



Klinikum rechts der Isar /Klinik für Anaesthesiologie

(Direktor: Univ.-Prof. Dr. E. Kochs)

**Analysis of anesthetic-induced effects on extracellular
electrophysiological activity in cortical and subcortical neuronal
networks**

Matthias Kreuzer

Vollständiger Abdruck der von der Fakultät für Medizin der Technischen Universität
München zur Erlangung des akademischen Grades eines

Doktors der Naturwissenschaften (Dr. rer. nat.)

genehmigten Dissertation

Vorsitzende(r): Univ.-Prof. Dr. Thomas Misgeld

Prüfer der Dissertation:

1. Univ.-Prof. Dr. Eberhard Kochs
2. Univ.-Prof. Dr. Michael Schemann

Die Dissertation wurde am 01.08.2013 bei der Technischen Universität München eingereicht
und durch die Fakultät für Medizin am 11.12.2013 angenommen.

Table of contents

Pre-releases	V
Nomenclature	VI
Abbreviations.....	VII
1 Introduction	1
1.1 General background.....	1
1.2 Working hypotheses of this thesis	4
2 Electrophysiological recordings of the brain: from action potentials to EEG	6
2.1 The Neuron	6
2.2 Neuronal Conduction	8
2.2.1 The action potential	8
2.2.2 The local field potential.....	10
2.3 The electroencephalogram	11
2.3.1 Classical EEG frequency ranges	13
2.3.2 A more modern approach of EEG interpretation	14
3 Anesthetic drugs.....	15
3.1 Propofol.....	15
3.2 Sevoflurane.....	16
3.3 Isoflurane.....	16
3.4 Enflurane	16
3.5 Halothane	17
3.6 Potency of volatile anesthetics, the MAC concept.....	17
3.7 The GABA _A receptor	18
3.8 Other relevant receptors	19
4 Observable anesthetic-induced effects on neuronal network activity	20
4.1 Isolated cortical networks.....	20
4.2 In vivo cortical networks	21
4.3 Hippocampal networks in vivo	22
4.4 Electroencephalogram	24
5 Experimental setups.....	26
5.1 Organotypic slice cultures	26
5.1.1 Preparation of neocortical organotypic slice cultures.....	26
5.1.2 Anesthetic protocol and sequence selection.....	27
5.1.3 Data preprocessing and parameter settings	29
5.1.4 Setting to compare LFP against noise and blocked neuronal activity	29
5.1.5 Setting to evaluate the GABAergic effect of sevoflurane	30

5.2	Cortical in vivo experiments with volatile anesthetics.....	30
5.2.1	Electrode implantation and LFP recording from rat neocortex	31
5.2.2	Selection of LFP data segments	32
5.2.3	Data preprocessing and parameter settings	33
5.3	Cortico-hippocampal experiments with propofol.....	33
5.3.1	LFP recordings from neocortical and hippocampal areas	34
5.3.2	Data preprocessing and parameter settings	34
5.4	Single-channel steady state study.....	35
5.4.1	Selection of volunteers and anesthetic protocol.....	35
5.4.2	Data preprocessing and parameter settings	36
5.5	Single-channel transition studies.....	36
5.5.1	Selection of patients and anesthetic protocol.....	37
5.5.2	Data preprocessing and parameter settings	38
5.6	Multi-channel-study.....	39
5.6.1	Selection of patients and anesthetic protocol.....	40
5.6.2	Data preprocessing and parameter settings	40
6	Analysis methods of cortical activity.....	41
6.1	Data preprocessing steps	44
6.2	Linear analysis.....	47
6.2.1	Power spectral density.....	47
6.2.2	Slew rate analysis.....	48
6.3	Non-linear analysis	51
6.3.1	The concept of entropy	51
6.3.2	Approximate entropy.....	54
6.3.3	Permutation entropy	58
6.3.4	Order recurrence rate	61
6.3.5	Examples comparing the cardinal and ordinal measures	63
6.3.6	Cross approximate entropy	66
6.3.7	Bivariate permutation entropy	68
6.3.8	Symbolic transfer entropy	69
7	Statistical methods	72
7.1	Prediction probability	72
7.2	Wilcoxon Test.....	74
7.3	Sign Test	74
7.4	Pearson's Correlation	74
7.5	Boxplots	75
7.6	Exponential regression.....	75
7.7	Stationarity.....	76

8	Anesthetic-induced effects on cortical network activity <i>in vitro</i>	77
8.1	Anesthetic effects on PSD in the complete recordings and down-states only	77
8.2	Down-state activity is different from noise.....	80
8.2.1	Results of the experiments with noise	80
8.2.2	Results of the experiments with the blocked neuronal activity.....	81
8.3	Approximate Entropy of cortical down-states.....	82
8.4	Permutation Entropy of cortical down-states	85
8.5	Order Recurrence Rate of cortical down-states	85
8.6	Evaluating the GABAergic effects of sevoflurane.....	87
8.7	Anesthetic-induced effects on cortical down-states <i>in vitro</i> : Discussing the results.....	90
8.8	Conclusion.....	91
9	Volatile anesthetic effects on local cortical network activity <i>in vivo</i>	92
9.1	Power Spectral Density	92
9.2	Approximate Entropy, Permutation Entropy and Order Recurrence Rate	94
9.3	Evaluation of spatiotemporal effects of volatile anesthetics on LFP with XApEn	99
9.4	Volatiles temporally and spatially affect local cortical activity: Discussing the results.....	103
9.5	Conclusions.....	105
10	Propofol-induced effects on cortex, hippocampus and the cortico-hippocampal pathway ..	106
10.1	Power spectral density.....	106
10.2	Cross Approximate Entropy	108
10.3	Bivariate Permutation Entropy.....	109
10.4	Symbolic Transfer Entropy.....	112
10.5	Propofol affects the cortico-hippocampal pathway: Discussing the results	114
10.6	Conclusion.....	115
11	Anesthetic effects on frontal EEG recordings at steady state conditions	117
11.1	Power spectral density changes	117
11.2	Approximate entropy.....	118
11.3	Permutation Entropy and Order Recurrence Rate	121
11.4	Parameter performance in the classical frequency ranges.....	122
11.5	Non-linear measures can reliably separate anesthetic levels: Discussing the results.....	124
12	Anesthetic effects on single-channel frontal EEG recordings at state transitions	125
12.1	Modeled propofol concentrations at LOC and ROC	125
12.2	Spectral but not complexity measures follow paradoxical excitation	125
12.3	Different frequencies adapt to the switched state with different delays	131
12.4	Permutation entropy reflects altered signal information content and reveals time hysteresis in EEG: Discussing the results.....	131
12.4.1	Propofol concentrations at LOC and ROC	131
12.4.2	Biphasic response during LOC	132

12.4.3	Time hysteresis during LOC and ROC.....	133
12.4.4	Conclusion.....	135
13	Spatio-temporal anesthetic effects on multi-channel EEG.....	136
13.1	Power spectral density.....	136
13.2	Approximate and Cross Approximate Entropy in β -frequencies.....	137
13.3	Evaluating electroencephalographic synchrony in classic frequency bands.....	138
13.3.1	Cross Approximate Entropy.....	138
13.3.2	Bivariate Permutation Entropy.....	138
13.3.3	Symbolic transfer entropy.....	139
13.4	Anesthetics affect EEG synchrony and information processing: Discussing the results..	140
13.4.1	Detection of adequate EEG recording positions.....	140
13.4.2	Evaluating spatial EEG properties.....	141
13.5	Conclusion.....	143
14	Limitations.....	144
15	Anesthetic-induced unconsciousness – a cortical point of view.....	146
15.1	Summary of the findings.....	146
15.1.1	LFP <i>in vitro</i>	146
15.1.2	LFP <i>in vivo</i>	146
15.1.3	Single and multi-channel EEG.....	146
15.2	Discussing the role of the cortex.....	147
16	A cortical curiosity: Brain electrical activity obeys Benford’s Law.....	152
16.1	Background.....	152
16.2	Methods.....	153
16.3	Results.....	155
16.4	Discussion.....	159
16.5	Conclusion.....	161
17	Reference list.....	162
18	Supplement.....	176
	List of figures.....	176
	List of tables.....	185
	Acknowledgements.....	186
	Publications.....	187
	Selected Abstracts / contributions to a congress.....	189
	Curriculum Vitae.....	191

Pre-releases

Parts of this thesis have been published as:

Kreuzer M[§], Hentschke H[§], Antkowiak B, Schwarz C, Kochs E, Schneider G: *Cross-approximate entropy of cortical local field potentials quantifies effects of anesthesia - a pilot study in rats*. BMC Neuroscience 2010; 11: 122

Drexler B[§], **Kreuzer M[§]**, Jordan D, Antkowiak B, Schneider G: *Sevoflurane-induced loss of consciousness is paralleled by a prominent modification of neural activity during cortical down-states*. Neuroscience Letters 2013; 548: 149-154

Kreuzer M, Jordan D, Antkowiak B, Drexler B, Kochs EF, Schneider G: *Brain electrical activity obeys Benford's Law*, Anesthesia & Analgesia 2014; 118(1):183-191

[§]: both authors contributed equally

Nomenclature

Parameter and indices

AEP	auditory evoked potentials
$ApEn$	approximate entropy
BIS	bispectral index
$BPeEn$	bivariate permutation entropy
ORR	order reoccurrence rate
$PeEn$	permutation entropy
PSD	power spectral density
PSI	Patient State Index
SR	slew rate
sTE	symbolic transfer entropy
$XApEn$	cross approximate entropy

Symbols

A	number of reverse arrangements
$\delta(t)$	Dirac δ -impulse
$\mathcal{E}\{\}$	expectation value
f_{\max}	Nyquist frequency
f_s	sampling rate
H	Shannon entropy
I	Information content
L	set of letters of an alphabet
l_{abc}	single letters of the alphabet
M	length of an alphabet
m	embedding dimension
N	number of data points in the time series
$p(a)$	probability of event a
$p(a,b)$	joint probability
$p(a b)$	conditional probability
P_K	prediction probability
π_k	permutation/order pattern
r_c	Pearson's correlation coefficient
S	thermal entropy
\bar{s}	system state vector
T_s	time between samples
$\bar{T}\{\dots\}$	transformation operator

τ	lag parameter
W	number of independent microstates
$x(t)$	continuous time signal
$x[n]$	discrete time signal
$X[k]$	frequency spectrum of $x[n]$
\bar{x}	mean of a time series

Constants and variables

E_m	resting membrane potential
E_K	potassium equilibrium potential
E_{Na}	sodium equilibrium potential
F	Faraday constant: $9.64853399 \cdot 10^4 \text{ C mol}^{-1}$
k_B	Boltzmann constant: $1.3806488 \cdot 10^{-23} \text{ m}^2 \text{ kg s}^{-2} \text{ K}^{-1}$
$[K^+]_i$	intracellular potassium concentration
$[K^+]_o$	extracellular potassium concentration
M_r	molar mass
R	universal gas constant: $8.314 \text{ J mol}^{-1} \text{ K}^{-1}$
T	temperature in Kelvin

Abbreviations

ACSF	artificial cerebrospinal fluid
ASA	American Society of Anesthesiologists
BS	burst suppression
C_{eff}	effect-site concentration
CTC	Cortico-thalamo-cortical
EEG	Electroencephalogram
EMG	Electromyogram
EPSP	excitatory postsynaptic potential
GABA	γ -aminobutyric acid
hipp	Hippocampus
HVRS	high voltage rhythmic spikes
IPSC	inhibitory postsynaptic current
IPSP	inhibitory postsynaptic potential
KSE	Kolmogorov-Sinai entropy
LFP	local field potential
LOC	loss of consciousness
LORR	loss of righting reflex
MAC	minimum alveolar concentration
ncx	Neocortex
OTC	organotypic slice cultures

Nomenclature

PK/PD	pharmacokinetic/pharmacodynamic
QQ-plot	quantile-quantile-plot
ROC	return of consciousness
SD	standard deviation
TCR	thalamic relay nuclei

1 Introduction

1.1 General background

General anesthesia is defined as a drug-induced reversible state of unconsciousness including hypnosis, amnesia, analgesia and akinesia, but stable cardiovascular and respiratory systems (Brown, Lydic et al. 2010). Until today the underlying mechanisms of anesthesia remain unclear. Seminal observations on cellular changes involved in anesthetic effects were reported by Meyer and Overton. They were the first to independently suggest that anesthetics affect lipid layers in the membranes of neuronal cells. The hypothesis was that the potency of an anesthetic drug is closely related to its lipophilicity (Meyer 1899; Overton 1901). In the 1980s this model was strongly questioned by Franks and Lieb. They established the model in which anesthetics act by directly binding on protein targets and so to affect cell membrane channel activity (Franks and Lieb 1982). The current situation proposes the theory that anesthetics affect excitatory and inhibitory neurotransmitter and hence influence neuronal network activity. The anesthetic effect on neuronal activity can be observed at all scales, starting from isolated cortical networks *in vitro* to cortical extracellular local field potentials (LFP), that can be considered as micro-EEG (Buzsáki, Anastassiou et al. 2012), *in vivo* in and surface electroencephalogram (EEG) recordings. An EEG consists of cumulated activity of the underlying cortical neuronal network (Cooper, Winter et al. 1965; Elul and Carl 1972). Anesthetic effects on molecular and cell membrane level have been studied extensively. Intravenous regimens such as propofol or etomidate almost exclusively affect the GABA_A (γ -aminobutyric acid) receptor, especially β_2 - and β_3 -subunits (Rudolph and Antkowiak 2004; Franks 2008). Volatile anesthetics, e.g., sevoflurane, isoflurane or halothane cause effects on a wider range of receptors like GABA_A, glycine, glutamate or nicotinic acetylcholine receptors (Campagna, Miller et al. 2003; Rudolph and Antkowiak 2004) as well as Ca²⁺ activated potassium channels. But the most prominent major player is probably the GABA_A receptor. One thesis on the mechanism of anesthesia claims that if GABA is enhanced by anesthetics, thalamo-cortical neurons are depressed and the loss of consciousness (LOC) occurs (Alkire, Haier et al. 2000). Another theory contends that drug-induced changes in cortico-cortical synchrony are essential for inducing the state of anesthesia. The disruption or distortion of these communication structures can either be caused by “loss of cortical integration”, i.e., disruption of the cortical network’s communication structure or by “loss of information capacity”, i.e., reduction of the cortical

state space (Alkire, Hudetz et al. 2008). Anesthetics seem to impair large-scale integration of information hypothesized to be a prerequisite to proper brain function, particularly conscious perception (Lamme, Zipser et al. 1998; Varela, Lachaux et al. 2001; Buzsaki 2007; Uhlhaas, Pipa et al. 2009). Numerous experimental observations are in agreement with this concept. Rats which were stimulated with light flashes showed that volatile anesthetics disrupt anterior-posterior phase synchronization of field responses (Imas, Ropella et al. 2006) and depressed long-latency spike responses in visual cortex thought to arise from cortico-cortical interactions (Hudetz, Vizuite et al. 2009). In humans, during the transition from awake to LOC, various general anesthetics decoupled γ -rhythms between anterior and posterior cortical areas as well as between homologous areas in different hemispheres (John, Prichep et al. 2001). A theoretical approach to explain the LOC was formulated by John et al. in the form of an anesthetic cascade. They explain the process in six, not necessarily consecutive steps as “bottom-up” approach starting with brain stem depression and finally leading to suppression of activity in the prefrontal cortex (John and Prichep 2005). In a direct contradicting response a “top-down approach” is suggested (Antkowiak 2005). Experimental results point towards a cortical effect as trigger for LOC (Velly, Rey et al. 2007). Imaging studies confirmed the role of cortex and thalamus as important targets for anesthetics (Fiset, Paus et al. 1999; Alkire, Haier et al. 2000). All these findings indicate that anesthetics temporally and spatially alter neuronal network activity. These changes can either be observed by recordings of electrophysiological activity such as the EEG or LFP or imaging methods can be used to detect changes in neuronal activity in different regions. EEG and LFP directly reflect activity of cortical neurons whereas imaging studies like functional magnetic resonance imaging indirectly measure cortical activity. There, changes in blood oxygen consumption are measured and since higher neuronal activity seems associated with higher oxygen consumption the neuronal activity can be evaluated. Imaging studies are characterized by high spatial, but low temporal resolution, whereas when using electrophysiological recordings high temporal resolution can be achieved at the expense of spatial resolution. In recent years non-linear analysis methods were introduced in the analyses of electrophysiological signals such as EEG and LFP. These non-linear parameters for instance evaluate signal complexity or dimensionality and are able to deliver additional information to results obtained from correlation, coherence or spectral analyses. The more prominent univariate parameters are approximate entropy (*ApEn*) (Pincus 1991; Bruhn, Ropcke et al. 2000) and permutation entropy (*PeEn*) (Bandt and Pompe 2002; Jordan, Stockmanns et al. 2008). They showed better performance in separating different levels of anesthesia during EEG studies than spectral measures (Jordan, Stockmanns et al. 2008;

Jordan 2010). This result remains true for LFP experiments (Kreuzer, Hentschke et al. 2010; Silva, Cardoso-Cruz et al. 2010). The better performance may be based in the fact that non-linear signal components are also considered (Jordan, Hock et al. 2008; Jordan, Kreuzer et al. 2009). Modification of these parameters to bivariate measures, e.g., cross-approximate-entropy (*XApEn*) (Pincus, Mulligan et al. 1996) are potent to additionally detect drug-induced spatial effects between two recording sites. EEG and LFP synchronizing effects could be revealed with this method (Hudetz 2002; Hudetz, Wood et al. 2003). On the whole uni- and bivariate parameters seem to be suitable for analysis of anesthetic-induced effects on electrophysiological signals. The work presented here describes the application of non-linear parameters on electrophysiological activity of neuronal networks of different size, starting from LFP recorded *in vitro* up to multi-channel EEG, to detect anesthetic-induced changes of neuronal network activity. These analyses may help to obtain information regarding the neuronal mechanisms that lead to anesthetic-induced unconsciousness. On the one hand, different types of neuronal activity are analyzed using the same set of tools, acquiring comparability among the results and on the other hand, leading to new insights toward possible mechanisms. The least complex analyzed neuronal networks are organotypic slice cultures (OTC) from the rat neocortex. Extracellular LFP was recorded from these *in vitro* networks lacking subcortical inputs. This means that observed drug-induced effects are of purely cortical origin. The OTC were treated with sevoflurane and propofol and the drug-induced effect on LFP activity was evaluated (Drexler, Kreuzer et al. 2013). The next data set consisted of LFP recordings *in vivo*. That means that compared to OTC the activity recorded was influenced by the entire neuronal network in contrast to the pure cortical activity. Therefore, LFP was recorded from multi-electrode arrays located in a rat's barrel cortex. These recordings represent intra- and inter-cortical activity but can be influenced from the thalamus, another major target for anesthetics (Alkire, McReynolds et al. 2007) or other subcortical regions. The effect of different volatile regimens on the recorded LFP was determined. Additionally to the experiments with multi-channel recordings from the barrel cortex, simultaneous recordings from multi-electrode arrays placed in the mouse prefrontal neocortex and hippocampus were performed. The change of LFP activity caused by propofol was investigated. In a following step, transferring the analyses from rodents to humans, single and multi-channel EEG recordings were used for examination. EEG recordings represent the activity of a much bigger underlying neuronal network than LFP do. Nevertheless, it is recorded from electrodes placed on the scalp. Hence, the EEG represents a signal filtered by the skull and other tissue located between the EEG generating neurons and the recording site. This leads to a change of temporal signal

properties compared to LFP (Nunez 1989). But results obtained during cortical LFP and surface EEG using the same analysis methods may be quantitatively compared with each other. With the presented experimental cascade of setups (isolated cortex *in vitro* → intra-cortical and hippocampal multi-electrode arrays *in vivo* → frontal single-channel EEG → multi-channel EEG recordings) and a unified set of non-linear parameters cortical anesthetic effects can be analyzed on different scales and compared. This approach might provide some new insights into the mechanisms of anesthesia and may prove helpful in the quest of identifying the trigger of consciousness. The data used in this manuscript was retrospectively analyzed with the described methods, i.e., the study protocols could not be influenced. The focus was set on a logical succession of experimental setups and the parameters that yielded most informative results. The approaches and results presented can help to better understand the effects of anesthetics on neuronal network activity. These findings may also have clinical relevance in order to monitor the patients' level of anesthesia more reliably. Increased understanding of anesthetic-induced effects on electrophysiological recordings may prove helpful in the design of devices monitoring the anesthetic level of a patient during surgery. Right now, these monitors are capable of detecting changes in the EEG waveforms caused by the anesthetic drug. But the sources and triggers of these changes are unknown.

1.2 Working hypotheses of this thesis

As mentioned in the previous section, anesthetics were used to induce hypnosis and anesthesia for the last one and a half century. However, one question has is still unsolved: How do anesthetics induce the state of anesthesia? This thesis deals with the approach to apply non-linear signal processing parameters on electrophysiological activity recorded from the brain or single cerebral structures. With this setup it may be possible to gain new insight into anesthetic-induced effects that alter neuronal network activity and hence the signals in a substance-specific manner. Thus the following hypotheses were investigated:

- The non-linear analysis methods are suitable to determine effects of anesthetics on neuronal activity and provide new insights compared to established (spectral) analysis methods;
- The observed anesthetic-induced temporal and spatial effects help to reveal changes in the information processing structure of the neuronal networks. Thus giving insight into potential mechanistic processes;

- Analyzing signal changes during state transition phases helps to understand how (and where) processes that trigger anesthetic-related effects are released.
- Effects observed in distinct frequency ranges, e.g., 4-12 Hz as communication frequency in the cortico-hippocampal pathway responsible for mnemonic processes, can help to understand how anesthetics trigger amnesia and hypnosis;

2 Electrophysiological recordings of the brain: from action potentials to EEG

Electrophysiological recordings reflect the electrical properties of biological cells or tissues. In this work, the focus lies on the electrical activity generated by neurons and neuronal networks located in cortical and subcortical areas of the brain. The generated electrical activity was recorded either as LFP or EEG. The containing voltage fluctuations are sensitive to anesthetic regimens and as a consequence they can be used to detect anesthetic-induced effects on the brain.

2.1 The Neuron

The neuron (Greek: νεῦρον, *neûron* = “nerve”) or nerve cell consists of a cell body (soma), the branch-like dendrites and a long nerve fiber, the axon as shown in Figure 2.1. Neuronal activity transmits information throughout neuronal networks of the central nervous system. Therefore, dendrites collect action potentials from the axons of other cells. The connection between dendrite and axon is called synapse. The dendrites of a single cell can be connected with up to 200.000 axons of other cells (Bower and Parsons 2003). The information of a received action potential is transferred to the soma and from there to the axon. The axon transmits action potentials to the synapses and from there it encroaches to the dendrite of another cell with an axonal transmission speed of up to about 100 m/s (Miller 2005).

Generally, cell to cell signaling through the synapse can take part either through chemical or electrical transmission (Johansson 2006), depending on whether the synapse is of electrical or chemical kind. In electrical synapses, pre- and postsynaptic cells are very close together (~3.5 nm) and the cells are coupled via gap junction channels. Signal transmission occurs directly via ion transfer through the gap junctions without noticeable delay and can be bidirectional (Figure 2.2). Chemical synapses transmit signals unidirectional with a time delay of ≥ 0.3 ms or often more. Pre- and postsynaptic cells are about 20-40 nm apart and the signal is processed with the help of neurotransmitters, e.g., glutamate. That means that the action potential is transformed into a chemical signal, i.e., flow of the neurotransmitter from axon to dendrite and then retransformed into an ion current (Figure 2.2). Depending on the kind of neurotransmitter spilled into the synaptic cleft, inhibitory postsynaptic potentials (IPSP) or excitatory postsynaptic potentials (EPSP) can occur on the postsynaptic membrane. IPSP hyperpolarize the cell membrane and aggravate releasing an action

potential. EPSP depolarize the cell membrane supporting action potential release. The most important inhibitory neurotransmitters are GABA and glycine while glutamate represents the most powerful excitatory neurotransmitter.

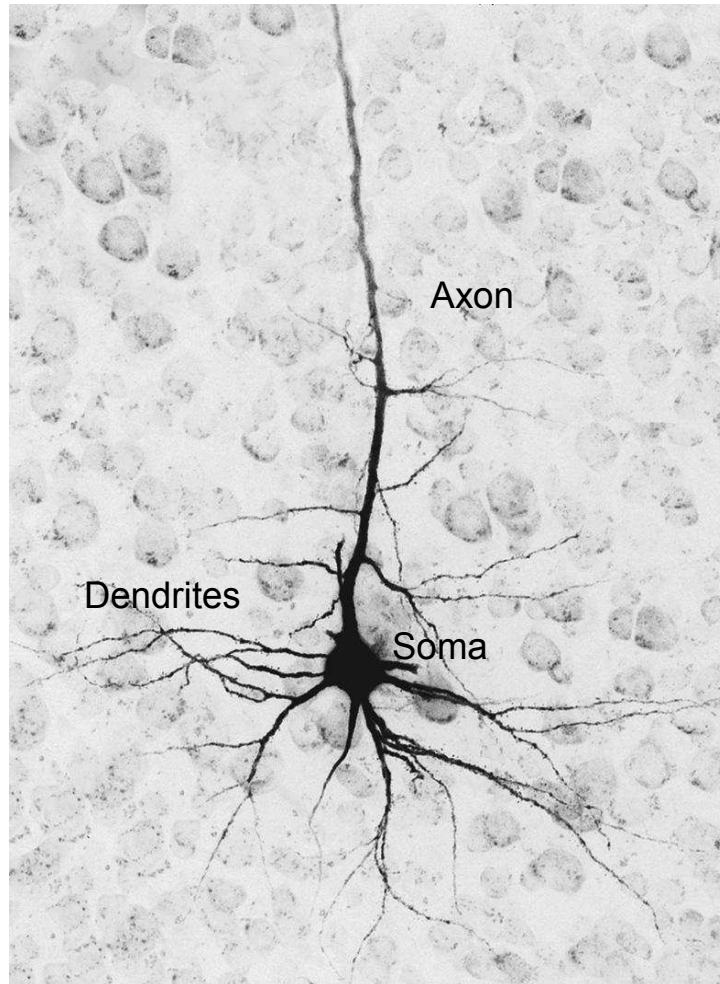


Figure 2.1: The neuron consists of the soma where dendrites and one axon are spreading from. The dendrites are forming connections with other cells' axons and vice versa, hence building up a neuronal network where action potentials can be transmitted. (Pryor 2007)

Inhibitory receptors influence potassium or chloride ion channels, causing hyperpolarization of the postsynaptic membrane thus impeding action potential release. Excitatory neurotransmitters depolarize postsynaptic membranes making it easier for an action potential to be released, thus facilitating signal transmission. Excitatory receptors influence sodium and calcium channels. These receptors have also been identified as targets of anesthetic regimen (Campagna, Miller et al. 2003; Franks 2006; Alkire, Hudetz et al. 2008). Anesthetics can substance-dependently have an activating effect on inhibitory neurotransmitters and/or inhibit excitatory neurotransmitters. As result, cell to cell communication is interfered.

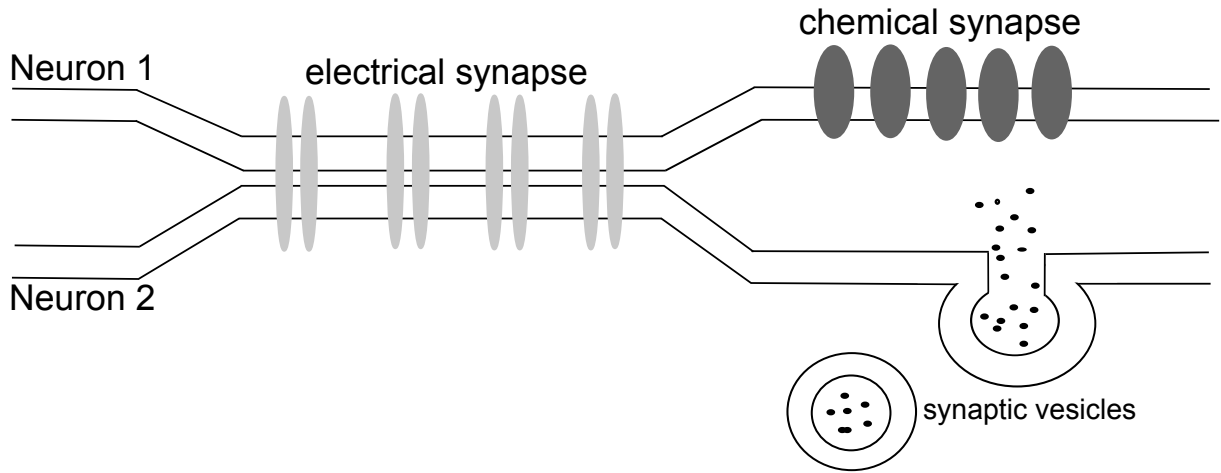


Figure 2.2: Two neurons can either communicate through direct coupling with gap junction channels (left) or via neurotransmitters through the synaptic cleft (right) (Johansson 2006).

2.2 Neuronal Conduction

As mentioned, neurons conduct information through the release and transfer of action potentials. An action potential is characterized by rapid changes in the neuron's membrane potential. Neuronal networks are dependent on action potentials as most important form of cell to cell communication. These action potentials are generated by ion flux through voltage gated ion channels.

2.2.1 The action potential

The resting membrane potential E_m in a neuron is approximately the potassium equilibrium potential E_K that can be calculated according to the Nernst equation.

$$E_m \approx E_K = \left(\frac{-RT}{F} \right) \ln \left(\frac{[K^+]_i}{[K^+]_o} \right) \quad (2.1)$$

$R = 8.314 \text{ J mol}^{-1} \text{ K}^{-1}$ is the universal gas constant, $F = 9.65 \times 10^4 \text{ } ^\circ\text{C mol}^{-1}$ the Faraday constant and T the current temperature in Kelvin. $[K^+]_i$ and $[K^+]_o$ are the potassium concentrations inside and outside the cell, respectively. Equation 2.1 leads to E_K values of -70 to -80 mV. The value is negative because $[K^+]_i > [K^+]_o$. It is the opposite for sodium where the concentration outside the cell is higher than inside (Miller 2005). Hence, E_{Na} is around 60 mV. During this resting state sodium channels are closed and open potassium channels trigger the resting potential. If the cell receives a depolarizing impulse that raises the membrane

potential over its threshold potential, potassium and sodium channels open up and allow a positive ion flow into the cell. The membrane potential becomes even more positive. During this depolarization more and more ion channels open and the membrane potential increases fast to positive values up to 20-30 mV where an overshoot takes place. Before reaching the maximum potential, fast sodium channels close and with some delay potassium starts to drift out of the cell. Repolarization begins and the membrane potential decreases below the resting potential. During the hyperpolarization phase the membrane potential increases to the resting potential. In a neuron the entire action potential process takes about 1-2 ms. After an absolute refractory period of about 0.5 ms the cell is ready to fire again, but with increased threshold potential. Action potentials can be released at the natural threshold potential after approximately 3.5 ms, resulting in a maximum firing frequency of circa 200 Hz. After an action potential is released it is transmitted through the axon in the according way. The schematic course and ion flow of an action potential is displayed in Figure 2.3.

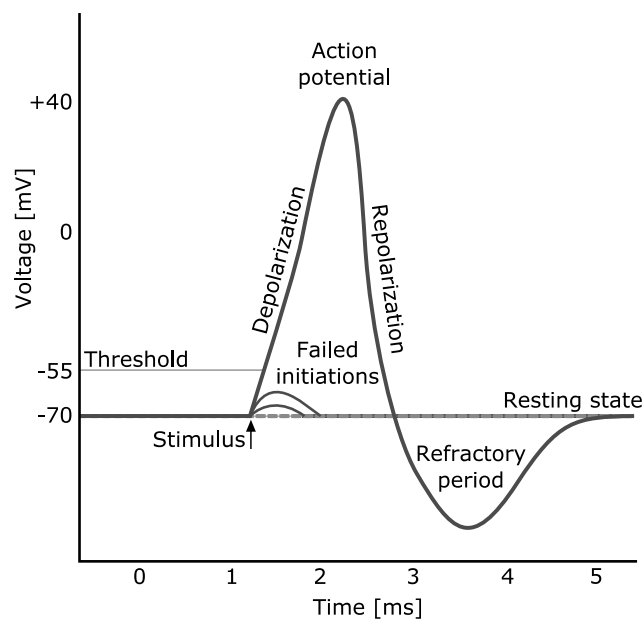


Figure 2.3: Schematic course of an action potential (Chris73).

Direct transduction from one cell's axon to the next cell's dendrite is not possible, due to the synaptic cleft. The action potential causes chemical neurotransmitters to spill into the cleft and diffuse to the dendrite. Here, these transmitters can force ion channels to react. If these processes simultaneously take place in a number of synapses, action potentials can be released.

2.2.2 The local field potential

A LFP consists of multi unit activity and represents the sum of dendritic currents within a cutout of the neuronal network recorded from low impedance microelectrodes that are placed extracellularly (Berens, Keliris et al. 2008). In contrast to action potentials LFPs are much slower and seem to represent synchronized dendritic activity within an area of up to approximately 140-300 μm around the electrode tip where a large number of neurons contribute to LFP generation (Legatt, Arezzo et al. 1980; Gray, Maldonado et al. 1995). LFP may represent the synchronized input into the observed cutout of the network and may be considered as micro-EEG (Buzsáki, Anastassiou et al. 2012). Action potentials are too fast to participate in LFP generation. The major players in generating LFPs are somato-dendritic currents and postsynaptic potentials, i.e., EPSP and IPSP. Since LFP activity is a slow process, the signal containing the LFP is usually low-pass filtered with a cutoff frequency of 200-300 Hz to exclude non LFP activity such as high-frequency parts like spike components coming from action potentials (Figure 2.4). Generally, the unfiltered signal represents the sum of action potentials of participating cells. Further, LFPs are believed to measure synchronized synaptic signals (Mitzdorf 1987), sub-threshold membrane oscillations (Kamondi, Acsady et al. 1998) and spike afterpotentials (Buzsaki and Kandel 1998). LFP recordings consist of up- and down-state activity. Up-states are characterized by ongoing activity that is disrupted by sequences where no spiking can be observed, so called down-states. Up-states are triggered by glutamate release and are maintained as long as glutamate is available (Poskanzer and Yuste 2011). Following this up-state, the network enters a down-state, sometimes considered neuronal silence (Cash, Halgren et al. 2009) and the glutamate reserves are refilled until the next up-state can be released.

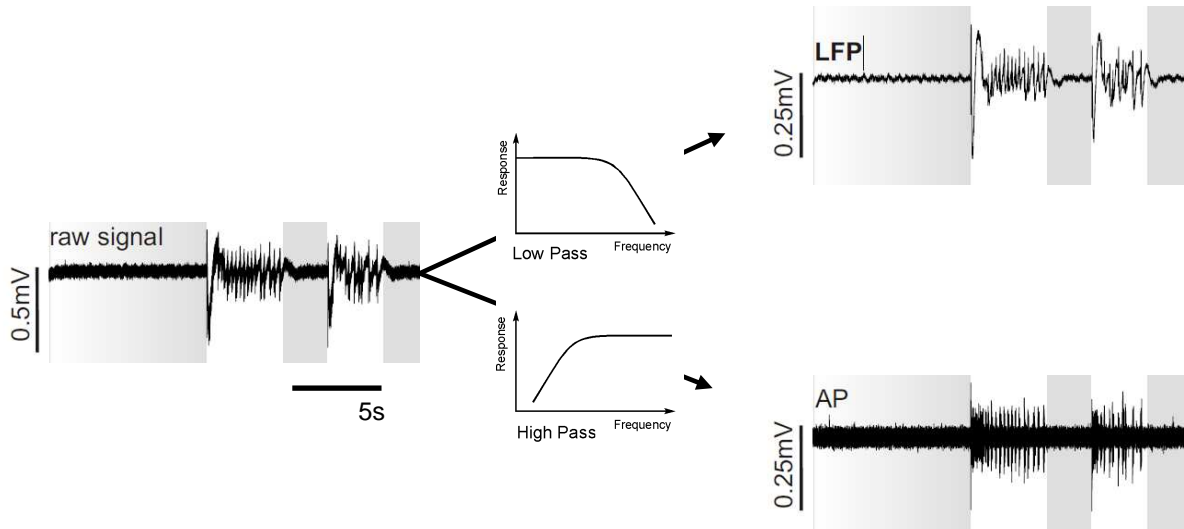


Figure 2.4: left side: recorded neuronal activity from an electrode that is placed extracellularly in an OTC (raw signal). This signal is processed by either low-pass or high-pass filtering to isolate LFP and action potentials. Right side: top: low frequent LFPs, bottom: action potentials; if action potential bursts are generated, simultaneously low frequent LFPs can be observed. These recordings were obtained from extracellular recordings in cortical OTC described in section 5.1. The action potentials can be extracted from the raw signal through high pass filtering, LFPs through low-pass filtering.

2.3 The electroencephalogram

The EEG represents the cerebral electrical activity measured on the scalp generated from a distinct section of the cortical neuronal network, i.e., it represents the sum of LFP in this area. The German psychiatrist Hans Berger was the first to detect these potential changes caused by the human brain (Berger 1929). Generators of this activity are cortical neurons, i.e., the accumulated activity of pyramidal cells located in the cortical layer V. There, these pyramidal cells, a specific type of neurons, are vertically, column-like, orientated throughout the cortex and form the majority of neurons in the cortex (Schmidt, Müller et al. 2008). The term "pyramidal cells" is derived from the shape of the cell bodies. The EEG is the summed activity of 10^7 up to 10^{10} pyramidal neurons (Nunez 1989; Nauck, Klawonn et al. 1996), and effective contributions to EEG generation come mostly from synchronized cortical activity (von Stein, Rappelsberger et al. 1999). A surface EEG electrode measures the neuronal activity of an underlying cortical area of around 6 cm^2 (Cooper, Winter et al. 1965). Thereby, negative potentials cause positive and positive potentials cause negative EEG amplitudes as displayed in Figure 2.5. The acquired EEG is characterized by distinct patterns and frequencies that can be associated with different cerebral states or tasks. But the underlying neuronal mechanisms of EEG generation and how to interpret it are not yet

totally revealed (Korn and Faure 2003). However, EEG includes information from the cortex as well as information from subcortical areas that project to the cortex, since pyramidal neurons also receive input from these regions. The EEG is a compound of oscillations of different frequencies generated and transmitted by different cerebral structures. Throughout the EEG research approaches were made to allocate defined EEG frequency ranges to different cerebral tasks, respectively states.

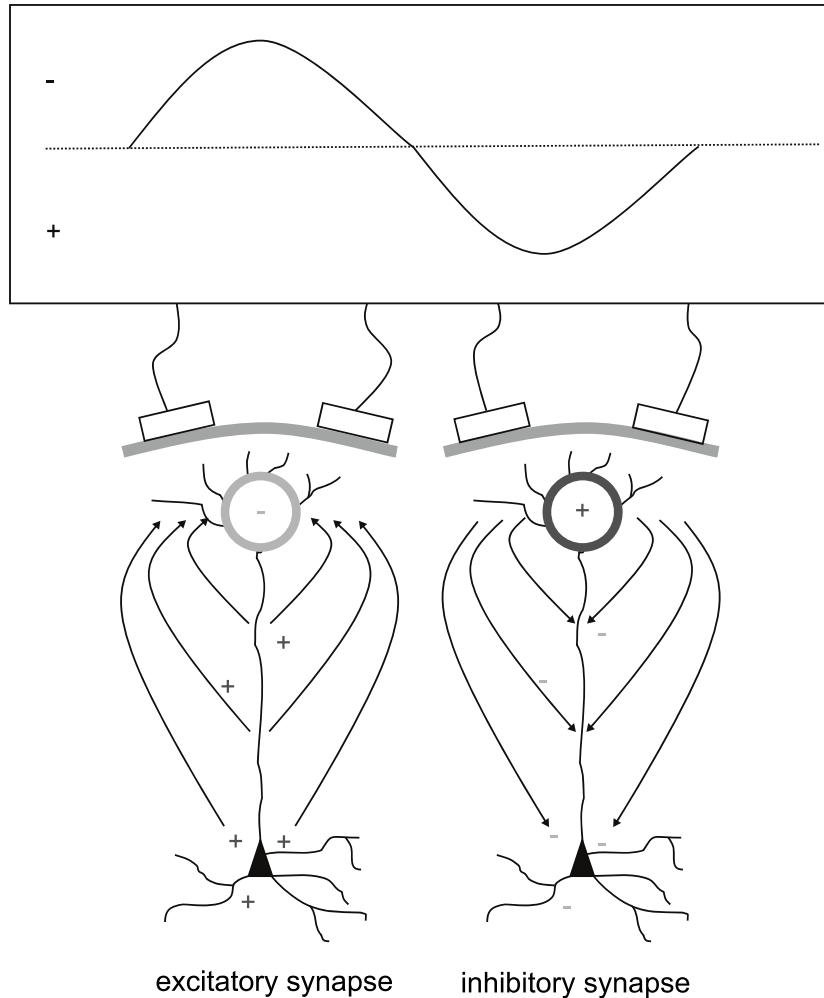


Figure 2.5: EEG generators: excitatory (left) and inhibitory (right) synapses generate an electrical signal on the scalp (Schmidt, Müller et al. 2008).

2.3.1 Classical EEG frequency ranges

Classically, EEG frequencies are classified by five frequency bands, namely α -, β -, γ -, δ -, and θ -band. Possible allocations of these frequency ranges to specific cerebral tasks or states are presented in Table 2.1. Roughly speaking, the EEG-frequencies and the tasks presented in the table may be assigned to different cerebral structures. EEG δ -waves seem to arise from the cortex and the thalamus. θ - and α -waves are considered crucial for information processing during mnemonic tasks in cortico-hippocampal pathways, the hippocampus or the amygdala. EEG β -oscillations spread over the entire cortex serving cortico-cortical transmission and γ -oscillations are mainly of short range, e.g., as in intra-cortical processes. The impression of cerebral activity being the sum of different oscillations justifies the adaption of spectral analysis methods. But since these spectral analyses are linear not the entire information content of the signal may be revealed as discussed in the next section.

<i>Label</i>	<i>Frequencies</i>	<i>Task</i>
α	~8-13 Hz	<ul style="list-style-type: none"> - demands related to attention (Ray and Cole 1985) - attention and semantic memory performance (Klimesch 1999) - gate to the thalamus (John and Prichep 2005)
β	~13-30 Hz	<ul style="list-style-type: none"> - emotional and cognitive processes (Ray and Cole 1985) - establishment of long-distance synchrony; that is, over transmission delays of 10–50 ms (Varela, Lachaux et al. 2001). - reflects intra-cortical transactions (John and Prichep 2005)
γ	~30-70 Hz	<ul style="list-style-type: none"> - formation of local patches of synchrony; labile for long-distance connections (Varela, Lachaux et al. 2001) - reflects cortico-cortical and cortico-thalamo-cortical transactions (John and Prichep 2005) - cortex layer I/V comparison (John and Prichep 2005)
δ	~0.5-4 Hz	<ul style="list-style-type: none"> - may be related to attention and to internal processing during the performance of a task (Harmony, Fernandez et al. 1996) - resting state when cortex gets decoupled from the thalamus (John and Prichep 2005)
θ	~4-8 Hz	<ul style="list-style-type: none"> - episodic memory and encoding of new information (Klimesch 1999)

Table 2.1: Classic EEG frequencies and some of their assumed cerebral processing tasks

2.3.2 A more modern approach of EEG interpretation

A more modern approach of EEG interpretation is to see the EEG as representative of the prevalent state of the brains cortical and subcortical systems (Faure and Korn 2001; Thakor and Tong 2004). While a single addition of cortical activities leads to a linear system, the system state approach yields a high-dimensional and non-linear system. For the definition of linearity see section 6.1. With this system state perception, EEG shows non-linear properties as cellular activity itself is non-linear (Elbert, Ray et al. 1994; Buzsáki 2006). A confusing number of independent cortical networks contribute to EEG generation. These networks interact with each other in a very complex and almost irreproducible way. An explicit answer to the question whether EEG is stochastic or deterministic is not possible, but both properties may be coexistent (Faure and Korn 2001). Generally, EEG is a non-stationary signal, though it can contain stationary sequences (Kawabata 1976; Cohen and Sances 1977; Kreuzer, Jordan et al. 2010). With the alluded properties of this signal an analysis with non-linear parameters of EEG and underlying LFP within *in vivo* and *in vitro* networks seems plausible. When the activity of cerebral neuronal networks is manipulated by the use of anesthetic drugs, specific alterations in the electrophysiological signal can be observed (Antkowiak 1999; Antkowiak 2002; Hentschke, Schwarz et al. 2005). Further, an approach of applying non-linear analysis methods on distinct EEG-frequencies could help to gain new insights to anesthetic processes.

3 Anesthetic drugs

Anesthetic drugs that are used in the course of general anesthesia aim towards suppression of consciousness and pain during a surgical procedure. The beginning of modern anesthesia goes back to October 16, 1846 when William Morton performed the first general anesthesia using ether. As time went on, several other drugs such as chloroform or nitrous oxide were used to induce unconsciousness in patients. Nowadays either intravenous or inhalational anesthetics are administered. A short compendium of the properties of the anesthetics used for this work is presented in the next sections.

3.1 Propofol

Propofol ($C_{12}H_{18}O$, $M_r=178.3g/mol$, 2,6-bis(propan-2-yl)phenol) is a short acting, intravenously administered anesthetic used for induction and maintenance of anesthesia. It rapidly induces hypnosis and causes loss of consciousness. Recovery from propofol anesthesia is quick and smooth (Bryson, Fulton et al. 1995). The behavioral effects of propofol are concentration-dependent. Low concentrations lead to mild sedation and memory impairment and high concentrations produce deep sedation, hypnosis and immobility (Rudolph and Antkowiak 2004). Propofol has no remarkable analgesic effect and its hypnotic effect is revealed by mainly acting on the GABA_A receptor's β_2 - and β_3 -subunits (Grasshoff and Antkowiak 2004; Rudolph and Antkowiak 2004). Chloride membrane currents are potentiated by propofol revealing inhibitory influence on neuronal network activity. The chemical structure of propofol is displayed in Figure 3.1.

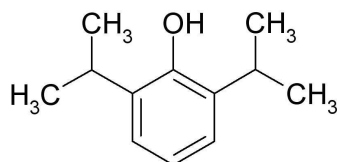


Figure 3.1: Chemical structure of propofol

3.2 Sevoflurane

Sevoflurane ($C_4H_3F_7O$, $M_r = 200.1$ g/mol, 1,1,1,3,3,3-hexafluoro-2-(fluoromethoxy)propane) is a halogenated ether with its structure displayed in Figure 3.2. It is the commonly used inhalational anesthetic used for induction and maintenance of anesthesia. It is a colorless, non-flammable liquid that has widely substituted other inhalational agents like isoflurane and halothane. In contrast to propofol it affects a wide range of molecular targets. $GABA_A$ and glycine receptors are enhanced while glutamate and acetylcholine receptors are inhibited (Campagna, Miller et al. 2003; Grasshoff and Antkowiak 2004) as well as the large conductance Ca^{2+} activated potassium channel, but its mode of action still remains unclear. It has good hypnotic and weak analgesic and relaxant effects. Compared to propofol, extubation times after sevoflurane anesthesia are better predictable. Its solubility in blood is lower than for isoflurane and halothane and, hence, recovery is faster (Patel and Goa 1996).

3.3 Isoflurane

Isoflurane from the class of carboxylic acids ($C_3H_2ClF_5O$, $M_r = 184.5$ g/mol, 2-chloro-2-(difluoromethoxy)-1,1,1-trifluoroethane) is another volatile anesthetic. It is a clear and colorless liquid with pungent smell. And has a good hypnotic and relaxant but weak analgesic effect that is often used for induction of anesthesia. Similar to sevoflurane it affects multiple molecular targets, especially $GABA_A$, glycine, glutamate receptors and the large conductance Ca^{2+} activated potassium channel. The exact mechanism of action is still matter of discussion. The chemical structure of isoflurane is displayed in Figure 3.2.

3.4 Enflurane

Enflurane ($C_3H_2ClF_5O$, $M_r=184.5$ g/mol, 2-chloro-1-(difluoromethoxy)-1,1,2-trifluoroethane) from the class of carboxylic acids is an isomer of isoflurane. It is extremely stable and allows fast adjustments of the anesthetic level without affecting pulse or respiratory rate to a big degree. It is a colorless liquid with sweet smell and has a good hypnotic and relaxant but weak analgesic effect. Enflurane is not used in clinical practice anymore. Enflurane seems to affect different molecular targets such as $GABA_A$, glycine and glutamate receptors as well as the large conductance Ca^{2+} activated potassium channel but its complete mechanism of action is not yet revealed. In Figure 3.2 the chemical structure of enflurane is presented.

3.5 Halothane

Halothane ($C_2HBrClF_3$, $M_r=197.4$ g/mol, 2-bromo-2-chloro-1,1,1-trifluoroethane), another volatile anesthetic, is a halogenated hydrocarbon in the class of alkyl halides. It has been substituted in clinical practice by sevoflurane and isoflurane due to its liver toxicity. Halothane probably also affects $GABA_A$, glutamate and glycine receptors as well as potassium channels, but its concrete mechanism of causing anesthesia has not been revealed yet. Halothane's chemical structure is presented in Figure 3.2 below

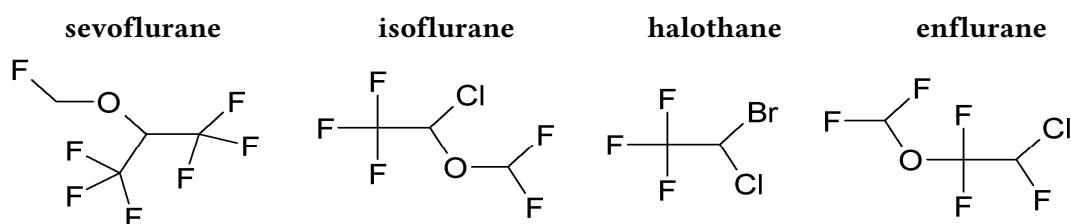


Figure 3.2: Chemical structure the used volatile anesthetics

3.6 Potency of volatile anesthetics, the MAC concept

The potency of volatile anesthetics is represented as minimum alveolar concentration (MAC). MAC is defined as the concentration that is necessary to prevent a movement reaction on a defined pain stimulus in 50% of the subjects. The lower the MAC, the more potent the volatile anesthetic gets (Eger, Saidman et al. 1965). In the course of this work, the above mentioned anesthetic regimens were used during the studies described in section 5. Halothane has a MAC of 0.8%, the MAC of isoflurane is 1.2% and sevoflurane and enflurane have the MAC at 1.7%. A special form of MAC is the MAC_{awake} , which is the alveolar concentration where 50% of the subjects do not verbally respond to a command.

The *in vitro* experiments were performed with sevoflurane and propofol. For the *in vivo* animal experiments in rats' barrel cortex the inhalational anesthetics isoflurane, enflurane and halothane were used. *In vivo* studies of anesthetic effects on the cortico-hippocampal pathway were conducted with propofol. EEG recordings were accomplished under propofol or sevoflurane anesthesia. One proposed major target of anesthetics is the inhibitory $GABA_A$ receptor. Since it seems to be the most relevant target for the process of unconsciousness, especially for propofol, the receptor's structure is explained in detail in the next section.

3.7 The GABA_A receptor

GABA_A receptors are densely distributed throughout the brain and the central nervous system and especially in areas that are sensitive to anesthetic regimens (Drexler, Grasshoff et al. 2006). The GABA_A receptor consists of five parts that are combined from different subunits as displayed in Figure 3.3 (c). In the brain, most GABA_A receptors are built from two α -, two β -, and one γ -subunit. If GABA binds to the pentameric GABA_A receptor chloride is spilled to the postsynaptic neuron causing a hyperpolarization of the cell membrane, aggravating cell to cell communication. In the presence of general anesthetics, the inhibitory postsynaptic current (IPSC) decays slower; hence, blocking the communication structure for a longer time span. Network activity is negatively influenced and this may represent a key mechanism of anesthesia-induced unconsciousness (Rudolph and Antkowiak 2004).

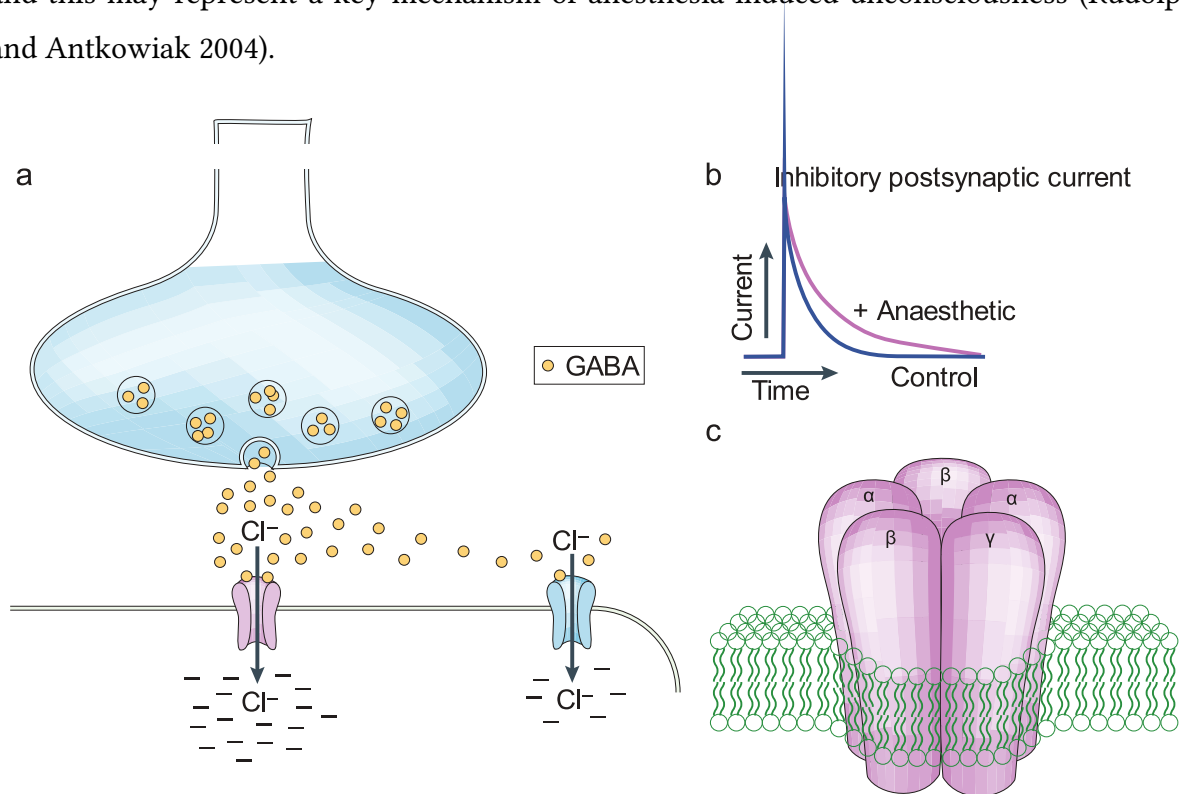


Figure 3.3: The figure was taken from the work of Rudolph and Antkowiak (Rudolph and Antkowiak 2004). (a) When GABA is activated, chloride is released and can flow in the postsynaptic cell; (b) in the presence of general anesthetics IPSC's decay slower and hyperpolarization of the postsynaptic cell membrane is increased due to longer chloride flux; (c) pentameric design of the GABA_A receptor.

3.8 Other relevant receptors

Other relevant receptors that are affected by the anesthetics used apart from the GABA_A receptor are glutamate and glycine receptors. The NMDA (N-methyl-D-aspartate) receptor is the most prominent glutamate receptor. It is essential in the control of synaptic plasticity and memory function (Li and Tsien 2009). Especially volatile anesthetics have an inhibiting effect on this receptor which leads to less opened ion channels being nonselective to cations. Hence neuronal signaling becomes impaired. The glycine receptor controls chloride currents like GABA_A does. Inhalational and intravenous anesthetics potentiate the glycine receptor (Alkire, Hudetz et al. 2008) and impede neuronal signaling. Ca²⁺ activated potassium channels are necessary to shape action potentials in neuronal cells and hence enable cell to cell signaling. Especially volatile anesthetics inhibit activity of these channels leading to impaired neuronal communication (Namba, Ishii et al. 2000). Another group of receptors that is affected by anesthetics are nicotinic and muscarinic acetylcholine receptors. Certain anesthetics obstruct these receptors and hence the movement of cations. In general, anesthetics influence a variety of membrane channels in a way that worsens neuronal conduction and hence communication within the neuronal network.

4 Observable anesthetic-induced effects on neuronal network activity

The introduced anesthetics affect cortical network activity by acting on different receptor targets that influence membrane ion channels with inhibiting or enhancing effect. These changes cause an observable effect in the electrophysiological recordings of neuronal network activity. The OTC's *in vitro* LFP traces show anesthetic specific effects on the networks up- and down-state behavior. The *in vivo* and EEG recordings that are characterized by a much larger generating neuron population in contrast to the isolated cortical OTC do not just show an alteration of the up- and down-state rate but on waveform behavior, i.e., anesthetic-induced changes in frequency and amplitude of cortical or hippocampal LFP or surface EEG. This section describes the effects of anesthetics that are visible to the naked eye.

4.1 Isolated cortical networks

OTC of neocortical cells that were treated with volatile anesthetics show a depression of action potential spikes in a concentration dependent manner (Antkowiak and Helfrich-Forster 1998). This effect could also be shown for propofol, which also reduces mean spike rates of action potentials but not the number of spikes per burst (Antognini, Wang et al. 1999). Extracellular LFP recordings as used for this work also show an observable effect when treated with sevoflurane or propofol. The conduction of these experiments is presented in section 5.1.2. With sevoflurane a concentration dependent depression of LFP activity can be observed as displayed in Figure 4.1 on the right side. The bursts or up-states become fewer but seem to last longer. With propofol the depression of activity is not as prominent but still detectable by just looking on the signal trace as shown in Figure 4.1 on the left side. The depression is weaker compared to sevoflurane as is the prolongation of the up-state. These alterations are at least partially caused by GABAergic inhibition, but especially for sevoflurane other receptors seem to be affected as well (Antkowiak and Helfrich-Forster 1998; Antkowiak 1999; Kreuzer, Schneider et al. 2008).

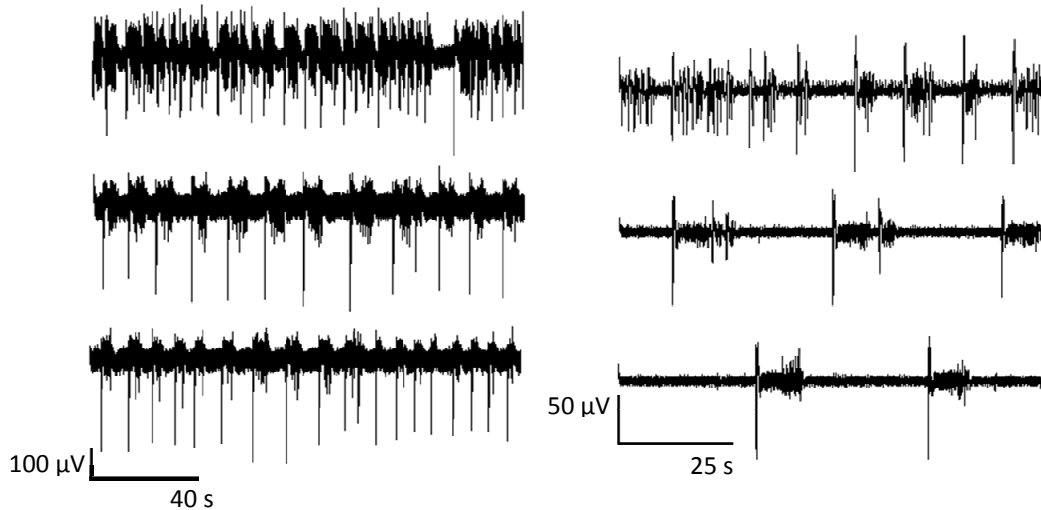


Figure 4.1: Anesthetic-induced changes in LFP observed from recordings used in this work; Left side (top down): Control, 0.2 μM , 0.4 μM propofol; Right side (top down): Control, 0.75 MAC, 1 MAC sevoflurane; The different spiking patterns for propofol and sevoflurane at control conditions (first row) may be due to the different age of the OTC. For the experiments with propofol older OTC were used (\rightarrow Section 5.1).

4.2 *In vivo cortical networks*

LFP recorded in a rat's somatosensory cortex *in vivo* from implanted multi-electrode arrays as described in section 5.2 show a clearly visible effect on the recorded waveforms. This effect is also based, as it is in the *in vitro* recordings, on depression of action potentials. Isoflurane, enflurane and halothane concentration dependently reduce firing rates of action potentials. In addition to reduced firing, the spiking activity pattern changed from tonic activity to burst-like patterns which are synchronized throughout the part of the cortex from which signals were recorded. The result of these burst- and synchronization-effects can be observed in a more regular LFP signal with higher amplitudes (Hentschke, Schwarz et al. 2005) and is exemplarily presented for isoflurane in Figure 4.2. If the derived spiking depressions caused by the three volatiles are compared to the *in vitro* results, similar effects can be observed for isoflurane and enflurane. This leads to the assumption that these two regimens mainly affect intrinsic neocortical targets. Halothane shows different action potential depression *in vitro* and *in vivo*. This could be explained by a halothane effect on extra-cortical areas that may partially control neocortical activity. The volatiles' effect on the GABA_A receptor seems to represent a key mechanism for the activity suppression, however, other receptors should also be considered (Hentschke, Schwarz et al. 2005).

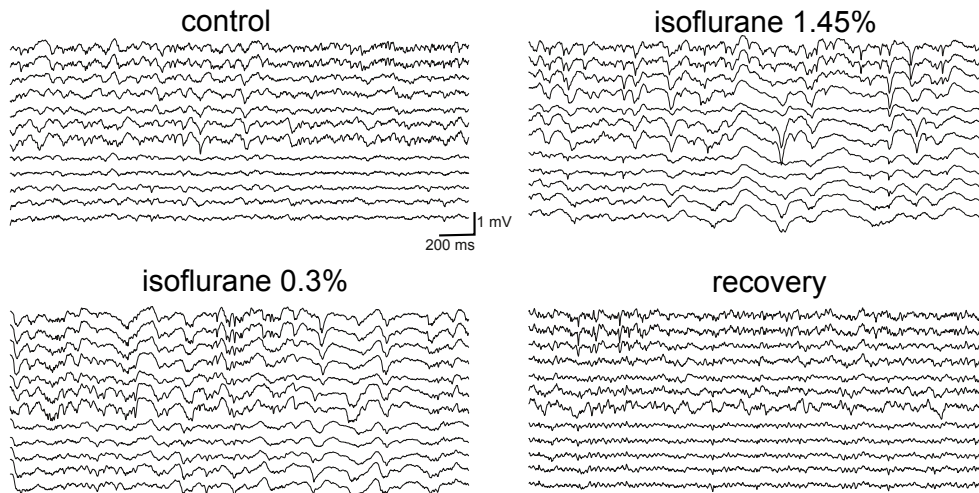


Figure 4.2: Exemplary raw LFP sequences of 2 s length recorded from a multi-electrode array located in the rat barrel cortex as described in section 5.2 and presented in the paper of Kreuzer et al. (Kreuzer, Hentschke et al. 2010) . The recorded signal was filtered between 0.5 and 200 Hz. The displayed traces were recorded in the same animal at control, at a sedating concentration and an anesthetic concentration of isoflurane and after recovery (Kreuzer, Hentschke et al. 2010). Note the similarity of the signals within each row (lines 1-7 and 9-14) and particularly between adjacent pairs of electrodes. Row two is placed approximately 300 μm deeper in the cortex than row one, possibly targeting another layer.

4.3 Hippocampal networks in vivo

In another set of experiments with wild type mice, propofol was delivered in hypnotic concentrations. LFP that are generated in the prefrontal cortex and in hippocampal areas were simultaneously recorded from multi-electrode arrays as described in section 5.3. The propofol induced waveform change in the prefrontal cortex is presented in Figure 4.3. With propofol the pattern becomes more sinus-like with dominating frequencies in the α -range. The regular patterns indicate high synchronization in these frequencies. With the naked eye propofol seems to cause similar effects as the volatiles mentioned above.

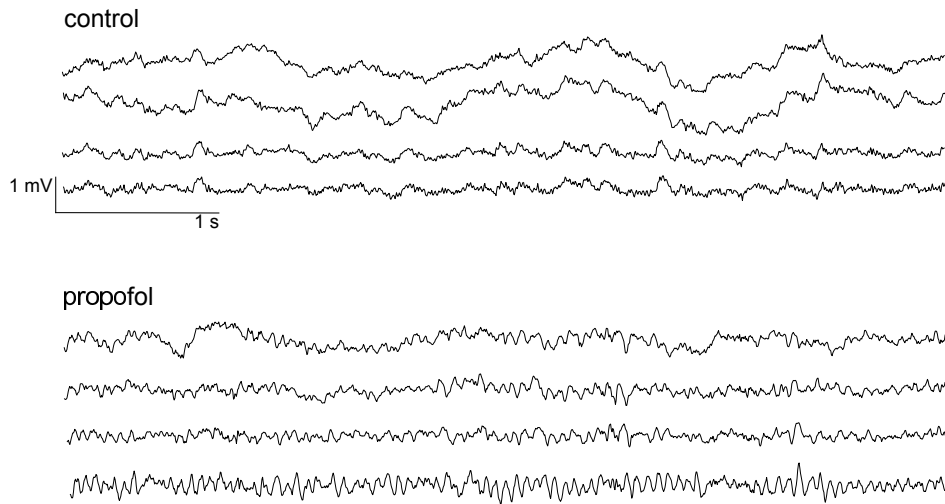


Figure 4.3: Excerpt from the recorded multi-channel LFP in mouse neocortex at control conditions and after a hypnotic dose of propofol. More regular oscillations in the α -range can be observed in the presence of propofol.

Hippocampal areas represent another major target for drug induced actions of general anesthetics. Actions of the anesthetic on neuronal activity in the hippocampus are associated with the alteration of mnemonic processes (Bland 1986). Figure 4.4 displays the modulation of hippocampal LFP when treated with hypnotic concentrations of propofol. Slow oscillations become more prominent resulting in increased signal amplitudes and the signal becomes more regular in general.

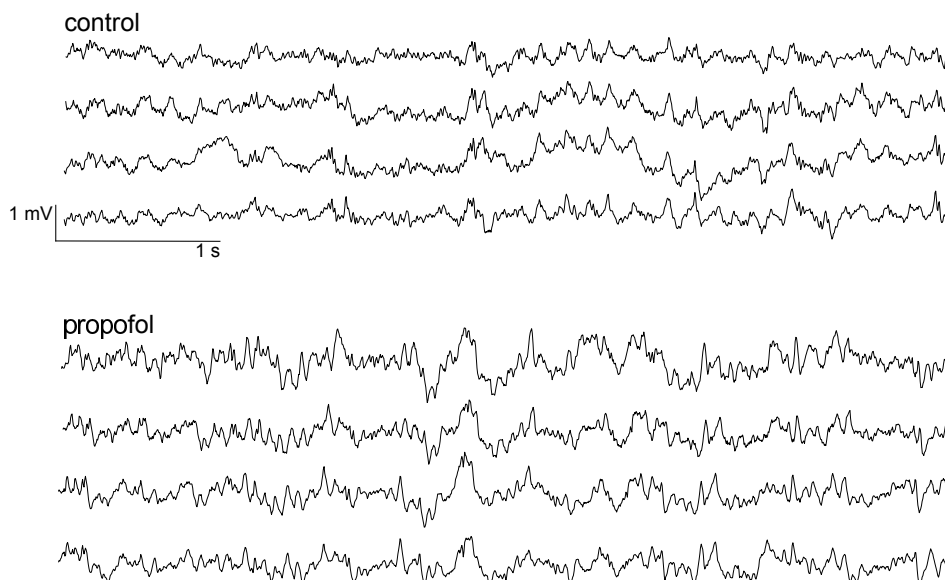


Figure 4.4: Excerpt from the recorded multi-channel LFP in mouse hippocampus at control conditions and after a hypnotic dose of propofol. Single rows display LFP traces obtained from the single recording electrodes. In the presence of propofol, dominating frequencies become slower and amplitudes increase. The signals seem to follow a more regular pattern.

Since anesthetic-induced changes can be observed within *in vitro* and *in vivo* networks the effect on EEG recordings should also be detectable by examining the waveforms at different concentration levels of the applied anesthetic.

4.4 Electroencephalogram

In healthy humans at a conscious state the EEG shows a mixture of dominating α - and β -frequencies. Additionally, γ -oscillations can be observed (Wilhelm, Bruhn et al. 2006; Schmidt, Müller et al. 2008). EEG-amplitudes are rather small and the signal appears rather stochastic. General anesthetics, in this work propofol and sevoflurane, visibly alter EEG characteristics. At sedating, subhypnotic concentrations of the delivered drug, α - and β -frequencies are activated (Gugino, Chabot et al. 2001; Wilhelm, Bruhn et al. 2006; Kortelainen, Koskinen et al. 2008). This phase is called paradoxical excitation since spectral parameters show a biphasic course indicating increased wakefulness during anesthesia induction (Kuizenga, Wierda et al. 2001). Deeper anesthesia causes a shift towards slower frequencies in the θ - and then in the δ -range (Wilhelm, Bruhn et al. 2006; Kortelainen, Koskinen et al. 2008; Schmidt, Müller et al. 2008). Amplitudes become higher and the signal seems to become more regular. At even higher concentrations of the drug, EEG is suppressed and only interrupted by short bursts with variable signal energy in the different frequency bands. Duration of the suppression sequences is drug specific and can last from seconds up to minutes. This waxing and waning pattern is called burst suppression (BS) (Rampil 1998). At maximum doses, these bursts disappear and a reversible total suppression occurs which is known as “cortical silence” (Wilhelm, Bruhn et al. 2006) and the waveform becomes quasi isoelectric. The depression of cortical activity represented by EEG waveform changes which are caused by GABAergic regimens can be triggered either by a direct cortical effect or by subcortical systems, e.g., brain stem and thalamus that potentiate arousal. Furthermore, the effect of GABAergic drugs on EEG may be as prominent, because a small number of GABAergic inhibitory interneurons controls a large amount of excitatory pyramidal cells. If the interneurons' inhibiting activity is potentiated by the anesthetic, large cortical areas could become deactivated (Brown, Lydic et al. 2010).

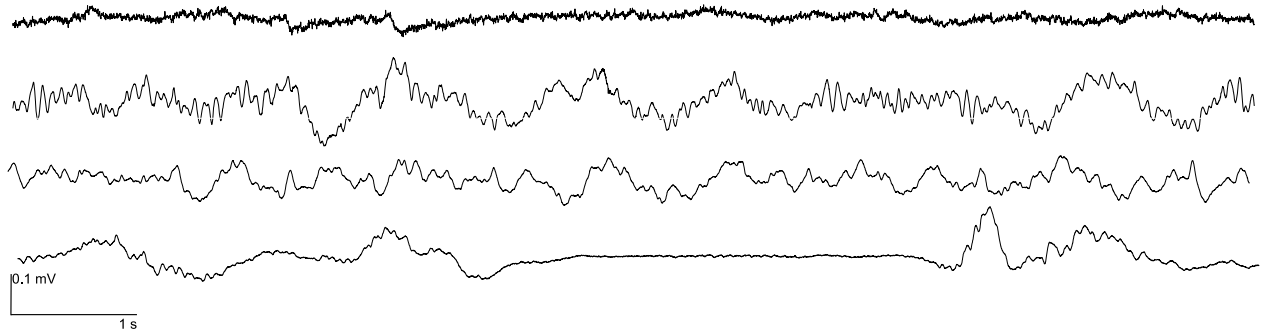


Figure 4.5: Anesthetic-induced changes in EEG patterns that were recorded from EEG-electrodes placed on the forehead. In a conscious subject EEG is characterized by high frequencies and low amplitudes (1st row). With increasing concentrations of the drug (2nd and 3rd row) the EEG becomes slower but of higher amplitude. At very high concentrations burst suppression represented by activity patterns interrupted by isoelectric sequences occurs (4th row).

5 Experimental setups

Data derived from different human and animal studies were analyzed within the framework of this thesis. All human studies were conducted after informed written consent and approval of the local ethics committee of the Technische Universität München, Munich, Germany. For the experiments including animals, all procedures were approved by the animal care committee (Eberhard Karls University, Tübingen, Germany) and were in accordance with the policy on the use of animals in neuroscience research of the Society for Neuroscience and German law. All efforts were made to minimize both the suffering and number of animals used. This section describes the experimental setups including drug protocols as well as data preprocessing used for LFP and EEG recording.

LFP was recorded from OTC *in vitro* as well as from multielectrode arrays placed in cortical and hippocampal areas *in vivo*. EEG data from three single-channel studies and one multi-channel study was used for the analytical experiments in this thesis. The single-channel steady state study and the multi-channel study were conducted with volunteers, whereas the transition studies were accomplished with patients.

5.1 Organotypic slice cultures

Extracellular LFP recordings from co-cultures of rat neocortex were recorded at the Section of Experimental Anesthesiology of the University of Tübingen, Germany. OTC represent an established model to evaluate effects *ex vivo* (Antkowiak and Helfrich-Forster 1998; Antkowiak 1999; Dai, Perouansky et al. 2009; Drexler, Hentschke et al. 2010). The used OTC represents an isolated cortical network lacking subcortical inputs. Anesthetic-induced effects that can be observed at this level can be considered as purely cortical.

5.1.1 Preparation of neocortical organotypic slice cultures

For preparation of OTC, 300 μm thick slices of neocortex (Area SI or SII), taken from wild type rats, were fixed on a glass cover slip with a coagulate of plasma and thrombin (Gahwiler 1981). They were transferred into plastic tubes (Nunc, Thermo Fisher Scientific Inc., Waltham, MA, USA) containing 750 μl of nutrition medium and incubated in a roller drum at 10 rev/h at 37°C. The medium consisted of 50% Eagle's basal medium, 25% Hank's balanced salt solution and 25% horse serum with a final concentration of 1 mM l-glutamine and 61 mM glucose (all reagents purchased from Gibco® (Life Technologies, Carlsbad, CA, USA)). The medium was changed twice a week and alternately supplemented with

antimitotics. Cultures were used after 9 to 35 days of incubation. LFP recordings were performed at 34 - 36°C under continuous perfusion with artificial cerebrospinal fluid (ACSF) consisting of NaCl (120 mM), KCl (3.3 mM), NaH₂PO₄ (1.13 mM), NaHCO₃ (26 mM), CaCl₂ (1.8 mM) and glucose (11 mM). ACSF was saturated with 95% oxygen and 5% carbon dioxide (O₂/CO₂ - saturated ACSF) (Antkowiak and Helfrich-Forster 1998). Sevoflurane or propofol were added in liquid form to the ACSF and applied via bath perfusion using syringe pumps (ZAK Medicine Technique, Marktheidenfeld, Germany), connected to the experimental chamber via Teflon tubing (Lee, Frankfurt, Germany). Recordings were carried out 10 minutes after changing the perfusate to ensure steady state conditions. This time interval has been proven to be sufficient for steady state conditions (Antkowiak 1999) as diffusion times in slice cultures are considerably shorter compared to acute slice preparations (Gredell, Turnquist et al. 2004; Benkwitz, Liao et al. 2007). Concentrations of sevoflurane are presented as MAC according to the MAC values proposed by Franks and Lieb (Franks and Lieb 1986). Based on this data a MAC equivalent of 0.35 mM was used for this study.

Extracellular LFP activity recordings were carried out with ACSF-filled glass electrodes with impedances of 3-5 MΩ and with the Axon Digidata 1200 analog-to-digital/digital-to-analog interface. Records were in addition stored on a Sony data recorder PC 204A (Racal Elektronik, Bergisch Gladbach, Germany) The extracellular recordings were low-pass filtered at 5 kHz, digitized at a sampling frequency $f_s = 10$ kHz, visualized and stored with the Axoscope software tool (Axon Instruments, Molecular Devices Corp., Chicago, IL, USA).

5.1.2 Anesthetic protocol and sequence selection

The age of the cell cultures ranged between 12 and 19 days for the sevoflurane and 14 to 35 days for the propofol experiments. Each cell culture was washed with sevoflurane at increasing concentrations, whereas two different washing routines were performed.

Routine one consisted of the concentration steps 0, 0.75, 1 and 1.5 MAC (group1, n=5) and the other routine was 0, 0.25 and 0.5 MAC (group2, n=7). In the propofol group three experiments with the routine 0, 0.2 μM and 0.4 μM propofol were performed. Duration of every LFP recording at equilibrated concentrations was 180 s. From each recording a total of three 2 s down-state episodes that were visually identified were extracted from the beginning the middle and the end of each recording using a self-programmed LabVIEW6i (National Instruments, Austin, TX, USA) routine. An exemplary selection of a down-state sequence is presented in Figure 5.1. Application of non-linear parameters was only performed on the down-states, because combined up- and down-state activity LFP activity is highly non-stationary (Masimore, Kakalios et al. 2004; Mehboob and Yin 2008). Further, only

anesthetic induced effects on up-state activity have been shown so far. Spontaneous action potential firing concentration dependently decreased with the delivery of volatile anesthetics and the duration of down-state episodes increased with the drug (Antkowiak and Helfrich-Forster 1998). Systematic investigations regarding anesthetic induced effects in these down-state episodes besides evaluating their duration have not been performed. The signal analytical approach used in this thesis may prove helpful to reveal effects in these unattended episodes. So far, cortical down-states have been considered neuronal silence (Cash, Halgren et al. 2009). No attempts were made to detect possible anesthetic-induced information changes in the signal in these episodes. This study tested the hypothesis that volatile anesthetics, rather than directly affecting neuronal up-states, reduce the probability that such persistent activity is induced by profound actions on phases of low neuronal activity, named down-states. Down-states are characterized not by absent, but by sparse and uncoordinated neuronal activity (Staley, Longacher et al. 1998) and make up the typical activity pattern that is present between two up-states as presented in Figure 5.1.

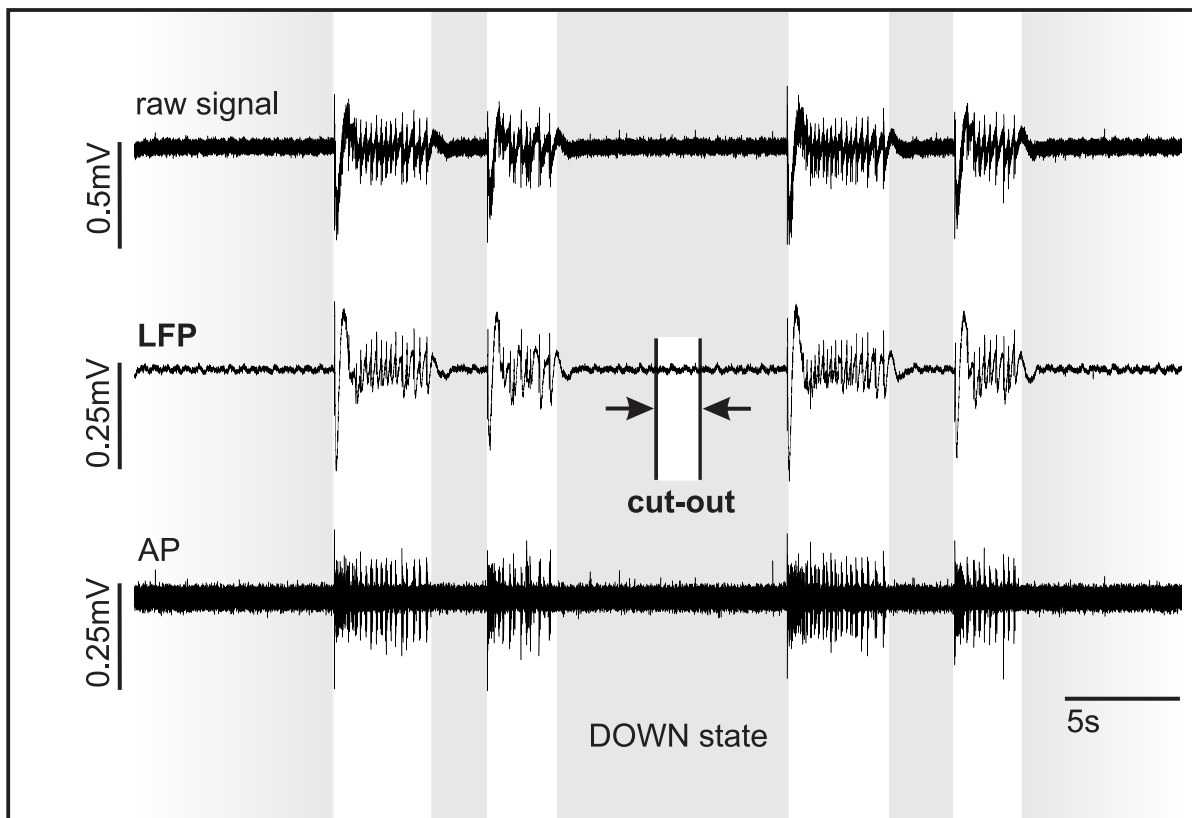


Figure 5.1: Extraction of a down-state episode from the *in vitro* recording. The recorded raw signal (1st row) was low-pass filtered to obtain the LFP trace (2nd row) or high-pass filtered to isolate action potentials (3rd row). Down-state sequences were extracted from the LFP trace. (Drexler, Kreuzer et al. 2013)

5.1.3 Data preprocessing and parameter settings

Power spectral density (*PSD*) was calculated over the entire 180 s of the recorded traces and over the extracted 2 s down-state episodes at each concentration level of sevoflurane or propofol. The non-linear parameters were calculated from the down-state sequences. Before conducting these analyses the signals were 0.5 to 100 Hz band-pass filtered applying a MATLAB (The MathWorks, Natick, MA, USA) based Butterworth filtering routine and down sampled to $f_s = 500$ Hz. The parameters *ApEn*, *PeEn* and order recurrence rate (*ORR*) were calculated for every selected data segment, i.e., over 1000 data points, at each anesthetic concentration level. A detailed description of the parameters is given in section 6.

5.1.4 Setting to compare LFP against noise and blocked neuronal activity

In order to ensure that the down-state recordings differ from noise, fifteen noise-sequences with a sample frequency of $f_s = 500$ Hz were generated using the LabVIEW “Uniform White Noise” module. The “white noise approach” was chosen to compare the recorded neuronal activity that is considered different from a equally distributed power spectrum to such a frequency distribution. Further, 15 pink noise ($1/f$ -noise) sequences were generated using MATLAB. Pink noise may be better suited to reflect a physiological signal because of its $1/f$ -frequency distribution). The pink noise sequences also had a $f_s = 500$ Hz. Noise amplitude was adjusted to the amplitude range of the LFP down-state recordings. The sequences consisting of 1000 data points were equally filtered to the 0.5 to 100 Hz range as the LFP sequences. *ApEn* and *ORR* were calculated for the sequences.

Additional experiments with a drug cocktail that blocked almost all cellular activity (n=7) and recordings without cell cultures, in the ACSF filled recording chamber (n=7) were performed in order to ensure that the analyzed signal information in the recordings did not belong to non-cellular processes. Again, three 2 s episodes were extracted from the recording. Sampling rate was $f_s = 500$ Hz and the frequency range was again 0.5 to 100 Hz. *PSD* and *ApEn* were calculated to determine differences between the recordings without cells, the recordings with cells, but blocked neuronal activity and the recordings of normal neuronal activity.

5.1.5 Setting to evaluate the GABAergic effect of sevoflurane

In an additional series of experiment 100 μM bicuculline was applied to the OTC ($n=5$, age of the cultures: 9 days) before they were washed with 0.75 MAC sevoflurane analog to the procedure described in section 5.1.2. Bicuculline is a GABA_A antagonist and the used dose of 100 μM is sufficient to block the GABA_A receptor, i.e., the sevoflurane-induced effects that were detected in the presence of bicuculline are based on non-GABAergic effects. Again, from the 5 LFP recordings three down-state sequences of 2 s length were extracted and analyzed. As in the other in vitro experiments $f_s = 500$ Hz and the frequency range was from 0.5-100 Hz. *PSD*, *ApEn* and *ORR* were calculated in order to evaluate the influence of bicuculline, i.e., the lack of the GABAergic effect.

5.2 Cortical in vivo experiments with volatile anesthetics

The experimental procedures were identical to those described in Hentschke et al. (Hentschke, Schwarz et al. 2005) and the field potential data analyzed here were taken from three of the four animals of the study described in their article. In contrast to the *in vitro* experiments the described *in vivo* network represents activity from a larger amount of cortical neurons and subcortical inputs are not absent. Hence, these *in vivo* recordings can possibly be explained as a halfway house between the *in vitro* LFP obtained from OTC and the human EEG recordings. Opposed to anesthetic EEG effects, it is less clear at present in which manner anesthetics impair information processing on this much smaller spatial scale. In local cortical networks, sub-networks defined by strong excitatory connections exist which may operate quite independently of each other (Song, Sjöström et al. 2005; Kampa, Letzkus et al. 2006). With anesthetics, their independence of operation may be compromised by a general decrease of cortical neuronal excitability (Simons, Carvell et al. 1992; Erchova, Lebedev et al. 2002; Hentschke, Schwarz et al. 2005; Berger, Borgdorff et al. 2007; Sleight, Vizuite et al. 2009). Moreover, inhibitory interneurons project locally and have a great potential to pace their postsynaptic targets (Blatow, Rozov et al. 2003; Hasenstaub, Shu et al. 2005). Under conditions of pharmacologically enhanced GABAergic transmission, they may coerce independent sub-networks into more synchronous, uniform activity patterns (Jurd, Arras et al. 2005; Verbny, Merriam et al. 2005). In section 9 results of an investigation on the degree of how anesthetics alter signal independence in the somatosensory ('barrel') cortex of the rat are presented. LFP activity was recorded from multiple, closely spaced electrodes, which sample from a much smaller subset of neurons than EEG electrodes (Creutzfeldt,

Fuster et al. 1964; Katzner, Nauhaus et al. 2009). The effects of volatile anesthetics isoflurane, enflurane and halothane were evaluated in three animals.

5.2.1 Electrode implantation and LFP recording from rat neocortex

Briefly, male or female Sprague-Dawley rats aged 12-16 weeks were anesthetized with ketamine/xylazine (100 mg/kg and 15 mg/kg, respectively). A craniectomy over the right hemisphere was made, the dura was removed and a steel ring with 5 mm outer diameter was placed on the pial surface. 4-16 custom-made etched tungsten microelectrodes (impedance 1-5 M Ω , tip separation \sim 180 μ m) arranged as single or double linear arrays (one animal, 1x4; two animals, 2x8) were implanted through the steel ring into the neocortical somatosensory representation of the mystacial vibrissae (“barrel cortex”). The array was oriented at an angle of 30-40° relative to the cortical surface so that the medial electrode row touched the cortical surface first and thus was located in a deeper cortical lamina than the lateral electrode row. The latter was aimed at the border of layers IV and V (depth of penetration for this row from the point of contact with the pia was approximately 1100 μ m). Proper location of the electrodes within barrel cortex as shown in Figure 5.2 was verified by mapping of neuronal responses elicited by manual deflection of individual vibrissae.

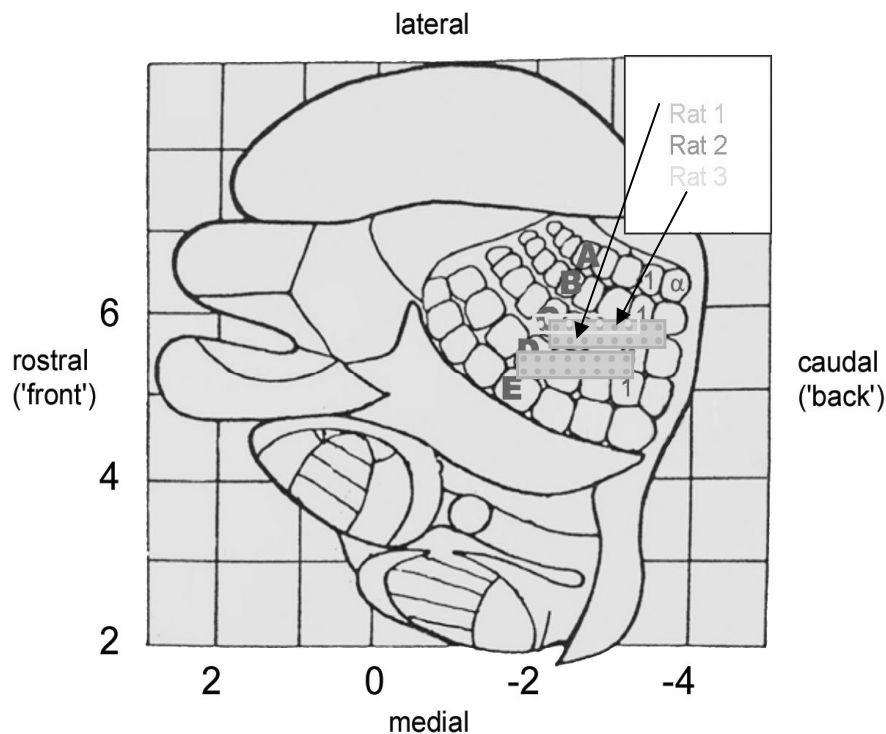


Figure 5.2: Positions of the multi-electrode arrays in the somatosensory (“barrel”) cortex of the rats. (Hentschke, Schwarz et al. 2005; Kreuzer, Hentschke et al. 2010)

The electrode array and a head post were then fixed with dental cement and via 7-9 stainless steel screws driven into the skull. Recordings commenced after a recovery period of 2-4 days. The animals were head-restrained and placed in a sealable Plexiglas box into which vaporizers (Drägerwerke, Lübeck, Germany) driven by air pumps delivered the anesthetics. The volatile's concentration in the box was monitored with an anesthetic gas monitor (Hewlett-Packard M1025A, Hewlett-Packard, Palo Alto, CA, USA). For any given concentration, animals were exposed for periods of 27-39 min to the anesthetic. After discontinuation of the anesthetic, the animals were exposed to air for 40-60 min. A maximum of one recording session was performed per day. Voltage traces recorded from the electrodes with a multi-channel extracellular recording system (Multi Channel Systems, Reutlingen, Germany) were referenced to the steel ring (rat1 and rat2) or to one of the electrodes (rat3), amplified and then passed through a band pass filter (-3 dB pass band 0.5-200 Hz), digitized at $f_s = 20$ kHz and stored with a multi-channel extracellular recording system (Multi Channel Systems, Reutlingen, Germany). They were down sampled to 500 Hz prior to analysis. Deteriorated, low-impedance electrodes characterized by small signal amplitudes were excluded from analysis. The number of useable electrodes was 3 (rat3), 6 (rat2) and 12 (rat1). Anesthetic concentration is expressed in volume-% or as MAC as given in the article of Mazze et al. (Mazze, Rice et al. 1985). They determined the MAC of isoflurane at 1.46%, the MAC of enflurane at 2.21%, and the MAC of halothane at 1.03%.

5.2.2 Selection of LFP data segments

Under control conditions, LFP contained episodes of oscillatory activity with a dominant peak at 8-9 Hz (θ -component) and an additional (non-harmonic) peak at 13-16 Hz (β -component) (an example is given in Figure 9.8 A). The nature of these oscillations, also termed 'high voltage rhythmic spikes' (HVRS), is a matter of debate. They appear in resting animals, often in conjunction with low-amplitude whisker movements (Semba and Komisaruk 1984) (whisker 'twitching') and may reflect a specific kind of idling, responsive state of the whisker sensory system (Kaplan 1985; Nicolelis and Fanselow 2002; Wiest and Nicolelis 2003). Others consider HVRS manifestations of absence epilepsies (Meeren, Pijn et al. 2002; Shaw 2004; Polack and Charpier 2006). It could be observed that at hypnotic to sub-anesthetic concentrations (isoflurane, 0.3-0.7%; enflurane, 0.5-1.2%; halothane, 0.65-1.05%) the oscillations changed appearance in several ways. Most notably, they were less coherent across channels and lasted for shorter periods. Furthermore, the dominant frequency was between 13 and 16 Hz. At the highest concentrations, which were equal to or above MAC (isoflurane, 1.45%; enflurane, 2.4%; halothane, 1.6%) the oscillations subsided and low-

frequency components and/or burst suppression patterns dominated. Data that contained HVRS was excluded from analysis due to the unresolved nature of this activity and because the computational load of the applied analyses restricted the amount of data that could be analyzed in reasonable time to about 10 seconds per recording. To this end, the data acquired under control conditions were divided into segments of 2048 points overlapping by 730 points. From these, the spectral power of the signals in the range 7-9 Hz was computed for all channels. Of the resulting segment-wise power values, the 75th and 90th percentile were determined for each channel. Segments with a power greater than the 90th percentile on any of the recorded channels and/or with a power larger than the 75th percentile on half or more of all recorded channels were rejected. The procedure was repeated for recordings with anesthetics, but with power determined in the range 10-16 Hz. Finally, within each recording, groups of four consecutive (overlapping) intervals which satisfied the criteria above were combined to yield segments of 60002 points length, corresponding to ~3 s. Three of such segments per recording, picked randomly from the beginning, middle and end of each recording were subjected to the subsequent analysis.

5.2.3 Data preprocessing and parameter settings

As in the *in vitro* experiments *PSD* and univariate *ApEn*, *PeEn* and *ORR* were calculated for every selected data segment from each electrode at each anesthetic concentration level. Advantage of the multi-electrode recording layout was taken to gather information regarding spatiotemporal processes within these small cortical networks. Pearson's correlation was utilized as "established" measure to compare two signals and in a next step *XApEn* was calculated over all channel combinations to reveal changes in inter-channel dissimilarity caused by the volatiles. Prior to the analyses, the selected LFP sequences were down-sampled to $f_s = 500$ Hz as mentioned. The frequency range was from 0.5 to 200 Hz. The calculations were conducted over the 3 s LFP episodes consisting of 1500 data points.

5.3 Cortico-hippocampal experiments with propofol

The setting is similar to the ones described by Dr Butovas, the conductor of the experiments described below, in his 2010 paper (Butovas, Rudolph et al. 2010).

Generally, the hippocampus and neocortical areas represent sensitive targets for anesthetic drugs (Rudolph and Antkowiak 2004; Heinke and Koelsch 2005). Analysis of the data showed that LFP-oscillations in the θ - and α -range of around 5-15 Hz are affected by propofol. The drug causes a widely described shift towards a lower peak frequency in the

Fourier spectrum (Perouansky, Rau et al. 2010). Synchronized oscillations in this frequency seem to represent a key mechanism for structuring interactions between neuronal networks in different cerebral regions. Inside the hippocampus these θ -oscillations are responsible for mnemonic tasks whereas in the neocortex, θ -oscillations seem to trigger working tasks. In general, the cortical-hippocampal system seems responsible for memory consolidation (Butovas, Rudolph et al. 2010).

5.3.1 LFP recordings from neocortical and hippocampal areas

Surgical procedures to implant the electrode arrays were similar to those described in section 5.2.1. Each mouse had two custom made linear arrays of four microelectrodes implanted. The used electrodes were made of an alloy of iridium and platinum with a glass coating (shank diameter: 80 μm ; diameter of the metal core: 23 μm , free tip length: 10 μm and impedance: $> 1 \text{ M}\Omega$; Thomas Recording, Giessen, Germany) the array frame was made of polyimide (HV Technologies, Trenton, GA, USA). The electrodes were connected to Teflon-insulated silver wires (Science Products, Hofheim, Germany) that were connected to a microplug (Bürklin, Munich, Germany). The data was recorded with the same setup described in section 5.2.1. The first array was implanted in the prefrontal cortex 200 μm below the pia, presumably recording activity from layer II. The second array was inserted through the somatosensory cortex at 900 μm below the pia, targeting the hippocampus (Butovas, Rudolph et al. 2010). Propofol was delivered in hypnotic doses (30 mg/kg) and during control conditions and at a steady state propofol level, LFP was recorded with sampling rate $f_s = 20 \text{ kHz}$, a bandwidth of 0.5 to 200 Hz and a gain of 5000. In total, nine experiments from four animals were analyzed. Therefore, the LFP were filtered to frequency bands corresponding to the selection made in Dr. Butovas' paper (Butovas, Rudolph et al. 2010) and the classical θ -, α - and β - frequency bands. An artifact-free 5 s LFP sequence was visually identified and extracted from the recordings at control conditions and under propofol.

5.3.2 Data preprocessing and parameter settings

Before the analyses were performed, the recorded LFP sequences derived from neocortical and hippocampal regions were low-pass (band-pass) filtered to (i) 100 Hz, (ii) θ : 4-8 Hz, (iii) α : 8-12 Hz and (iv) β : 12-24 Hz and down sampled to 250 Hz or 50 Hz using a MATLAB based filtering routine. Hence the parameters were applied on LFP episodes of 1250, respectively 250 data points. In order to get a more specific insight in the mechanisms triggered by propofol, the θ -band used for hippocampal analysis that ranges from

approximately 2-15 Hz -different publications define different θ -ranges- was defined in this thesis as α - and θ -band, according to the classical EEG frequency bands described in section 2.3.1. *PSD* was calculated from the 100 Hz low pass filtered data. Further *XApEn*, *BPeEn* and *STE* were calculated for all channel combinations within one region (prefrontal cortex or hippocampus) and for all channel combinations between prefrontal cortex and hippocampus from the different frequency bands.

5.4 Single-channel steady state study

5.4.1 Selection of volunteers and anesthetic protocol

After ethics committee approval, 15 adult male test subjects with an American Society of Anesthesiologists physical (ASA) status of I, i.e., healthy volunteers, gave written, informed consent and were recruited to the study. No premedication was used. Exclusion criteria from the study were contraindications to one of the study drugs, a history of psychiatric or neurologic disease, drug abuse or medication known to affect the central nervous system, indication for rapid sequence induction or impairment of the auditory system. All subjects were given both, sevoflurane and propofol mono anesthesia in randomized order in two consecutive sessions following a non-blinded crossover design. EEG from the test person was recorded at five different anesthetic concentrations of sevoflurane (Horn, Pilge et al. 2009) [awake, loss of LOC, inter1, inter2 and BS (Rampil 1998)]. The course of the study is shown in Figure 5.3.

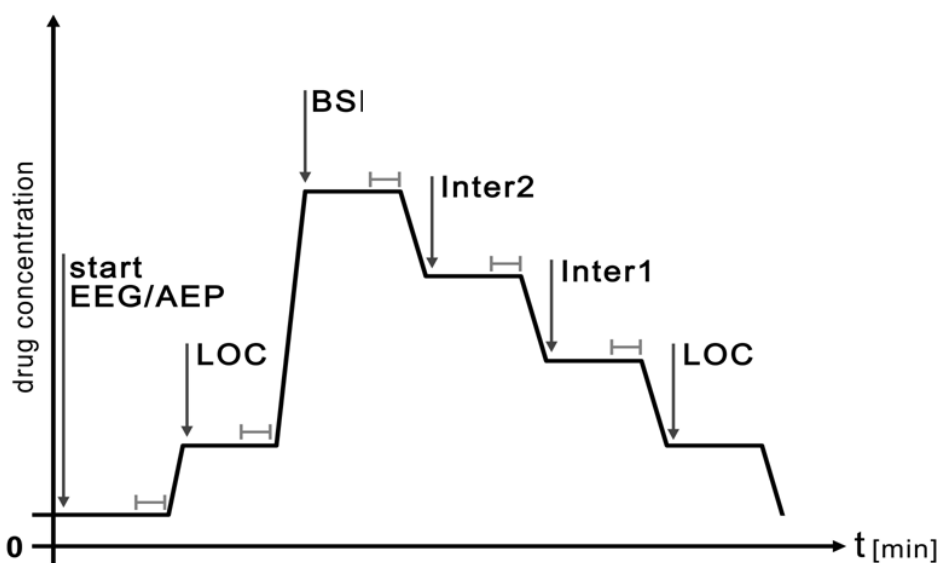


Figure 5.3: Course of the anesthetic concentration vs. time in the EEG recording protocol. Arrows indicate the starting point of the steady concentration level. Horizontal bars mark the time of EEG recording. (Jordan 2010)

Standard monitoring parameters were continuously measured with a Datex AS/3 compact monitor (GE Healthcare, Helsinki, Finland). A two-channel EEG was recorded with a specifically designed device (Jordan, Weller et al. 1995) at positions AT1, M2, Fz (reference), Fpz (ground) according to the international 10-20 system using ZipPrep electrodes (Aspect Medical Systems, Natick, MA, USA). Electrode impedances were always below 5 k Ω and the signal was filtered with a 0.5 to 400 Hz band pass followed by a digitization of the signal with $f_s = 1$ kHz. The EEG data was also analyzed after an additional 30 Hz low-pass filtering using LabVIEW6i in order to eliminate EMG and other high frequency artifacts. EEG in the frequency range above 30 Hz is subject to be superposed by EMG distortions (Bonhomme and Hans 2007). Propofol was applied via a TCI pump (openTCI, Space infusion pump, BBraun Medical, Melsungen, Germany) and for sevoflurane a standard vaporizer was used. Anesthesia was slowly induced (TCI: 0.1 $\mu\text{g/ml}$ effect concentration; vaporizer: 0.1 Vol%) in a stepwise manner until the volunteers did no longer respond to the “squeeze my hand” command (LOC). Anesthetic concentrations were increased until EEG showed BS. The individually determined anesthetic concentrations to induce level “inter2” and subsequently “inter1” were administered. A part of the conducted analyses was also included in Dr. Jordan’s thesis (Jordan 2010).

5.4.2 Data preprocessing and parameter settings

At each concentration level, EEG was recorded for 15 minutes as outlined in Figure 5.3. From these recordings a 120 s sequence was extracted and utilized for further analysis. For conducting the analyses, either the unfiltered signals were used or the signals were 30 Hz low pass filtered and down-sampled to 200 Hz, i.e. the analyzed episodes consisted of 120000 or 24000 data points. Additional analyses were also performed in the classical δ -, θ -, α -, β -, and γ -frequency bands. *PSD* was calculated up to 50 Hz in order to determine anesthetic-induced changes in the EEG power spectrum. Propofol and sevoflurane effects on EEG complexity were evaluated with *ApEn*, *PeEn* and *ORR*.

5.5 Single-channel transition studies

In order to gain insights in electrophysiological processes, the states transitions from wakefulness to unconsciousness and vice versa are of great importance. The analysis of electrophysiological recordings allows a high time resolution and may be superior to imaging approaches that show only weak time resolution for detecting anesthetic-induced

effects during these transitions. Therefore state transitions with propofol were analyzed. During the course of general anesthesia with propofol, LOC occurs at higher propofol concentrations when compared to the return of consciousness (ROC) (Gugino, Chabot et al. 2001; Nunes, Ferreira et al. 2009). This phenomenon indicates a drug hysteresis and might lead to the assumption that the patients' state is not equal at LOC and ROC. Hence, differences in the EEG characteristics at LOC and ROC may be observed. Evaluating EEG activity to assess the patients hypnotic state gains more and more popularity. Commercially available monitors like the bispectral index (BIS, Aspect Medical Systems, Natick, MA, USA) or state and response entropy from the EntropyTM Module (Datex Ohmeda, Helsinki, Finland) apply spectral analysis methods on EEG recorded from the forehead to evaluate the patients anesthetic state (Rampil 1998; Viertio-Oja, Maja et al. 2004). These EEG monitors seem to be unreliable in detecting the correct time of transition between conscious and unconscious states (Schneider, Kochs et al. 2004; Schneider, Hollweck et al. 2005; Pilge, Blum et al. 2011). A main reason may be due to the time delay of these monitors to represent the actual level of anesthesia (Pilge, Zanner et al. 2006; Zanner, Pilge et al. 2009; Kreuzer, Zanner et al. 2012). The time delays mainly originate from the length of analysis windows and additionally applied smoothing algorithms to stabilize the course of the index. Another issue may be the phenomenon of EEG activation in α - and β -frequencies during LOC. Spectral indices and *ApEn* (Figure 11.3) may indicate increased wakefulness instead of sedation during this transition phase. Since these methods are not able to reliably detect the transitions in time other measures are required to evaluate EEG changes during LOC and ROC. *PeEn* may analyze other signal properties of EEG and does not follow the course of paradoxical excitation during LOC. Hence we concentrated on *PeEn* performance in this section. *PeEn* is capable of reliably separating conscious from unconscious EEG (Jordan, Stockmanns et al. 2008; Olofsen, Sleight et al. 2008; Jordan 2010). Therefore propofol-induced effects at LOC and ROC in the classical EEG frequency bands were analyzed with *SR*, an established parameter for evaluation of the paradoxical excitation, and *PeEn*. The analysis was based on frontal EEG data derived from 35 patients during the two patient studies described below. Effect site concentration (C_{eff}) at the LOC/ROC transition was assessed using a PK/PD Schnider model (Schnider, Minto et al. 1999).

5.5.1 Selection of patients and anesthetic protocol

The data derived from the transition studies were used to evaluate propofol effect during LOC and ROC. These studies were conducted to analyze the performance of depth of anesthesia monitors, i.e., the patient state index (Physiometrix Inc., North Billerica, MA,

USA) and BIS (PSI study) (Schneider, Gelb et al. 2003) or BIS and acoustic evoked potentials (AEP study) (Schneider, Hollweck et al. 2005). In the PSI study, $f_s = 256$ Hz and only a 0.25 Hz high pass was used on the software side. The adequate low pass filtering was hardware-based. In the AEP study the signal was filtered from 0.5 to 400 Hz and $f_s = 1$ kHz was used. The test subject collective consisted of patients with ASA status I and II, i.e., healthy patients or patients with mild systemic disease. There were no significant differences of the patients' demographic data between the different drug groups. Nevertheless, only the EEG recordings of patients receiving propofol were used for analysis within the framework of this thesis. A special feature of the studies' design was a short period of simulated intraoperative awareness. Propofol delivery was discontinued after the first LOC which was also detected by asking the patient to squeeze the investigators hand. After intubation propofol delivery was discontinued until the patient started to repeatedly react on the "squeeze hand" command. This event was defined as ROC1. Then propofol was turned on again and the second loss of consciousness was annotated. After finishing surgical procedure anesthesia was emerged and the patients first squeeze of hand was defined ROC2. Propofol was injected with a first dose of 0.7 mg/kg, followed by doses of 20 mg every 30 s. For analysis only the first LOC and the second ROC were taken, for the time between ROC1 and LOC2 was often quite short, hence, influencing possible time relevant effects in EEG.

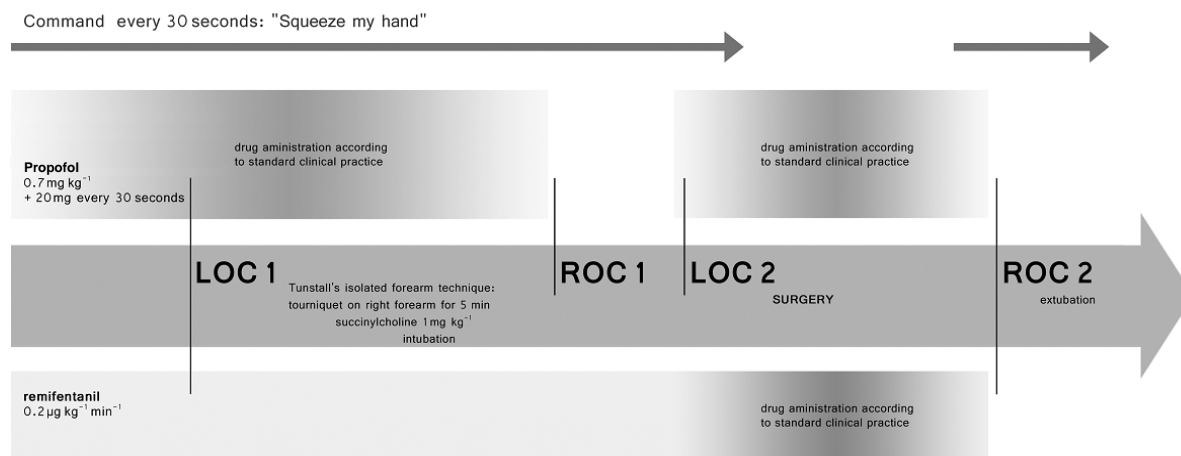


Figure 5.4: Study design with simulated intraoperative awareness. The figure was taken from (Pilge, Blum et al. 2011) and modified.

5.5.2 Data preprocessing and parameter settings

A ten minute EEG sequence ranging from 300 s before, until 300 s after the transition event was extracted from the recordings and processed for further analysis. All extracted

segments were band-pass filtered to following classical EEG frequency ranges: (i) δ (0.5-4 Hz), (ii) θ (4-8 Hz), (iii) α (8-12 Hz), (iv) β (12-24 Hz), (v) γ (24-47 Hz). Filtering was performed using a MATLAB based Butterworth forward backward zero phase band-pass routine. In a next step the 1 kHz recordings (AEP study) were down-sampled to 100 Hz, the 256 Hz recordings (PSI study) to 128 Hz. *SR* and *PeEn* were calculated over non-overlapping 4 s (400 / 512 data points) EEG sequences using LabVIEW6i. A possible paradoxical biphasic excitation effect was evaluated by comparing normalized *PeEn* and *SR* values in the α - and β -band obtained 60 s before LOC with values (i) 8 s, (ii) 60 s and (iii) 92 s after LOC. In order to detect a possible temporal hysteresis between the different frequency bands the point of intersection of *PeEn* during LOC and ROC in the θ - to γ -frequency band was determined for each patient. The time points of intersection in the frequency bands were compared by using a two-sample Wilcoxon test with Bonferroni correction (threshold $p < 0.05$ corrected). In a further step, each parameter time course was normalized by division through their mean and additional analyses were conducted. For the analysis of possible hysteresis effects in the different frequency bands the data sets corresponding to one time point in the LOC and ROC transition were tested using a Wilcoxon two-sample test performed with MATLAB. For instance, all *PeEn* values from the -8 s to -4 s segments before LOC in the α -band were tested against all *PeEn* values from 4 s to 8 s after LOC in the α -band. This procedure delivers information after what time *PeEn* is able to significantly distinguish consciousness from unconsciousness in the frequency bands at the state transition.

5.6 Multi-channel-study

Neuronal synchrony might be associated with the neural correlate of consciousness. There is evidence for a relation between synchronous oscillatory activity in β - and γ - frequencies and cognitive functions (Uhlhaas, Pipa et al. 2009). In EEG recordings, synchrony in different frequencies seems to conduct different perceptual tasks. α -activity (8-12 Hz) is assumed to play a role in mental processing and attentional demands while β -frequencies (12-24 Hz) reflect emotional and cognitive processes (Ray and Cole 1985). In particular, the β -band seems to be responsible for establishing long-distance synchrony of cortico-cortical regions (von Stein, Rappelsberger et al. 1999; Varela, Lachaux et al. 2001). There is wide acceptance in analyzing anesthetic-induced changes in EEG with non-linear parameters such as *ApEn* and *PeEn* (Bruhn, Ropcke et al. 2000; Jordan, Stockmanns et al. 2008; Jordan 2010). These parameters are single-channel measures and determine temporal changes in

EEG caused by anesthetic regimen. As next step, multi-channel EEG was used to perform bivariate analyses, i.e., to evaluate spatiotemporal EEG properties. Therefore, as first approach, to evaluate whether additional spatial information contributes to better performance in distinguishing consciousness and unconsciousness, the β -band was chosen as a frequency range because it was identified as being responsible for long-range cortico-cortical communication and hence should be most sensitive for spatial effects. Anesthetic-induced effects in β -synchrony were evaluated using *XApEn*. Therefore, EEG was recorded from 29 electrodes spread over the scalp. At levels “awake” and “unconscious” a 60 s EEG sequence was recorded from each electrode.

5.6.1 Selection of patients and anesthetic protocol

After approval of the ethics committee and informed written consent, 15 healthy male volunteers (aged between 21 and 32 years) were enrolled into the study. Standard monitoring parameters were measured with a Datex AS/3 compact anesthesia monitor. In addition, EEG was collected using a 32-channel electrode cap according to the 10-20-system (Easy-Cap, Brain Products, Gilching, Germany) with $f_s = 5$ kHz sampling rate (BrainVision Recorder, Brain Products, Gilching, Germany). Recordings from 29 channels were used for analysis. After 15 minutes baseline EEG, propofol was infused until LOC using a target controlled infusion pump. LOC was determined as missing reaction to a command to squeeze the investigators hand as mentioned before in section 5.5.1. At this level, propofol infusion was continued for 15 minutes. Basic artifact rejection, average reference and independent component analysis for blind source separation of non-cortical signal components were computed using BrainVision Analyzer 1 (Brain Products, Gilching, Germany).

5.6.2 Data preprocessing and parameter settings

From each channel 60 s EEG sequences were extracted at equilibrated anesthetic levels and used for analysis after adequate band-pass filtering to the classical frequency bands and down-sampling to $f_s = 200$ Hz. Hence, analyses were performed with EEG episodes consisting of 12000 data points. The frequency bands were (i) δ : 0.5-4 Hz, (ii) θ : 4-8 Hz, (iii) α : 8-12 Hz, (iv) β : 12-24 Hz and (v) γ : 25-47 Hz. Filtering and down sampling to 25, 50 or 100 Hz, depending on the analyzed frequency range was performed with MATLAB routines. For all channels, *ApEn* and for all channel combinations *XApEn*, *BPeEn* and *sTE* were calculated.

6 Analysis methods of cortical activity

In the presented experimental setups brain electrical activity is recorded from neuronal networks of different size. The approach of evaluating activity in these networks is the same at all levels. An electrode records the sum electrical activity of a certain amount of neurons, i.e., potential changes in the neuronal network that are generated by coordinated activity of the neurons. The recorded signal contains the potential changes in the network over time.

Generally, brain electrical activity is generated by the interplay of excitatory and inhibitory elements. For EEG and LFP generation excitatory pyramidal cells and inhibitory interneurons are the contributors. In general, the underlying network the recorded activity originates from is a dynamical system (Izhikevich 2007). Spontaneous or evoked stimuli can act as input into this neuronal system. These inputs are processed by the dynamic of this system and lead to a system output that is recorded by the electrodes. If the system's dynamic can be described by a set of linear differential equations, the system is called linear. Generally, a system is the mathematical model of how an initial input state leads to another state over time.

This means that the mathematical model or transformation operator $\bar{T}\{\dots\}$ generates an time-continuous output signal $y(t)$ based on an time-continuous input signal $x(t)$.

Generally systems can be either static or dynamic. In a static system the output $y(t)$ does only depend on the input $x(t)$ the point in time t . Hence it can be described as:

$$y(t) = \bar{T}\{x(t)\} \quad (6.1)$$

In short, for static linear systems the principle of superposition is valid as presented in Figure 6.1.

A system $y(t) = \bar{T}\{x(t)\}$ with two input signals $x_1(t)$ and $x_2(t)$ that run through a transformation operator $\bar{T}\{\dots\}$ and lead to the output signal $y(t)$ can be considered linear if the principle of superposition is valid, i.e., if

$$\bar{T}\{ax_1(t) + bx_2(t)\} = a\bar{T}\{x_1(t)\} + b\bar{T}\{x_2(t)\} \quad (6.2)$$

That means, if two inputs are summed and then fed into the linear system, the output is equal as if the inputs are fed into the system individually and their outputs are added. Examples for linear operators are integrators or differentiators.

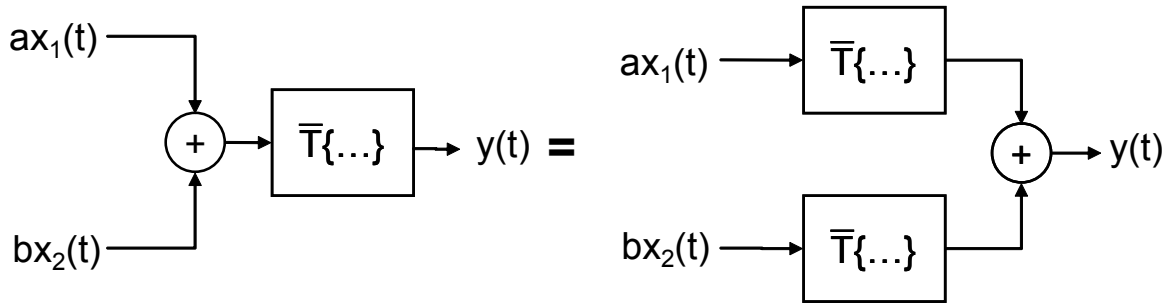


Figure 6.1: A system can be considered linear if the sum of inputs sequences that is transformed leads to the same output signal as the sum of transformed input signals. It does not matter, if signals $ax_1(t)$ and $bx_2(t)$ are added before or after the transformation operation. The resulting output $y(t)$ will be equal.

If this it not the case and the output of the system is not directly proportional to the output the system is non-linear.

Example:

Given are two continuous input signals $x_1(t) = 2t$ and $x_2(t) = t^2$

An example for a linear system is a system with a differentiator as transformer, i.e.,

$$y(t) = \bar{T}\{x(t)\} = x(t)'$$

1. As summed input:

$$y(t) = \bar{T}\{ax_1(t) + bx_2(t)\} = (a(2t) + bt^2)' = 2a + 2t$$

2. As individual inputs fed into a differentiator each and added afterwards

$$y(t) = a\bar{T}\{x_1(t)\} + b\bar{T}\{x_2(t)\} = (a(2t))' + (bt^2)' = 2a + 2t$$

This means that the equality criterion holds and the system is linear

$$\bar{T}\{ax_1(t) + bx_2(t)\} = a\bar{T}\{x_1(t)\} + b\bar{T}\{x_2(t)\}$$

Non-linear: Both inputs are fed to a transformer, squaring block, i.e.,

$$y(t) = \bar{T}\{x(t)\} = x(t)^2 :$$

1. As summed input:

$$y(t) = \bar{T}\{ax_1(t) + bx_2(t)\} = (a(2t) + bt^2)^2 = 4t^2 + 4t^3 + t^4$$

2. As individual inputs fed into a differentiator each and added afterwards

$$y(t) = a\bar{T}\{x_1(t)\} + b\bar{T}\{x_2(t)\} = (a(2t))^2 + (bt^2)^2 = 4t^2 + t^4$$

Here the linearity equality criterion does not hold and the system is non-linear

$$\bar{T}\{ax_1(t) + bx_2(t)\} \neq a\bar{T}\{x_1(t)\} + b\bar{T}\{x_2(t)\}$$

For description of a dynamic system also a state space vector $\vec{s}(t)$ has to be defined. This vector describes the memory of the system, i.e., the output $y(t)$ does not only depend on the input $x(t)$ at t , but also on the past.

The system state $\vec{s}(t)$ is the number of state variables that have to be specified in order to describe the development of the system $\vec{s}(t), t \geq t_0$ based on given inputs $\vec{x}(t), t \geq t_0$. Usually dynamical systems can be described using following approach:

$$\dot{\vec{s}} = \vec{f}(\vec{s}, \vec{x}, t) \quad (6.3)$$

$$\vec{y} = \vec{g}(\vec{s}, \vec{x}, t) \quad (6.4)$$

$$\vec{s} \in \mathfrak{R}^n, \vec{x} \in \mathfrak{R}^r, \vec{y} \in \mathfrak{R}^q, \vec{t} \in \mathfrak{R}$$

These state equations consist on one hand of a set of n ordinary differential equations describing the actual intrinsic system behavior as well as keeping information of the past. On the other hand a set of q output equations \vec{y} describes the output behavior. Since \vec{s} represents the intrinsic features of the system the output equation according to 6.1 can be written as

$$y(t) = \vec{T}\{t, x(t)\} \quad (6.5)$$

These set of equations together with the (nonlinear and time variant) functions $\vec{f}(\cdot)$ and $\vec{g}(\cdot)$ describe a nonlinear and time variant system.

If initial values $\vec{s}(t_0) = \vec{s}^0$ and input signals $\vec{x}(t), t \geq t_0$ are known, $\vec{s}(t)$ and $\vec{y}(t)$ can be calculated.

As a special case, the linear model can be described. In case of a single input, single output system it can be written as

$$\dot{\vec{s}}T = A(\vec{s}) + b(x) \quad (6.6)$$

$$y = \vec{c}^T \vec{s} + du \quad (6.7)$$

with the state vector $\vec{s} \in \mathfrak{R}^n$, the system input $\vec{x} \in \mathfrak{R}$ and the system output $\vec{y} \in \mathfrak{R}$. $A \in \mathfrak{R}^{n \times n}$ defines the system matrix, $b \in \mathfrak{R}$ the input coefficient, and $c \in \mathfrak{R}^n$ the output coefficient vector and $d \in \mathfrak{R}$ the feed through coefficient.

If the coefficient matrices A, b, \vec{c} and d do not depend on the time, i.e. the matrix elements are constants, the model describes a linear time invariant system, otherwise the system is linear time variant. Again, for linear systems the principle of superposition applies:

$$\vec{x}_1(t) + \vec{x}_2(t) = \vec{y}_1(t) + \vec{y}_2(t) \quad (6.8)$$

This description of dynamic linear systems is according to the script of Prof. G. Schmidt (Schmidt 2001).

If a system is completely predictable, i.e., it can be completely described by mathematical equations, it is called deterministic. The opposite of a deterministic system is the random or stochastic system. There, the dynamic in the system cannot be described, i.e., the output of a defined input cannot be predicted.

Chaotic systems are deterministic, but the output strongly depends on the initial conditions of the system. Slight changes of the system's initial condition can lead to different output signals. Still, the chaotic system can be mathematically described by non-linear equations. The recorded signal can be considered as output of the dynamical system, the neuronal network.

This recorded univariate signal, LFP or EEG can be regarded as one-dimensional signal, since it only depends on the time. If more than one channel is recorded LFP and EEG also contain spatial information. If the signal is generated by a deterministic system, it only contains little information (Norton and Karczub 2003), whereas if the signal was generated by a higher dynamic the information content can be higher and more complex. A classification of the recorded brain electrical activity is difficult. It consists of many contributing components and because of its unknown neuronal actions it is highly complex. A general assumption regarding the signal properties of brain electrical activity is that it consists of chaotic and stochastic elements (Faure and Korn 2001; Jordan 2010). Hence the signal analytical methods used to quantify anesthetic induced effects on EEG and LFP recordings should be suitable to deal with this kind of signal.

In an initial step, the recorded signal has to be preprocessed and stored, so that the signal analyses can be performed. In the first section of this chapter the signal processing steps are described that are necessary to store the recorded signals on a computer and make them available for the signal analysis. The analytical methods that were applied on the recorded brain electrical activity are presented in second part of this section.

6.1 Data preprocessing steps

All signals that were recorded from the different experimental settings employed in this thesis have to be preprocessed so that they can be used for the analyses. In a first step the brain electrical signal is captured by a recording electrode as analog, time continuous signal $x(t)$. Since the electric potentials recorded as LFP or EEG have only small amplitudes in the μV and low mV range these signals have to be amplified, preferably as close to the recording site as possible to prevent the influence of surrounding noise. A stronger noise influence on the recording will impair the quality of your useful signal, the LFP or EEG, by decreasing

the signal to noise ratio. In a next step the signal has to be digitized so that it can be used for the computer based signal analysis. The digitizing step contains an initial hardware based low pass filtering of the signal so that the highest frequency that occurs in the signal is smaller than two times the digitizing (sampling) rate f_s , i.e., the digitized signal has to fulfill the Shannon-Nyquist theorem:

$$f_s > 2f_{\max}$$

where f_s is the sampling frequency and f_{\max} is the highest frequency in the signal defined by the low pass filter, the so called Nyquist frequency. If this requirement is not met, aliasing can occur and the discrete signal can be falsified as presented in the example in Figure 6.2 B.

After the filtering step the time-continuous signal $x(t); -\infty < t < \infty$ can be discretized to a discrete time series with equally spaced data points $x[n]; -\infty < n < \infty; n \in Z$, where the time between T_s two data points is defined by $T_s = 1/f_s$. The procedure to obtain $x[n]$ from $x(t)$ is as follows

In order to come from a continuous signal $x(t)$ to a continuous but sampled signal $x_s(t)$ a multiplication of $x(t)$ with a train of Dirac impulses has to take part.

A Dirac impulse $\delta(t)$ can be defined with following assignment rule:

$$\int_{-\infty}^{\infty} x(t)\delta(t)dt \stackrel{\text{per def}}{=} x(0) \quad (6.9)$$

The integral is of value $x(0)$, if $x(t)$ is continuous at $t = 0$.

If the signal $x(t)$ is multiplied with a train of Dirac impulses that occur every T_s time points, the sampled signal $x_s(t)$ can be written as:

$$x_s(t) = x(t) \sum_{s=-\infty}^{\infty} \delta(t - sT_s) = \sum_{s=-\infty}^{\infty} x(sT_s) \delta(t - sT_s); \quad -\infty < t < \infty \quad (6.10)$$

$x_s(t)$ is still a continuous signal with amplitude values every T_s steps.

The transition to the discrete series $x[n]$ is made by the conversion

$$x[n] = x_s(sT_s) \quad (6.11)$$

This means that the discrete time signal $x[n]$ represents samples of the analog time signal $x(t)$ every T_s seconds. An example of the discrete time series $x[n]$ derived from $x(t)$ is presented in Figure 6.2.

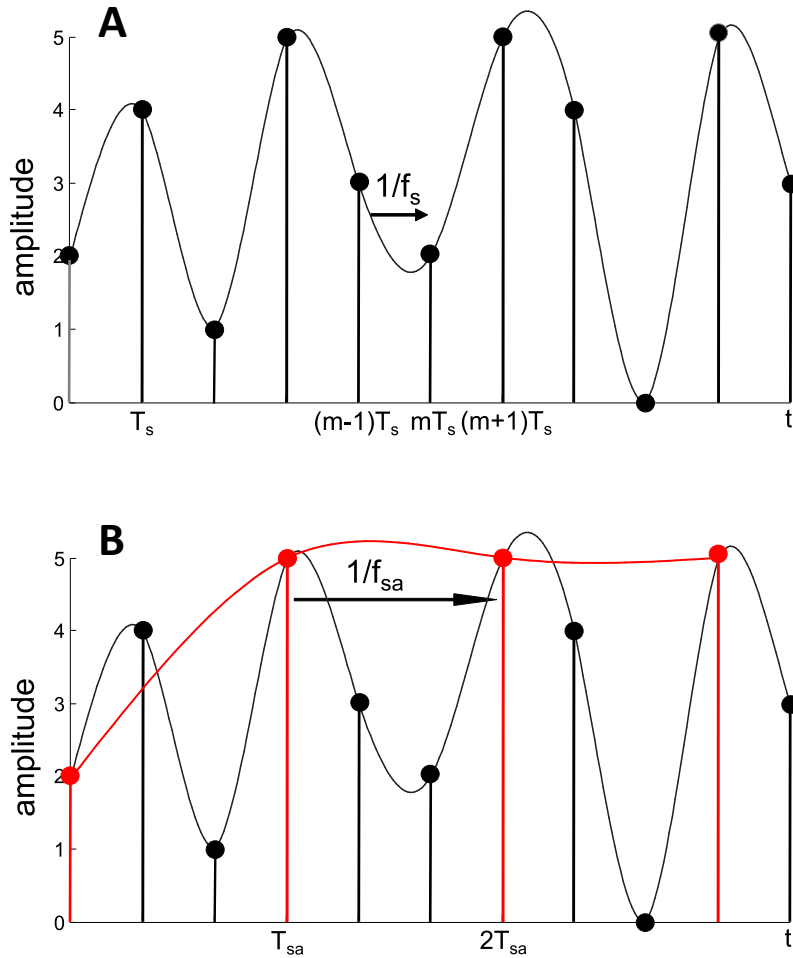


Figure 6.2: A: The continuous time series $x(t)$ can be presented as series of equally spaced and weighted, Dirac impulses leading to a discrete time series $x[n]$, according to formulas 6.10 and 6.11. The time between the Dirac impulses is defined by the sampling rate f_s , i.e. $T_s = 1/f_s$. That means that only the amplitude values of $x(t)$ at the time points defined by f_s are considered for further processing. B: Example for aliasing: In case of a too low f_s , here f_{sa} , too little sample points are recorded and the original cannot be assumed. Instead something like the red signal will be estimated. Once aliasing has occurred the lost information cannot be regained.

In order to store a digitized signal, the discrete time series as presented in Figure 6.2 has to be quantized, i.e., the potential values at the discrete time points have to be discretized as well. Because of the high quantization resolution of the EEG and LFP recording setups, quantization uncertainty can be neglected in this thesis. Consider a EEG recording range from -0.5 to 0.5 mV and a 12-Bit quantization resolution. The discrete value steps are $1/2^{12} \text{ mv} = 244\text{nV}$. The signals recorded during the experiments were consequently stored as such digitized time series, where the single data points represent the recorded potential values (with respect to quantization) at the sampled time points. The used settings of the data analyzed in this work are presented in Table 6.1.

Setup	f_s [kHz]	Quantization
In vitro OTC	10	12-bit
In vivo cortex	20	16-bit
In vivo cortex/hippocampus	20	16-bit
EEG steady state	1	12-bit
EEG transition I (AEP)	1	12-bit
EEG transition II (PSI)	0.256	16-bit
EEG Multi-channel	5	14-bit

Table 6.1: Sampling rates and quantization resolution of the data that was recorded in the single experiments

6.2 Linear analysis

Under the consideration that the recorded activity was probably generated by a mixture of chaotic and stochastic dynamics, the signal represents the output of a non-linear system. Still, linear questions regarding the network, for instance the search for the contributing parts of certain oscillations that are contained in the recorded brain electrical activity can be answered by linear analysis methods. An often used method to represent a frequency's participation to a signal is the use of Fourier based methods like the power spectral density (*PSD*). In this work, *PSD* was used to gain some insight of the power of single frequencies that contribute to the signal and changes in the frequencies' power distribution due to the anesthetic. The *PSD* measures power per frequency units and can only evaluate the autonomous contribution of single frequencies to the analyzed signal, but not their interaction. Since brain electrical activity lives from these interactions, where small changes in distinct frequencies may lead to relevant changes of the total brain electrical activity, the Fourier based approaches may not be able to process the entire information content of the signal, because they cannot deal with the highly complex dynamic in the underlying neuronal network. E.g., sudden phase shifts may not be detected. Nevertheless, these approaches seem useful to get a first impression of what is going on.

6.2.1 Power spectral density

The first step to derive the *PSD* is the calculation of the discrete Fourier spectrum utilizing the discrete Fourier transformation DFT. The complex, discrete Fourier spectrum $X[k]$ for a finite and aperiodic time series $x[n]$ of length N can be written as:

$$X[k] = \sum_{n=0}^{N-1} x[n] e^{\frac{-i2\pi kn}{N}} \quad (6.12)$$

The spectrum $X[k]$ delivers information regarding the amplitude and phase of oscillations in your analyzed signal sequence. $|X[k]|$ is the amplitude spectrum and $\arg(X[k])$ is the phase spectrum. The amplitude spectrum's information can be used to evaluate the power per frequency by estimating the *PSD* with $|X[k]|^2$. The results of *PSD* analysis are used to evaluate anesthetic-induced changes on oscillation properties of the EEG / LFP sequence analyzed. The *PSD* for signal sequences was calculated using MATLAB. In the presented results the unit is usually $\mu\text{V}^2/\text{Hz}$.

6.2.2 Slew rate analysis

Further, for one single experiment, the evaluation of anesthetic-induced effects during LOC, the so called slew rate analysis *SR* was used. This measure is capable of reflecting the biphasic excitation during the state transition. This biphasic course, also termed paradoxical excitation is a phenomenon that can occur during induction of anesthesia. EEG activity between 13-25 Hz that is usually suppressed during anesthesia shows activation during this transition phase (Kuizenga, Wierda et al. 2001; Brown, Lydic et al. 2010). This paradoxical activation effect was described using the *SR* approach. The presented method evaluates the slope of the EEG oscillations. When applied to EEG, filtered to the relevant frequency range, recorded during LOC, *SR* increased reflecting the stronger slopes due to higher amplitudes that occur if EEG oscillations in the selected frequency range are activated (Kuizenga, Wierda et al. 2001). The algorithm is based on the paper by Gregory and Pettus (Gregory and Pettus 1986), where they termed this method aperiodic analysis. It is "*a method that analyzes the EEG signal in the time domain by measuring the rate at which the signal slews between consecutive peaks and troughs*" (Steyn-Ross 2002). The method was included in this thesis, since Kuizenga used it in his experiments where he described the biphasic course of EEG activity during LOC for numerous drugs. The *SR* unit is potential/time, i.e., in EEG / LFP analysis usually $\mu\text{V}/\text{s}$ (Kuizenga, Wierda et al. 2001). According to Steyn-Ross, the slew rate is similar to the Fourier analysis of the waveform's time-derivative, i.e., the velocity of potential changes (Steyn-Ross 2002). To evaluate *SR* for a discrete time series $x[n]$, here EEG sequences, local minima are detected and the time delay between these local minima is accounted. A local minimum is defined when EEG voltage trend turns from a decreasing slope to increasing values. The turning point is defined as a local minimum. The time of the first detected local minimum in the time series, also termed valley, is denoted v_1 , the second

v_2 and so on. Between the first two valleys the temporal location of the voltage peak is denoted p_1 . A graphical presentation of defining valleys and peaks can be found in Figure 6.3. Based on the series of valleys and peaks, SR can be calculated based on detection of the average amplitude and frequency.

In a first step, the averaged amplitude A of an oscillation between two valleys, here v_1 and v_2 is defined as

$$A = \frac{[(V[p_1] - V[v_1]) + (V[p_1] - V[v_2])]}{2} \quad (6.13)$$

V represents the EEG amplitude, i.e. the potential at the certain time points v_1 , v_2 , and p_1 . Since the peak potential, e.g., $V[p_1]$ is always larger than the valley potentials, here $V[v_1]$ and $V[v_2]$, A will be positive. The frequency f of this oscillation defined by the two valleys is derived by calculating the inverse of the time span between the first and the second valley.

$$f = \frac{1}{v_2 - v_1} \quad (6.14)$$

Based on these equations the slew rate SR of one wave, i.e., the potential velocity of each wave can be evaluated.

$$SR = Af \quad (6.15)$$

Finally, the SR values of each detected oscillation in a sample are averaged, leading to an estimated dominating oscillation speed. In order to correctly apply this method, appropriate filtering, i.e., de-noising of the signal is necessary. Otherwise the valley and peak detection may not be correct, too many valleys and peaks would be detected and this would lead to erroneous results. SR was used on EEG signals that were band pass filtered to a certain frequency range, i.e., the classical EEG frequency bands.

Example:

Based on the time series presented in Figure 6.3, SR is calculated.

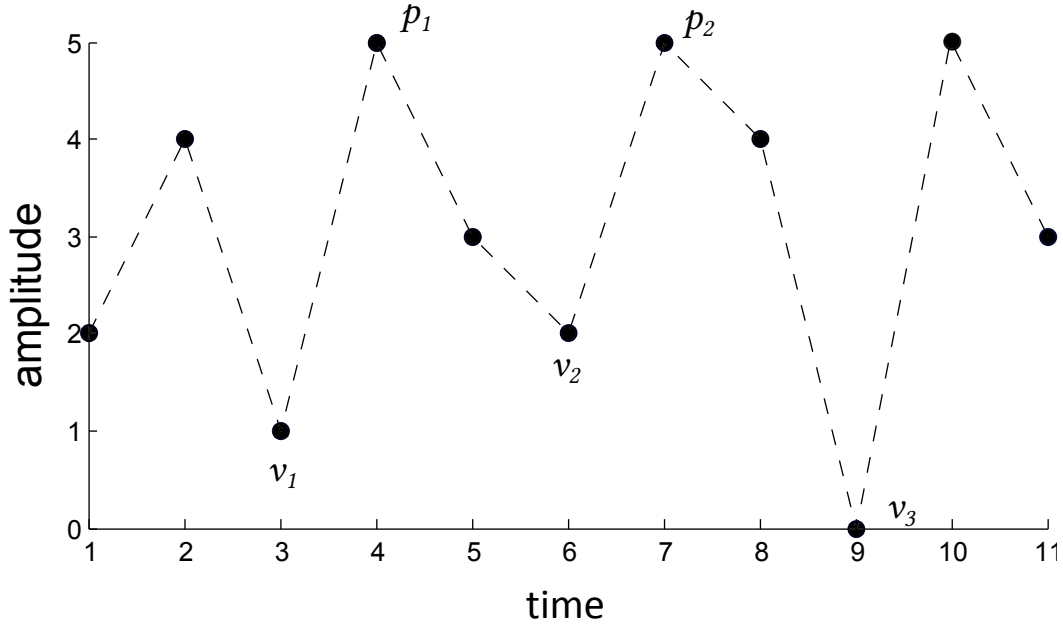


Figure 6.3: Exemplary time series $x[t]$ of length $N = 11$ used for description of the SR calculation.

Three valleys can be identified in the time series $x[n]$ at $v_1 = 3$, $v_2 = 6$, and $v_3 = 9$ with corresponding amplitude values $V[v_1] = 1$, $V[v_2] = 2$, and $V[v_3] = 0$. The two peaks $V[p_1] = V[p_2] = 5$ occur at $p_1 = 4$, and $p_2 = 7$.

$$f_1 = \frac{1}{v_2 - v_1} = \frac{1}{3}; \quad f_2 = \frac{1}{v_3 - v_2} = \frac{1}{3}$$

$$A_1 = \frac{[(V[p_1] - V[v_1]) + (V[p_1] - V[v_2])]}{2} = \frac{[5 - 1 + 5 - 2]}{2} = 3.5$$

$$A_2 = \frac{[(V[p_2] - V[v_2]) + (V[p_2] - V[v_3])]}{2} = \frac{[5 - 2 + 5 - 0]}{2} = 4$$

$$SR_1 = A_1 f_1 = 3.5/3; \quad SR_2 = A_2 f_2 = 4/3;$$

$$SR = \frac{SR_1 + SR_2}{2} = 1.25$$

6.3 Non-linear analysis

The introduced analytical methods of *PSD* and *SR* evaluate oscillating properties of the signal. *PSD* evaluates the contribution of single frequencies to the signal. If one frequency is dominating the signal, the spectral power of this frequency will be high. It evaluates the composition of oscillations the recorded signal. *SR* directly evaluates effects in the recorded signal and not just its composition. So *SR* may function as an interim stage between the pure spectral analysis (*PSD*) and the non-linear analyses introduced in this section. In order to evaluate a bigger amount of EEG / LFP properties, non-linear analysis techniques may prove better suited. As described in section 2.3.2 neuronal network activity per se is non-linear. In the context of EEG-based depth of anesthesia monitoring, experiments with surrogate EEG revealed that additional signal content can be analyzed with non-linear approaches in contrast to commercially available monitoring systems that evaluate the EEG with spectral approaches (Jordan, Kreuzer et al. 2009; Jordan, Stockmanns et al. 2009). Non-linear parameters that are established for scientific depth of anesthesia monitoring are based on the concept of entropy (Bruhn, Ropcke et al. 2000; Jordan, Stockmanns et al. 2008; Olofsen, Sleight et al. 2008; Jordan 2010).

6.3.1 The concept of entropy

Generally, entropy is defined as "*a way of measuring the lack of order in a system*" in the Oxford Advanced Learner's Dictionary (Hornby and Turnbull 2010). It was initially introduced in the field of thermodynamics and goes back to Claudius and Boltzmann (Clausius 1867). The central statement is that the entropy S of a system is proportional to the logarithm of the number of independent microstates W in a system.

$$S = k_B \ln W \quad k_B: \text{Boltzmann constant} \quad (6.16)$$

Shannon transferred entropy to the field of information theory to evaluate the information content of a message, where the amount of different letters in the message correspond to the amount of different microstates W in thermodynamics (Shannon 1948). He defined "*a logarithmic measure of the rate of transfer of information in a particular message*" (Soanes and Stevenson 2005).

Imagine a text consisting only of letters also termed events of a finite alphabet of length M : $L = \{l_1, l_2, l_3, \dots, l_M\}$. The probability $p(l_{abc})$ of a distinct event abc , i.e., a distinct letter of the alphabet, occurring in this text will be the rate of the event occurring in the text divided by the entire text length, i.e., the total number of letters. According to Claude Shannon, the information content I can be derived for each letter through

$$I(l_{abc}) = -\log_2 p(l_{abc}) \quad \text{for } 0 \leq p(l_{abc}) \leq 1 \quad (6.17)$$

The Shannon-Entropy H is the expectation value \mathcal{E} of I per event.

$$\mathcal{E}\{I(l_{abc})\} = H(L) = -\sum_{abc=1}^M p(l_{abc}) \log_2 p(l_{abc}) \geq 0 \quad (6.18)$$

$H(L)$ will always be ≥ 0 and it will only reach 0 if the probability of one event is 1 and all other probabilities are zero.

The maximum $H(L)$ is $\log_2 M$ and will only be reached, if all probabilities are equal.

This leads to $0 \leq H(L) \leq \log_2 M$. The unit of $H(L)$ is bit.

Example:

If a message can only consist of the three letters A , B and C ($M=3$), a message "AAAAAA" will lead to minimum $H=0$.

$$p(A) = 1;$$

$$p(B) = p(C) = 0;$$

$$H = -(1\log_2 1 + 0\log_2 0 + 0\log_2 0) = 0$$

Note that $0\log_2 0 = 0$ according to L'Hopital's rule. The intuitive description is that

$x \log x = \frac{\log x}{x^{-1}}$ and if x converges towards zero, $\log x$ converges faster towards infinity than x^{-1} .

A message "ABCBCA" will lead to a maximum $H = \log_2 3 = 1.585$ since

$$p(A) = p(B) = p(C) = \frac{2}{6} = 0.33;$$

$$H = -(0.33\log_2 0.33 + 0.33\log_2 0.33 + 0.33\log_2 0.33) = 1.585$$

Transferred to the exemplary time series in Figure 6.4 that was also used for the SR description, the Shannon entropy can be calculated as follows, under the assumption that the alphabet $M = \{0,1,2,3,4,5\}$, i.e., it consists of the possible amplitude values in the time series.

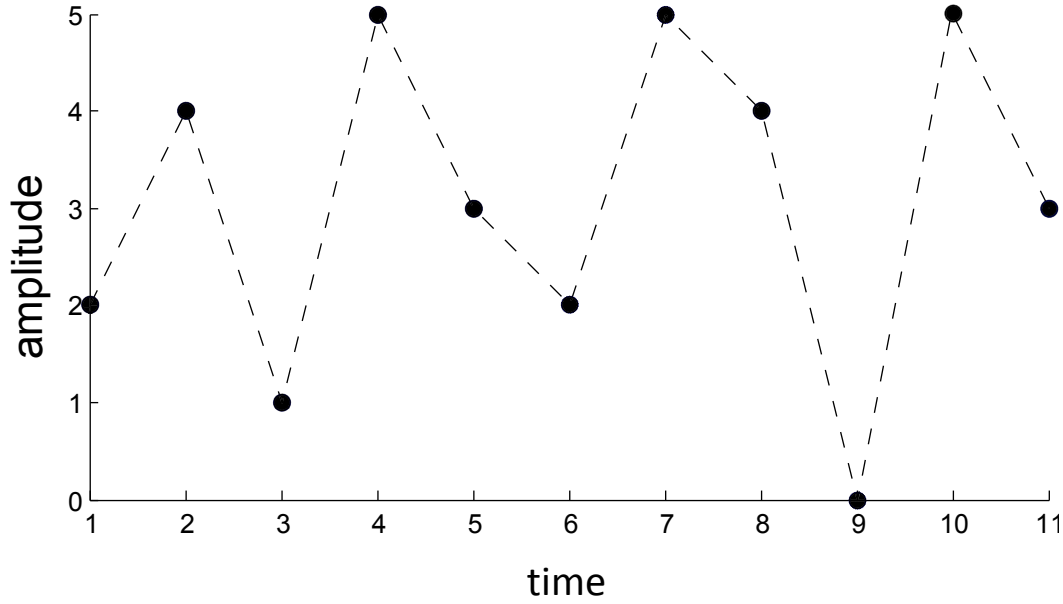


Figure 6.4: Exemplary time series $x[n]$ of length $N = 11$ used for description of the Shannon-Entropy calculation.

The time series $x[n]$ is then described by the message, i.e. the amplitude values, “2,4,1,5,3,2,5,4,0,5,3”.

$$p(0) = p(1) = \frac{1}{11}$$

$$p(2) = p(4) = p(3) = \frac{2}{11}$$

$$p(5) = \frac{3}{11}$$

$$H = -\left(2\left(\frac{1}{11} \log_2 \frac{1}{11}\right) + 3\left(\frac{2}{11} \log_2 \frac{2}{11}\right) + \frac{3}{11} \log_2 \frac{3}{11}\right) = 2.418$$

This concept of estimating probabilities of occurring events lies the fundament for entropy based methods already used in EEG analysis to detect the current level of anesthesia (Bruhn, Ropcke et al. 2000; Jordan, Stockmanns et al. 2008; Olofsen, Sleigh et al. 2008; Jordan 2010). Application of these methods seems suitable since entropy as a statistical parameter can be used to describe deterministic systems as well as stochastic systems (Jordan 2010). A set of entropy based parameters established in EEG anesthesia monitoring was used in this thesis. In order to evaluate information in the signal the utilized parameters use single chunks of that signal as bits of information.

The length of these chunks is defined by an embedding dimension m . For the *PeEn*, *ORR*, *BPeEn* and *sTE* algorithms this embedding dimension defines the number of possible

permutations, i.e., to how many different coded patterns the time series can be reduced. See Figure 6.6 for the generation procedure of the permutations. In the *ApEn* and *XApEn* algorithm, the embedding dimension defines the length of chunks that are compared with each other for similarity (section 6.3.2). The time lag τ defines a lag in the time series, i.e., the patterns of length m that are used for analysis consist of data points $(x[i], x[i + \tau], \dots, x[i + (m - 1)\tau])$. In the course of this work, τ was set to 1 for the parameter calculations unless stated otherwise.

If you use the exemplary time series $x[n] = [2, 4, 1, 5, 3, 2, 5, 4, 0, 5, 3]$ and you have an embedding dimension of $m = 3$ and $\tau = 1$, following patterns are derived from the series: $[2, 4, 1], [4, 1, 5], [1, 5, 3], [5, 3, 2], [3, 2, 5], [2, 5, 4], [5, 4, 0], [4, 0, 5], [0, 5, 4]$.

6.3.2 Approximate entropy

The approximate entropy *ApEn* introduced by Pincus (Pincus 1991) is a modification of the Kolmogorov-Sinai Entropy for the analysis of biosignals as a measure of signal predictability. The Kolmogorov-Sinai Entropy was designed for the analysis of chaotic systems and quantified the information content of the attractor of the system. In order to calculate accurate entropy, a lot of data is necessary and system noise can be of big influence (Pincus 1991). *ApEn* was introduced to overcome these issues. It evaluates signal predictability, where a higher *ApEn* value indicates a more chaotic and less predictable signal based on following idea:

If common patterns of m data points are detected in a time series $x[n]$, how big is the probability that the extended $m + 1$ data point patterns are also similar? The higher the probability of repetitive patterns, the lower will be *ApEn*.

ApEn found its way into biosignal analysis because it works with relatively few data values. A $N > 10^m$ was suggested by Pincus (Pincus 1991). Further, *ApEn* seems robust against noise artifacts to some extent due to a tolerance variable r (Pincus 1991). *ApEn* was first used in biosignal analysis for the evaluation of heart rate variability and interbeat intervals (Ho, Moody et al. 1997; Pikkujamsa, Makikallio et al. 1999) until it was introduced to EEG analysis by Bruhn et al. (Bruhn, Ropcke et al. 2000). Due to the fact that *ApEn* is finite for chaotic time series and the EEG probably represents a mixture of stochastic and chaotic processes (Fell, Röschke et al. 1996), application of *ApEn* to the data sets in this thesis seems suitable. The *ApEn* of a time series $x[n]$ with N data points can be defined as follows (Pincus 1991):

Short signal patterns $u[j]$ of length m starting at j are extracted from the time series with j ranging from $j=0$ to $j=N-m$ leading to $u[j]=[u_j, u_{j+\tau}, \dots, u_{j+(m-1)\tau}]$, i.e., as consequence the time series is presented as series of patterns. These patterns are compared to each other. Two patterns $u[i]$ and $u[j]$ are similar by means of a defined tolerance r , if:

$$\max\{|u[i+k]-u[j+k]|, k \in \{0, \dots, m-1\}\} \leq r \quad (6.19)$$

In biosignal analysis this tolerance r acts as a noise filter, i.e., if a small content of noise is added to the measuring signal, two signals are still considered similar if r is chosen appropriately. In a next step, the probability $C_i^m(r)$ of patterns similar to $u[i]$ is calculated. The index i ranges from $i=0$ to $i=N-m$, i.e. i runs over the entire time series selected.

$$C_i^m(r) = \frac{n_i^m(r)}{N-m+1} \quad (6.20) \text{ With } \tau \text{ set to } 1$$

N is the length of the data series and $n_i^m(r)$ counts the patterns similar to $u[i]$ to the defined tolerance r . With $C^m(r)$ being the means of $C_i^m(r)$. $ApEn$ can be defined as the natural logarithm of the quotient of the averaged probability of similar patterns of length m and the averaged probability of similar patterns of length $m+1$:

$$ApEn(m, r) = \log\left(\frac{C^m(r)}{C^{m+1}(r)}\right) \quad (6.21)$$

or with

$$\begin{aligned} \Phi^m(r) &= \log(C^m(r)) \\ ApEn(m, r) &= \Phi^m(r) - \Phi^{m+1}(r) \end{aligned} \quad (6.22)$$

As noted, $ApEn$ evaluates predictability by detecting similar patterns and assuming the probability that and the continuation of these patterns will also be similar and can hence be predicted. Hence $ApEn$ quantifies the predictability of a time series. $ApEn$ is high, when it is least predictable. If for every similar pattern of length m found, the extended $m+1$ pattern is also similar, $ApEn$ equals zero. The advantage of applying $ApEn$ lies in its noise

tolerance due to the tolerance element r . A limiting factor is the count of self matches. Each pattern used for comparison against the other patterns will be counted as hit if compared to itself. This procedure is necessary to prevent the occurrence of $\log(0)$ (Richman and Moorman 2000). As a consequence, $ApEn$ may be lower than expected for short data sets.

The $ApEn$ algorithm routine used in the experiments was realized with C++ according to the definitions in the papers of Ho and Bruhn (Ho, Moody et al. 1997; Bruhn, Ropcke et al. 2000) in order to minimize calculation time. The variables window length m and tolerance r of $ApEn$ were set to $m = 2$ and $r = 0.2SD$ (standard deviation of the time series) in this thesis. This choice is based on the findings of Bruhn et al., Silva et al. and Pincus et al. (Pincus and Goldberger 1994; Bruhn, Ropcke et al. 2000; Silva, Cardoso-Cruz et al. 2010). Bruhn et al. showed in a patient study that using this parameter setting is best suitable as indicator for an EEG based prediction of desflurane concentrations (Bruhn, Ropcke et al. 2000). Silva et al. calculated $ApEn$ with these settings from LFP recordings that were derived from rat somatosensory cortex and ventroposterolateral thalamic nuclei. These recordings were used to evaluate the performance of $ApEn$ to distinguish different anesthetic levels and also to investigate the existence of correlated or disrupted thalamo-cortical activity at isoflurane concentration levels corresponding to general anesthesia. $ApEn$ showed a good correlation with endtidal isoflurane concentrations. Further, the authors assumed based on their findings that a remaining thalamo-cortical connection during general anesthesia does exist (Silva, Cardoso-Cruz et al. 2010).

A $r = 0.2SD$ indicates that distortions smaller 20% of the analyzed time series' standard deviation are considered noise and consequently neglected.

Example:

The mode of action of $ApEn$ calculation is described with help of the exemplary time series $x[n] = (2,4,1,5,3,2,5,4,0,5,3)$ in Figure 6.5

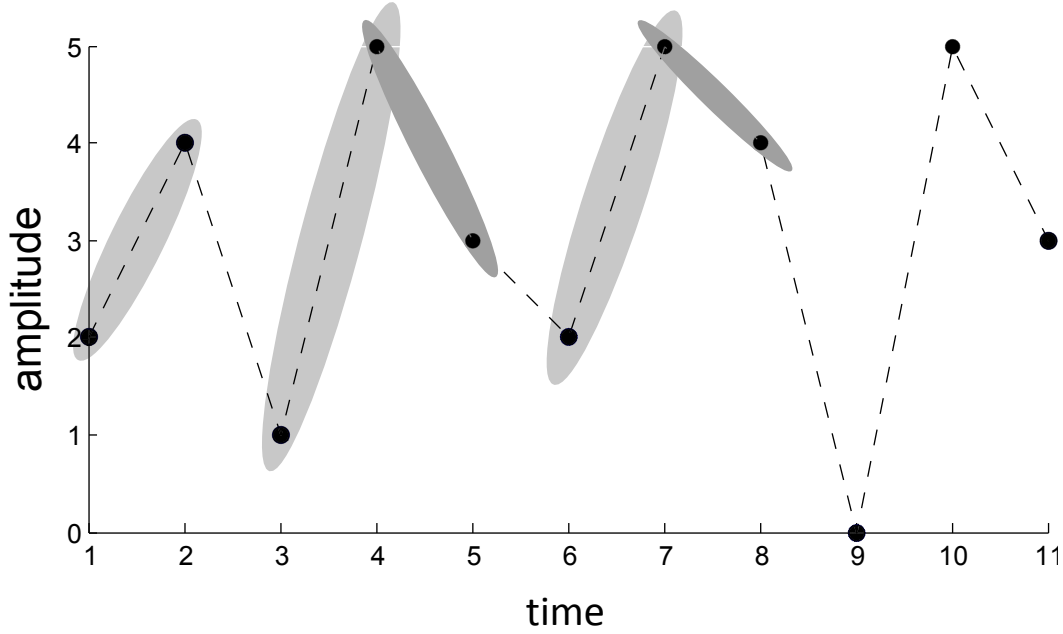


Figure 6.5: Exemplary time series $x[n]$ of length $N=11$ used for description of the $ApEn$ calculation.

Based on an embedding dimension of $m = 2$ and a tolerance $r = 1$, the patterns similar to the pattern $x_3 = (x[3], x[4]) = (1,5)$ are depicted with light grey shading in Figure 6.3. These are $x_1 = (x[1], x[2]) = (2,4)$ and $x_6 = (x[6], x[7]) = (2,5)$ and the self match. This leads to

$$n_3^2(1) = 3 \quad \text{hence to } C_3^2(1) = \frac{n_3^2(1)}{N - m + 1} = \frac{3}{10} = 0.3. \quad \text{After extension of the } x_1 \text{ pattern to}$$

$m + 1 = 3$, only the extended pattern starting at x_6 can also be considered similar besides the extended self match. This is denoted by the dark grey shading in Figure 6.3.

$$\text{Hence } n_3^{2+1}(1) = 1 \text{ and } C_3^3(1) = \frac{n_3^{2+1}(1)}{N - m + 1} = \frac{2}{10} = 0.2. \quad \text{If these steps are performed for all time}$$

points, $ApEn$ can be calculated according to formulas 6.21 and 6.22.

6.3.3 Permutation entropy

Permutation entropy $PeEn$ is an ordinal parameter that makes even less demands on the time series to be analyzed. It can be applied to signals consisting of stochastic and deterministic components (Bandt and Pompe 2002) and it has the further advantage that it works with relatively few data points compared to other approaches.

Because for $PeEn$ calculation the signal is considered as series of ranks and absolute amplitude values are dismissed, the state space, i.e., the possible amplitude values $x[n]$, here, the potential values the EEG or LFP can attain, can be decreased to a big degree (Bandt and Pompe 2002). In order to generate a series of ranks of length m (the embedding dimension), the course of the amplitudes of m data points is coded to permutation patterns π_k as displayed in Figure 6.6. The number of possible permutations k is depended on m , with $k = m!$

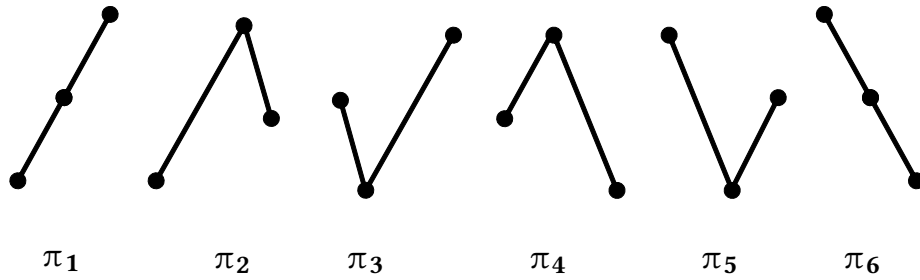


Figure 6.6: The six possible order patterns for a dimension of $m = 3$ adapted from Groth's article (Groth 2006).

In order to obtain $PeEn$, amplitude patterns $u[i]$ of length m are cut out of time series $x[n]$ in the same way as for $ApEn$, i.e., $u[i] = [u_i, u_{i+\tau}, \dots, u_{i+(m-1)\tau}]$. These amplitude patterns are coded to a series of ranks. The highest rank $m - 1$ is assigned to the highest amplitude value in the pattern. For instance a $m = 3$ amplitude pattern of 10, 20, 5 will lead to a rank series of 1, 2, 0. These rank series are defined permutations and denoted π_k as mentioned.

For example, if $m = 3$ then six different permutations π_k can be generated because of $k = m!$. Hence, $p(\pi_k)$ of a time series $x[n] = [x_1, x_2, \dots, x_N]$ can be calculated to (Bandt and Pompe 2002)

$$p(\pi_k) = \frac{|\{n \mid 0 \leq n \leq N - m, (x[n], \dots, x[n + m]) \text{ is of type } \pi_k\}|}{N - m + 1} \quad (6.23)$$

$PeEn$ can then be defined analogue to the Shannon entropy as:

$$PeEn = -\sum_k p(\pi_k) \log p(\pi_k) \quad (6.24),$$

where the sum runs over the number of all possible permutations π_k (Bandt and Pompe 2002).

As for the Shannon Entropy, $PeEn$ can range from $0 \leq PeEn \leq \log m!$. $PeEn$ is zero, when only one pattern can be detected, e.g., $x[n]$ is strictly monotonically decreasing or increasing. $PeEn$ will be maximal when all permutations π_k arise with the same probability, i.e., for a completely random system (Bandt and Pompe 2002).

In the context of EEG based depth of anesthesia monitoring, $PeEn$ was capable to reliably distinguish between consciousness and unconsciousness and hence highly suitable for monitoring anesthetic-induced EEG changes (Jordan, Stockmanns et al. 2008). They obtained equal or better results than other monitoring methods, but they used EEG frequencies only up to 30 Hz, which is lower than for the other analysis methods, i.e., the risk of analyzing EMG distortions is lower (Jordan, Kochs et al. 2008). Other groups confirmed the applicability of $PeEn$ (Olofsen, Sleigh et al. 2008).

In contrast to $ApEn$, where similarities of absolute amplitude values are evaluated, $PeEn$ follows a different approach and quantifies the probabilities of patterns of ranks in the analyzed non-linear signal. It seems advantageous to $ApEn$ in the analysis of time series containing only a few data points. For example, $PeEn$ delivers reliable results of separating consciousness from unconsciousness for EEG-sequences as short as 2 seconds (Jordan, Stockmanns et al. 2010). Another main advantage of $PeEn$ is its fast calculation time and the little demands that have to be made on the time series. Still, there are some limitations or things that have to be kept in mind. Possible information that is contained in the amplitude of the signal is lost and small and big changes in potential lead to the same permutation pattern. Smallest amplitude changes may be generated due to noise influence and patterns deriving from these changes are treated in the same way as "real" signal changes (Fadlallah, Chen et al. 2013). A partial solution to this issue may be the adequate low pass filtering of the signal. The length N of the time series analyzed should be $N > m!$ in order to reliably reflect the different permutations (Jordan 2010). Typically embedding dimensions of $m = \{3, \dots, 7\}$ are recommended (Bandt and Pompe 2002). This embedding

dimension interval was also validated by Jordan et al. for the purpose of distinguishing consciousness from unconsciousness based on EEG recordings (Jordan, Stockmanns et al. 2008). Hence an embedding dimension of $m = 5$ was chosen for the investigation of anesthetic-induced effects on brain electrical analysis in this work. Calculations were performed with LabVIEW 6i (Jordan 2010).

Example:

The steps of *PeEn* calculation are described with help of the exemplary time series $x[n] = (2,4,1,5,3,2,5,4,0,5,3)$ with $N = 11$ in Figure 6.7. This description is based on an example from Denis Jordan's work. (Jordan 2010)

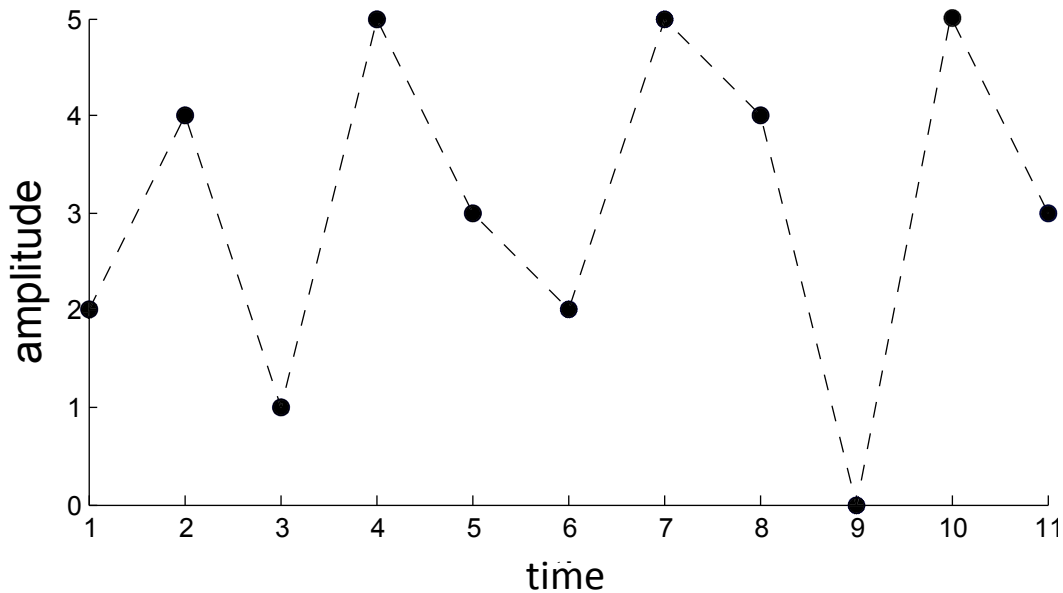


Figure 6.7: Exemplary time series $x[n]$ of length $N = 11$ used for description of the *PeEn* calculation.

For a defined time lag of $\tau = 1$, following amplitude presented in the table below values are used for generating the permutations for an embedding dimension of $m = 3$.

amplitudes	2 4 1	4 1 5	1 5 3	5 3 2	3 2 5	2 5 4	5 4 0	4 0 5	0 5 3
coded ranks	1 2 0	1 0 2	0 2 1	2 1 0	1 0 2	0 2 1	2 1 0	1 0 2	0 2 1
permutation π_k	π_1	π_2	π_3	π_4	π_2	π_3	π_4	π_2	π_3

This leads to following probabilities of the permutations:

$$\begin{aligned} p(\pi_1) &= 1/9 \\ p(\pi_2) &= p(\pi_3) = 3/9 \\ p(\pi_4) &= 2/9 \\ p(\pi_5) &= p(\pi_6) = 0 \end{aligned}$$

and consequently to

$$PeEn = -\sum p(\pi_k) \log p(\pi_k) = -\left(\frac{1}{9}\right) \log \frac{1}{9} + 2\left(\frac{3}{9}\right) \log \frac{3}{9} + \left(\frac{2}{9}\right) \log \frac{2}{9} = 0.569$$

Maximum $PeEn$ would be $PeEn_{\max} = \log 3! = 0.778$, so $PeEn$ of the exemplary time series differs from a completely random signal.

6.3.4 Order recurrence rate

As a third non-linear parameter used in this thesis the order recurrence rate ORR was applied to the data sets. This parameter is not entropy based but follows the idea of evaluating the relative quantity of recurring ordinal patterns, presented by permutations as in $PeEn$. This idea is implemented in the order recurrence rate ORR introduced by Andreas Groth (Groth 2006). In exemplary EEG time series he justified the use of ORR on these signals. The introduction of this measure to evaluate anesthetic-induced EEG changes was by Jordan et al. (Jordan, Stockmanns et al. 2008). Again, patterns of ranks of embedding dimension m are formed from a given time series $x[n]$ and the time series can then be presented as sequence of these $m!$ possible patterns denoted π_k , $k \in \{1, \dots, m!\}$. The advantage of this method, like of $PeEn$, is the fact that the data of the time series is reduced to order patterns π_k overcoming the problem of changing amplitudes and offsets with the time. For all possible order patterns a number of recurring patterns can be $R(i, \tau)$ derived. τ denotes the step in the time series, i.e., which patterns π_k are compared. If $\tau = 1$, consecutive patterns are evaluated and if $\tau = 3$, the selected pattern is compared with the pattern following 3rd. A hit is counted if the order pattern i is the same as the order pattern at $i + \tau$.

$$R(i, \tau) = \begin{cases} 1, & \pi_k(i) = \pi_k(i + \tau) \\ 0, & \text{otherwise} \end{cases} \quad k \in 1, \dots, m! \quad (6.25)$$

The order recurrence rate can be written as the sum of all detected hits for all $m!$ order patterns and as normalization step divided by the number of total comparisons (Jordan, Stockmanns et al. 2008):

$$ORR(\tau_\pi) = \frac{1}{N - m - \tau + 1} \sum_i R(i, \tau) \quad (6.26)$$

In general, if all compared patterns would lead to a hit ORR would be 1 and in the worst case, if no hit could be counted, ORR would be zero.

ORR represents a measure of statistical similarities in a time series dependent on a defined lag τ that was set to 1 in this work. Further, embedding dimension was set to $m = 4$. A $m = 4$ was chosen because in the paper of Jordan et al. good separation of conscious from unconsciousness based on EEG analysis could be obtained with this setting (Jordan, Stockmanns et al. 2008). Calculations were performed with LabVIEW 6i (Jordan, Stockmanns et al. 2008). As for other ordinal measures the coding of the time series may be of help and a limitation at the same time. The reduction of the state space leads to a more robust and faster algorithm. But if there is information content transferred by absolute amplitude values, it is lost in the coding step. Further, as described in the $PeEn$ section, distorting noise can influence the parameter, since "correct" amplitude changes and changes due to noise may be coded to the same pattern.

Example:

The steps of ORR calculation are described with help of the exemplary time series $x[n] = (2,4,1,5,3,2,5,4,0,5,3)$ with $N = 11$ in Figure 6.8.

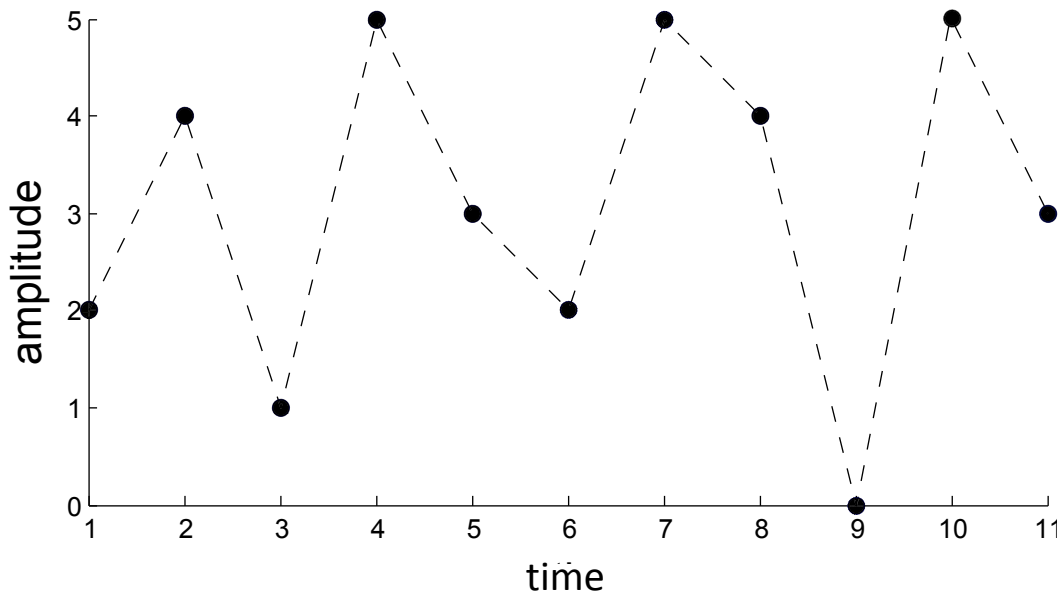


Figure 6.8: Exemplary time series $x[t]$ of length $N = 11$ used for description of the ORR calculation.

amplitudes	2 4 1	4 1 5	1 5 3	5 3 2	3 2 5	2 5 4	5 4 0	4 0 5	0 5 3
coded ranks	1 2 0	1 0 2	0 2 1	2 1 0	1 0 2	0 2 1	2 1 0	1 0 2	0 2 1
permutation $\pi_k(i)$	π_1	π_2	π_3	π_4	π_2	π_3	π_4	π_2	π_3
permutation $\pi_k(i+3)$	π_4	π_2	π_3	π_4	π_2	π_3			
recurring at $\tau = 3$?		Y	Y	Y	Y	Y			

For this example, the embedding dimension was set to $m = 3$ and the time lag was set to $\tau = 3$. This leads to a total sum of recurring patterns $\sum R(i, \tau) = 5$, as indicated by the Y(es) in the table. Y indicates that three permutations later ($\tau = 3$) the same permutation π_k is detected. Hence, the analysis leads to

$$ORR(3) = \frac{5}{11 - 3 - 3 + 1} = 0.833$$

6.3.5 Examples comparing the cardinal and ordinal measures

In the following section examples are presented displaying the different properties of the used parameters. The first example deals with the influence of noise on the signal.

An exemplary discrete time series $x[n]$ of 1 s with $f_s = 1$ kHz consisting of added 30 Hz and 17 Hz sine waves was created with MATLAB.

$$x[n] = \sin(2\pi 30n) + 0.67 \sin(2\pi 17n)$$

In two steps, random noise of maximum amplitudes 0.1 (step 1) and 0.25 (step 2) was added to the raw signal.

$ApEn$ was calculated for these signals with $m = 2$ and $r = 0.2SD$, $PeEn$ with $m = 5$, and ORR with $m = 4$ as used in the experiments. τ was set to 1. The results and the signals are presented in Figure 6.9.

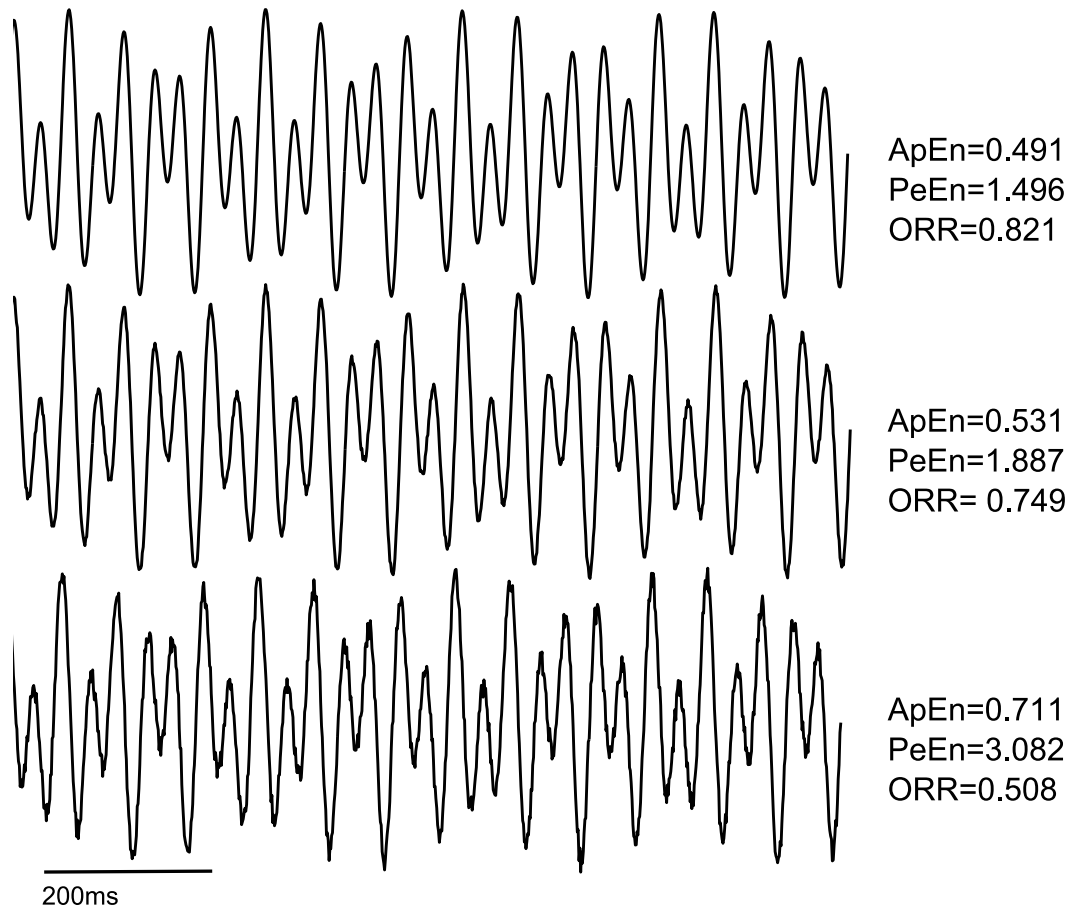


Figure 6.9: *ApEn*, *PeEn*, and *ORR* of the undistorted exemplary time series (top) and with increasing influence of random noise (center and bottom). *ApEn* is less influenced than *PeEn* and *ORR*.

The *ApEn* and *PeEn* values derived for the undisturbed raw signal are increased by noise that influences the signal. *ORR* values decrease. The change of *ApEn* (+7.3% at noise step 1 and +30.8% at noise step 2) is less pronounced than the change of *ORR* (-8.8% at noise step 1 and -38.1% at noise step 2). The biggest change can be observed for *PeEn* (+20.7% at noise step 1 and +51.5% at noise step 2). This example elucidates that *ApEn* seems more robust to noise influences than ordinal measures as represented by *PeEn* and *ORR*. In the second example the influence of a signal drift is investigated, i.e., what happens if the signal becomes nonstationary. Hence the time series is added with a linear slope as presented in Figure 6.10.

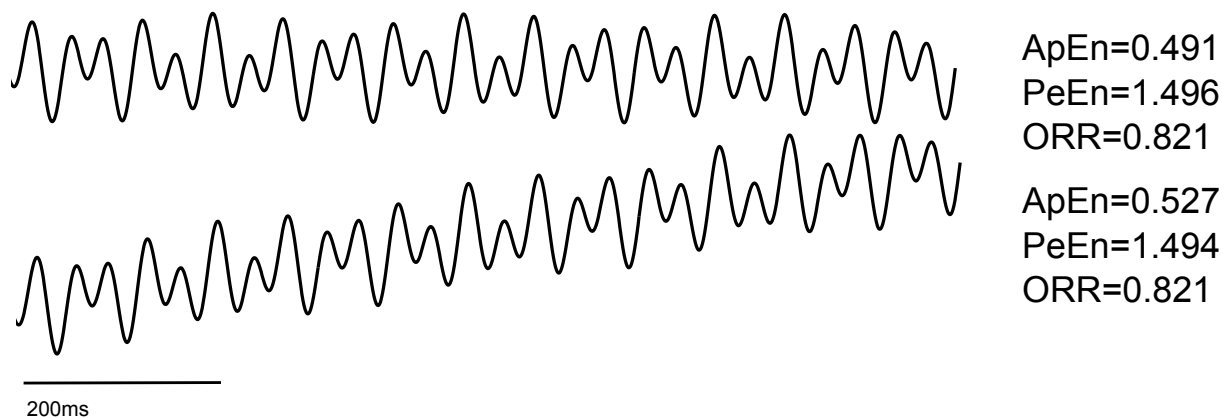


Figure 6.10: *ApEn*, *PeEn*, and *ORR* of the undistorted exemplary time series (top) and with a linear drift (bottom). *ORR* and *PeEn* are not influenced by the drift, whereas *ApEn* increases.

The linear drift does not influence *ORR* and almost not influence *PeEn* performance. The change of *PeEn* is 0.2%. *ApEn* values in contrast show an increase of 6.6%, since less similar patterns can be detected due to the drift. This example pronounces the advantage of ordinal measures if the recorded signal is prone to be distorted by drifts, for instance due to changing recording electrode impedances. All these non-linear methods described so far have been proven useful in evaluating anesthetic-induced effects on EEG recordings (Bruhn, Ropcke et al. 2000; Jordan, Stockmanns et al. 2008; Olofsen, Sleight et al. 2008). Since LFP, recorded from a smaller patch of the neuronal network can be seen as micro-EEG (Buzsáki, Anastassiou et al. 2012). The LFP generators comply with the EEG generators, only that EEG is recorded outside the skull and LFP electrodes are placed in the neuronal network. The *in vitro* LFP lacking subcortical inputs is characterized by alternating up- and down-state activity. In order to control these highly non-stationary signals we focused on analysis of the down-states, showing stationary behavior. Hence, application of these methods to recordings of brain electrical activity in form of LFP derived from neuronal networks of different size seems suitable. The presented methods evaluate changes in univariate time series, i.e., temporal effects can be analyzed. In a next step the ideas of *ApEn* and *PeEn* are extended to bivariate measures cross approximate entropy (*XApEn*), bivariate Permutation entropy (*BPeEn*) and symbolic transfer entropy (*sTE*) to quantify effects of the anesthetics on brain electrical activity spatio-temporally. Changes in inter channel similarity and synchrony can be evaluated with these measures. This spatio-temporal approach may deliver insights of how anesthetics change relations of brain electrical activity between recording sites on local and global levels of the neuronal network.

6.3.6 Cross approximate entropy

The cross approximate entropy $XApEn$ is an extension of $ApEn$ to two channels and was also introduced by Pincus and colleagues. They claimed that $XApEn$ seems capable of quantifying asynchrony (i.e., conditional irregularity) in interconnected networks (Pincus, Mulligan et al. 1996). $XApEn$ was used to quantify interhemispheric effects of volatile anesthetics on EEG recordings in the rat (Hudetz 2002). The procedure to derive $XApEn$ is similar to the way of calculating $ApEn$, only that patterns derived from one channel are compared to the patterns of the other channel. Since $XApEn$ is a cardinal measure evaluating absolute EEG / LFP amplitude values, and the baseline of the channels is included in the analysis, the given time series $x[n]$ and $y[n]$ are standardized to $x^*[n]$ and $y^*[n]$ according to

$$x^*[n] = \frac{x[n] - \bar{x}}{SD(x)} \quad (6.27)$$

\bar{x} is the mean of the time series $x[n]$ and $SD(x)$ is its standard deviation (Pincus, Mulligan et al. 1996). From these standardized series of N data points, short signal patterns $u[i]$ and $v[j]$ of length m are extracted from $x^*[n]$ and $y^*[n]$. The patterns $u[i]$ with i ranging from $i = 0$ to $i = N - m$ are compared to the patterns $v[j]$ with j also ranging from 0 to $N - m$.

Similar to $ApEn$, $C_i^m(r)(x \| y)$ depicts the probability of similar patterns found in $y^*[n]$ to a selected pattern from $x^*[n]$. After the averaging step over all $C_i^m(r)(x \| y)$ to $C^m(r)(x \| y)$, $XApEn$ can be defined as:

$$XApEn(m, r)(x \| y) = \log \left(\frac{C^m(r)(x \| y)}{C^{m+1}(r)(x \| y)} \right) = \Phi^m(r)(x \| y) - \Phi^{m+1}(r)(x \| y) \quad (6.28)$$

For analysis of the LFP channels window length m was set to 1 and tolerance r was 20% of the standard deviation of the time series $x[n]$. This setting was chosen since Pincus showed that $m = 1$ and the extending step to $m + 1 = 2$ in the algorithm seems applicable (Pincus, Mulligan et al. 1996) and to keep calculation time of the MATLAB based algorithm tolerable. Since some electrode layouts used in the *in vivo* experiments in this study contained 14 electrodes, 91 possible channel combinations had to be evaluated, as well as 411 combinations for evaluating all possible combinations of the 29 channel EEG used in the

volunteer studies. *XApEn* was applied to LFP activity to evaluate anesthetic-induced changes in the cortical network and between cortical and hippocampal regions on a local scale as well as the global evaluation of cortical activity represented in multielectrode EEG recordings. A limitation that has to be noted is the possibility of the occurrence of $\log(0)$ if no similar patterns between $x[n]$ and $y[n]$ are found.

Example:

The basic idea of *XApEn* calculation is presented in this example and in Figure 6.11.

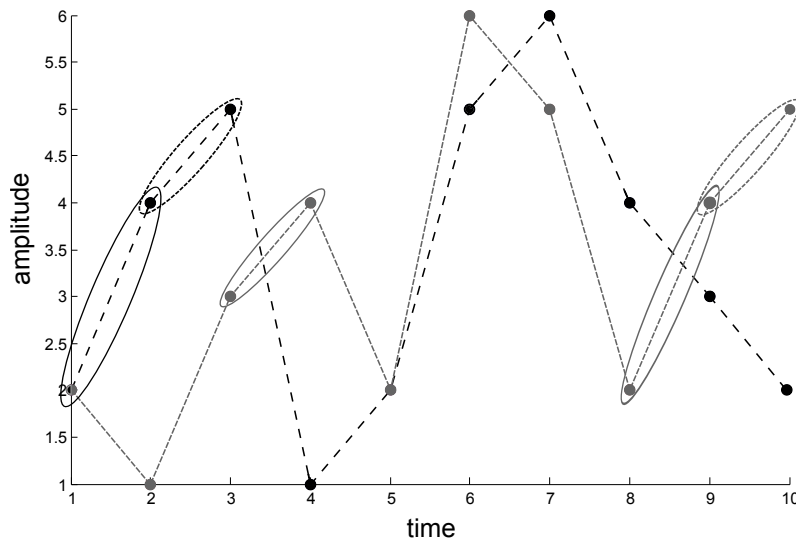


Figure 6.11: Exemplary time series $x[n]$ (black, long dashes) and $y[n]$ (grey, short dashes) of length $N = 10$ used for description of the *XApEn* calculation.

Based on an embedding dimension of $m = 2$ and a tolerance $r = 1$, the patterns similar to the pattern $x_1 = (x[1], x[2]) = (2, 4)$ marked with the black circle in $y[n]$ are depicted with grey circles in Figure 6.11. These are $y_3 = (y[3], y[4]) = (3, 4)$ and $y_8 = (y[8], y[9]) = (2, 4)$. This leads to $n_1^2(1)(x \parallel y) = 2$ hence to

$$C_1^2(1)(x \parallel y) = \frac{n_3^2(1)(x \parallel y)}{N - m + 1} = \frac{2}{9}. \text{ After extension of the } x_1 \text{ pattern to } m + 1 = 3 \text{ depicted by the}$$

black, dashed circle, only the extended y_8 (grey, dashed circle) can also be considered

similar. Hence $n_1^{2+1}(1)(x \parallel y) = 1$ and $C_1^{2+1}(1)(x \parallel y) = \frac{n_1^{2+1}(1)(x \parallel y)}{N - m + 1} = \frac{1}{9}$. If these steps are

performed for all time points, *XApEn* can be calculated according to formula 6.28.

6.3.7 Bivariate permutation entropy

The extension from *PeEn* to the bivariate permutation entropy *BPeEn* transfers the advantages of this ordinal measure to bivariate time series analysis. *BPeEn* calculations were performed with LabVIEW 6i. As described for *PeEn*, the amplitude values of two time series $x[n]$ and $y[n]$ are coded to patterns of ranks depending on the embedding dimension m . This leads to a series of permutations $\pi_{k,x}$ for $x[n]$ and $\pi_{k,y}$ for $y[n]$ with $k \in \{1, \dots, m!\}$. For every occurring permutation $\pi_{k,x}$ the corresponding number of $\pi_{k,y}$ is counted and used for calculation of *BPeEn*. In a preceding step, $p(\pi_k(x))$ and $p(\pi_k(y))$ are calculated according to

$$p(\pi_k(y)) = \frac{|\{n \mid 0 \leq n \leq N - m, (x[n], \dots, x[n+m]) \text{ is of type } \pi_{k,x}\}|}{N - m + 1}$$

$$p(\pi_k(x)) = \frac{|\{n \mid 0 \leq n \leq N - m, (x[n], \dots, x[n+m]) \text{ is of type } \pi_{k,y}\}|}{N - m + 1} \quad (6.29)$$

In the presented results of this thesis *BPeEn* was the averaged result of $BPeEn(\pi_k(x))$ and $BPeEn(\pi_k(y))$. As for *PeEn*, m was set to 5 for the analyses performed in this thesis.

Example:

An exemplary calculation of *BPeEn* for two short times series is described below and clarified using Figure 6.12.

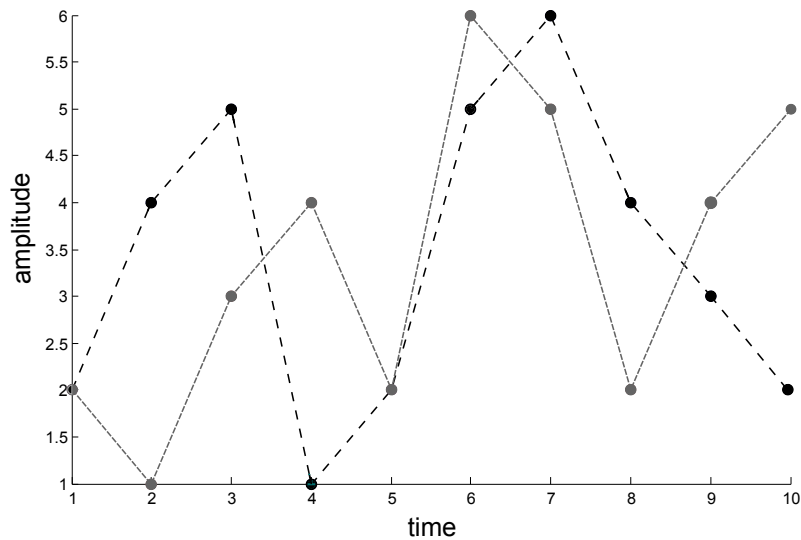


Figure 6.12: Exemplary time series $x[n]$ (black, long dashes) and $y[t]$ (grey, short dashes) of length $N = 10$ used for description of the *BPeEn* calculation.

The amplitudes of the time series $x[t]$ and $y[n]$ are coded to ranks as performed in the table below.

amplitudes $x[n]$	2 4 5	4 5 1	5 1 2	1 2 5	2 5 6	5 6 4	6 4 3	4 3 2
coded ranks $x[n]$	0 1 2	1 2 0	2 0 1	0 1 2	0 1 2	1 2 0	2 1 0	2 1 0
	$\pi_{1,x}$	$\pi_{2,x}$	$\pi_{3,x}$	$\pi_{1,x}$	$\pi_{1,x}$	$\pi_{2,x}$	$\pi_{4,x}$	$\pi_{4,x}$
amplitudes $y[n]$	2 1 3	1 3 4	3 4 2	4 2 6	2 6 5	6 5 2	5 2 4	2 4 5
coded ranks $y[n]$	1 0 2	0 1 2	1 2 0	1 0 2	0 2 1	2 1 0	2 0 1	0 1 2
	$\pi_{5,y}$	$\pi_{1,y}$	$\pi_{2,y}$	$\pi_{5,y}$	$\pi_{6,y}$	$\pi_{4,y}$	$\pi_{3,y}$	$\pi_{1,y}$

This leads to following probabilities:

$$\begin{aligned}
 p(\pi_1(y)) &= 2/8 & p(\pi_1(x)) &= 3/8 \\
 p(\pi_2(y)) &= 1/8 & p(\pi_2(x)) &= 2/8 \\
 p(\pi_3(y)) &= 1/8 & p(\pi_3(x)) &= 1/8 \\
 p(\pi_4(y)) &= 1/8 & p(\pi_4(x)) &= 2/8 \\
 p(\pi_5(y)) &= p(\pi_6(y)) = 0 & p(\pi_5(x)) &= p(\pi_6(x)) = 0
 \end{aligned}$$

6.3.8 Symbolic transfer entropy

The symbolic transfer entropy sTE was designed by Staniek et al. (Staniek and Lehnertz 2008). It is also a nonparametric measure like $PeEn$ and quantifies directed information flow between two time series $x[n]$ and $y[n]$, in this case, EEG or LFP recordings from two different channels. It was initially used to quantify anesthetic induced changes on cortical activity by Denis Jordan et al. (Jordan, Paprotny et al. 2011; Jordan, Ilg et al. 2013). Both time series are coded to a sequence of rank patterns of embedding dimension m , as also performed for $PeEn$. Based on a defined time lag τ , the permutation patterns can be generated from amplitude values derived at $(x[n], x[n + \tau], \dots, x[n + (m - 1)\tau])$. For each time point k the permutations obtained are denoted $\pi_{k,x}$, respectively $\pi_{k,y}$. Now the degree of prediction $p(\pi_{k,x})$ from past information of the other channel $p(\pi_{k-\delta,y})$ is reflected by a general Markov property, i.e., that the present information only depends on the observed past information. δ is a defined and constant delay, i.e., how far the considered information from $y[n]$ lies in the past. In order to dismiss prediction within the same signal, $p(\pi_{k,x-\delta})$ is

subtracted. This leads to a definition of sTE that information is transferred from $y[n]$ to $x[n]$

$$sTE_{y,x} = \sum p(\pi_{k,x}, \pi_{k,x-\delta}, \pi_{k,y-\delta}) \log_2 \left(\frac{p(\pi_{k,x} | \pi_{k,x-\delta}, \pi_{k,y-\delta})}{p(\pi_{k,x} | \pi_{k,x-\delta})} \right) \quad (6.30). \text{ (Jordan, Ilg et al. 2013)}$$

with conditional probabilities $P(A | B) = \frac{P(A \cap B)}{P(B)}$ and joint probabilities

$$P(A, B) = P(A \cap B).$$

The information transfer from $x[n]$ to $y[n]$ can be calculated accordingly.

sTE is the difference

$$sTE = sTE_{x,y} - sTE_{y,x} \quad (6.31)$$

The sign of sTE gives indication about the direction of the information flow, i.e., if a channel is sending or receiving information. In this thesis $|sTE|$ was used in the analyses, i.e. only the amount of information flowing was investigated and the direction of the flow was dismissed. This measure has been successfully used to quantify anesthetic-induced changes in cortical connectivity (Jordan, Paprotny et al. 2011; Ku, Lee et al. 2011; Jordan, Ilg et al. 2013). In this thesis it was mainly used to quantify propofol-induced effects in the information processing between prefrontal cortex and hippocampus. Therefore the calculations were conducted with LabVIEW 6i (Jordan, Ilg et al. 2013). sTE ($m = 3, \tau = 5, \delta = 6$) was used in this thesis. Since the delay parameter δ specifies a step in time it is dependent on the sampling frequency f_s of the analyzed time series $x[n]$. For the analyses performed and the corresponding results presented in section 10.4 and 13.3.3 the down-sampling rate was adapted to the analyzed frequency range.

Example:

The influence of extrinsic and intrinsic information, the concept of sTE is based on is described in the following text and in Figure 6.13.

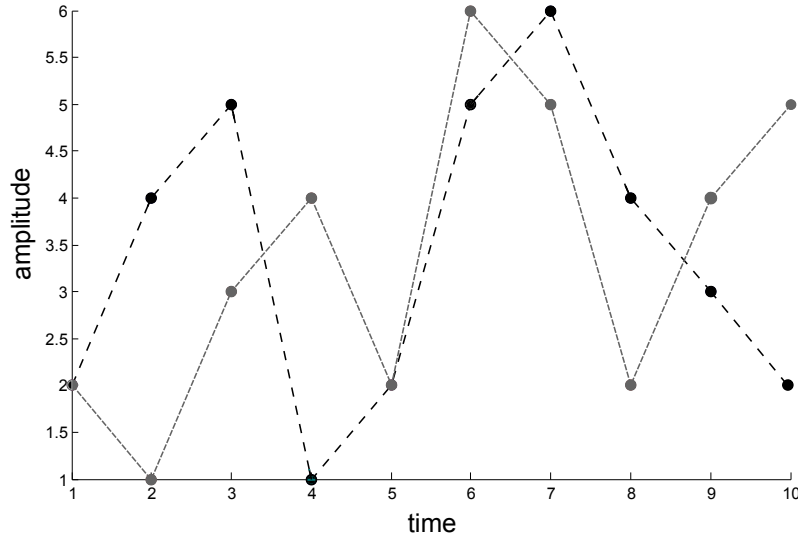


Figure 6.13: Exemplary time series $x[n]$ (black, long dashes) and $y[n]$ (grey, short dashes) of length $N = 10$ used for description of sTE calculation.

For a defined time lag of here exemplarily $\tau = 1$, following amplitude values presented in the table below are used for generating the permutations for an embedding dimension of $m = 3$.

amplitudes $x[n]$	2 4 5	4 5 1	5 1 2	1 2 5	2 5 6	5 6 4	6 4 3	4 3 2
coded ranks $x[n]$	0 1 2	1 2 0	2 0 1	0 1 2	0 1 2	1 2 0	2 1 0	2 1 0
amplitudes $y[n]$	2 1 3	1 3 4	3 4 2	4 2 6	2 6 5	6 5 2	5 2 4	2 4 5
coded ranks $y[n]$	1 0 2	0 1 2	1 2 0	1 0 2	0 2 1	2 1 0	2 0 1	0 1 2

With a defined delay $\delta = 3$, the coded (1 2 0) pattern from the coded $y[n]$ series, is transferred to the coded series of $x[n]$ three steps later. This transfer is without intrinsic information from $x[n]$ from three steps before. The pattern there is (2 0 1).

The relevant patterns are shaded grey in the table.

7 Statistical methods

7.1 Prediction probability

Prediction probability P_K was introduced to the field of anesthesia to evaluate a parameter's performance to distinguish different levels of anesthesia (Smith, Dutton et al. 1996). It can be used on dichotomous and non-dichotomous classifiers, i.e., on separation of two or more anesthetic levels. Classifiers are the parameters used to estimate the anesthetic level. P_K is a nonparametric test without any conditions regarding distribution of the classifier values and it is independent from any defined thresholds defining separation between two levels. This is of great advantage for the evaluation of anesthetic effects because a strict parameter threshold cannot be defined since underlying mechanisms of state transitions are unknown. The mode of action of P_K calculation is as follows (Jordan 2010).

In a set of classifier values $\vec{c} = (c_1, \dots, c_N)$ and their corresponding states $\vec{z} = (z_1, \dots, z_N)$, where z_i belongs to the dichotomous states $s_i \in \{"awake", "unconscious"\}$ and "*awake*" > "*unconscious*". Based on this p_d (frequency of discordance), p_c (frequency of concordance) and p_t (frequency of ties) can be evaluated. Therefore, two random pairs $\{c_i, \dots, c_i\}$ and $\{c_j, \dots, c_j\}$ with $(i, j \in \{1, \dots, N\}, i \neq j)$ and $z_i \neq z_j$ are drawn. Then p_c means $z_i > z_j$ and $c_i > c_j$, p_d indicates $z_i > z_j$ and $c_i < c_j$, and p_t expresses $z_i > z_j$ and $c_i = c_j$.

For dichotomous data P_K can be defined as

$$P_K = \frac{1}{2} \left(\frac{p_c - p_d}{p_c + p_d + p_t} + 1 \right) \quad (7.1)$$

A P_K of one indicates perfect separation of different states according to the calculated classifier values. $P_K = 0.5$ means that the chance to correctly assign a classifier value to an anesthetic level is no more than fifty-fifty. $P_K = 0$ expresses that every classifier is assigned to the wrong state in dichotomous data sets. This leads to the fact that there is often no separation between $P_K = 0$ and $P_K = 1$ and by calculating the absolute of the frequency quotient, P_K can be limited to the interval $[0.5, 1]$.

$$P_K = \frac{1}{2} \left(\left| \frac{p_c - p_d}{p_c + p_d + p_t} \right| + 1 \right) \quad (7.2)$$

The following Figure 7.1 displays a graphical example for different P_K values.

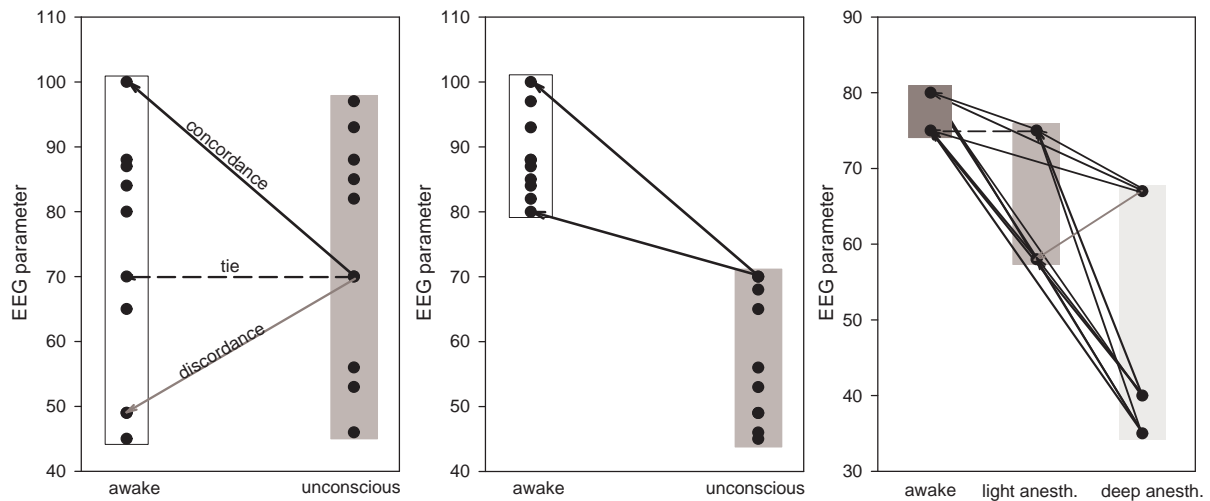


Figure 7.1: Left side & center: Example for different distributions of an EEG parameter values at states “awake” and “unconscious”. On the left side, the example represents a P_K of 0.56 and the arrows indicate concordant (parameter at “awake” > parameter at “unconscious”, solid black line), discordant (parameter at “awake” < parameter at “unconscious”, solid gray line), and tied (parameter at “awake” = parameter at “unconscious”, dashed black line), relationships. The right side represents a distribution with $P_K = 1$, i.e., there is perfect separation of the parameter values derived from the different levels. Only concordant relationships exist. Right side: In case of using P_K to evaluate a parameter's performance of separating different anesthetic levels, the evaluation of relationships has to be performed over all combinations of states. Here for "awake" vs. "light anesthesia", "awake" vs. "deep anesthesia" and "light anesthesia" vs. "deep anesthesia".

In the case of evaluating the performance of a parameter to distinguish between different anesthetic levels or concentration stages, the described mode of calculation has to be performed over all combinations of levels, i.e., over the number of different level less 1.

For P_K calculation the LabVIEW based “ P_K -Tool” was used as presented in the paper of Jordan et al. (Jordan, Steiner et al. 2010). This software also includes the calculation of 95% confidence intervals. These intervals are obtained using bootstrapping. From a set of classifiers and their corresponding anesthetic levels, a new set of same size and same number samples from each state is created by variation with repetition and P_K is calculated. Recommended are 1000 rounds of this procedure to obtain a reliable distribution. Non-overlapping confidence intervals represent a conservative measure of estimating significance from P_K values.

7.2 *Wilcoxon Test*

The Wilcoxon test was used to evaluate significant differences between two data sets. It is a nonparametric method and does not make conditions regarding distribution of data in one sample. Its parametric pendant t-test for example requires normally distributed samples. In contrast to the t-test, the Wilcoxon test is better suited for small sample sizes. The data does not have to be normally distributed. The Wilcoxon test was used in order to test the hypothesis if two samples have equal medians. The unpaired Wilcoxon test is equivalent to the Mann-Whitney U-test. The two tested samples can be of different size. The significance level was set to $p < 0.05$. In this thesis, anesthetic-induced changes on brain electrical activity at different concentration levels during one experiment were compared to control conditions. This led to multiple comparisons against control.

It means that multiple hypotheses are tested. The more hypotheses are tested, the higher the probability will be that a hypothesis is falsely accepted. In order to counteract this risk, the Bonferroni correction is the most conservative method. For each test, the significance level is lowered to the original level set divided by the number of hypotheses, i.e., the comparisons performed. Hence, the significance level was adjusted according to the Bonferroni correction and the level was set to $p < 0.05/nc$, where nc is the number of comparisons performed.

7.3 *Sign Test*

The sign test was used to evaluate a possible trend in the propofol induced change in LFP activity between neocortex and hippocampus in section 10. It is a very insensitive test. In this work the relative change of the bivariate parameter value for single electrode combinations due to propofol was calculated. If the parameter value increased with propofol, a '+' was noted, if it decreased with propofol, a '-' was noted. The amount of '+' and '-' are used to assess a possible trend towards an increasing or decreasing parameter value due to propofol.

7.4 *Pearson's Correlation*

Pearson's Product Moment Correlation, for short Pearson's Correlation, reflects the degree of linear relationship between two variables. It ranges from -1 to 1 where 1 indicates perfect positive relationship and -1 indicates perfect negative relationship. The Pearson's correlation coefficient r_c for two time series $x[n]$ and $y[n]$ can be calculated as follows

$$r_c = \frac{\sum_{n=1}^N (x[n] - \bar{x})(y[n] - \bar{y})}{\sqrt{\sum_{n=1}^N (x[n] - \bar{x})^2 \sum_{n=1}^N (y[n] - \bar{y})^2}} \quad (7.3)$$

\bar{x} and \bar{y} are the mean of the time series $x[n]$ and $y[n]$. The correlation coefficient was calculated using LabVIEW6i. Pearson's correlation was used in the analysis of the *in vivo* LFP recordings to give an impression regarding similarity between the channels. It was further compared against *XApEn* to highlight the advantages of *XApEn* to detect anesthetic-induced effects as exemplarily presented in Figure 9.8 A.

7.5 Boxplots

Boxplots (box-and-whisker) charts are a good way to give an impression on how data is distributed and how big their variance is. The box represents the area where the central 50% of the data are located (25th and 75th percentile as upper and lower limit and the median as intermediate line). A median that is off center indicates asymmetry in the distribution. 95% of the data are within the whiskers and outliers are displayed as dots (Riffenburgh 1999). Boxplots are used to compare the results of different anesthetic levels. Boxplots were created with SigmaPlot 8.0 (Systat Software Inc, Chicago, IL, USA).

7.6 Exponential regression

Exponential regression was calculated with SigmaPlot 8.0 in the cortical *in vivo* experiments to compare the effect of the different anesthetic regimen on *XApEn* with each other. The data points, i.e., parameter values obtained for one drug at different concentration levels was fitted according to the monoexponential function $y = a \exp(-x/b)$.

The parameter b describes the decreasing course of *XApEn* at increasing dosages of the applied anesthetic. The parameter a is the initial parameter value at control conditions. Presented R^2 values represent a goodness of fit measure. R^2 ranges between 0 and 1. $R^2=1$ means that all data points lie exactly on the calculated regression line, i.e., a perfect fit. Whereas $R^2=0$ means that there is no exponential relationship between x and y .

7.7 Stationarity

Weak stationarity analysis was performed as described by Bendat and Piersol (Bendat and Piersol 1986). Therefore, the selected sequences were divided in non-overlapping LFP or EEG samples and root mean square RMS was calculated over these segments. For a time series $x[n] = (x_1, x_2, \dots, x_N)$ the RMS is:

$$RMS = \sqrt{\frac{1}{N}(x_1^2 + x_2^2 + \dots + x_N^2)} \quad (7.4)$$

The obtained RMS values of each sample were used for the reverse arrangement test as a criterion for weak stationarity. Z-score was calculated according to Beck et al. (Beck, Housh et al. 2006) using equation

$$z = \frac{A - \left[\frac{N_s(N_s - 1)}{4} \right]}{\sqrt{\frac{2N_s^3 + 3N_s^2 - 5N_s}{72}}} \quad (7.5)$$

A is the number of reverse arrangements in the samples and N_s is the total number of samples in the sequence. Significance level to reject the null hypothesis that there is no underlying trend and the analyzed sequence is stationary, was set to $p < 0.05$, i.e., a z-score of $|z| \leq 1.96$. The test for stationarity was performed with LabVIEW 6i.

8 Anesthetic-induced effects on cortical network activity *in vitro*

In the following section the results of the analyses from the OTC LFP recordings are presented. Some parts of these results are also presented in the paper of Drexler et al. (Drexler, Kreuzer et al. 2013)

8.1 Anesthetic effects on PSD in the complete recordings and down-states only

PSD changes concentration dependently during sevoflurane or propofol administration. In the propofol group *PSD* of the entire recordings decreased monotonously over the entire frequency range observed (Figure 8.1). *PSD* spectrum of the propofol down-states showed a very similar behavior and, hence, is not shown in an extra graph. In the experiments with sevoflurane *PSD* increases at 0.25 MAC over the entire frequency range and a concentration of 0.5 MAC causes a depression of *PSD* in the lower frequencies up to 10 Hz and an activation of higher frequencies in the 15 to 25 Hz range. At sevoflurane concentrations of 0.75 MAC and above, which is higher than the MAC_{awake} that lies between 0.5 and 0.75 MAC (Hobbhahn and Conzen 2003), spectral power is suppressed in the entire frequency range (Figure 8.2 & Figure 8.3). If only down-state activity is considered, these effects can also be observed. Generally, substance specific changes of PSD can be determined and combined activity consisting of up- and down-states and down-state only activity are modulated in similar manner. These findings indicate relevant activity in the down-state episodes that are analyzed more closely by the non-linear measures in the following sections.

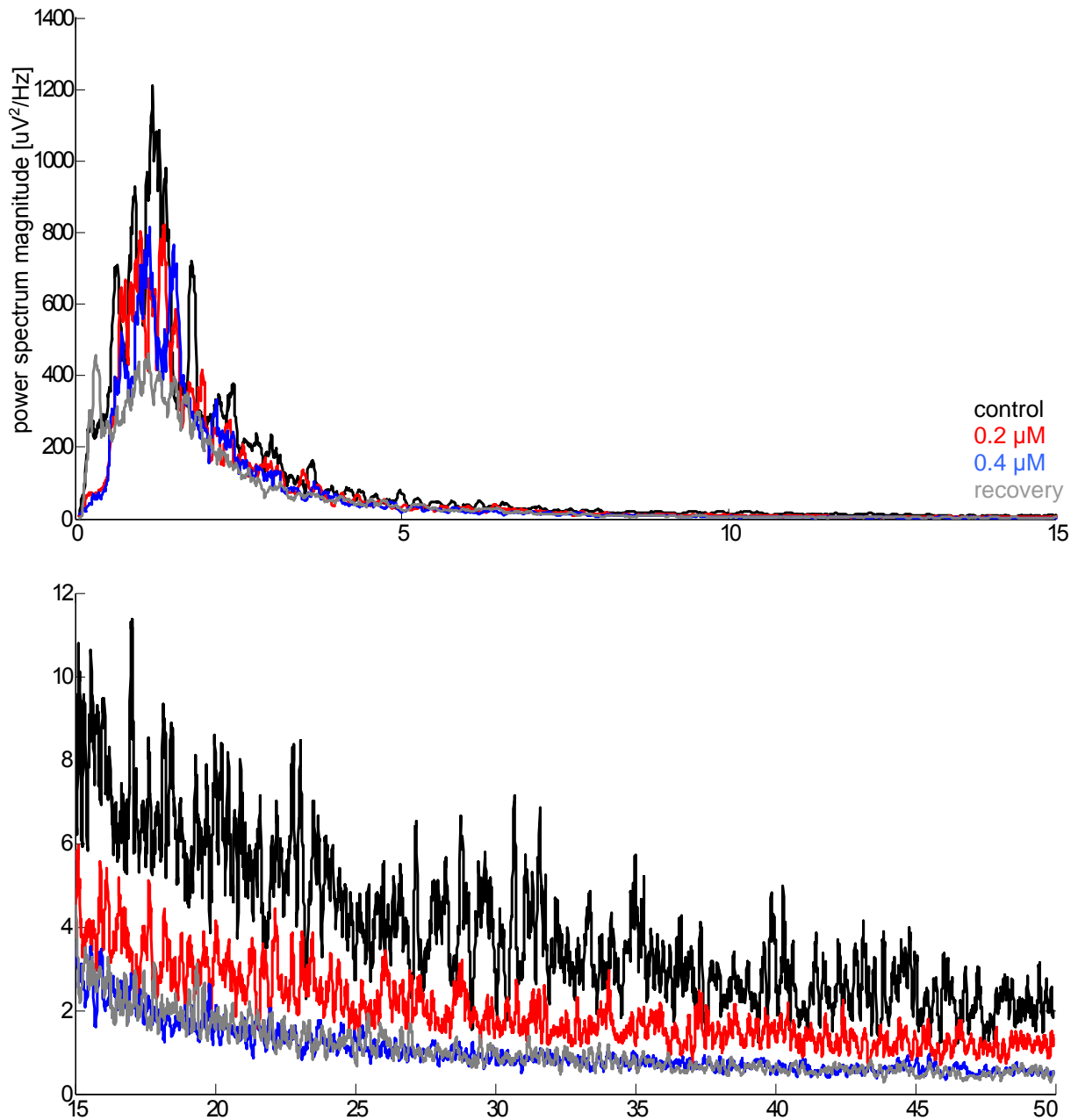


Figure 8.1: *PSD* average of all propofol recordings; top: low frequencies 0-15 Hz, bottom: high frequencies 15-50 Hz; Low frequencies up to approximately 4 Hz are dominant. With increasing propofol concentration, *PSD* decreases.

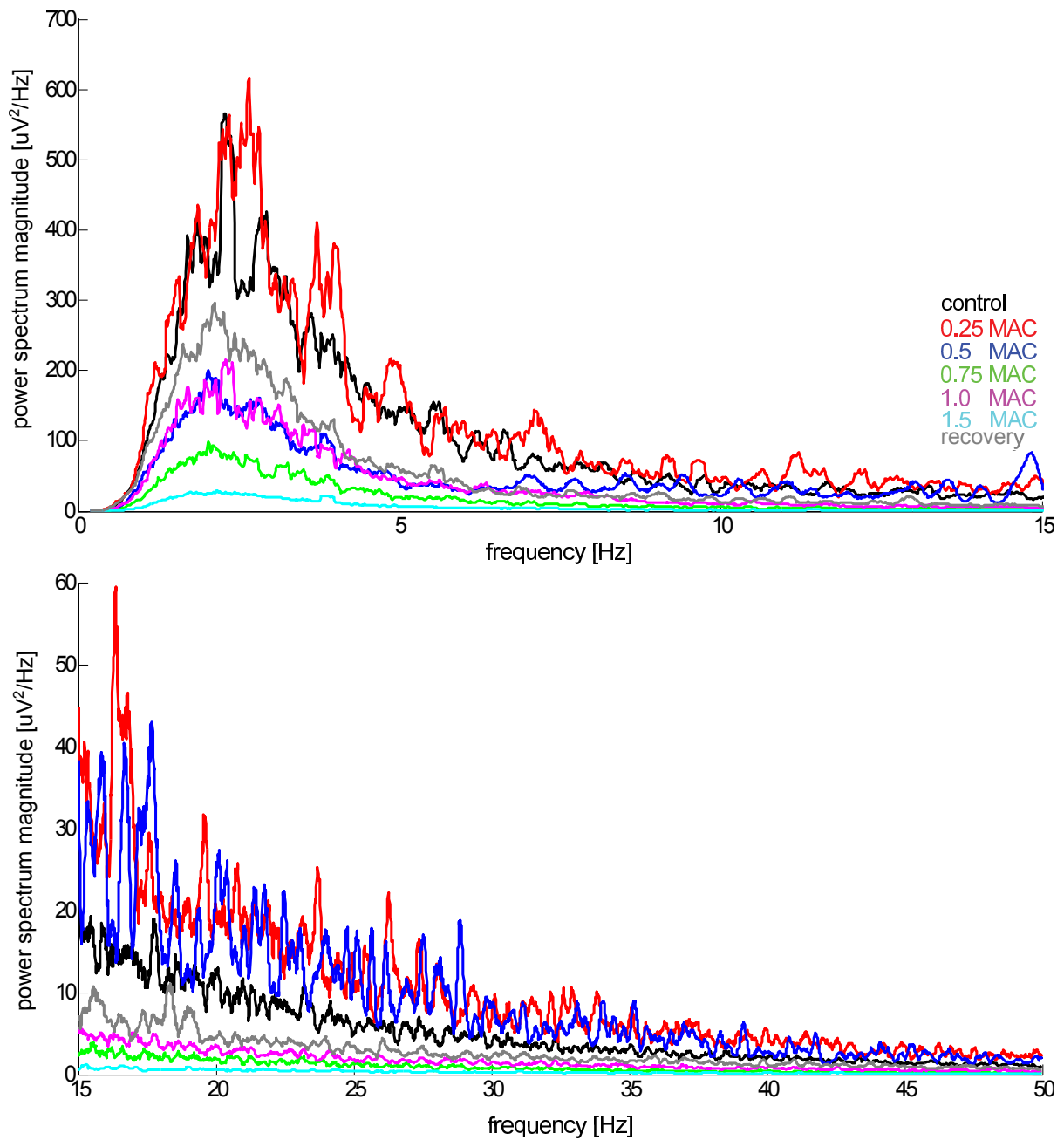


Figure 8.2: *PSD* average of all sevoflurane recordings; top: low frequencies 0-15 Hz, bottom: high frequencies 15-50 Hz; *PSD* shows activation at low concentrations at 0.25 MAC followed by suppression at higher concentrations.

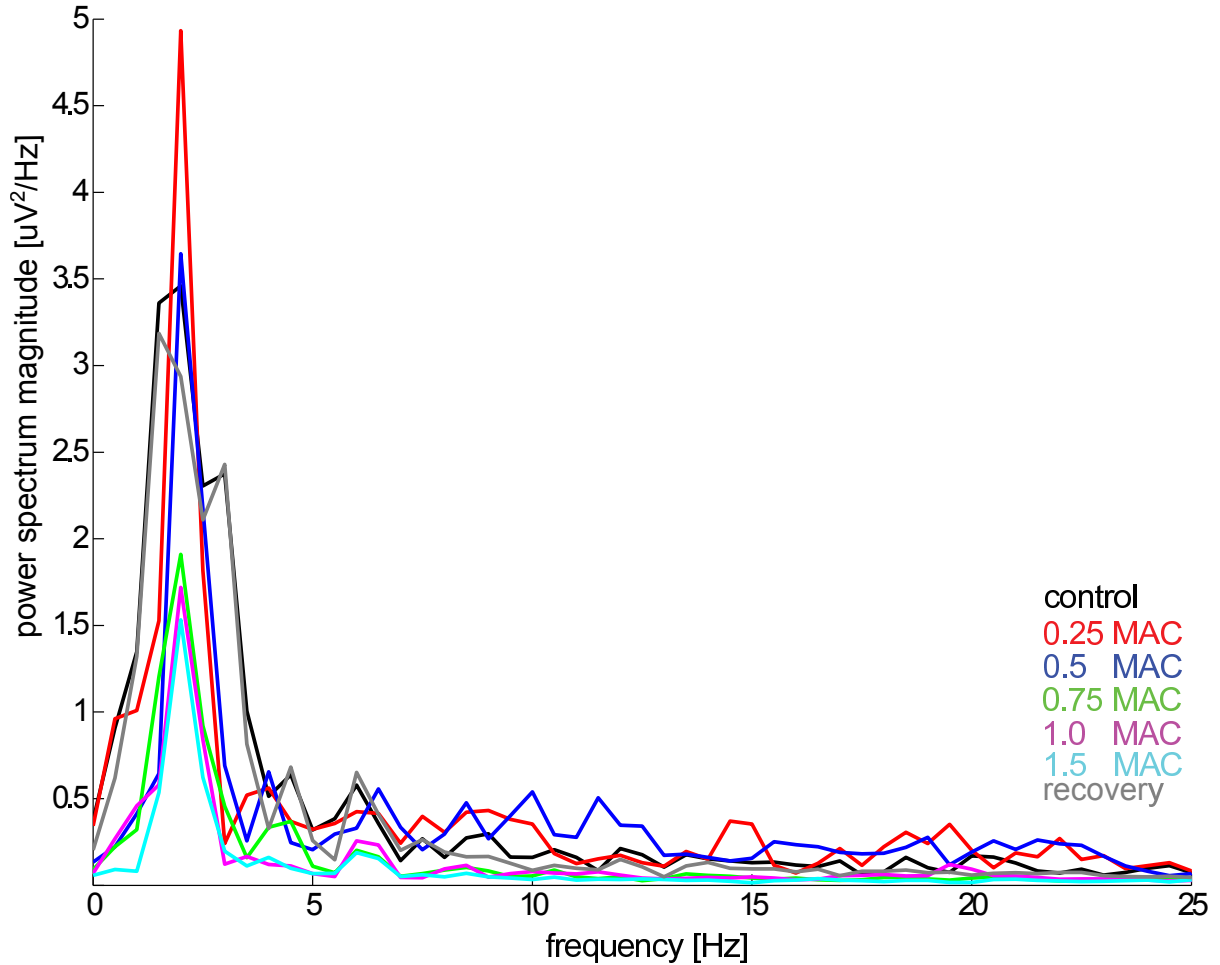


Figure 8.3: Averaged *PSD* of down-state sequences. The power spectrum shows activation especially in low frequencies for low doses (0.25 and partially 0.5 MAC) and strong inhibition at higher doses. At 0 MAC and recovery a small side peak at approx. 4 Hz is visible.

8.2 Down-state activity is different from noise

8.2.1 Results of the experiments with noise

$ApEn$ ($m = 2, r = 0.2SD$) and ORR ($m = 4$) of the noise sequences significantly differed from the parameter values obtained for the 0 MAC recordings from OTC (Wilcoxon test, white noise vs. 0 MAC: $ApEn$: $p < 0.0001$; ORR : $p < 0.0001$). For white noise, $ApEn$ was 0.86 ± 0.12 (mean \pm standard deviation) at control conditions and 1.63 ± 0.02 for the noise episodes. Hence, $ApEn$ of noise showed maximum values compared to $ApEn$ of down-states indicating less predictability. The difference between noise and LFP recordings was smaller in the ORR analyses. ORR was 0.89 ± 0.15 at control conditions and ORR of noise was 0.64 ± 0.01 . This means that white noise sequences were more chaotic than ORR of down-states. $ApEn$ of pink noise was 0.39 ± 0.05 and hence significantly lower than $ApEn$ at

0 MAC (Pink noise vs. 0 MAC: $ApEn$: $p < 0.0001$). The ORR of pink noise was 0.14 ± 0.01 which is significantly higher than ORR of LFP at 0 MAC. (Pink noise vs. 0 MAC: ORR : $p < 0.0001$). The results indicate that information content in the down-state recordings is different from white noise and pink noise.

The results indicate that information content in the down-state recordings is different from noise. The difference in $ApEn$ and ORR performance may be due to the fact that $ApEn$ mainly reflects changes in the lower frequencies of the analyzed frequency band since a tolerance is included in the detection of “similar patterns” that works like a low-pass filter. ORR may analyze the higher frequencies in the band since every data point contributes to the rank pattern generation. These experimental results seem to confirm a relevant information content in cortical down-states that differs from noise.

8.2.2 Results of the experiments with the blocked neuronal activity

In the experiments using recordings from the empty setup and blocked neuronal activity, PSD was determined in order to confirm the correct experimental setup. PSD of the recordings without cells showed a more equally distributed PSD than it was in the presence of cells (Figure 8.4), indicating increased slow frequency activity when recordings are performed from OTC with blocked neuronal network activity.

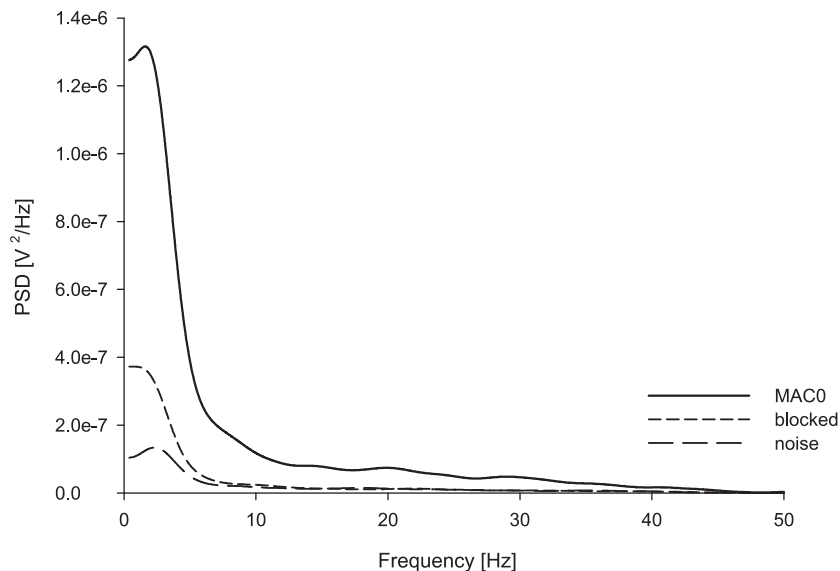


Figure 8.4: PSD at control conditions, of blocked cellular activity and recordings of background and setup noise only (empty cell). PSD was highest during control conditions at low frequencies when cells were put in the measuring container, and was still above the PSD of background noise even if their activity was blocked.

$ApEn$ ($m = 2, r = 0.2SD$) was calculated for the blocked cells and the experimental setup recordings. $ApEn$ of the recordings without cells in the tube was significantly lower than for the experiments with blocked activity (Wilcoxon test, $p < 0.05$), indicating higher information content in the cellular recordings.

8.3 Approximate Entropy of cortical down-states

The settings used for presented parameter calculation were window length $m = 2$ and tolerance $r = 0.2SD$ as recommended by for EEG analysis by Bruhn et al. (Bruhn, Ropcke et al. 2000). Other settings showed comparable results. The effects of clinically relevant concentrations of sevoflurane on $ApEn$ of cortical down-states are demonstrated in Figure 8.5. For comparison of sevoflurane effects on cortical down-states three different groups were defined: The first group is represented by the control condition, i.e., absence of sevoflurane (0 MAC), representing the cortical state “awake”. The second group is formed by low concentrations of sevoflurane (0.25 and 0.5 MAC; below concentrations corresponding to MAC_{awake}), representing “sedation”. The third group corresponds to “general anesthesia” with concentrations from 0.75 to 1.5 MAC sevoflurane (above MAC_{awake}). For both the low concentration (“sedation”) group and the high concentration group (“general anesthesia”), the $ApEn$ was significantly increased compared to control condition (Wilcoxon; 0 MAC vs. “sedation”: $p < 0.0001$; 0 MAC vs. “general anesthesia”: $p < 0.0001$, significance level $p < 0.05$, Bonferroni corrected). $ApEn$ did not indicate differences between low concentrations of sevoflurane corresponding to “sedation” (group 2) and high concentrations corresponding to “general anesthesia” (group 3).

Differentiation between anesthetic concentrations of propofol was not possible with $ApEn$ down-state analysis as displayed in Figure 8.5 in the bottom graph. P_K analysis also showed that different propofol concentrations cannot be distinguished with $ApEn$ down-state analysis. P_K values were 0.54 (0.50-0.66) for distinguishing all three propofol concentrations and 0.55 (0.50-0.70) for distinguishing propofol concentrations from control conditions. For sevoflurane P_K analysis obtained good results for $ApEn$ separating 0 MAC from sevoflurane concentrations. Further, in order to prevent dressed-up results because of the selection of three LFP episodes of at each concentration P_K was also calculated from parameter values that were averaged over the three values obtained at each culture at each concentration. Results are presented in Table 8.3. The results were not different. Accuracy

of discrimination of the single concentrations showed a rather poor result and so did the separating sedating concentrations below MAC_{awake} from concentration levels above (Table 8.2).

MAC Sevoflurane	<i>ApEn</i>
0	0.86 ± 0.12
0.25	1.11 ± 0.10 *
0.5	1.12 ± 0.14 *
0.75	1.05 ± 0.09 *
1	1.10 ± 0.07 *
1.5	1.07 ± 0.12 *

Table 8.1: *ApEn* in the absence and presence of sevoflurane calculated from 2 s LFP down-state epochs obtained from cortical OTC. *Indicates significance ($p < 0.05$, Bonferroni corrected) of an anesthetic concentration level vs. control conditions.

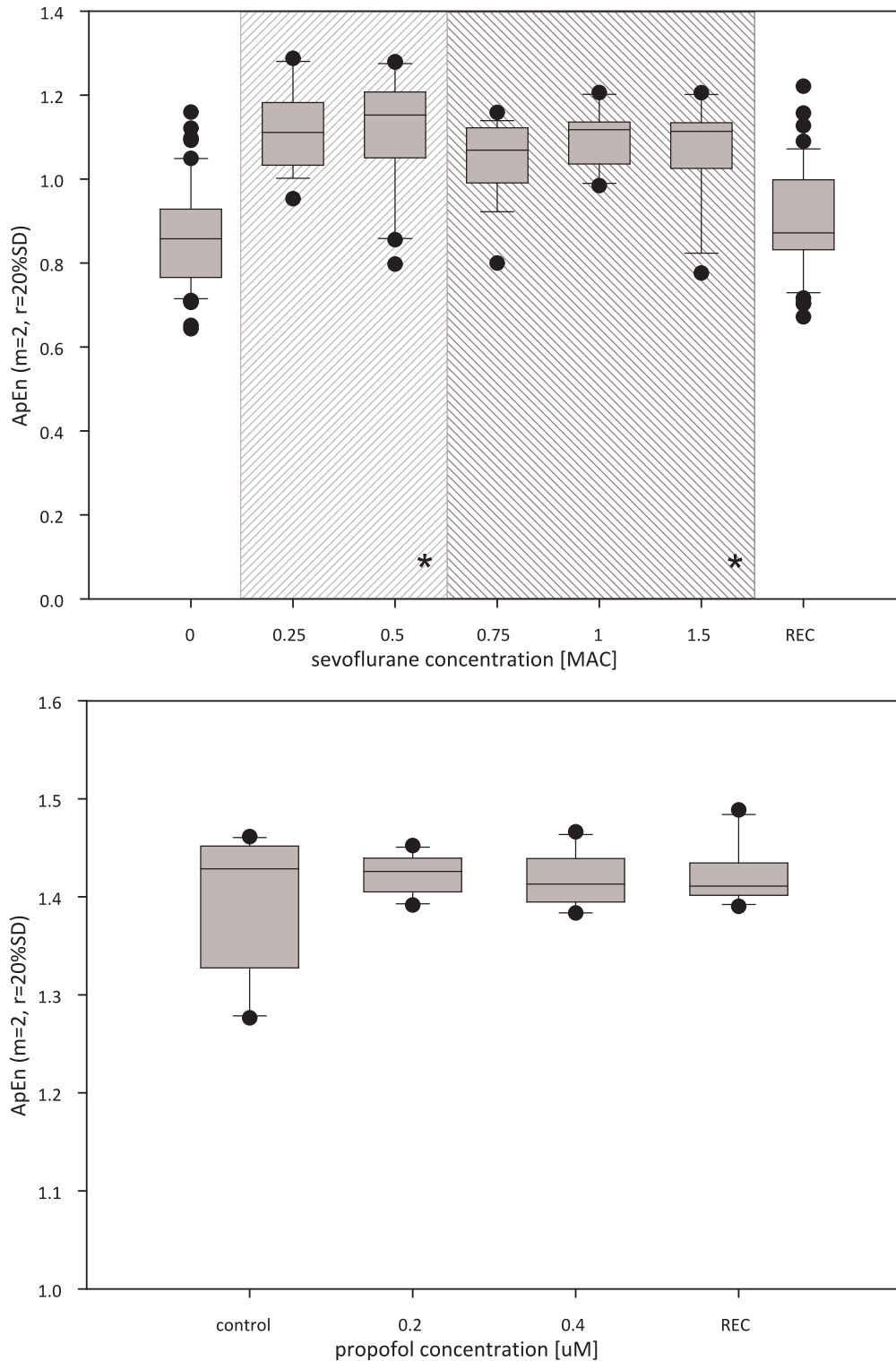


Figure 8.5: Top: $ApEn$ of down-states rises significantly with sevoflurane. *Pooled sedating concentrations (light grey) and hypnotic concentrations (grey) significantly differ from control conditions ($p < 0.05$, Bonferroni corrected). Bottom: Different propofol concentrations cannot be distinguished with $ApEn$. $ApEn$ at control conditions and recovery do not differ significantly, neither for sevoflurane nor for propofol. Higher $ApEn$ at propofol control conditions compared to sevoflurane may be explained by the different age of the OTC used for the experiments.

8.4 Permutation Entropy of cortical down-states

The obtained results are comparable to $ApEn$. Levels of sevoflurane can be significantly distinguished from the control experiments (without sevoflurane). Separation of propofol concentrations in down-states was also not possible with $PeEn$. P_K analysis revealed an acceptable separation between 0 MAC and the different sevoflurane concentrations, but it was worse than P_K of $ApEn$. Discrimination of all different levels and concentrations below versus above MAC “awake” was quite poor (Table 8.2).

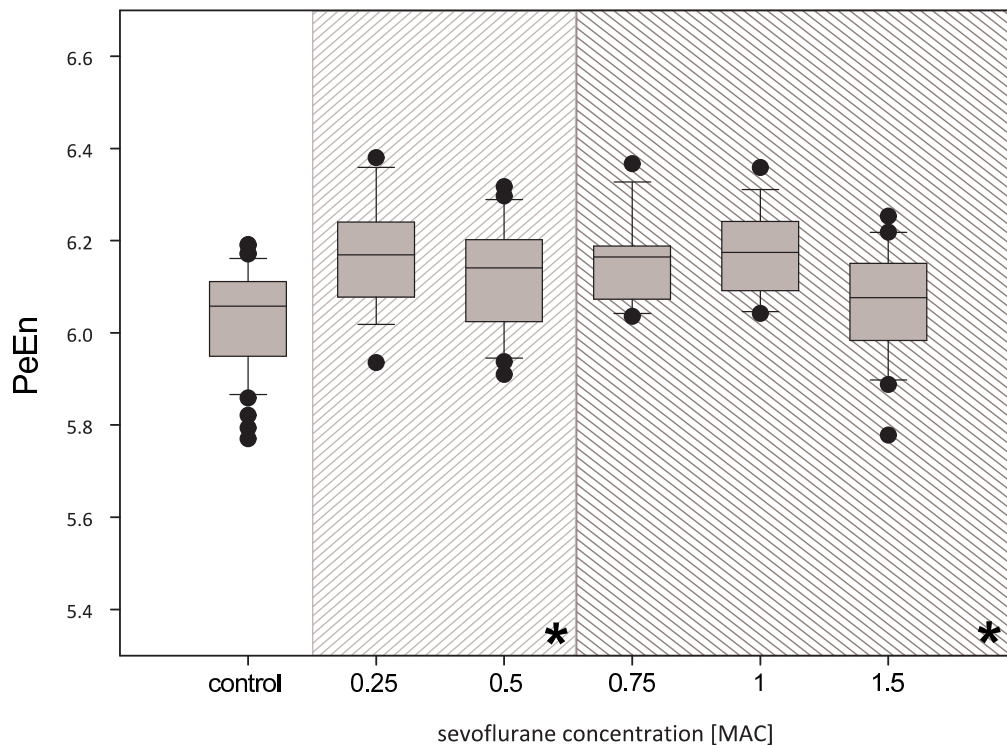


Figure 8.6: $PeEn$ rises significantly (*, $p < 0.05$, Bonferroni corrected) with sevoflurane for grouped sedating (light grey) and hypnotic (grey) concentrations.

8.5 Order Recurrence Rate of cortical down-states

The actions of sevoflurane on ORR derived from LFP down-states are displayed in Figure 8.8. In contrast to $ApEn$, the ORR did not change in the presence of low concentrations of sevoflurane (0.25 and 0.5 MAC, group 2). However, ORR decreased abruptly at concentrations higher than 0.5 MAC. ORR of sevoflurane above 0.5 MAC (group 3) was significantly different from concentrations of 0.5 MAC and below. ORR significantly decreased at concentrations ≥ 0.75 MAC. Note that this sudden switch appears at concentrations around the MAC_{awake} . Hence, this parameter might be able to reflect the

transition from “consciousness” to “unconsciousness”. P_K analysis pronounced the switch-like behavior with best P_K for separation of sevoflurane concentrations below and above the MAC_{awake} . However, in contrast to $ApEn$ and $PeEn$ discrimination of control conditions from sevoflurane was rather poor (Table 8.2).

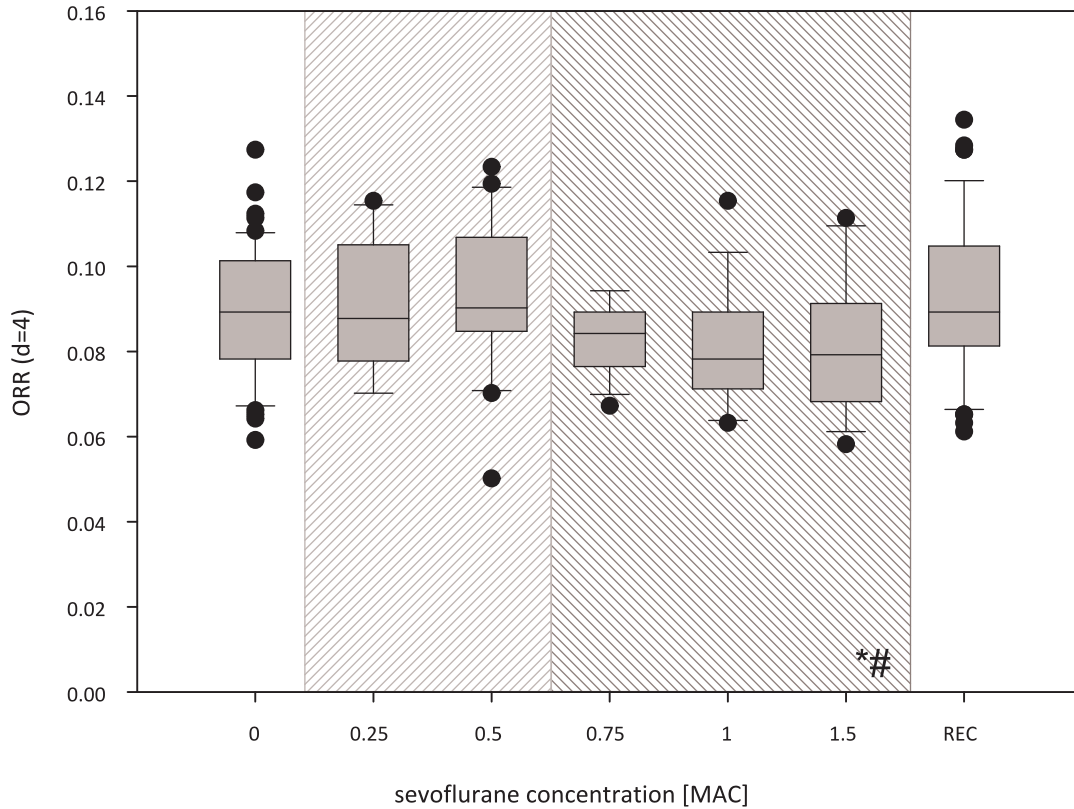


Figure 8.7: ORR ($m = 4$) significantly separates control conditions from hypnotic concentrations (*, light grey, 0.75 -1.5 MAC) as well as sedating concentrations from hypnotic concentrations (#, 0.25 & 0.5 MAC vs. 0.75 to 1.5 MAC, grey) of sevoflurane. ($p < 0.05$, Bonferroni corrected) It shows a switch-like behavior at concentrations around the MAC_{awake} . ORR at control conditions and recovery is not significantly different.

	$ApEn$		$PeEn$		ORR	
	P_K	CI	P_K	CI	P_K	CI
All levels	0.714	(0.670-0.760)	0.621	(0.564-0.686)	0.609	(0.533-0.667)
0 MAC vs. conc.	0.904	(0.844-0.952)	0.700	(0.609-0.789)	0.587	(0.508-0.684)
0-0.5 vs. 0.75-1.5 MAC	0.662	(0.566-0.747)	0.632	(0.534-0.729)	0.691	(0.598-0.776)

Table 8.2: P_K values and their confidence intervals of the different non-linear parameters for distinguishing (i) the different levels from each other, (ii) 0 MAC vs. all other concentrations and (iii) concentrations below MAC “awake” vs. concentrations above the MAC “awake”.

Average over the three segments	<i>ApEn</i>		<i>PeEn</i>		<i>ORR</i>	
	P_K	<i>CI</i>	P_K	<i>CI</i>	P_K	<i>CI</i>
All levels	0.748	(0.682-0.833)	0.631	(0.566-0.699)	0.611	(0.526-0.711)
0 MAC vs. conc.	0.939	(0.876-0.996)	0.833	(0.720-0.937)	0.567	(0.504-0.757)
0-0.5 vs. 0.75-1.5 MAC	0.690	(0.535-0.838)	0.639	(0.512-0.790)	0.737	(0.584-0.870)

Table 8.3: P_K values and their confidence intervals of the different non-linear parameters for distinguishing (i) the different levels from each other, (ii) 0 MAC vs. all other concentrations and (iii) concentrations below MAC “awake” vs. concentrations above the MAC “awake” for the parameter average of the three selected down-state episodes.

8.6 Evaluating the GABAergic effects of sevoflurane

The presented results are derived from analysis of LFP activity at control conditions with bicuculline and at 0.75 MAC sevoflurane with bicuculline. A first analysis with *PSD* showed that sevoflurane causes strong depression of slow frequencies up to about 8 Hz as displayed in Figure 8.8. *ApEn* still showed a significant effect when cells were washed with a hypnotic dose of sevoflurane and increased from 1.31 ± 0.06 (mean \pm standard deviation) to 1.36 ± 0.04 , whereas *ORR* did not but remained stable at 0.14 ± 0.02 . The parameter boxplots are presented in Figure 8.9. These results deliver another hint that *ApEn* rather analyses lower frequencies than *ORR* does. *ApEn* reflects the depression of the 0-8 Hz range and *ORR* does not detect a significant effect in the high frequencies of the analyzed range. A potential explanation for the different absolute parameter values derived from the down-state analyses and the bicuculline analyses may be the different age of the used OTC. The obtained results could lead to a hypothesis that the GABAergic effect detected with *ORR* around 0.75 MAC that is absent with bicuculline may correspond to the process of inducing hypnosis. This hypothesis needs to be further examined in the future.

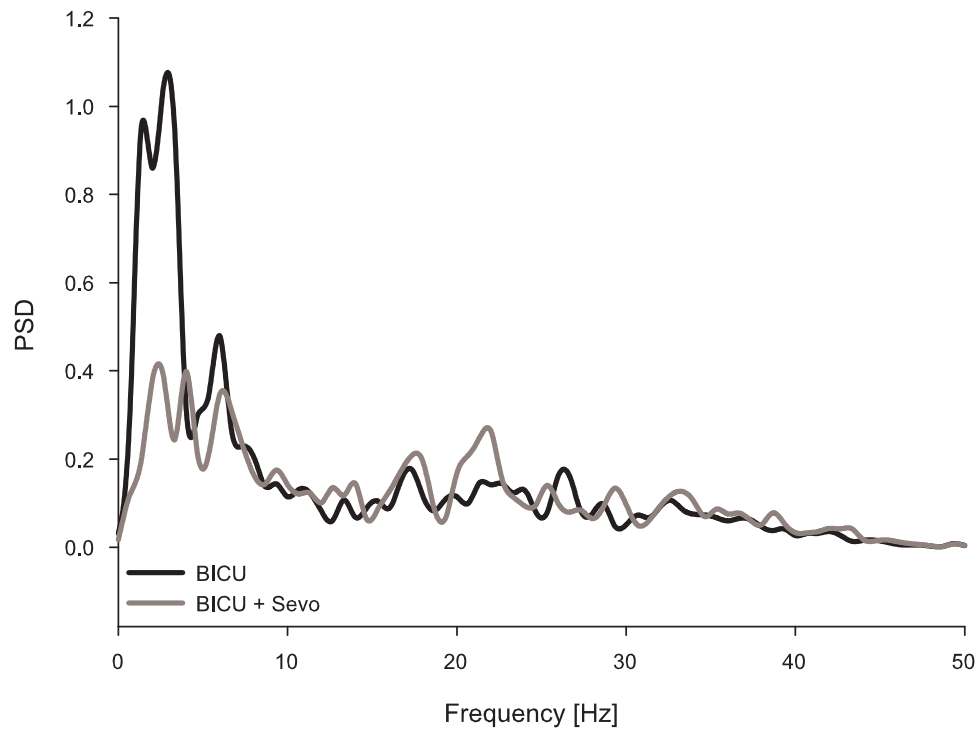


Figure 8.8: *PSD* of the recordings from cultures with the GABA antagonist bicuculline (black) and bicuculline and 0.75 MAC sevoflurane. *PSD* generally decreases as soon as sevoflurane is delivered pointing to a non GABAergic effect of sevoflurane on network activity.

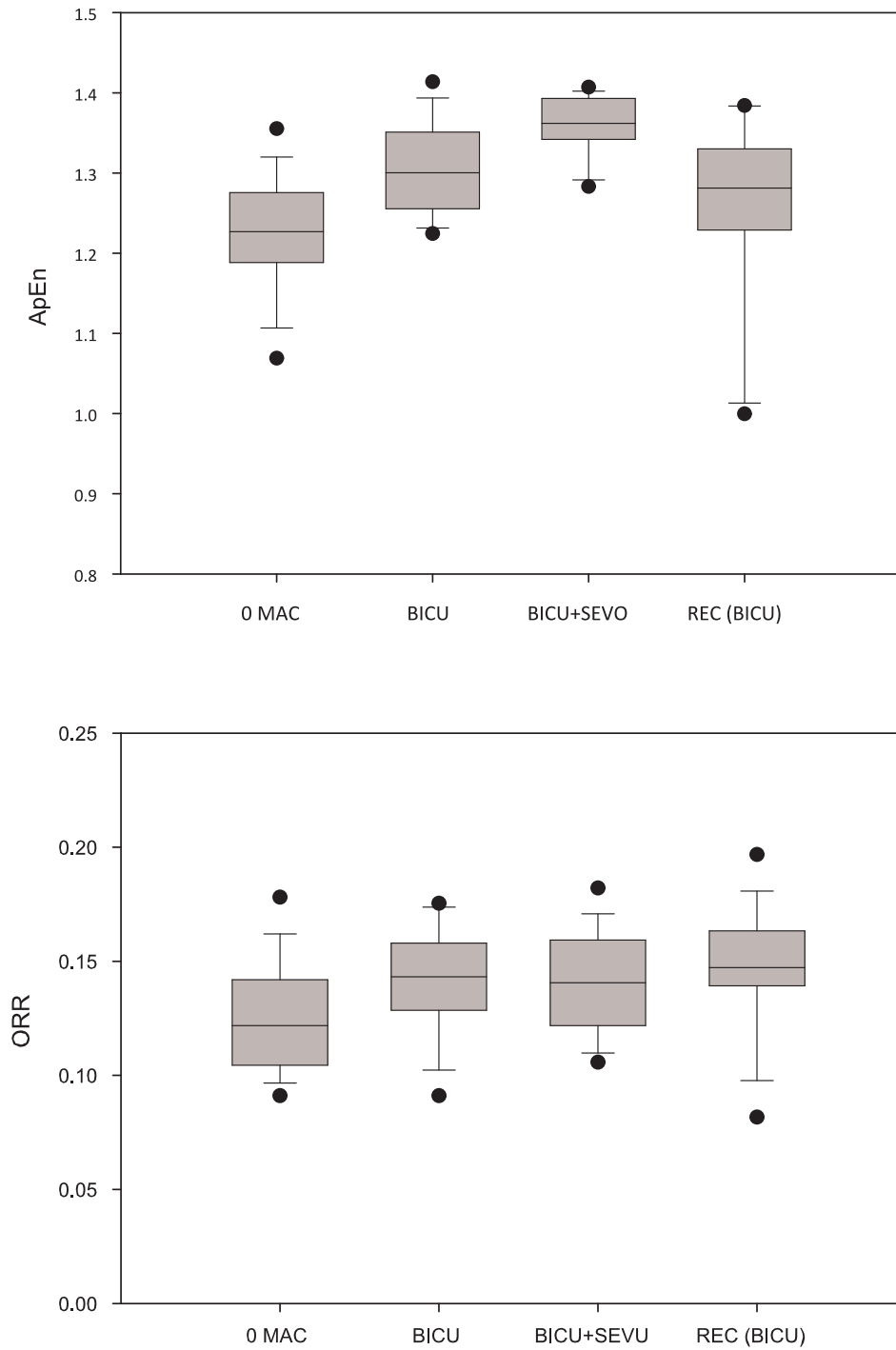


Figure 8.9: Top: Even in the presence of the GABA antagonist bicuculline $ApEn$ ($m = 2, r = 0.2SD$) shows a significant ($p < 0.05$) increase after delivery of 0.75 MAC sevoflurane, a hypnotic concentration. *Significantly different from BICU. Bottom: In contrast to the experiments without bicuculline, there is no significant effect to ORR ($m = 4$) when 0.75 MAC sevoflurane was applied.

8.7 Anesthetic-induced effects on cortical down-states *in vitro*: Discussing the results

The principal finding of these *in vitro* experiments is that the volatile anesthetic sevoflurane substantially alters neuronal activity during cortical down-states *ex vivo*. These phases of low neuronal activity have been neglected for signal analysis so far. The changes in *ApEn*, *PeEn* and *ORR* induced by sevoflurane as presented in sections 8.3 to 8.5, appearing at concentrations corresponding to sedation and levels of general anesthesia in a clinical environment indicate that the complexity of the LFP signal is increased in the presence of the volatile anesthetic. A gradual separation of different anesthetic concentrations can be observed for the presented *in vitro* down-state analysis. *ORR* as an ordinal measure has been proven as reliable measure to separate wakefulness from unconscious patients in human EEG studies (Jordan, Stockmanns et al. 2008; Jordan 2010). This behavior seems to be reflected by the sudden, switch-like change of *ORR* values at the MAC_{awake} as displayed in Figure 8.7. In contrast, propofol did not seem to affect down-state activity in a systematic and significant manner. None of the applied non-linear measures indicated a significant effect of the drug on the recorded LFP activity.

It was previously reported that volatile anesthetics prolong the duration of cortical down-states (Antkowiak and Helfrich-Forster 1998). The presented results provide evidence for marked actions of sevoflurane in isolated cortical networks during down-states. *ApEn* reacted significantly on the delivery of sevoflurane, i.e., it revealed effects primarily associated with causing sedation rather than hypnosis (section 8.3). Also *in vivo*, action potential activity was significantly reduced with sedating concentrations of volatile anesthetics (Hentschke, Schwarz et al. 2005). Furthermore, observed effects of these volatile anesthetics *in vitro* and *in vivo* were almost identical. *ApEn* reflected this sedating effect very well in the down-state sequences, but the parameter was not able to detect an effect at hypnotic concentrations. In contrast, using *ORR* made it possible to uncover the hypnotic effect of sevoflurane (section 8.5). The difference in parameter performance leads to the suggestion that sedative and hypnotic concentrations of sevoflurane have a qualitatively distinct effect on down-state activity. *ApEn* indicates less predictable signals with sevoflurane probably caused by less signal content and, hence, worse signal to noise ratio in the signal, suggesting less ordered neuronal activity possibly caused by disruption of communication in the observed neuronal network area. *ApEn* probably reflects changes in the lower frequencies, i.e., the suppression of frequencies below 5 Hz as observed in the spectrum in Figure 8.3. The *ApEn* design contains a tolerance variable r that acts in a

similar fashion than a low-pass filter, i.e., values are considered identical if they are within a defined value range, making the parameter resistant to a certain amount of noise as presented in the example in section 6.3.5. *ORR* uses the recorded absolute values of every data point for order generation without such a correcting step as described in section 6.3.4. Hence, *ORR* seems capable of analyzing higher frequencies in the recording. *ORR* detects a sudden change in signal complexity around the MAC_{awake} , i.e., the hypnotic component is evaluated. Sevoflurane initially seems to enhance GABA mediated inhibition as shown in Figure 8.8 and Figure 8.9. In the presence of the GABA_A antagonist bicuculline, *ApEn* does still expose an effect of sevoflurane on network activity, whereas the effect on *ORR* is diminished. At sedative concentrations an effect on LFP is observable but at 0.75 MAC another threshold seems to exist, causing a sudden switch in *ORR* assuming suppressed activity.

8.8 Conclusion

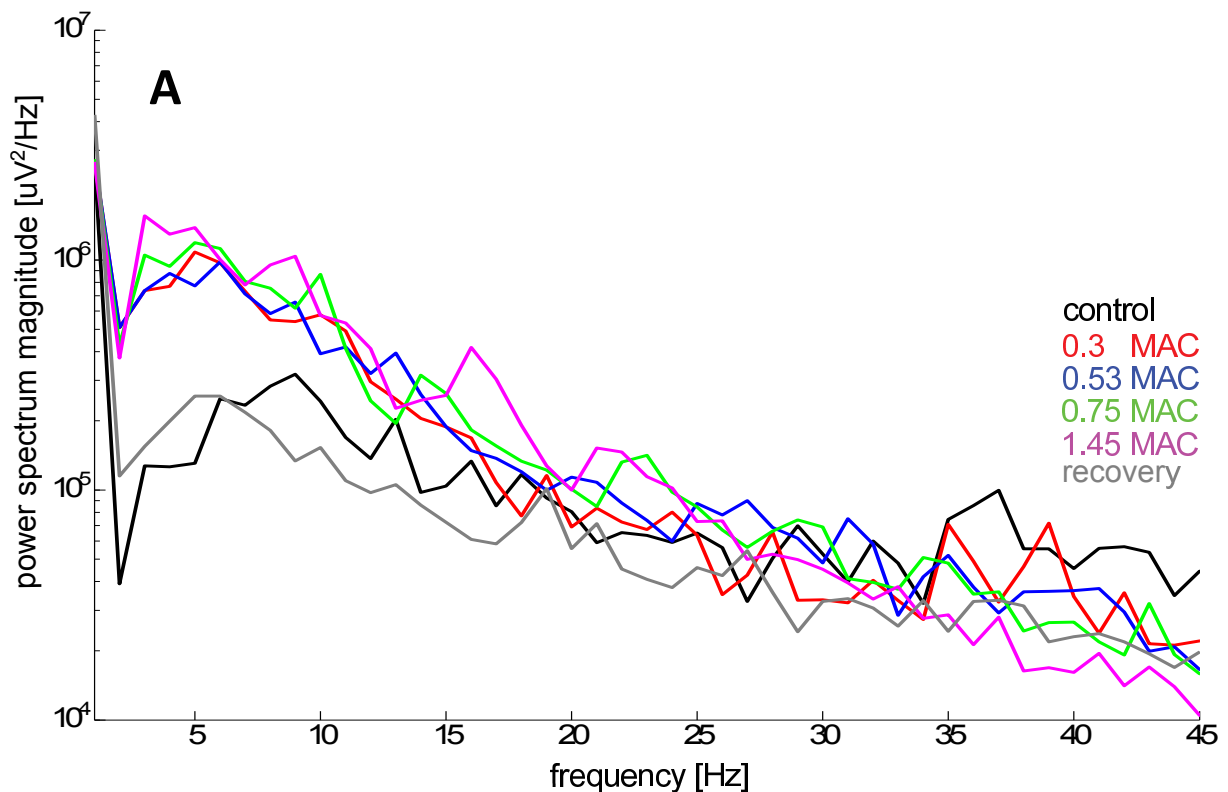
In summary, cortical down-state activity seems to be sensitive to volatile anesthetics in a concentration-dependent manner. Neuronal activity is significantly altered at sedating concentrations of sevoflurane. At hypnotic concentrations around the MAC_{awake} a sudden change in activity can be observed. This effect disappears with bicuculline, indicating a GABAergic effect at the state transition.

9 Volatile anesthetic effects on local cortical network activity *in vivo*

The results of the analyses of the data set described in section 5.2 are presented on the following pages. These results and the according discussion are also presented in part in the paper of Kreuzer et al. (Kreuzer, Hentschke et al. 2010)

9.1 Power Spectral Density

Mainly, *PSD* increased with the concentration of the anesthetic regimen and showed a good reversible effect with recovery. *PSD* increase was strongest at low frequencies in the δ - and θ -range but still visible at α - and β -frequencies. At high frequencies above 30 Hz, *PSD* was suppressed by the respective anesthetic. The results strongly differed depending on the delivered drug. Detailed courses of *PSD* for the single anesthetic regimen are displayed in Figure 9.1.



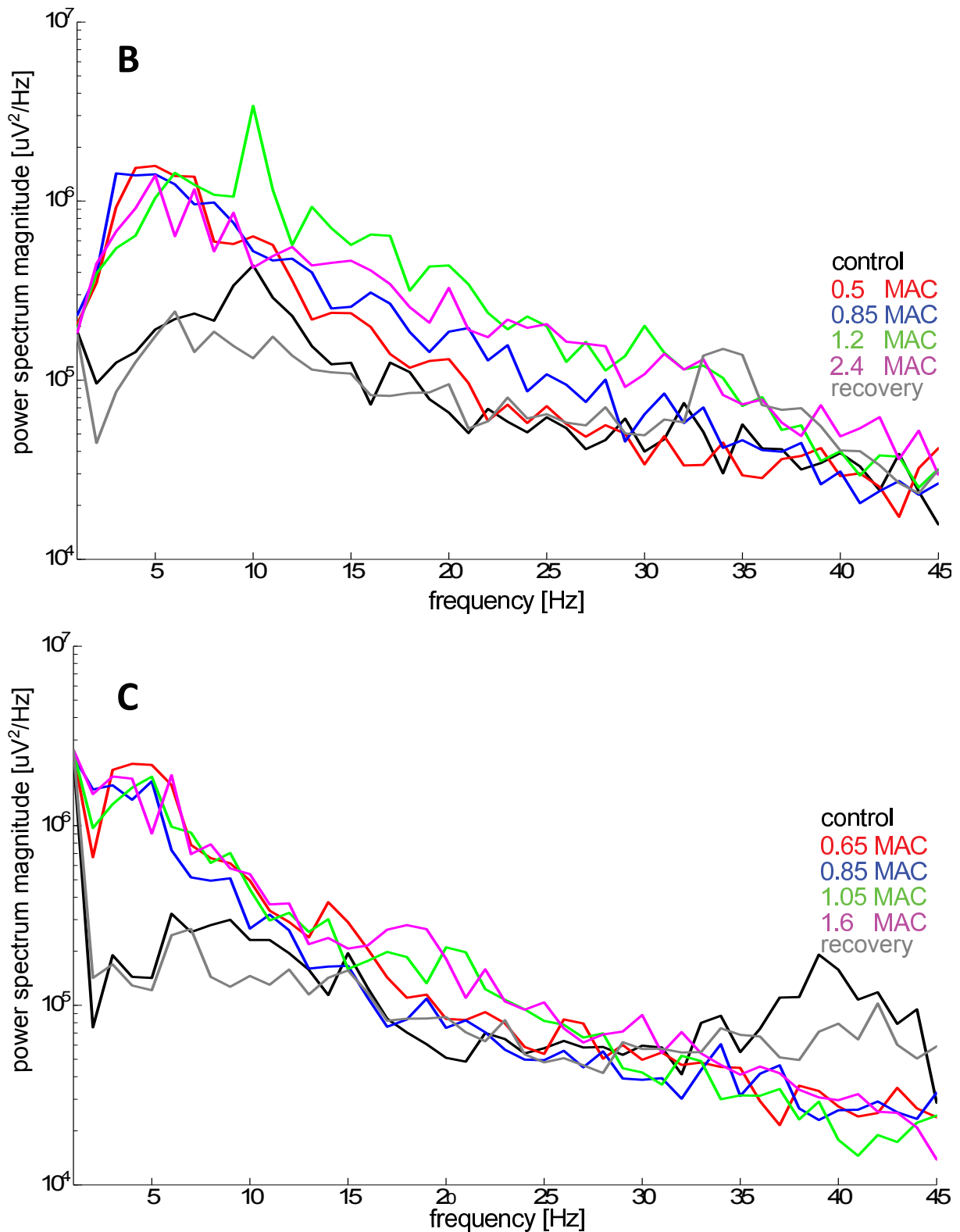


Figure 9.1: averaged *PSD* of the selected sequences for isoflurane (A), enflurane (B) and halothane (C). *PSD* differs depending on the used anesthetic agent, but generally it shows activation at low δ - to α - frequencies and suppression at high frequencies in the γ -band. Note the logarithmic representation.

9.2 Approximate Entropy, Permutation Entropy and Order Recurrence Rate

ApEn ($m=2, r=0.2SD$) decreased with increasing concentrations of the volatile anesthetics. The course of *ApEn* averaged over all channels for all three animals is displayed in Figure 9.2. For better comparison, *ApEn* values were normalized. *ApEn* at control conditions was set to 1. *ApEn* values dropped from control conditions to the first anesthetic concentration of all three regimens, followed by a smooth *ApEn* decrease to deeper anesthetic levels. *ApEn* at anesthetic concentrations could be significantly distinguished from the control recordings. In order to evaluate the potency of anesthetic-induced decrease of *ApEn* for each regimen, obtained *ApEn* values of the three animals were pooled and exponential regression was fitted according to $y = a \exp(-x/b)$. *ApEn* of isoflurane showed the steepest course with $a = 0.94(\text{std.error}:0.05)$ and $b = 0.57(0.10)$ followed by enflurane $a = 0.93(0.06)$ and $b = 0.42(0.08)$. *ApEn* for halothane had the smoothest course with $a = 0.97(0.04)$ and $b = 0.42(0.05)$. This result is consistent with the anesthetics' cortical effects found by Hentschke et al. (Hentschke, Schwarz et al. 2005). However, it stands in contrast to findings concerning the MAC, since halothane has the strongest potency in terms of MAC with a concentration ratio causing MAC values of 0.46 (halothane/enflurane) and 0.72 (halothane/isoflurane) (Drummond 1985). Adjusted R^2 values ranged from 0.89 to 0.93. Regression plots are displayed in Figure 9.3. *PeEn* ($m=5$) was calculated and averaged over all channels and all animals and showed a decrease for increasing MAC. All regimens seem to show a biphasic course with increasing *PeEn* at the highest anesthetic concentration applied. At lower concentrations enflurane caused the strongest decline of *PeEn* while halothane had the lightest effect on the parameter (Figure 9.4). This result is in concordance to the *ApEn* analyses. Halothane seems to influence signal complexity and predictability weaker than isoflurane and enflurane. *ORR* ($m=4$) tended to rise at increasing concentrations of the used anesthetic regimen also indicating more regularity. In contrast to the *in vitro* observations the switch-like behavior around the MAC_{awake} of *ORR* could not be obtained in the *in vivo* experiments. Here, the transition was not switch-like but smooth. The biphasic course at high MAC as observed for *PeEn* also occurred for *ORR*.

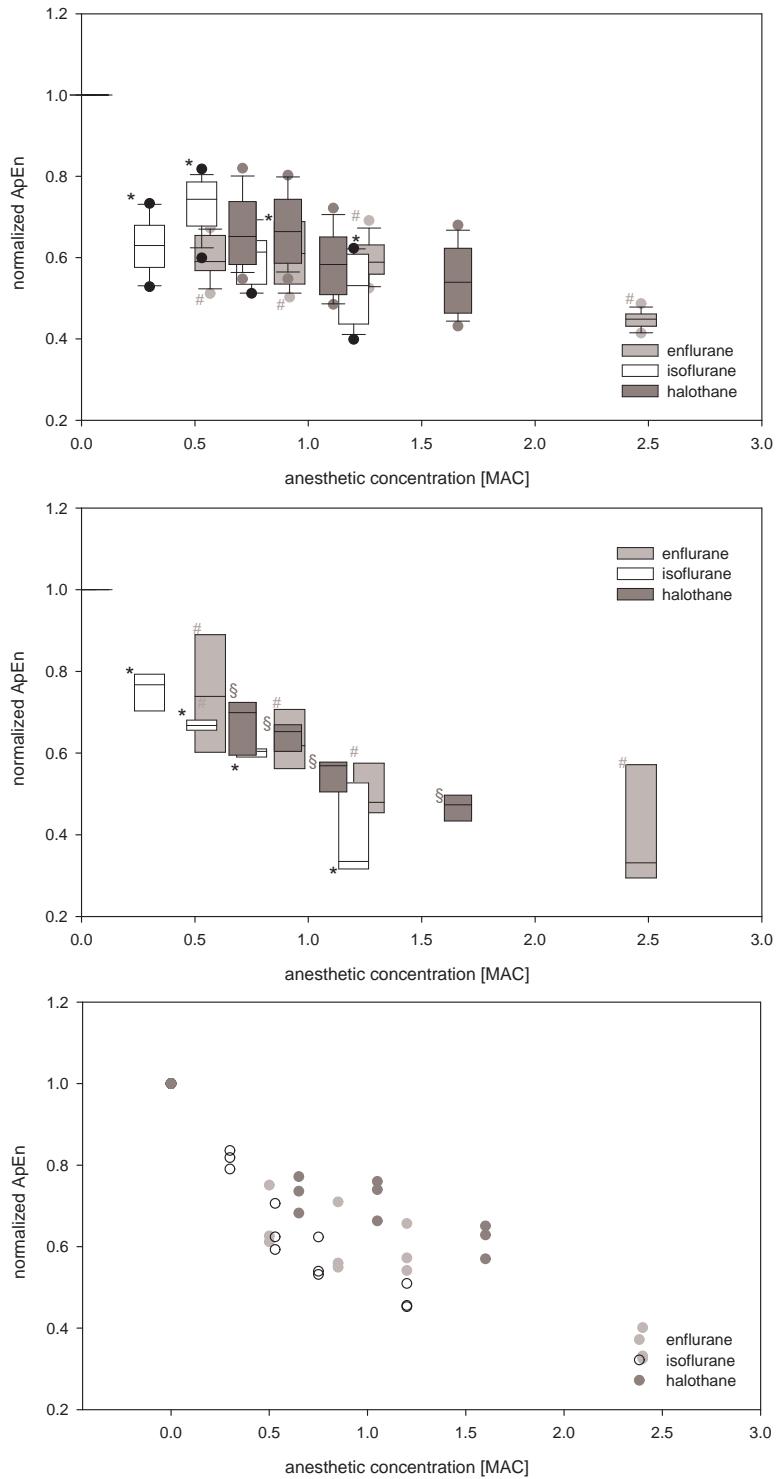


Figure 9.2: Normalized $ApEn$ ($m = 2, r = 0.2SD$) for the single recording channels in the single animals (from top to bottom: rat1, rat2, rat3). For each channel at each level the mean parameter value of the analysis of the three segments was used. $ApEn$ decreases with increasing MAC for all three regimens, whereas halothane seems to show the lightest decline. Significant difference $ApEn$ values compared to control conditions are marked with * (isoflurane), # (enflurane) and § (halothane), ($p < 0.05$, Bonferroni corrected). In rat3 we desisted from significance testing because of only three recording channels.

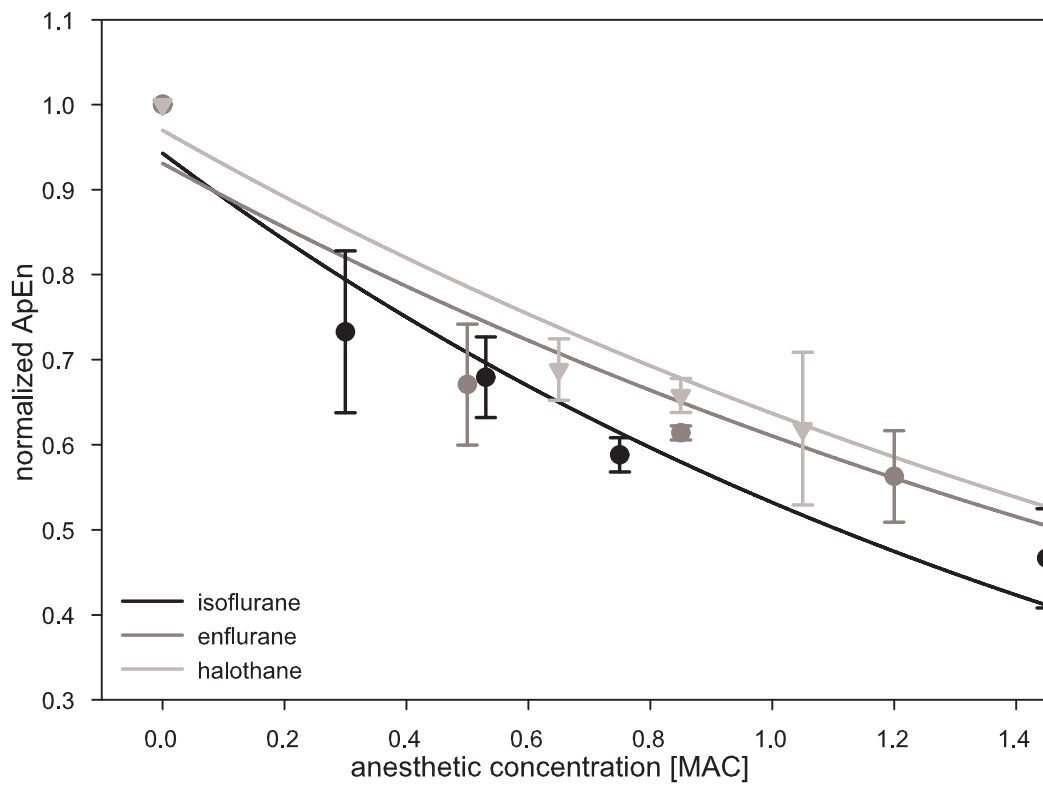


Figure 9.3: Exponential regression of $ApEn$. Isoflurane shows strongest concentration-dependent decrease.

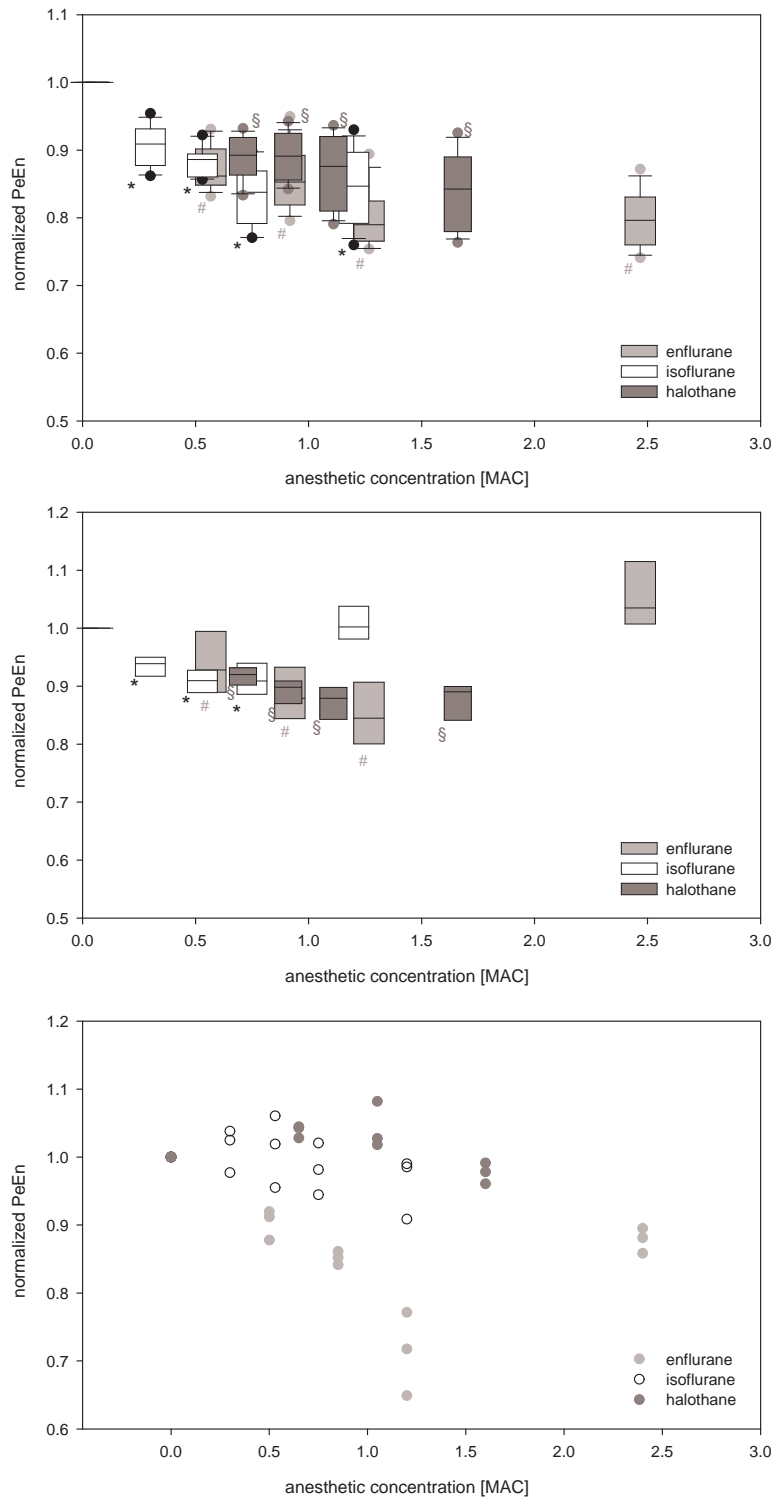


Figure 9.4: Normalized $PeEn$ ($m = 5$) for the single recording channels in the single animals (from top to bottom: rat1, rat2, rat3). For each channel at each level the mean parameter value of the analysis of the three segments was used. $PeEn$ tends to decrease with increasing MAC for all three regimens, whereas halothane seems to show the lightest decline. Significant difference $PeEn$ values compared to control conditions are marked with * (isoflurane), # (enflurane) and § (halothane), ($p < 0.05$, Bonferroni corrected). In rat3 we desisted from significance testing because of only three recording channels.

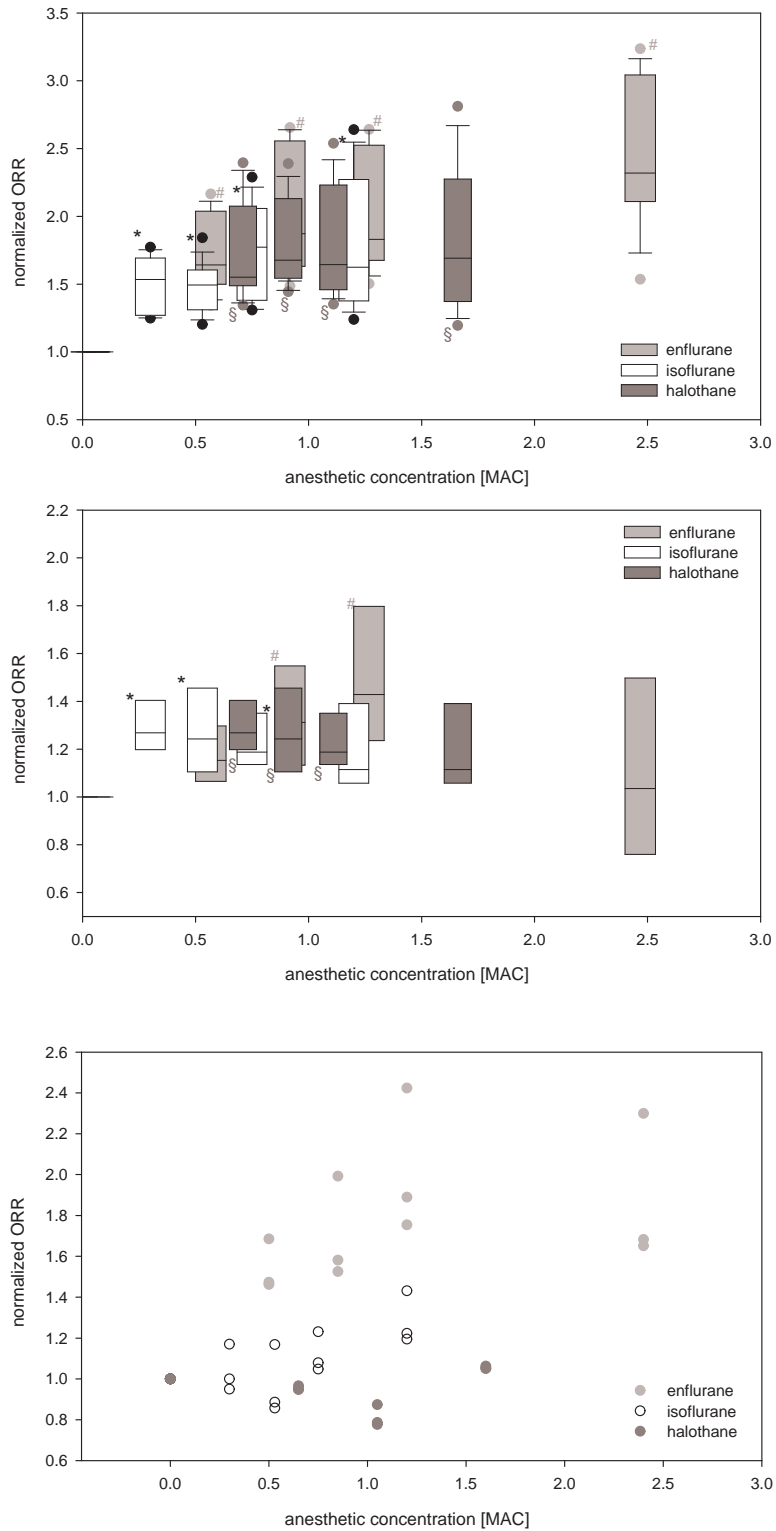


Figure 9.5: Normalized ORR ($m = 4$) for the single recording channels in the single animals (from top to bottom: rat1, rat2, rat3). For each channel at each level the mean parameter value of the analysis of the three segments was used. ORR tends to increase with increasing MAC for all three regimens, whereas halothane seems to show the lightest increase. Significant difference ORR values compared to control conditions are marked with * (isoflurane), # (enflurane) and § (halothane), ($p < 0.05$, Bonferroni corrected). In rat3 we desisted from significance testing because of only three recording channels.

9.3 Evaluation of spatiotemporal effects of volatile anesthetics on LFP with XApEn

XApEn quantifies the independence of patterns in a pair of time series. *XApEn* values were subsequently computed with $m=1$ and $r=0.2SD$ for all channel combinations as depicted in the intensity plots in Figure 9.6 (Kreuzer, Hentschke et al. 2010). This figure compares two different experimental sessions with one animal, at an interval of one day, with isoflurane and halothane administration, respectively. As can be seen most clearly under control conditions, the matrices formed fingerprint-like patterns that did not seem to depend on the spatial relations between electrodes. The patterns were quite similar in the two presented control measurements indicating that no major changes of the cortical network had occurred meanwhile. In general, *XApEn* patterns were remarkably stable over the period of several days in which the experiments were conducted: cross correlation coefficients of the normalized *XApEn* values of the control conditions ranged from 0.86 to 0.99 (median values 0.94, 0.99 and 0.99 for the three animals, each of which was subjected to three recording sessions on separate days).

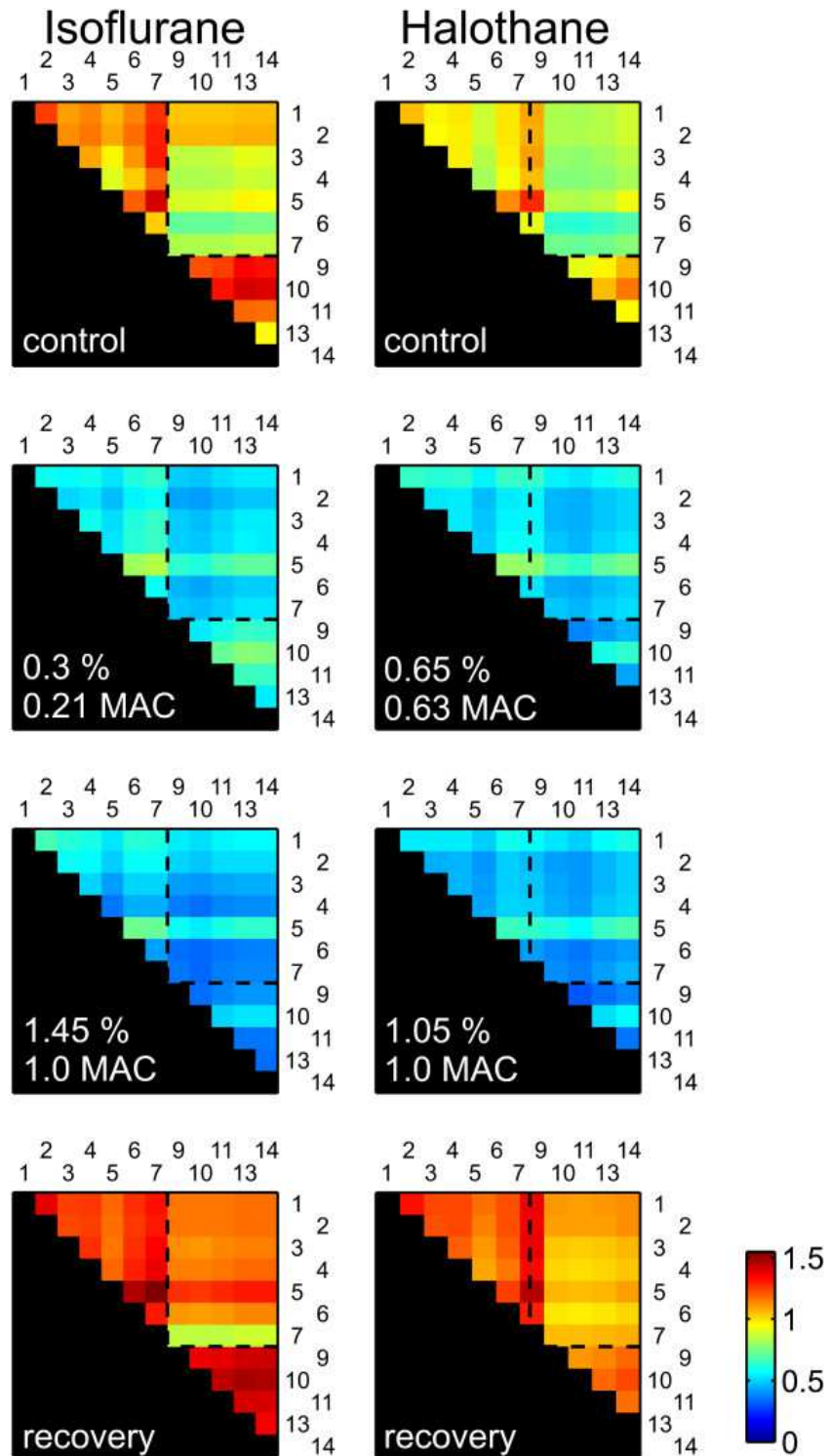


Figure 9.6: Anesthetic-induced changes of $XApEn$. Each color-coded matrix contains values obtained from non-redundant paired combinations of recording sites. The animal was exposed, in separate experimental sessions, to increasing concentrations of isoflurane (left subcolumn) and halothane (right subcolumn). Increasing blue colors indicate more similarity among the compared channels. (Kreuzer, Hentschke et al. 2010). x- and y- axis represent the single channels of the electrode array

Volatile anesthetics strongly and reversibly decreased $XApEn$. In the experiments shown in Figure 9.7, the lowest doses of isoflurane (0.3%) and halothane (0.65%) reduced $XApEn$ values to approximately 50%. Concentration increases to 1 MAC produced only minor additional changes, suggesting a non-linear dependence of $XApEn$ on anesthetic concentration. In Figure 9.7 the data points, normalized to control values, were fitted with the monoexponential function $y = \exp(-x/b)$ to obtain a dose response curve of $XApEn$ on the increasing concentrations of the volatile. The free parameter b , describing the decrease of $XApEn$ with anesthetic concentration expressed in MAC, was (95% confidence intervals in parentheses) 0.72 [0.58 0.86] for isoflurane, 0.72 [0.58 0.86] for enflurane and 1.70 [1.49 1.90] for halothane with R^2 values ranging from 0.85 to 0.91. Thus, halothane affected the cortical network less strongly than isoflurane and enflurane, in agreement with the differing action potential-depressing capabilities of the agents (Hentschke, Schwarz et al. 2005) and the results with the univariate parameters.

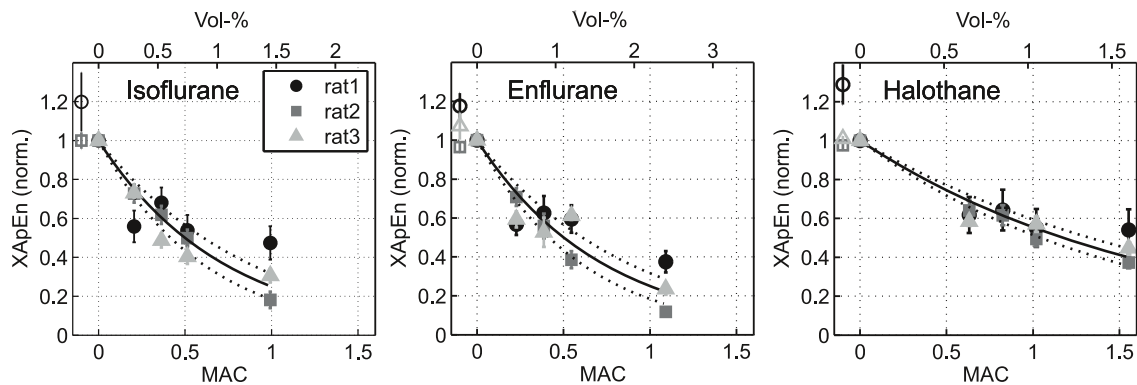


Figure 9.7: Dose-response curves of $XApEn$. Dependence of $XApEn$ on anesthetic concentration is expressed in MAC. The data points represent values from all non-redundant paired combinations of recording sites, normalized to control and averaged (\pm standard deviation). Single detached data points at negative abscissa values represent values after recovery (open symbols; no recovery data were recorded for rat 3). The lines are fits of the data to the monoexponential function $y = \exp(-x/b)$ with b as the only free parameter. Adjusted R^2 values ranged from 0.85 to 0.91, indicating that the fits were adequate. (Kreuzer, Hentschke et al. 2010)

Representative signal episodes were analyzed with $XApEn$ and Pearson's correlation to illustrate the effect of sudden signal changes compared to correlation measures (Figure 9.8). At the onset of synchronized spiking in both channels $XApEn$ reacts stronger than Pearson's correlation coefficient as displayed in Figure 9.8. The figure shows LFP excerpts recorded from three electrodes under control conditions, including the sudden appearance

of an episode of HVRS described in section 5.2.2. $XApEn$ values of all three channel combinations (Figure 9.8 B) were very similar throughout the length of the segment although their cross correlations (Figure 9.8C) differed substantially, in agreement with physical electrode distance. Moreover, $XApEn$ reacted very sensitively to HVRS, declining during this episode. Cross correlation coefficients also changed during HVRS, but the relative change was much smaller than that of $XApEn$. Thus, this analysis illustrates that $XApEn$ captures characteristics of cortical LFP activity beyond similarity as quantified by cross correlation, and emphasizes that $XApEn$ is well suited to detect changes in cortical network patterns.

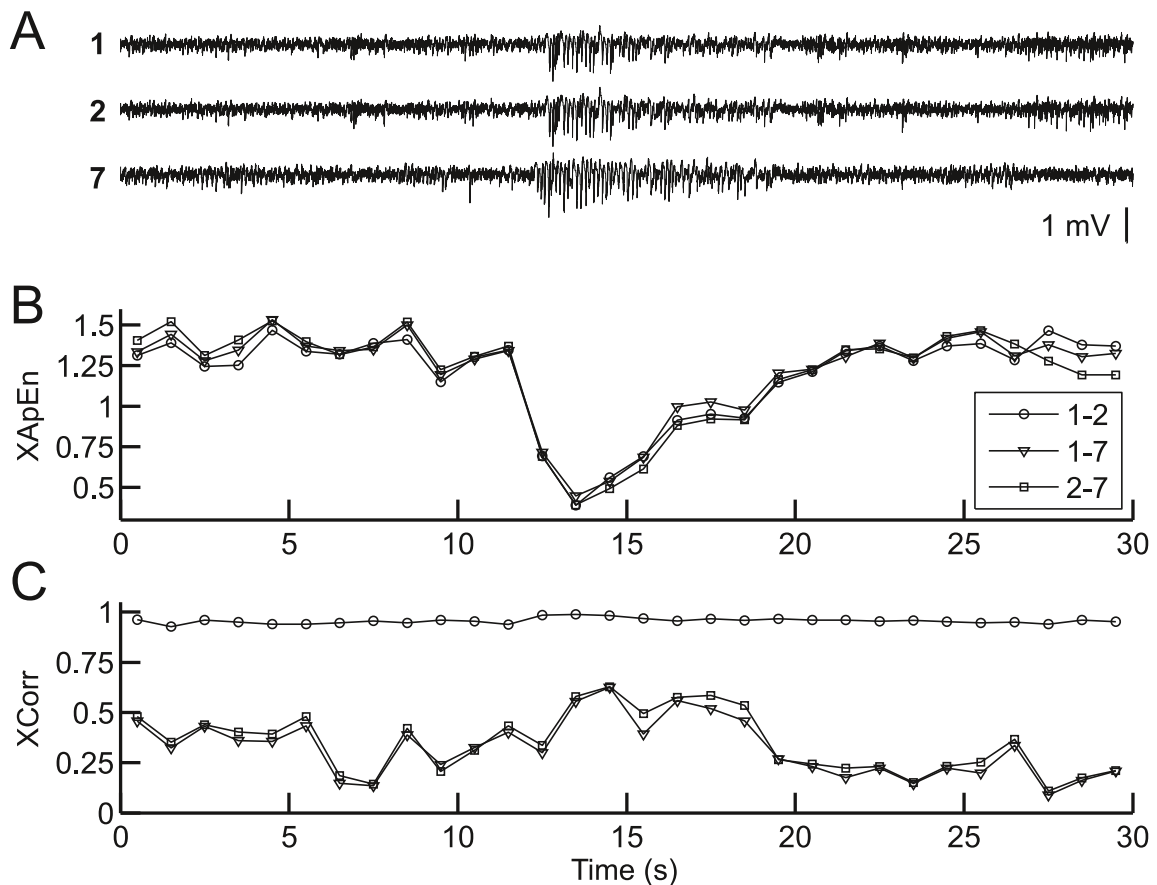


Figure 9.8: $XApEn$ compared to cross correlation: A: raw data excerpts of 30 s length from channels 1, 2 and 7 of the same recording as shown in Figure 4.2 (control condition). Note the sequence of 'high voltage rhythmic spikes' (HVRS) starting at ~12 s. B: $XApEn$ values calculated from non-overlapping 1 s sequences of all combinations of the three channels shown. C: peak cross correlation values of the same channel combinations and time intervals as shown in B. The peak of each non-overlapping 1 second segment was determined from the respective cross correlation function in an interval of ± 50 ms relative to zero lag. (Kreuzer, Hentschke et al. 2010)

9.4 Volatiles temporally and spatially affect local cortical activity: Discussing the results

Non-linear univariate analysis revealed significant changes in local cortical LFP activity. With delivery of the anesthetic agent the recorded signals become more regular (section 9.2). This change is concentration-dependent and not as abrupt as observed in the *in vitro* experiments described in section 8. With the multi-electrode design bivariate analysis with *XApEn* could also be performed. *XApEn* calculated from the LFP of closely spaced intra-cortical sites showed significant changes with anesthetic concentrations (section 9.3). This finding demonstrates that volatile anesthetics coerce small cortical sub-networks, here represented by rat barrel cortex into uniform, synchronized activity patterns.

Barrel cortex forms a large part of rodent somatosensory cortex, characterized by a one-to-one correspondence between the sensory organs (follicles at the base of the large facial whiskers) and cytoarchitectonically segregated structures in layer IV termed 'barrels' (Woolsey and Van der Loos 1970; Welker, Hoogland et al. 1988; Chmielowska, Carvell et al. 1989). This columnar, somatotopic organization results in an orderly bottom-up spread of sensory-evoked activity which, in the initial stage of processing, is spatially restricted to the discrete termination zones of the major thalamic afferents (Laaris, Carlson et al. 2000; Petersen and Diamond 2000; Petersen, Grinvald et al. 2003). Moreover, the barrel cortex and neocortex in general are also characterized by a large degree of synaptic divergence as well as interconnectivity (Braitenberg V and A 1998). Axons of pyramidal neurons may span several barrels, especially in layers II/III (Hoeflinger, Bennett-Clarke et al. 1995; Petersen, Grinvald et al. 2003), and other cortical areas including contralateral barrel cortex and form reciprocal, spatially dispersed connections (Welker, Hoogland et al. 1988; Cauller, Clancy et al. 1998). Probably owing to this high degree of cortical interconnectivity, the permanent, ongoing activity therein, unrelated to sensory input, has a spatiotemporal profile which is largely independent from the barrel architecture (Ferezou, Bolea et al. 2006; Kerr, de Kock et al. 2007). This activity was recorded and analyzed. Signal characteristics showed a dramatic and fundamental change during administration of volatile anesthetics. The decrease of *XApEn* with all three volatile anesthetics as reported in section 9.3 presented in Figure 9.7 suggests that these agents transform the diversity of synaptic inputs impinging on closely spaced pyramidal cells into a more uniform, synchronous pattern. These patterns may arise from an enhancement of GABAergic currents and a weakening of glutamatergic currents (MacIver, Mandema et al. 1996), which bias synaptic communication towards inhibition. Specifically, GABAergic interneurons likely gain in influence on cortical activity patterns by

entraining local networks to common rhythms. Both the relative insensitivity of some interneuron classes to GABAergic inhibition (Vardya, Drasbek et al. 2008) and the finding that inhibitory inputs in neighboring pyramidal neurons are more synchronous than excitatory inputs (Hasenstaub, Shu et al. 2005) are compatible with this idea. Furthermore, input via long-range connections from other cortical areas is impaired under anesthesia (Chen, Friedman et al. 2005; Kuhn, Denk et al. 2008; Ferrarelli, Massimini et al. 2010). Experimental findings on figure-ground separation in monkey visual cortex could also be interpreted along the lines of a functional disconnection of cortical areas with anesthetics (Lamme, Zipser et al. 1998). Therefore, it appears possible that the long-range excitatory synaptic inputs emanating from various cortical areas have an overall desynchronizing influence on local network activity in barrel cortex, and, by extension that the impairment of this input of volatile anesthetics contributes to more local synchrony and thus the presented decrease of *XApEn* could be observed (section 9.3).

Given that intra-cortical connections outnumber subcortical afferents (Braitenberg V and A 1998) and that volatile anesthetics alter network activity in isolated cortical networks *in vitro* (Antkowiak and Helfrich-Forster 1998) as presented in section 8, one can argue that the decline of *XApEn* was to a substantial part due to intra-cortical effects of the anesthetics. In addition, decreases in *XApEn* probably reflect the anesthetic-induced transformation of activity in subcortical areas projecting to the cortex as well. In particular the thalamus, with its intricate reciprocal connections to the cortex must be considered (Welker, Hoogland et al. 1988; Chmielowska, Carvell et al. 1989; Alkire, Haier et al. 2000). Shown to be sensitive to volatile anesthetics and prone to bursting behavior, it may imprint its activity patterns on the cortex (Steriade, McCormick et al. 1993; Detsch, Vahle-Hinz et al. 1999; Gottschalk and Miotke 2009). Other likely candidates include the basal forebrain which modulates cortical activity via cholinergic, GABAergic and glutamatergic afferents (Detari, Rasmusson et al. 1997; Manns, Alonso et al. 2003; Goard and Dan 2009) as well as hypothalamic sleep pathways (Zecharia, Nelson et al. 2009).

The three volatile anesthetics differed in their potency to alter cortical activity patterns as quantified by *XApEn* (section 9.3). While isoflurane and enflurane were indistinguishable, halothane had significantly weaker effects. This finding fits the profile of this anesthetic, which has previously been found to exert weaker effects than isoflurane on *XApEn* computed from interhemispheric EEG (Hudetz 2002) and on spontaneous action potential activity in neocortex *in vitro* and *in vivo* (Antkowiak 2002; Hentschke, Schwarz et al. 2005). In rat visual cortex, Imas et al. found an enhancement of event-related γ -oscillations at

intermediate concentrations of halothane (Imas, Ropella et al. 2004), a finding which underlines the particular characteristic of this anesthetic.

It is surprising that isoflurane- and halothane-induced changes of $XApEn$ computed from interhemispheric EEG and LFP match qualitatively so well. Hudetz et al. used a different set of filter frequencies and computational parameters (frequency range: 1-100Hz, $m = 3$; $r = 0.25SD$), so that a quantitative comparison of values may not lead to valid results (Hudetz 2002; Hudetz, Wood et al. 2003). First, although the basal mechanisms underlying EEG and LFP signals are identical – synaptic population currents in pyramidal cells giving rise to extracellular potential gradients – the populations of cells sampled from are not. EEG electrodes record potentials from a much larger population than intra-cortical electrodes. Furthermore, EEG signals are dominated by the largest dipole-generating contributors, pyramidal cells of layer V, which extend their dendrites to layer I. Intra-cortical signals, by contrast, are sampled from a restricted spatial volume (Katzner, Nauhaus et al. 2009) and thus are lamina-dependent (Kandel and Buzsaki 1997; Haslinger, Ulbert et al. 2006). Second, cortical sites separated by less than 1-2 mm as in our experiments receive a great deal of common synaptic input (Lampl I, Reichova I et al. 1999; Hasenstaub, Shu et al. 2005), and as a consequence exhibit more synchronous activity than cortical networks in different hemispheres. Thus, the qualitatively similar depression of $XApEn$ values reported by Hudetz et al. (Hudetz 2002) and in this study show that anesthetics unfold synchronizing effects on widely different spatial scales.

9.5 Conclusions

Anesthetics affect intra-cortical connections as well as cortico-cortical connections and inputs from subcortical areas. A disconnection or suppression of communication between different cortical areas is hypothesized to be a key player in the process of unconsciousness (Tononi and Edelman 1998; Buzsaki 2007; Alkire, Hudetz et al. 2008). Parallel to these cortico-cortical effects of anesthetics the presented results show an anesthetic-induced synchronization of LFP recorded intra-cortically. This synchronization of neuronal activity reduces the capability to process information. Hence, anesthetics also affect intra-cortical neuronal activity as well as long range communication between cortical areas.

10 Propofol-induced effects on cortex, hippocampus and the cortico-hippocampal pathway

The obtained results of the volatile effect on intra-cortical LFP activity was extended by another data set for which LFP were simultaneously recorded in the mouse hippocampus and prefrontal cortex at control conditions and at hypnotic propofol concentrations using a multi-electrode design as described in section 5.3. The following section focuses on the potency of bivariate non-linear analysis methods to provide further insights on the propofol-induced effects on cortical and hippocampal activity. In intra-cortical multi-electrode recordings *in vivo*, derived from rat neocortex, *XApEn* revealed increasing regularity among the channel recordings when volatile anesthetics were administered as described in section 9. One major finding of these experiments presented in the previous chapter was that despite an anesthetic effect on LFP activity the functional structure of the observed cortical networks cut-out was not affected (Kreuzer, Hentschke et al. 2010). Working hypothesis for this section was that the used parameters are able to detect and quantify an effect caused by propofol on neocortical and hippocampal LFP activity and that an effect on cortico-hippocampal communication pathways can be detected. The results of the performed analyses are presented on the next pages.

10.1 Power spectral density

In the *PSD* analysis a prominent shift of hippocampal peak frequencies from 8 to approximate 5 Hz could be observed. In the neocortex, this shift could not be observed, but *PSD* increased in the 2 Hz range. The detailed spectra of the considered frequencies are displayed in Figure 10.1.

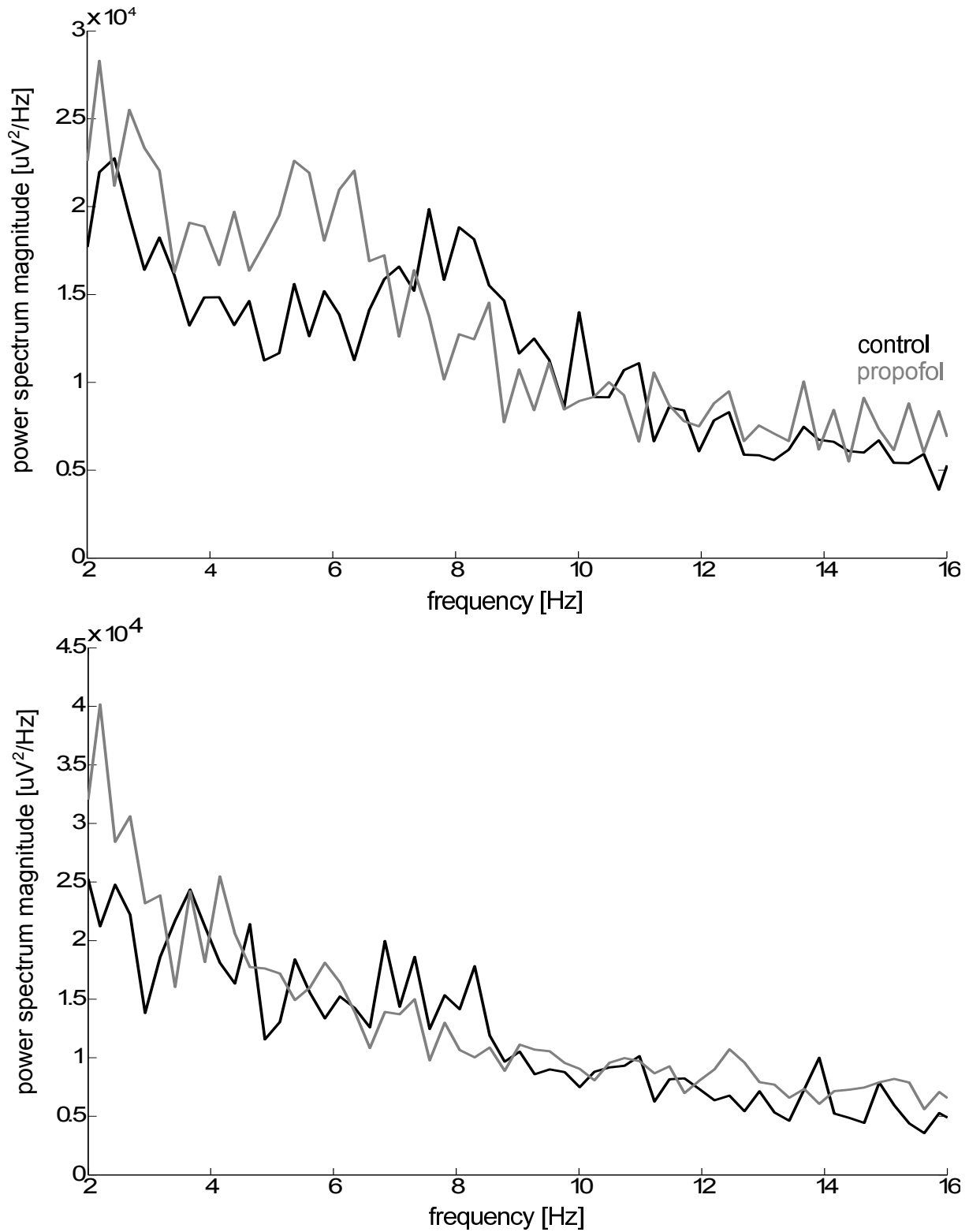


Figure 10.1: Propofol-induced modification of *PSD* in the 2-16 Hz range in the hippocampus (top) and the neocortex (bottom) at control conditions (black) and after delivery of propofol (grey). Besides the increase in the spectral power at very low frequencies ~2 Hz there are no changes in the neocortical power spectrum, whereas in the hippocampus a clear shift of peak frequency from approximately 8 to about 5 Hz is visible.

10.2 Cross Approximate Entropy

$XApEn$ ($m = 1, r = 0.2SD$) was calculated for all channel combinations within neocortex or hippocampus and for all combinations between those areas in the θ - and α -range. No significant effect of propofol on neocortical LFP could be detected in both frequency ranges. In the hippocampus α -oscillations seemed not affected but $XApEn$ significantly decreased for the θ -band analysis ($p=0.02$) indicating higher predictability. The same result could be observed for $XApEn_{hipp \leftrightarrow ncx}$ ($p=0.004$). Only θ -oscillations were significantly influenced, indicated by lower $XApEn$. Averaged $XApEn$ is listed in Table 10.1. Furthermore, to allow comparison regarding $XApEn$ derived from *in vivo* experiments with volatiles in section 5.2 the cortical and the hippocampal channels were analyzed with $XApEn$ after a 100 Hz low-pass filtering. Representative boxplots of the single recording sessions averaged over all channel combinations within hippocampus or prefrontal cortex are shown in Figure 10.2. Neither in the hippocampus nor in the cortex a significant effect of propofol could be detected. Based on these results no further analyses were performed with this parameter in this section. One remark should be made that $XApEn$ could not reveal an effect of intra-cortical recordings *in vivo* for propofol. This is in accordance with the *in vitro* findings presented in 8.3.

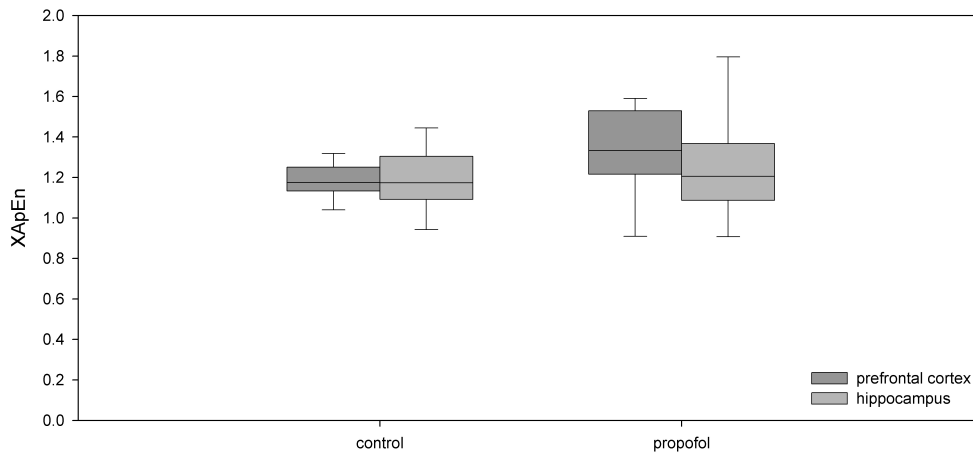


Figure 10.2: Boxplots of $XApEn$ analysis after 100 Hz low-pass filtering at control conditions and at hypnotic concentrations of propofol. No significant effect in the cerebral regions could be detected.

10.3 Bivariate Permutation Entropy

In the hippocampus, $BPeEn$ ($m=5$) averaged over all channel combinations was significantly affected in the θ -, α - and β - frequency ranges. $BPeEn_{hipp}(\theta)$ decreased from 4.59 (0.13) (mean(SD)) to 4.44 (0.19) ($p=0.02$) and the β -band showed a decrease in $BPeEn_{hipp}(\beta)$ from 7.63 (0.12) to 7.43 (0.16) ($p=0.02$). $BPeEn_{hipp}(\alpha)$ increased with propofol from 5.48 (0.18) to 5.75 (0.14) ($p=0.01$) and indicated higher irregularity among the channels. In the neocortical recordings, only the regularity in the α -band increased significantly, i.e., $BPeEn_{ncx}(\alpha)$ increased from 5.56 (0.20) to 5.73 (0.19) ($p=0.03$). Propofol induced changes in the other analyzed frequencies were not significant. Figure 10.3 displays the change of $BPeEn$ for all hippocampal channel combinations in the frequency bands, where a significant result could be obtained, as Figure 10.4 does it for the neocortical α -band. Functional structures seem to be unaffected by propofol in θ - and α -bands as displayed in the two figures, similar to the experiments from section 8. Analysis of $BPeEn_{hipp \leftrightarrow ncx}$ revealed no significant influence of propofol on $BPeEn_{hipp \leftrightarrow ncx}(\theta, \alpha)$, i.e., among the average of all neocortical-hippocampal channel combinations. Nevertheless, the plots in Figure 10.5 reveal a decreasing trend indicated by the sign test of $BPeEn_{hipp \leftrightarrow ncx}(\theta)$ and an increasing trend of $BPeEn_{hipp \leftrightarrow ncx}(\alpha)$, i.e., signals between hippocampus and neocortex become more regular in the θ -range and more irregular in the α -range. A detailed list of the propofol induced $BPeEn$ changes is presented in Table 10.1.

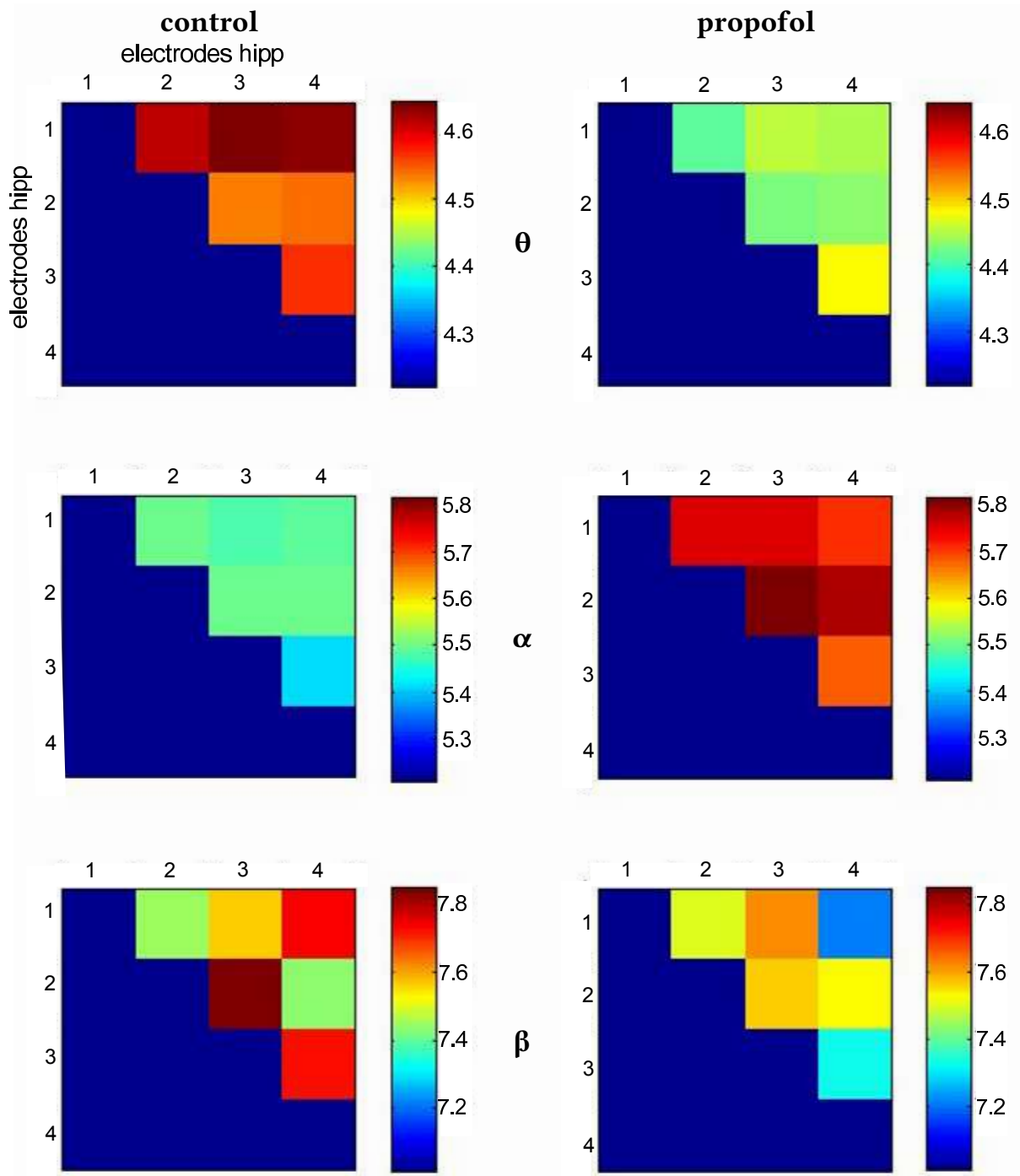


Figure 10.3: Propofol-induced, significant changes of *BPeEn* in the θ - (top), α - (middle) and β - (bottom) range in the hippocampus. Data presented in the left column were obtained during control conditions and in the right column after delivery of propofol. Channels become more regular in the θ -range and more irregular in the α -range for all channel combinations, whereas in the β -range *BPeEn* significantly decreases but the pattern is not as specific as observed for the other two slower frequencies.

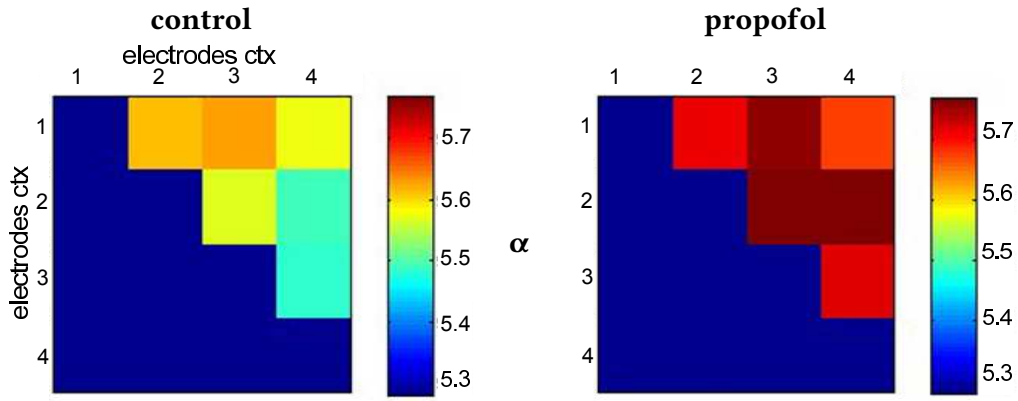


Figure 10.4: Propofol-induced, significant change of *BPeEn* in the α -range in the neocortical region. Left column was obtained during control conditions, the right one after delivery of propofol. Channels become more irregular in the α -range for all channel combinations.

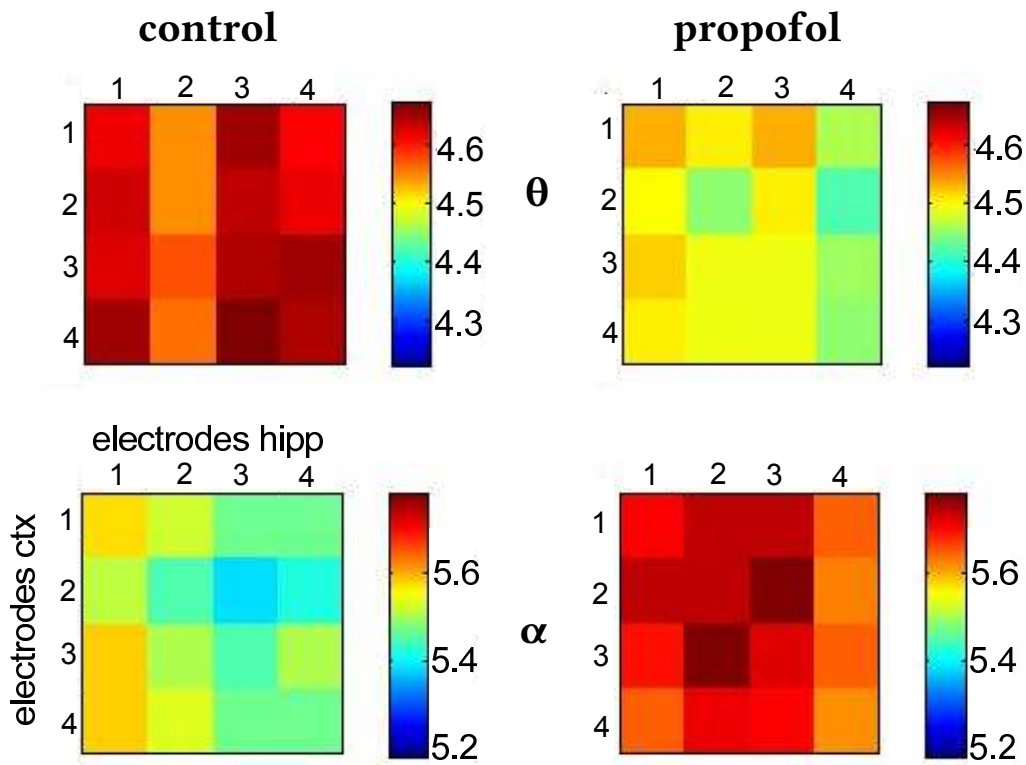


Figure 10.5: Propofol-induced, significant change of *BPeEn* in the θ - (top) and α -range (middle) between all hippocampus-neocortex channel combinations. Results in the left column were obtained during control conditions, in the right one after delivery of propofol. Channels become more regular in the θ -range and more irregular in the α -range for all channel combinations.

10.4 Symbolic Transfer Entropy

sTE ($m = 3, \tau = 5, \delta = 6$) was applied on all possible channel combinations within hippocampus and neocortex as well as on all combinations between these areas. Within the single areas, i.e. the channel combinations in the hippocampus or channel combinations in the prefrontal cortex, no significant results could be obtained. Only $sTE_{hipp}(\alpha)$ revealed a trend, indicated by the sign test, that information transfer within the hippocampus decreases with propofol. In contrast to the $BPeEn$ observations between hippocampal and neocortical areas, a significant effect on the α -band and a strong trend in the θ -band could be revealed. Between those areas information transfer decreased significantly with propofol, $sTE_{hipp \leftrightarrow ncx}(\alpha)$ from 0.30 (0.10) to 0.18 (0.09) ($p=0.02$) and $sTE_{hipp \leftrightarrow ncx}(\theta)$ decreased not significantly by means of the paired Wilcoxon test, but still by means of the sign test from 0.41 (0.16) to 0.30 (0.19) indicating a declining trend. All sTE results of the averaged channel combinations are displayed in Table 10.1.

	<i>Hipp</i>		<i>ncx</i>		<i>hipp ↔ ncx</i>		
		θ	α	θ	α	θ	α
<i>XApEn</i>	control	1.90(0.04)	2.09(0.04)	1.82(0.05)	2.06(0.06)	1.88(0.03)	2.08(0.05)
	propofol	1.77(0.11)	2.07(0.07)	1.71(0.27)	1.93(0.31)	1.73(0.15)	2.05(0.06)
<i>BPeEn</i>	control	4.59(0.13)	5.48(0.18)	4.61(0.14)	5.56(0.20)	4.62(0.08)	5.49(0.19)
	propofol	4.44(0.19)	5.75(0.14)	4.50(0.23)	5.73(0.19)	4.49(0.18)	5.68(0.22)
<i>sTE</i>	control	0.45(0.24)	0.36(0.12)	0.25(0.10)	0.20(0.07)	0.41(0.16)	0.30(0.10)
	propofol	0.43(0.32)	0.23(0.12)	0.25(0.13)	0.20(0.11)	0.30(0.19)	0.18(0.09)

Table 10.1: $BPeEn$ and sTE values (mean (standard deviation)) for the different analyses within and between the different regions. Displayed values represent the average over all channel combinations. Significant changes caused by propofol are printed in bold numbers. Non-significant changes that still reveal some propofol-induced trend are kept in bold and italic numbers.

The change in the single-channel combination sTE within and between the areas is presented by the intensity plots in Figure 10.6.

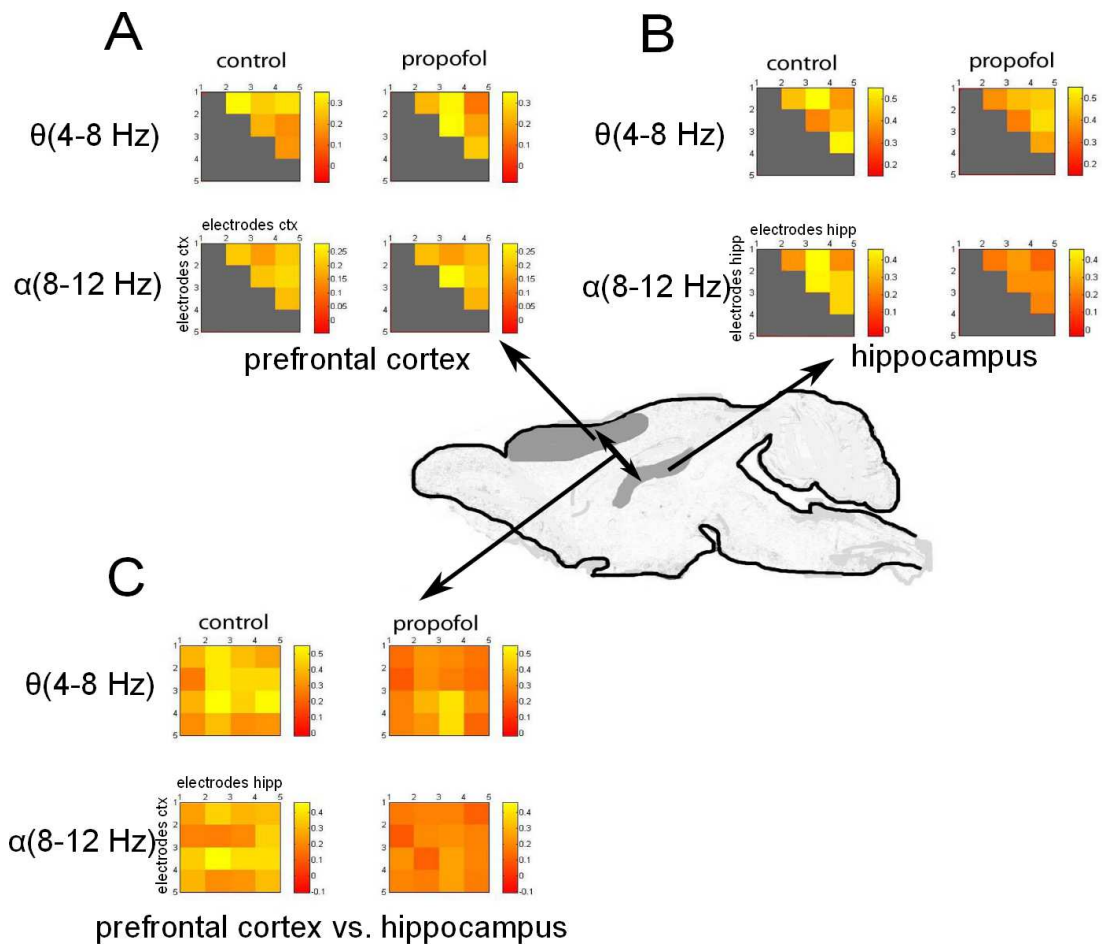


Figure 10.6: sTE in the θ - and α -range for all channel combinations within neocortical (A) and hippocampal regions (B) and between both areas (C). Within the single recording areas sTE does not alter significantly with delivery of propofol. Information flow, detected with sTE , significantly decreases between hippocampus and neocortex with propofol in the α -range. At θ -frequencies, sTE also decreases, but not significantly. Still, a trend can be revealed with a significantly decreasing result derived from the sign test whereas there is no unitary change in sTE (θ) within the areas.

10.5 Propofol affects the cortico-hippocampal pathway: Discussing the results

Neocortex and hippocampus are among the regions of the brain that are most sensitive to anesthetics and α - and θ -oscillations seem to represent key oscillations which structure the interaction between neuronal clusters in different brain regions (Butovas, Rudolph et al. 2010). The obtained results presented in sections 10.2 to 10.4 showed a significant effect of propofol on inter-channel LFP that can be revealed with different non-linear approaches such as *XApEn*, *BPeEn* and *sTE*. Analysis of the recordings with *XApEn* did reveal significant effect of propofol on hippocampal and hippocampal-neocortical θ -oscillations (section 10.2). Since *XApEn* or the univariate base *ApEn* are designed to analyze effects in time series of low complexity, one might suggest that the recordings in our experiments in the α -range had too complex signal characteristics. Another reason for the poor performance of *XApEn* may be caused by the chosen anesthetic regimen, propofol. Propofol may have a different effect on neuronal network activity in the cortex. For example, propofol and sevoflurane affect LFP recorded from cortical co-cultures *in vitro* differently (Antkowiak 1999). Also the analyses from section 8 revealed different effects of sevoflurane on isolated cortical network down-state activity. For the sevoflurane group, a significant effect on *ApEn* could be detected, whereas with propofol no separation between propofol and control conditions could be determined as described in section 8.3 (Kreuzer, Schneider et al. 2008; Drexler, Kreuzer et al. 2013). Further, as presented in section 10.3 the LFP data recorded from hippocampal and prefrontal cortical areas were also analyzed with *BPeEn*, a parameter that seems more suitable for complex signals (Bandt and Pompe 2002). With *BPeEn* analysis it was possible to reveal significant propofol induced effects among the channels within one recording area, i.e., all hippocampal channel combinations as well as all cortical channel combinations. The decrease of $BPeEn_{hipp}(\theta)$ and $XApEn_{hipp}(\theta)$ might be caused by the observed shift of spectral power peak frequency from the α -range to the slower θ -band. The increased power in the θ -band indicates that there is more synchronous activity going on in this frequency range, i.e., the recorded signals become more regular and the parameter values decrease. The shift towards slower frequencies in presence of anesthetic drugs was also observed by Perouansky et al. (Perouansky, Rau et al. 2010). Hippocampal function and hence learning is impaired, when θ -peak frequency drops below 6.5 Hz (Pan and McNaughton 1997). The drop in hippocampal $BPeEn(\theta)$ seems to represent less hippocampal integration and hence reflects impaired functionality of the hippocampus with propofol. In contrast, $BPeEn(\alpha)$ increases in neocortex and hippocampus, pointing towards more irregularity between the channels in the areas. There seems to be evidence for

the existence of an hippocampal-cortical network in the α -range responsible for stimuli processing (Schürmann, Demiralp et al. 2000). If synchrony within the hippocampus and neocortex decreases in the α -range, information pathways might be disrupted by propofol leading to increased *BPeEn* values. *sTE*, a parameter that evaluates the amount of information flow shows significant decrease of transferred information content between hippocampus and neocortex in both frequency bands with propofol as presented in section 10.4. Especially the prefrontal cortex is important for working memory but working memory tasks require intense interactions between different brain areas (Butovas, Rudolph et al. 2010). Siabas et al. found out that θ -entrained activity, here 4-10 Hz, across cortico-hippocampal circuits may be important for gating information flow and for guiding the plastic changes that are believed to underlie the storage of information across these networks (Siapas, Lubenov et al. 2005). Another hint for the importance of α -/ θ -oscillations comes from Paz et al. Their results indicated a strong role of θ -oscillations (here 4.5-10 Hz), generated in the hippocampus for synchronizing medial prefrontal cortex cells during learning tasks (Paz, Bauer et al. 2008). When it comes to animal studies with lower mammals, mice in this thesis, hippocampal θ -oscillations, here 5-11 Hz, seem to influence cortico-cortical long range synchronization in these animals, i.e., the hippocampus as mediator of these synchronizations might facilitate the control mechanisms of attention (Gollo, Mirasso et al. 2011). If θ -oscillation velocity is responsible for learning and perception tasks, i.e., slower θ -oscillations impair and faster θ -oscillations improve the performance (Perouansky, Rau et al. 2010), the decrease of information flow might be caused by the propofol induced left shift of θ -peak frequency in the hippocampus. Within the hippocampus α -information transfer is reduced with propofol, which most probably is also caused by slowing of prominent oscillations to the θ -range.

10.6 Conclusion

In summary calculation of bivariate, non-linear parameters is suitable to reveal anesthetic-induced effects in inter-channel regularity and information transfer between two recording sites. θ - and α -oscillations in the hippocampus are strongly affected by propofol. While θ -oscillations become more regular among the channels, α -regularity decreases as does the information transfer between hippocampus and prefrontal cortex in both frequency bands. This decrease might disrupt cortical integration and working memory formation and hence be a cause for anesthetic-induced amnesia and possibly unconsciousness.

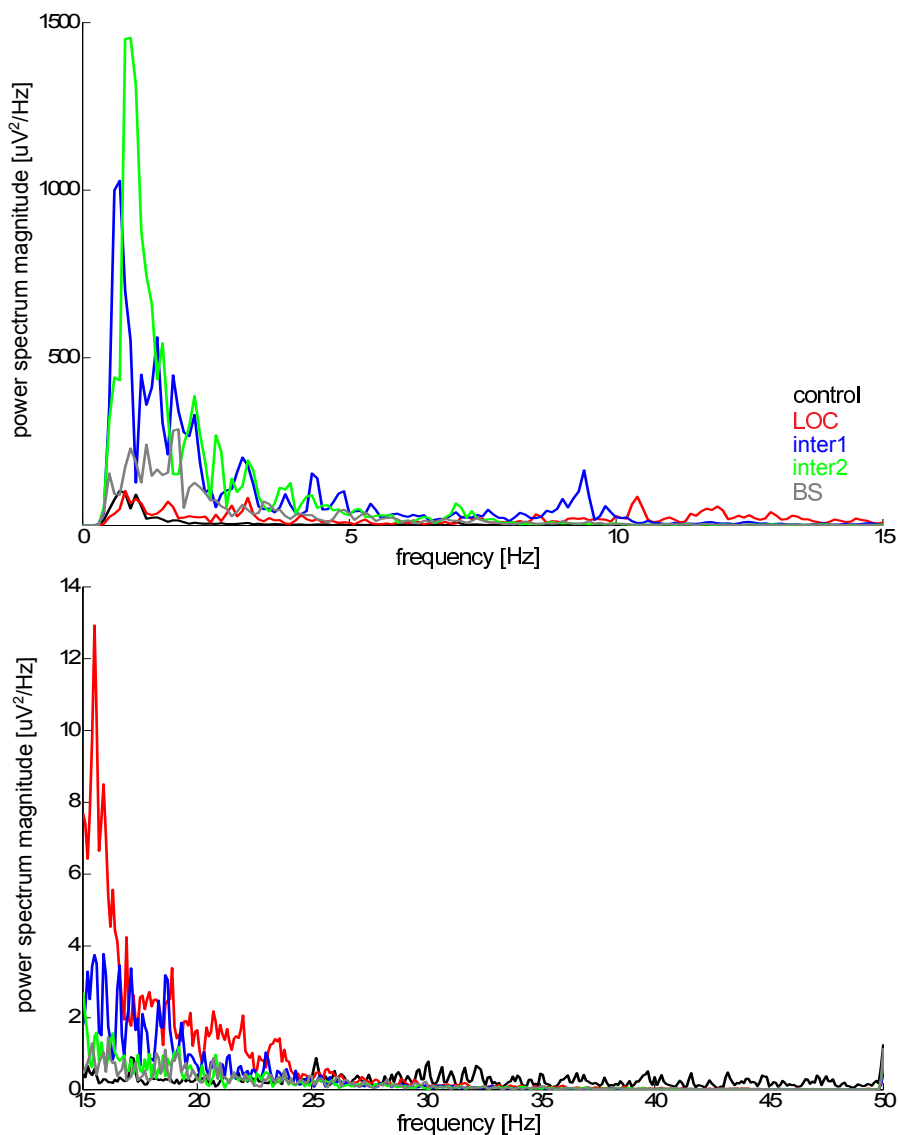
Another finding is that propofol and volatile anesthetics possibly affect cortical LFP activity *in vivo* differently as also observed *in vitro*. *XApEn* calculated for data which were not

filtered to the frequency bands, but only low-pass filtered showed a significant effect for volatile anesthetics, however, not for propofol. It can be argued, that electrode placement in the cortex was different and that the volatiles were applied to rats and propofol to mice, but nevertheless, results seem to confirm a potentially different mechanism of anesthetic action for inhalational and intravenous anesthetic regimen.

11 Anesthetic effects on frontal EEG recordings at steady state conditions

11.1 Power spectral density changes

PSD was calculated over 120 s samples that were extracted from each recording at the end of the equilibrated anesthetic levels. At concentrations corresponding to LOC, the low frequencies' PSD in the 0-5 Hz range was not altered. At levels inter1 and inter2 these frequencies were strongly activated with sevoflurane and propofol. At LOC α - and β -frequencies are activated by both drugs. This activation also persists at the anesthetic level inter1 but the activation peak frequency is shifted to the left. Above 30 Hz PSD is suppressed at the analyzed sevoflurane and propofol levels.



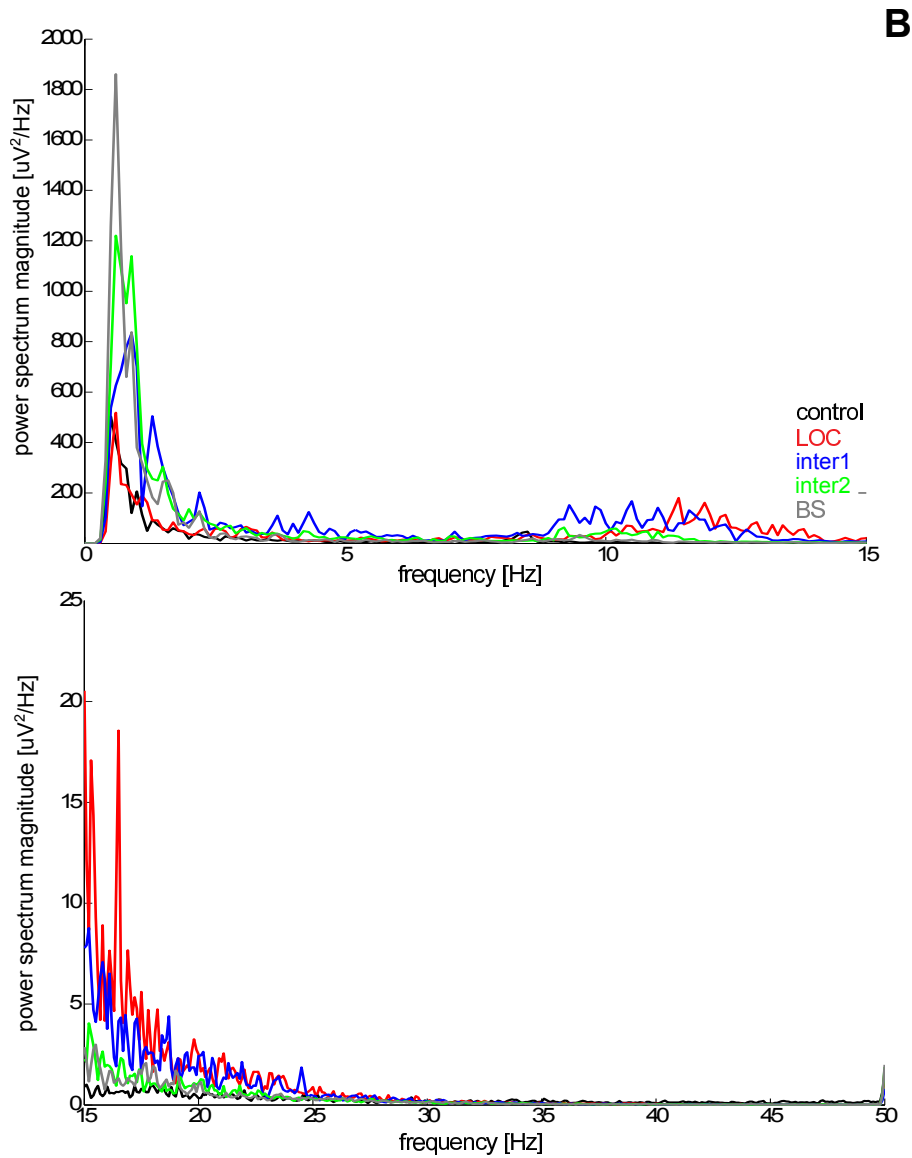


Figure 11.1: *PSD* (0-15 Hz/15-50 Hz) at different anesthetic levels for sevoflurane (A) and propofol (B) anesthesia. Low frequencies are activated with the used anesthetics, while high frequencies are suppressed. At levels LOC and inter1 α - and β -frequencies become activated.

11.2 Approximate entropy

ApEn ($m = 2, r = 0.2SD$) was computed over EEG sequences of 120 s length recorded at the five distinct levels of anesthesia for the frequency range 0.5–400 Hz and 0.5–30 Hz. *ApEn* of the 0.5-400 Hz signals significantly decreases with deeper anesthetic levels indicating a more predictable signal. The decrease is monotonously up to BS when frequencies over 30 Hz are included into computation. If these frequencies are excluded, *ApEn* shows a biphasic course with significantly increased values at LOC followed by *ApEn* decreasing till inter2. *ApEn* calculated at BS should not be used for interpretations

because this specific EEG signal may have non-stationary signal properties. The rise of *ApEn* (0.5-30 Hz) at LOC may be mainly due to α - and β -band activation (Kuizenga, Wierda et al. 2001; Brown, Lydic et al. 2010) and because the strong suppression of high frequency activity is not included in the analysis. The parameter courses are presented in Figure 11.2.

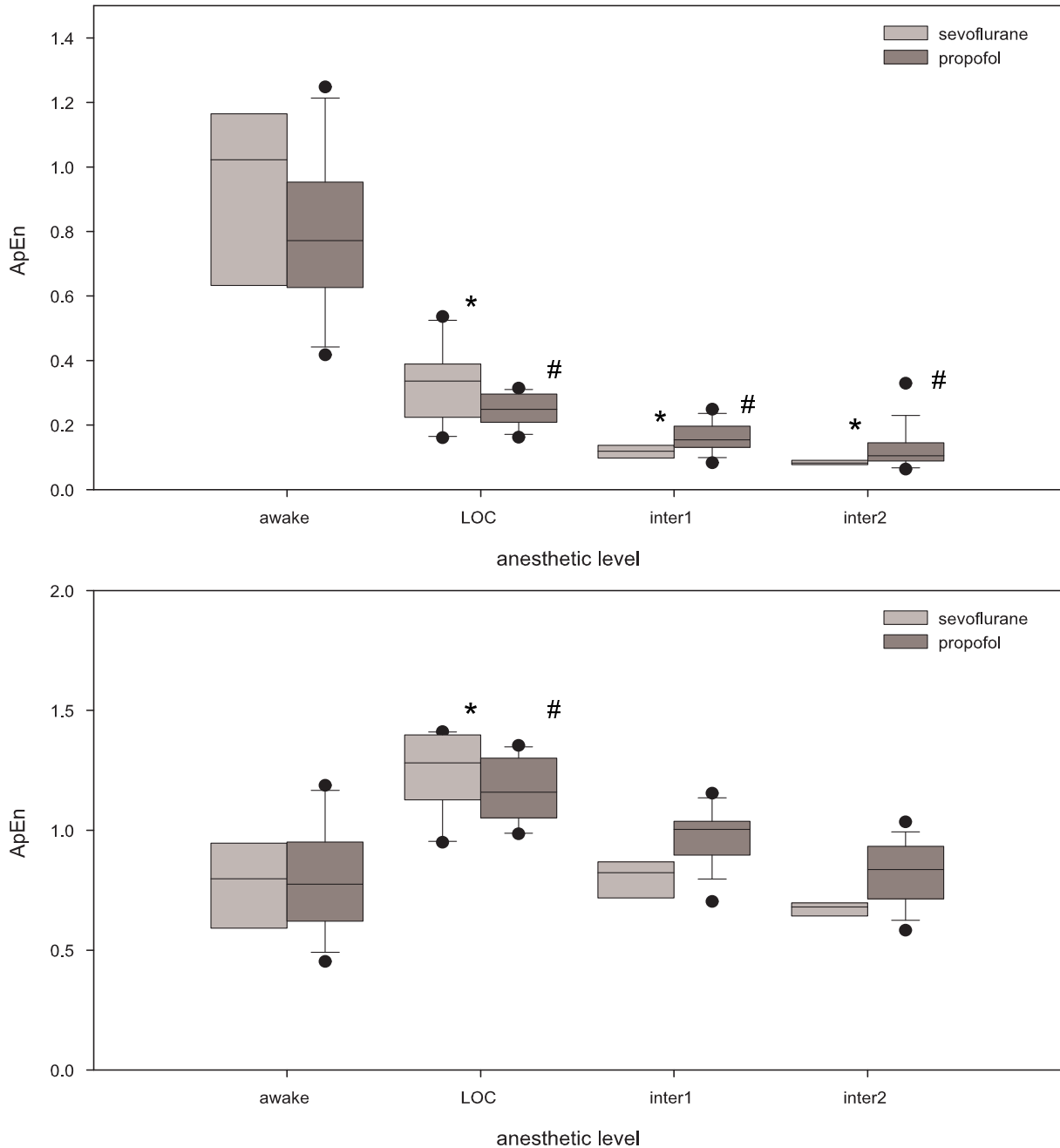


Figure 11.2: *ApEn* ($m = 2; r = 0.2SD$) of 0.5-400 Hz unfiltered (top) and 30 Hz low-pass filtered (bottom) EEG recorded at different anesthetic levels with sevoflurane and propofol. Significant differences from control conditions are indicated with * (sevoflurane) and # (propofol), ($p < 0.05$ Bonferroni corrected).

In a second step, the single concentrations that were necessary to achieve the stable anesthetic levels were converted to MAC values as described by Nickalls and Mapleson (Nickalls and Mapleson 2003). The shape of the *ApEn* (0.5-400 Hz) and *ApEn* (0.5-30 Hz) curves are very similar. At the single MAC values (>0 MAC) *ApEn* (0.5-30 Hz) was always 0.5 to 1.1 units bigger than *ApEn* (0.5-400 Hz). In addition, the activation of *ApEn* at subhypnotic sevoflurane concentrations can be observed. If high frequencies are included there is a strong drop in *ApEn* at the onset of sevoflurane that is not present in the analysis of the lower frequency range. P_K analysis showed that discriminating consciousness from unconsciousness and separating different anesthetic levels was not optimal for analysis up to 30 Hz (Table 11.1).

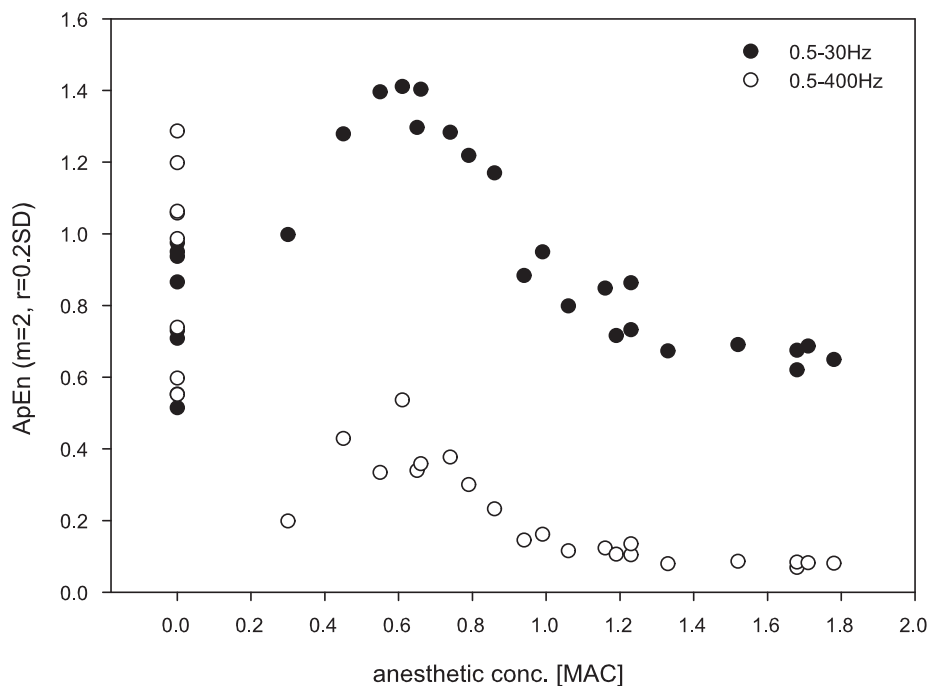


Figure 11.3: Course of *ApEn* related to MAC for the frequency bands 0.5 to 400 Hz (white) and 0.5 to 30 Hz (black). A biphasic course at subhypnotic sevoflurane concentrations can be observed followed by a steady decrease of *ApEn*. During high frequency analysis a strong drop of *ApEn* is visible at the onset of the drug.

Higher EEG frequencies above 30 Hz contain a number of anesthesia-relevant information. But the higher the frequencies the more they may become distorted by superimposed EMG. 30 Hz as peak frequency in the analysis range seem to represent an acceptable threshold. At frequencies below 30 Hz the influence of EMG on the recording seems to be negligible (Bonhomme and Hans 2007). With this aspect in mind, *ApEn* seems not able to separate

consciousness from unconscious states but as displayed in the bottom boxplot of Figure 11.2 and in Figure 11.3, the increasing concentrations of the anesthetic are reflected by decreasing $ApEn$ values.

11.3 Permutation Entropy and Order Recurrence Rate

$PeEn$ ($m = 5$) and ORR ($m = 4$) were calculated after a 30 Hz low-pass filtering of the EEG in order to reduce EMG distortions. Both parameters did not show any significant differences for the sevoflurane and propofol group. $PeEn$ decreased with the anesthetic level linearly to inter1 where it equilibrated. At BS, $PeEn$ increased pronouncing the exceptional position of this state. ORR showed a similar even though inverse pattern until inter1. But ORR had its turning point already at inter2. Still both parameters seem to be very useful to distinguish consciousness from an anesthetic level (except BS) by evaluating EEG only up to 30 Hz. P_K values were very good for $PeEn$ to distinguish between consciousness and unconsciousness and satisfying in the performance of distinguishing different anesthetic levels. P_K of ORR was better than P_K of $ApEn$ but ORR could not reach the qualitative results as $PeEn$ did (Table 11.1).

Parameter		P_K	CI
$ApEn$	Level	0.596	(0.533-0.656)
	Consc. vs. uncons.	0.720	(0.581-0.820)
	Anesthetic levels	0.896	(0.841-0.938)
$PeEn$	Level	0.789	(0.716-0.847)
	Consc. vs. uncons.	0.933	(0.839-1.000)
	Anesthetic levels	0.647	(0.536-7.38)
ORR	Level	0.714	(0.642-0.775)
	Consc. vs. uncons.	0.762	(0.641-0.867)
	Anesthetic levels	0.656	(0.543-0.751)

Table 11.1: P_K values and their confidence intervals of the different non-linear parameters for distinguishing (i) the different levels from each other and (ii) consciousness from unconsciousness. Recordings from BS were excluded from P_K analysis due to its special status. $PeEn$ seems potent to reliably distinguish between consciousness and unconsciousness whereas $ApEn$ seems suitable for separating different sedating and anesthetic levels. The presented results are from the 0.5-30 Hz analyses.

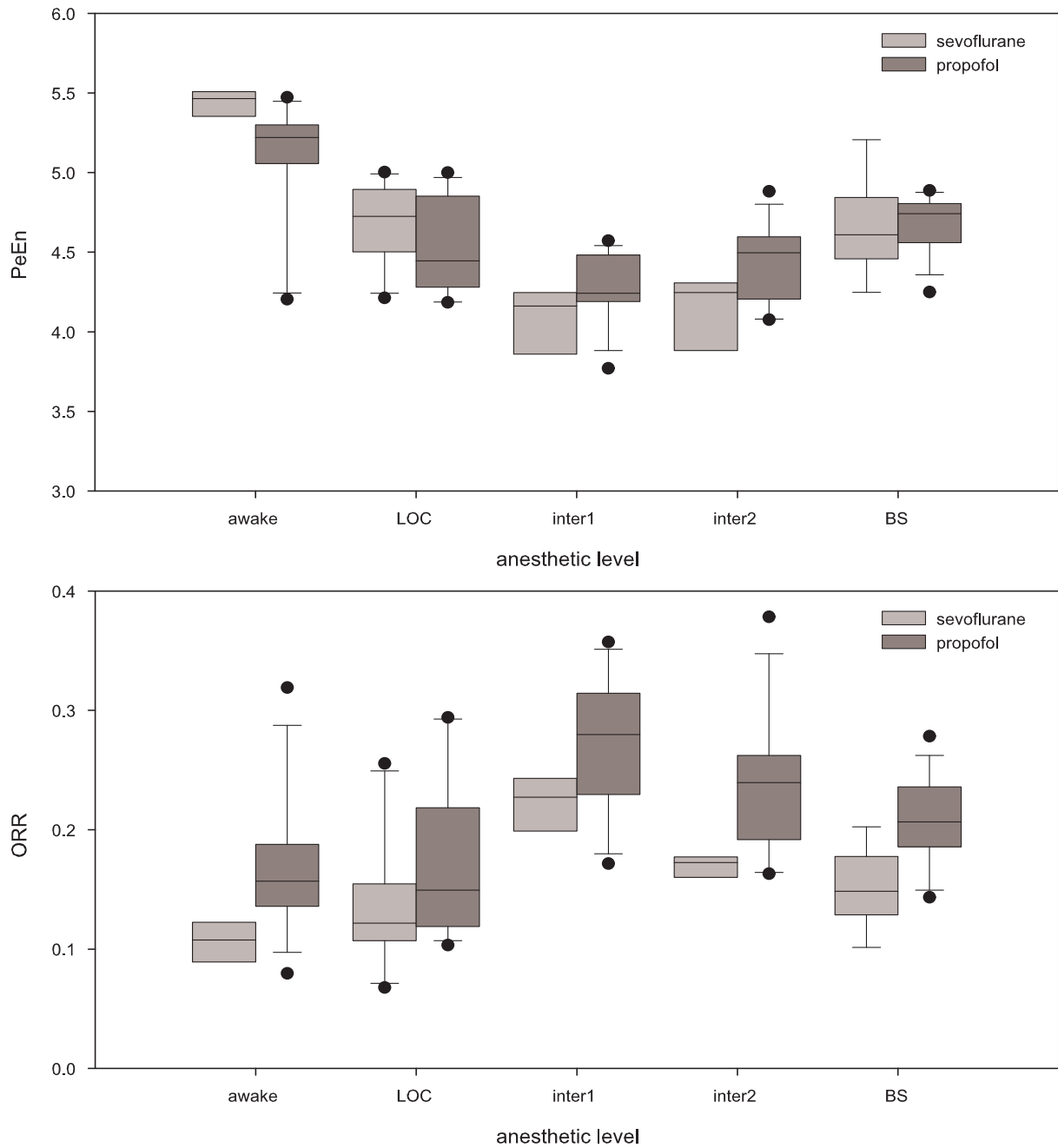


Figure 11.4: $PeEn$ ($m = 5$) (top) and ORR ($m = 4$) (bottom) at different anesthetic levels. Both parameters are affected by the anesthetic regimen and seem to be appropriate to be used for separation between the conscious state and anesthetic levels. Exception is the special state of BS. The detailed performance of separating different states is presented in Table 11.1

11.4 Parameter performance in the classical frequency ranges

In an additional set of analyses $PeEn$ (showing best performance in separating consciousness from unconsciousness Table 11.1) and $ApEn$ (showing best performance in distinguishing different anesthetic levels Table 11.1) were calculated from the EEG traces

filtered to the single frequency bands. Table 11.2 and Table 11.3 present the results of the *ApEn* and *PeEn* analyses.

		ApEn			
		awake	LOC	inter1	inter2
Delta	Sevoflurane	0.66 (0.02)	0.68 (0.04)	0.57 (0.14)	0.53 (0.10)
	Propofol	0.59 (0.11)	0.66 (0.05)	0.60 (0.13)	0.57 (0.10)
Theta	Sevoflurane	0.82 (0.13)	1.00 (0.13)	0.83 (0.14)	0.93 (0.09)
	Propofol	0.96 (0.10)	1.07 (0.11)	1.01 (0.26)	1.06 (0.17)
Alpha	Sevoflurane	0.93 (0.11)	1.02 (0.29)	0.93 (0.18)	1.29 (0.04)
	Propofol	1.06 (0.14)	0.77 (0.36)	0.60 (0.21)	0.93 (0.27)
Beta	Sevoflurane	1.89 (0.09)	1.03 (0.30)	1.55 (0.13)	1.83 (0.05)
	Propofol	1.93 (0.08)	0.85 (0.41)	1.07 (0.39)	1.50 (0.33)
Gamma	Sevoflurane	1.85 (0.16)	1.90 (0.12)	1.63 (0.17)	1.55 (0.16)
	Propofol	2.02 (0.08)	2.00 (0.07)	1.95 (0.09)	1.87 (0.13)

Table 11.2: *ApEn* values (mean and standard deviation) for the EEG sequences at different anesthetic levels filtered to the classical frequency ranges. Bold entries indicate significance against the awake state ($p < 0.05$, Bonferroni corrected)

		PeEn			
		awake	LOC	inter1	inter2
Delta	Sevoflurane	2.04 (0.06)	2.09 (0.04)	2.15 (0.03)	2.08 (0.04)
	Propofol	1.98 (0.10)	2.05 (0.06)	2.06 (0.09)	1.97 (0.09)
Theta	Sevoflurane	3.07 (0.06)	3.11 (0.04)	3.03 (0.04)	3.02 (0.07)
	Propofol	3.08 (0.09)	3.11 (0.03)	3.07 (0.05)	3.07 (0.05)
Alpha	Sevoflurane	3.69 (0.08)	3.82 (0.05)	3.62 (0.05)	3.69 (0.02)
	Propofol	3.67 (0.11)	3.81 (0.03)	3.71 (0.09)	3.71 (0.30)
Beta	Sevoflurane	5.20 (0.06)	4.79 (0.11)	4.85 (0.06)	4.97 (0.04)
	Propofol	5.15 (0.07)	4.68 (0.15)	4.82 (0.12)	4.93 (0.08)
Gamma	Sevoflurane	6.45 (0.05)	6.31 (0.10)	6.30 (0.02)	6.32 (0.03)
	Propofol	6.45 (0.04)	6.35 (0.08)	6.30 (0.05)	6.31 (0.07)

Table 11.3: *PeEn* values (mean and standard deviation) for the EEG sequences at different anesthetic levels filtered to the classical frequency ranges. Bold entries indicate significance against the awake state ($p < 0.05$, Bonferroni corrected)

The results in the tables indicate that the β -range may be especially suitable to distinguish between anesthetic levels and the awake state. *PeEn* showed significant decrease in the parameter values at all levels of sevoflurane and propofol in the higher β -, and γ -frequency bands.

11.5 Non-linear measures can reliably separate anesthetic levels: Discussing the results

The three non-linear measures were used to analyze EEG recordings from steady state conditions after a 30 Hz low-pass filtering. *ApEn* was not able to distinguish consciousness from unconsciousness. *ApEn* at LOC is maximal and hence *ApEn* seems to follow the course of paradoxical EEG excitation (section 11.2) . This activation phenomenon can be observed at low doses of anesthetics (Kuizenga, Wierda et al. 2001; Brown, Lydic et al. 2010). α - and β -frequencies are activated at these concentration levels before they are suppressed at higher doses. Ordinal measures, i.e., *PeEn* and *ORR* do not follow this biphasic course and are able to distinguish a conscious state from sedated or anesthetized levels as presented in section 11.3 for the analyses in the 0-30Hz range. The P_K values of the several comparisons are listed in Table 11.1. All P_K calculations were performed excluding results from burst suppression analysis. BS shows a very special EEG pattern characterized by a non-stationary waxing and waning signal (Rampil 1998). These alternating bursting and isoelectric episodes are also responsible that in commercially used EEG monitors this special state is detected by a specific algorithm called suppression ratio (Bruhn, Bouillon et al. 2000; Viertio-Oja, Maja et al. 2004). The obtained results confirm published findings and pronounce the capability of these parameters to be used in anesthetic monitoring (Jordan, Stockmanns et al. 2008; Olofsen, Sleight et al. 2008; Horn, Pilge et al. 2009). The analyses in the distinct frequency ranges presented in section 11.4 clearly underline the performance of *PeEn* to separate consciousness from unconsciousness. The high frequency bands (β - and γ -range) seem to be best suited for this task. A next logical step is to generate a multivariate measure based on these algorithms to explore their advantages in the particular concentration range. Nevertheless, these results were derived from analyzing steady state EEG sequences and no information can be gained regarding EEG changes in the transition from consciousness to unconsciousness and vice versa.

12 Anesthetic effects on single-channel frontal EEG recordings at state transitions

In this section the recent results of research in the transition phase between conscious and unconscious states in humans are presented

12.1 Modeled propofol concentrations at LOC and ROC

Calculated C_{eff} of propofol was significantly higher at LOC ($3.84 \pm 1.39 \mu\text{g/ml}$) than at ROC ($1.25 \pm 0.44 \mu\text{g/ml}$) (mean \pm SD; $p < 0.001$). These results indicate a drug hysteresis.

12.2 Spectral but not complexity measures follow paradoxical excitation

During LOC, SR follows the course of paradoxical excitation of EEG α - and β -frequencies indicated by increasing values with significant higher values after 92 s (α -band) and 8 s (β -band) compared to 60 s before the event of losing consciousness, i.e., when the patient was awake. $PeEn$ ($m = 5$) of α -frequencies remains mainly stable without significant changes and $PeEn$ ($m = 5$) of the β -band decreases during LOC with significant lower values. Detailed median values of the parameters at the selected time points are displayed in Table 12.1 and in the boxplots of Figure 12.1. The courses of averaged $PeEn$ and SR (mean \pm standard deviation) in the different frequency ranges are displayed in Figure 12.2 and Figure 12.3.

	-60s	8s	60s	92s
$PeEn(\alpha)$	0.99 (0.98, 1.03)	1.00 (0.98, 1.02)	1.00 (0.99, 1.01)	0.99 (0.98, 1.01)
$PeEn(\beta)$	1.04 (1.01, 1.05)	1.01* (0.99, 1.02)	0.99* (0.98, 1.00)	0.98* (0.97, 1.00)
$SR(\alpha)$	0.75 (0.61, 0.96)	0.83 (0.70, 0.95)	0.87 (0.71, 0.99)	1.03* (0.87, 1.18)
$SR(\beta)$	0.82 (0.66, 1.12)	1.04* (0.92, 1.35)	0.94 (0.88, 1.01)	1.04 (0.89, 1.10)

Table 12.1: Median values (25%-, 75%-quantile) of $PeEn$ and SR of the α - and β -band at selected time points 60 s before and 8, 60 and 92 s after LOC. * indicates a significant change of the parameter values compared to the time point “60 s before LOC”

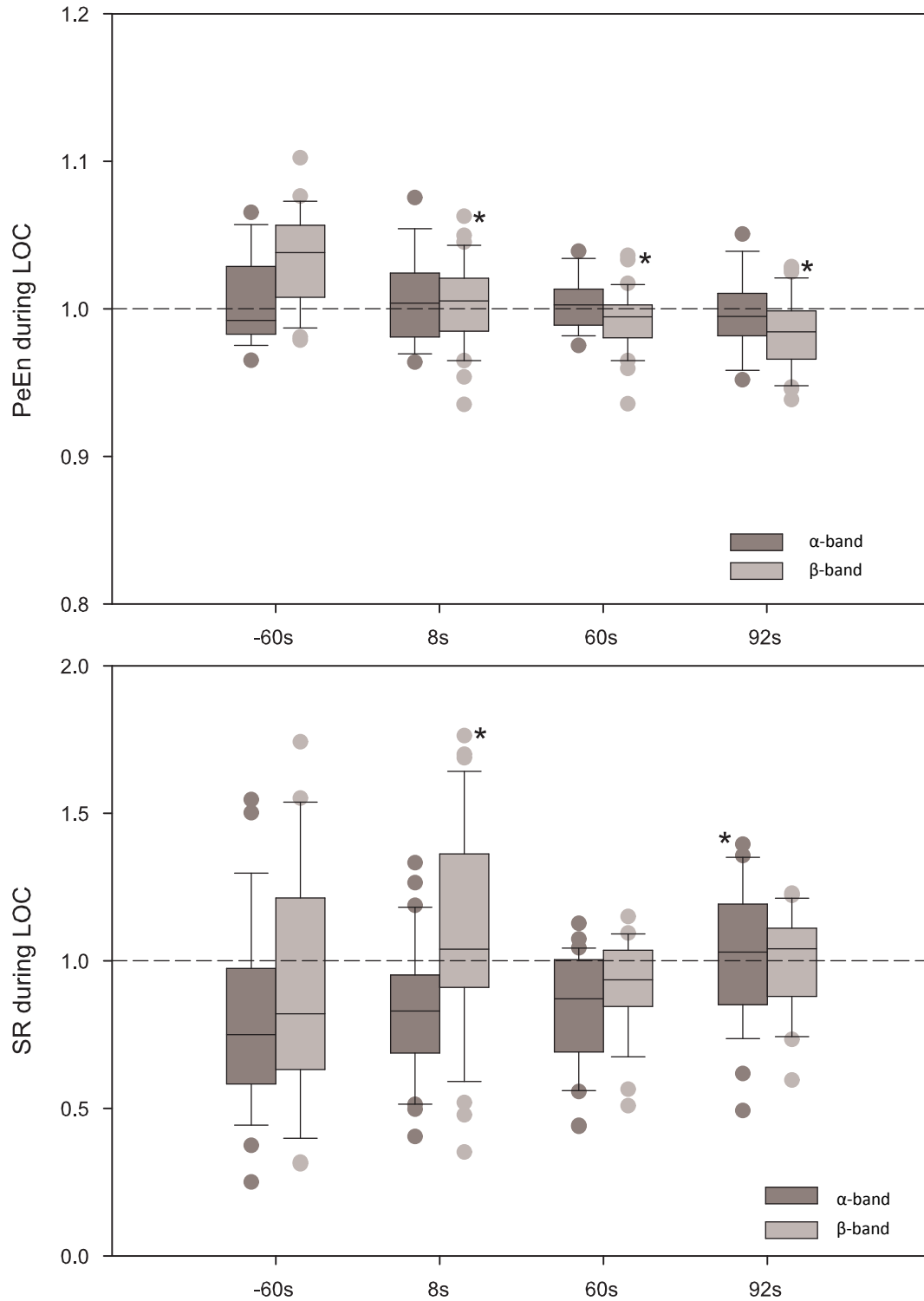
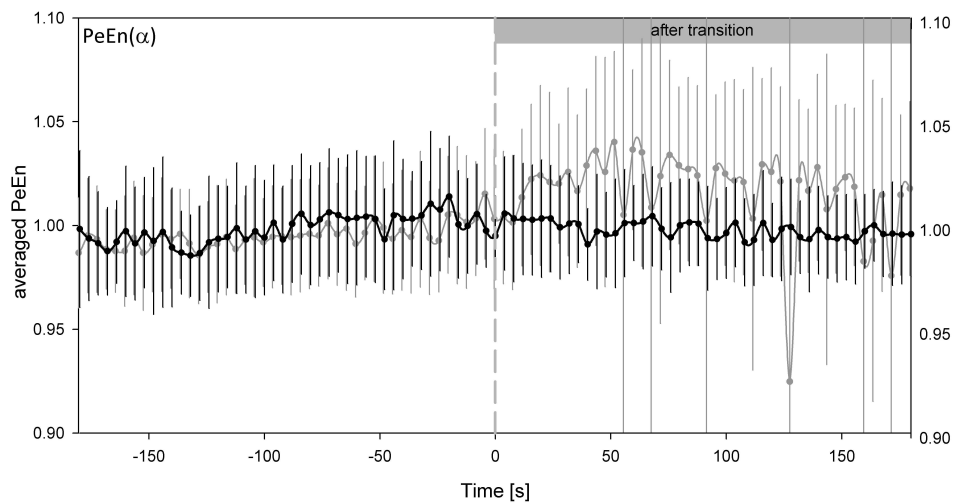
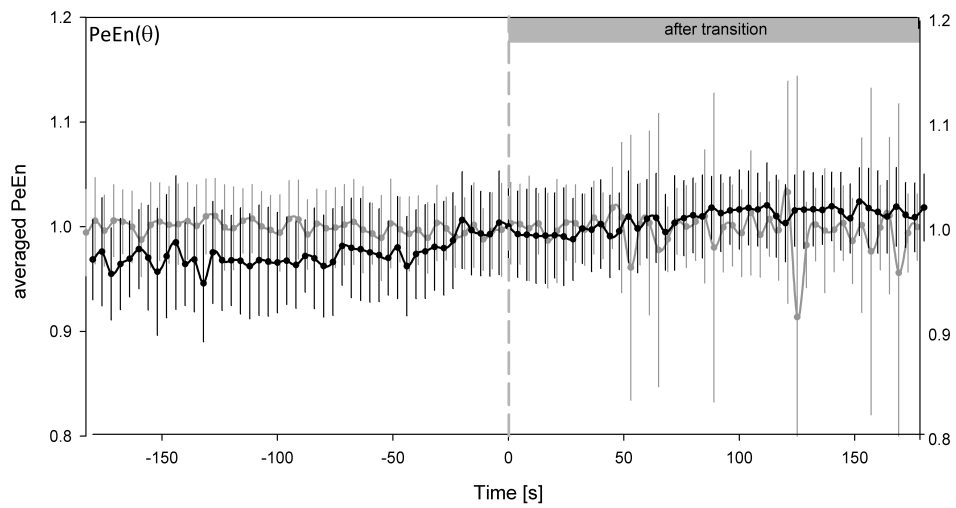
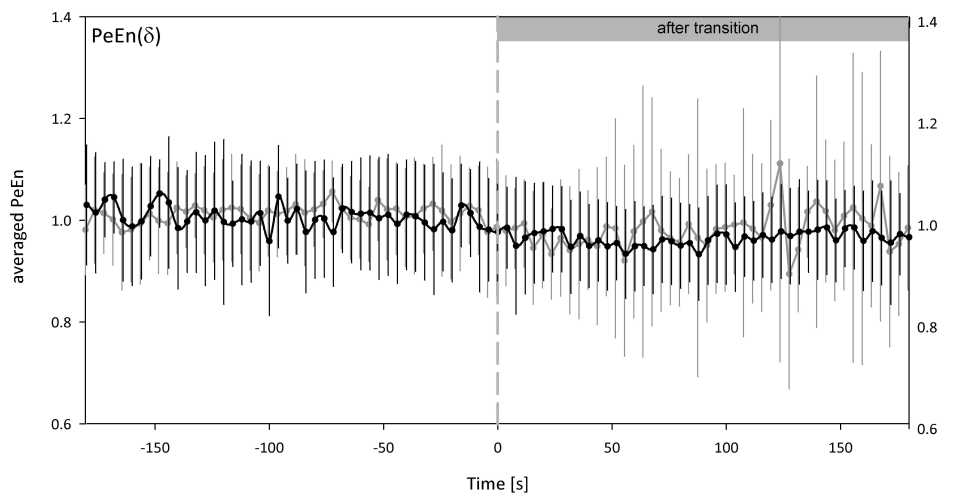


Figure 12.1: Boxplots for normalized $PeEn$ (top) and SR (bottom) of α - and β -frequencies during the transition from awake to LOC. $PeEn$ of α -frequencies shows no significant change during LOC but $PeEn$ (β) is significantly lower after LOC than before. SR (α) is significantly higher than 92 s after LOC compared to values derived from 60s before the event, indicating slow activation of these frequencies. SR (β) shows a biphasic activation with significant higher SR 8 s after LOC compared to SR 60 s before the transition. The dashed line at 1 was inserted for better orientation. *Significant compared to parameter value obtained at - 60 s.



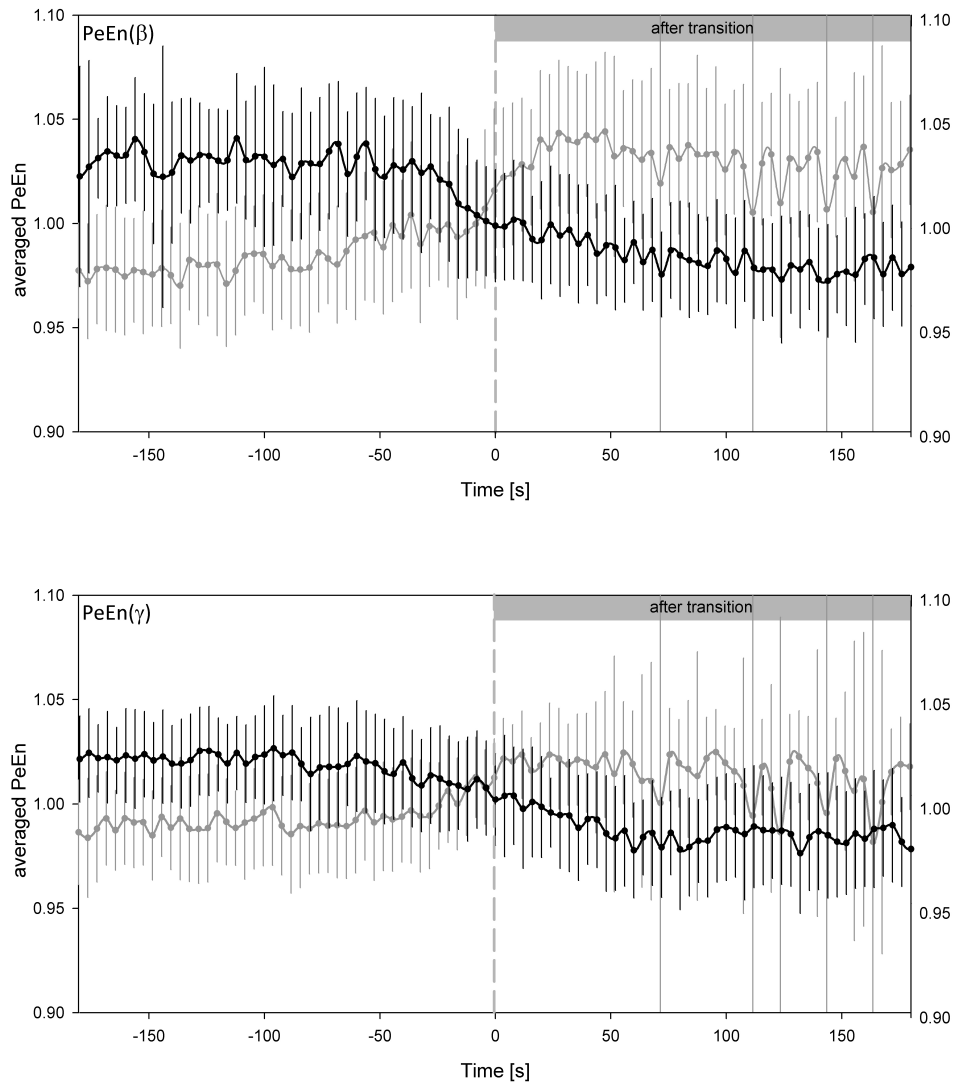
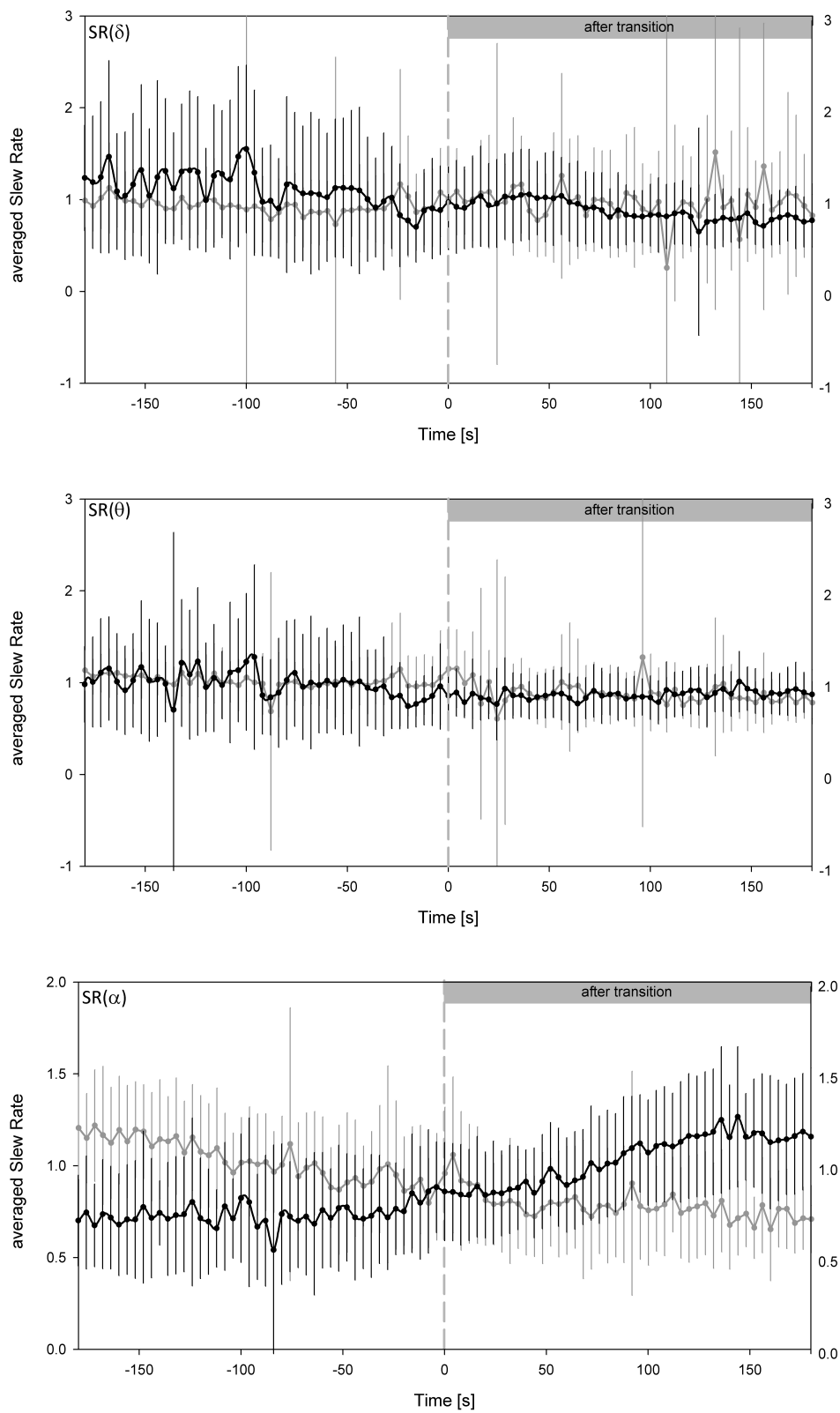


Figure 12.2: $PeEn$ of LOC (black) and ROC (dark grey) transitions in the different frequency bands. From top to bottom: δ -, θ -, α -, β -, γ -band. Data are presented as mean and standard deviation of the normalized parameter series. Mean $PeEn(\delta)$ shows no anesthetic-dependent effect in the state transitions. Mean $PeEn(\theta)$ increases during LOC and shows no change during ROC. Mean $PeEn(\alpha)$ does not react on changing propofol concentrations at LOC but increases after ROC. Mean $PeEn(\beta)$ and $PeEn(\gamma)$ decrease during LOC and increase with the emergence of anesthesia.



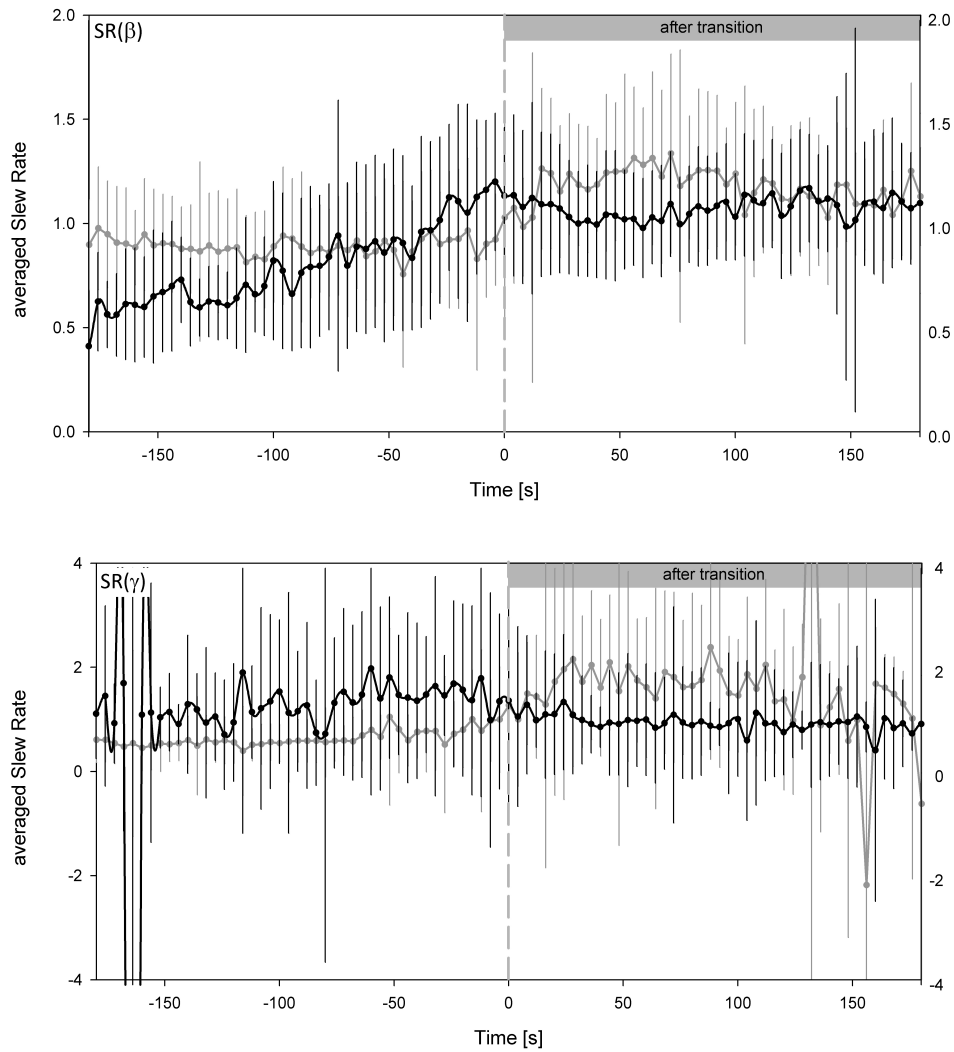


Figure 12.3: Slew Rate of LOC (black) and ROC (dark grey) transitions in the different frequency bands. From top to bottom: δ -, θ -, α -, β -, γ -band. Data is presented as mean and standard deviation from the normalized parameter series. Mean $SR(\delta)$ and $SR(\theta)$ show no obvious effects during LOC and ROC, only standard deviation is smaller after LOC. Mean $SR(\alpha)$ displays an activation in the transition from awake to LOC and steadily decreases during the recovery from anesthesia. Mean $SR(\beta)$ is also activated during induction and also increases during the recovery phase. Mean $SR(\gamma)$ decreases during LOC and increases at ROC.

12.3 Different frequencies adapt to the switched state with different delays

Analysis of time point when *PeEn* values intersect during LOC and ROC revealed a longer delay at lower frequencies. Intersection at γ -frequencies took place 12 ± 27 s before the event and hence significantly earlier than at all other analyzed frequencies. *PeEn* (β) intersection was 3 ± 34 s after LOC/ROC and *PeEn* (α) intersection 12 ± 31 s after LOC and these delays were not significantly different. *PeEn* at θ -frequencies was the last one to intersect 86 ± 51 s after the transition. It was significantly later than at all other frequencies. In the *PeEn* analysis, the lower frequencies did not show strong dependence on propofol during LOC. In the α -band there was no significant difference of *PeEn* values before and after LOC. In the θ -band values obtained 32-36 s before LOC could be distinguished from values 32-36 s after LOC. This delay of significant separation was 8-12 s for β - and 12-16 s for γ -frequencies. For ROC, there were no significant differences of *PeEn* before and after the transition in the θ -band. For the other frequencies the delays were 8-12 s (α) and 8-12 s and 0-4 s (β/γ).

12.4 Permutation entropy reflects altered signal information content and reveals time hysteresis in EEG: Discussing the results

In this section the results obtained from the transition studies' analyses presented in the section above are discussed.

12.4.1 Propofol concentrations at LOC and ROC

Modeled propofol concentration of the data set used was significantly higher during LOC than at ROC as shown in section 12.4.1. This observed drug hysteresis is assumed to be caused by an inherent resistance of the central nervous system to changes of the arousal state. (Friedman, Sun et al. 2010). Friedman et al. showed that hysteresis effects in the transitions cannot be completely explained by pharmacokinetics. They showed that these effects which they call neural inertia were not present in flies with a single gene mutation that does not affect uptake, distribution or metabolism of the anesthetic (Friedman, Sun et al. 2010). Further, Kelz et al. showed in experiments with mice that influencing orexinergic neurons impact emergence of anesthesia but not induction and hence the state transitions are non-symmetric processes in reverse order (Kelz, Sun et al. 2008). Orexinergic neurons play an essential role to maintain wakefulness. Reduced orexinergic signaling causes narcolepsy (Kelz, Sun et al. 2008). A state transition between consciousness and unconsciousness may be similar to a first order state transition observed in thermodynamics. Steyn-Ross et al. tried to model the state transitions LOC and ROC. Their model

revealed a drug hysteresis effect. This means that the patient requires a higher drug concentration to be put to sleep than to wake up. At the point of LOC/ROC the state switches from one stable branch to another causing the loss or return of consciousness. Since these transitions follow a hysteresis path, concentrations are different at LOC and ROC (Steyn-Ross, Steyn-Ross et al. 2004). The modeled results are also confirmed by the experiments from Friedman. They support the assumption that LOC and ROC are not mirrored processes but inducing these events requires different mechanisms (Friedman, Sun et al. 2010). Nevertheless, even with the mentioned drug hysteresis and different mechanisms causing LOC and ROC, an EEG measure reflecting the hypnotic component of anesthesia during these transitions should reliably reflect the patient's state independent from hysteresis processes.

12.4.2 Biphasic response during LOC

But *SR*, exemplary for spectral analysis methods, shows a paradoxical activation during LOC as presented in section 12.2. In the α - and β -frequency band the parameter values increase, indicating that the subject may be awake at and shortly after LOC. This paradoxical excitation was reported in the literature at different scales and with different anesthetic regimens. Kuizenga et al. showed a biphasic EEG effect on α - and β -frequencies during induction period with propofol and other common anesthetic agents except midazolam using *SR* as EEG parameter (Kuizenga, Wierda et al. 2001). Recently, β - and α -activation at sedation and LOC levels was observed during high density EEG experiments comparing propofol anesthesia to slow wave sleep. β -activation at LOC was distributed over the entire scalp while α -activation was mainly observed in frontal EEG recording locations (Murphy, Bruno et al. 2011). In experiments with rats activation of cortical and hippocampal EEG was observed during induction with thiopental. The peak power roughly corresponded with loss of righting reflex (LORR). The time of peak was also dependent on the selected EEG frequency range. In the α - and β -band the peak occurred shortly before LORR whereas slower frequencies showed the peak after LORR. Peaks were more pronounced in the cortex than in the hippocampus (MacIver, Mandema et al. 1996). Paradoxical excitation could be caused by a change of tonic inhibition of the thalamus through the globus pallidus interna. If GABAergic substances like propofol are used, this tonic inhibition could be suppressed and thalamo-cortical connections may be activated (Brown, Lydic et al. 2010). Another explanation may be a change in the level of interaction between GABA currents and intrinsic membrane slow potassium currents. Propofol changes the activity from baseline interneuron synchrony to interneuron asynchrony forcing pyramidal cells to ~20 Hz

oscillations (McCarthy, Brown et al. 2008). As aforementioned, during this excitation phase EEG amplitudes increase in the α - and β -band and cause parameters like *PSD* and *SR* to indicate a paradoxical turn towards consciousness. The results presented in section 12.4. show that *PeEn* does not reflect this activation but continues to decrease during LOC transition indicating less signal complexity. The different results for *SR* and *PeEn* lead to the conclusion that both parameters evaluate different properties derived from the EEG. The *SR* activation is caused by the observed synchronization of α - and β -frequencies during LOC. The underlying network becomes more synchronous leading to higher sum potentials in the EEG causing parameters like *SR* to increase. Measures based on information content of the EEG, such as *PeEn*, are suspected to be promising to indicate the hypnotic state, because unconsciousness is directly related to impaired cortical information processing. This impairment can be caused by synchronization processes as observed during the paradoxical excitation phase. In a modeling approach, increased α -synchrony, and hence activation was described through a reduction of the thalamo-cortical loops dimensionality caused by potentiation of GABA (Ching, Cimenser et al. 2010). Generally, spectral measures may indicate a paradoxical excitation because of synchronization effects in the relevant frequency bands. But because of this synchronization effect, the EEG becomes less complex, i.e., the information content decreases. This decrease is correctly reflected by decreasing *PeEn* values. Hence, *PeEn* may be suitable to reflect the patient's state correctly during this phase.

12.4.3 Time hysteresis during LOC and ROC

During analysis of effects on specific frequency bands the question arises whether different EEG frequencies react to propofol concentrations leading to LOC on comparable time scales as well as the emergence from anesthesia and the transition from ROC to awake. The presented *PeEn* results (section 12.3) show that higher frequencies react faster on the state transition than slower ones. In the γ -band a delay of 12-16 s at LOC and immediate reaction on the state change during ROC was observed. Generally, faster oscillations seem associated with cortical information processing, γ -frequencies represent intra-cortical communication especially as comparator between layer I and layer V or form patches of local synchrony (John and Prichep 2005) but are also subject to be superposed by EMG distortions, especially in the frequency range above 30 Hz (Bonhomme and Hans 2007). Besides the EMG questionability, the fast adaptation of *PeEn*(γ) to the changed state that could be revealed leads to a first hint towards a cortical mechanism causing transition to unconsciousness and return from it. In the β -band the delay at LOC was 8-12 s and the reaction at LOC was and

0-4 s. The decrease of $PeEn(\beta)$ during LOC is probably caused by synchronization of β -oscillations causing a state space reduction. $SR(\beta)$ increases during LOC, whereas $PeEn(\gamma)$ and $SR(\gamma)$ decrease during LOC indicating less neuronal γ -activity and an information reduction through depression of γ -network activity.

In general, β -oscillations seem responsible for cortical long-range information transfer and synchronization between neighboring cortices (von Stein, Rappelsberger et al. 1999; von Stein and Sarnthein 2000; John and Prichep 2005). In the α -band the reaction on the state transitions from awake to LOC and from ROC to awake were slower compared to the EEG β - and γ -frequencies. At LOC, α -frequencies become more synchronized but their information content is not significantly altered. α -synchronization may be caused by effects of propofol on the cortico-thalamo-cortical loop but because of the delay times of the α -oscillations, the process of LOC seems to be triggered by the higher frequencies, i.e., γ - and β -oscillations. Frequencies in the α - and θ -range seem associated with mnemonic tasks (Bland 1986) and structuring working memory and mental imagery (von Stein and Sarnthein 2000; Sauseng, Griesmayr et al. 2010). The slowest reaction on the state transition occurred in the θ -frequency range. Hence, these oscillation frequencies are probably not directly associated with triggering the state transition. $PeEn(\theta)$ increases slowly during LOC and could represent a propofol effect on the cortico-hippocampal pathway. For example, θ -oscillations derived from frontal midline recording sites are assumed to share functional relationships with hippocampal oscillations in this frequency range (Mitchell, McNaughton et al. 2008). Generally, inverse relation between scale of integration and frequency of interaction seems to exist, i.e., lower frequencies have a wider transmission range. And more generally low frequency interactions may be a characteristic feature for top-down interactions (von Stein and Sarnthein 2000). The presented experimental findings indicate that modifications of EEG θ -oscillations by anesthetics are probably less related to the hypnotic state than possibly the amnestic component of anesthesia. In animal experiments an anesthetic-induced frequency shift towards lower frequencies could be observed (section 10.1), hence impairing memory consolidation (Butovas, Rudolph et al. 2010; Perouansky, Rau et al. 2010). The time delays obtained show that faster frequencies adapt to the switched state more quickly than slower frequencies do. With the described associations of EEG-frequencies to working tasks, it seems that cortical activity reacts faster than subcortical activity. These findings are undermined by other experimental results. Velly et al. could show that EEG dramatically alters at the loss of consciousness but deeper brain areas were not significantly affected. This led to the hypothesis that the LOC transition is a mainly cortical process (Velly, Rey et al. 2007). The work of Velly et al. was

criticized because it was suggested that recorded EEG data and data from deep brain electrodes were generated by the same source, the cerebral cortex (Jäntti, Heikkinen et al. 2008). But still, Velly's work pronounces the role of cortical areas during LOC.

12.4.4 Conclusion

Our results for LOC analysis could lead to the assumption that LOC is released by fast changes on γ - and β -frequencies causing the cortex to lose its information capacity and at the same time triggering the transition towards unconsciousness. The transient course of $PeEn(\theta)$ may represent a gradual suppression or disruption of the connection between cortex and hippocampus and hence a depression of memory consolidation (Siapas, Lubenov et al. 2005). During ROC, $PeEn(\gamma)$ and $PeEn(\beta)$ react almost also switch-like to the transition, followed by a smoother and slower increase of $PeEn(\alpha)$. This chronological order may also pronounce the cortex as earliest target of propofol, at least as it can be observed in the EEG. The fact that $PeEn(\alpha)$ during LOC and $PeEn(\theta)$ during ROC do not change to significant degree may be explained through the propofol-induced shift from α - to θ -frequencies in the cortico-hippocampal pathway causing amnesia. (Perouansky, Rau et al. 2010) $PeEn(\theta)$ becomes higher during LOC and $PeEn(\alpha)$ during ROC indicating higher signal complexity and hence increased information content, possibly caused by the shift towards these frequencies. If we take $PeEn$ as a parameter evaluating information content in (frontal) cortical information processing, and similar network states are represented by similar $PeEn$ values in the relevant frequency band, our results lead to the conclusion that faster oscillation shows faster adaptation to the changed state and information content is lost or regained faster than at lower frequencies. Given the assumption that faster frequencies are responsible for cortical tasks and the slower the frequencies the deeper the communication structure projects to subcortical areas, the role of the cortex is strongly pronounced. These findings lead to the conclusion that propofol triggers intra- and cortico-cortical anesthetic-induced effects are triggered faster and more abruptly when compared to cortico-thalamo-cortical and cortico-hippocampal effects that are represented by slower oscillations. Furthermore, it may lead to the assumption that consciousness fades due to increased impaired cortical processing rather than subcortical mechanisms and hence LOC is cortically released. With the presented results the conclusion can be drawn that initial effects take part in the cortex and the mechanism of losing consciousness follows a top-down approach. This means that the cortical oscillations are suppressed (γ -waves), or hypersynchronized (β -waves) causing hypnosis. Effects in the EEG α - and θ -range may lead to distortions in processes cause amnesia.

13 Spatio-temporal anesthetic effects on multi-channel EEG

13.1 Power spectral density

PSD was determined for the “awake” and “propofol” level of the propofol multi-channel recordings where the level “propofol” corresponds to LOC in the single-channel study. *PSD* was calculated for every single-channel of each experiment and then averaged over all channels and experiments. Low frequencies in the δ -band are activated with propofol and there is also activation in the α - and β -band. At around 37 Hz *PSD* of the EEG recorded during wakefulness is higher than during propofol (Figure 13.1). These results agree with the ones obtained from the single-channel study presented in section 11.1.

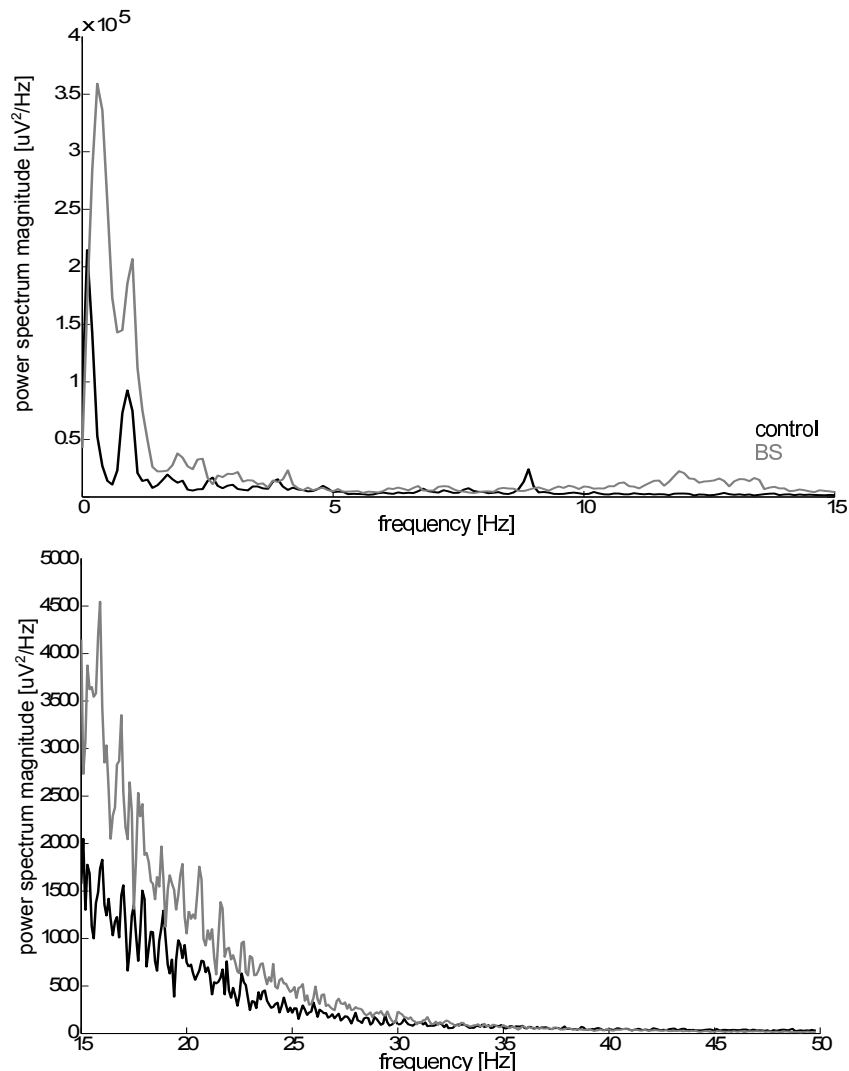


Figure 13.1: Averaged *PSD* obtained from the multi-channel study. With propofol activation at low frequencies and in the α - and β -band can be observed while *PSD* is higher during wakefulness at frequencies above approximately 37 Hz.

13.2 Approximate and Cross Approximate Entropy in β -frequencies

$ApEn$ ($m=2, r=0.2SD$) was calculated for every channel and $XApEn$ ($m=1, r=0.2SD$) was calculated over all possible channel combinations for the β -band. $ApEn$ and $XApEn$ values were averaged over all test subjects. P_K analysis was used to evaluate the parameters performance for differentiation of levels “awake” and “unconscious”. In the univariate analysis, overall performance of $ApEn$ used to distinguish between both anesthetic states, was rather poor. Performance of $ApEn$ could be represented by P_K values between 0.6 and 0.8 for most electrodes. Four channels located anterior temporal showed worst performance with P_K values below 0.6. EEG from an area over the left parietal lobe covered by three electrodes showed best performance for $ApEn$ with P_K values over 0.8. Maximum P_K of 0.83 was obtained in that area from the electrode located at C4. P_K computed from electrode locations usually used for monitoring the hypnotic component of anesthesia was 0.72 and 0.71 (FP1 and FP2). Performance of $XApEn$ was dependent on the location of involved electrodes. $XApEn$ including EEG recorded from frontal electrodes was poor with P_K values mainly below 0.6. If $XApEn$ was used with channels recorded from electrodes not placed on the frontal lobe, performance was better with P_K values always over 0.6 and some combinations with P_K values over 0.8. Best combination was Cz/CP6 with $P_K = 0.93$. $P_K(XApEn)$ was below 0.8 for channel combinations involving frontal electrodes (FP1/FP2). These findings indicate that using bivariate analyses lead to better performance since also spatial network properties and hence additional information are processed.

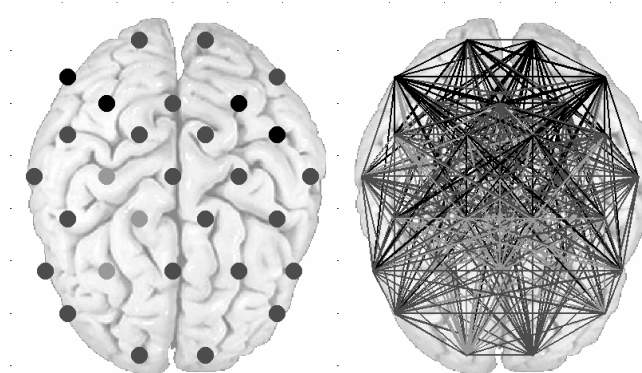


Figure 13.2: P_K for single-channel ($ApEn$, left) and all channel combinations ($XApEn$, right). Black dots/lines indicate $0.5 \leq P_K < 0.6$; dark grey represents $0.6 \leq P_K < 0.8$ and grey indicates $P_K \geq 0.8$. Orientation: top: frontal

13.3 Evaluating electroencephalographic synchrony in classic frequency bands

13.3.1 Cross Approximate Entropy

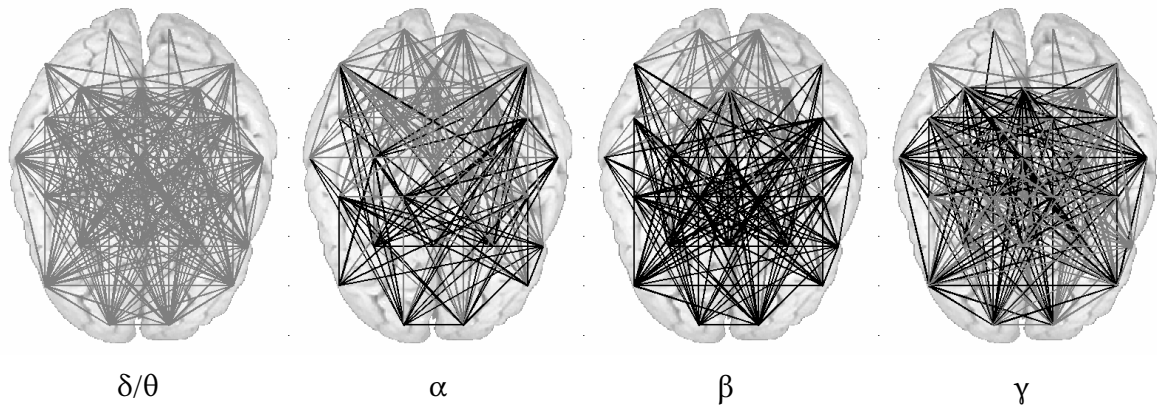


Figure 13.3: Significant propofol-induced changes of $XApEn$ in inter-channel synchrony in frequency bands: from left to right: 0.5-8 Hz; 8-12 Hz; 12-24 Hz; 25-47 Hz. Grey indicates increasing synchrony with propofol whereas black indicates a gain in asynchrony. Top: frontal;

Figure 13.3 shows the channel combinations with significant changes of $XApEn$ of EEG activity in the classic frequency bands. Asynchrony decreased over the entire cortex in the δ - and θ -frequencies indicating more synchronous behavior with propofol possibly caused by fewer network states. In the α - and even more pronounced in the β -band, asynchrony decreased in combinations with frontal electrodes involved, while it increased for combinations with parieto-occipital recordings. At γ -band frequencies, significant changes in both directions, towards synchrony and asynchrony can be observed over the cortex. For the low-frequent δ - and θ - oscillations as well as for the γ -band, only few channel combinations with frontal electrodes yielded significant $XApEn$ changes caused by propofol in contrast to the α - and β -band.

13.3.2 Bivariate Permutation Entropy

$BPeEn(\delta)$ and $BPeEn(\theta)$ decreased with propofol for most channel combinations, indicating more similarity among the channels. Analyzing the α - and β -band, $BPeEn$ increased significantly over all channel combinations. $BPeEn(\gamma)$ did not significantly change for all channel combinations. Significant changes were not unitary but changed towards synchrony or asynchrony similar to the observations with $XApEn$.

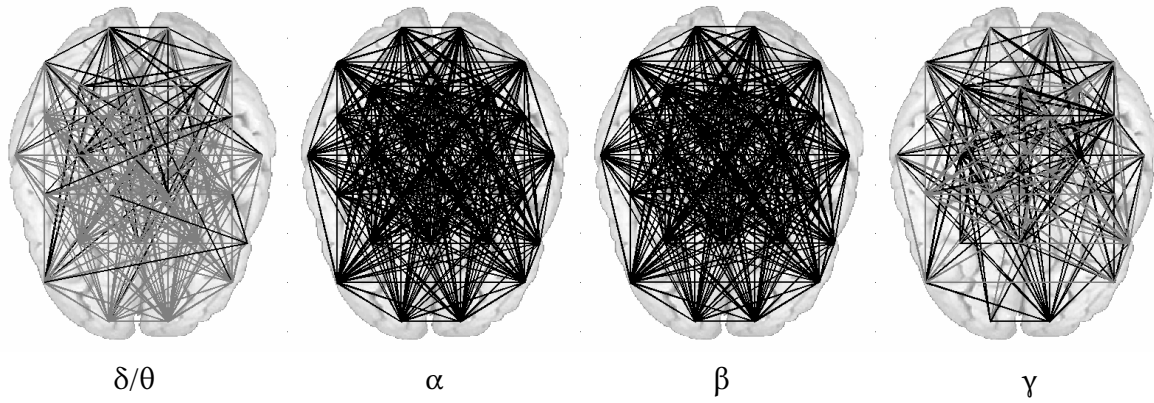


Figure 13.4: Significant propofol-induced changes of $BPeEn$ in inter-channel synchrony in frequency bands: from left to right: δ, θ : 0.5-8 Hz; α : 8-12 Hz; β : 12-24 Hz; γ : 25-47 Hz. Grey indicates increasing synchrony with propofol whereas black indicates a gain in asynchrony. Top: frontal;

Generally, anesthetics seem to have different synchronizing or desynchronizing effects in different EEG frequency ranges. $BPeEn$ and $XApEn$ seem suitable for evaluation of changes of spatial and temporal neuronal network properties locally *in vivo* (sections 9 and 10) and globally in multi-channel EEG recordings. There, one electrode records activity of approximately 10^7 to 10^{10} neurons (Nunez 1989) within a cut-out of the cortical network of about six to ten square centimeters (Cooper, Winter et al. 1965). This is in contrast to the *in vivo* recording area of only a few square millimeters, In a next step, sTE was used to detect changes in the information flow between single recording sites that were caused by the anesthetic regimen,

13.3.3 Symbolic transfer entropy

sTE evaluates changes of directed information flow between two channels. Significant results were obtained for EEG β -oscillations. In the presence of propofol concentrations corresponding to LOC, information transfer decreased for the channel combinations displayed in Figure 13.5. For the other frequencies information transfer was not systematically affected. These results confirm the role of EEG β -frequencies in the process of anesthetic-induced unconsciousness. In other experiments the β -band was identified as the frequency range were EEG based separation between wakefulness and unconsciousness is most reliable (Paprotny, Kreuzer et al. 2010). Since β -frequencies were identified as communication frequency between cortical long-range connections (von Stein, Rappelsberger et al. 1999; Varela, Lachaux et al. 2001), a reduced β -information flow between these areas may be responsible for a loss of communication structure and hence decoupling of these areas causing LOC.

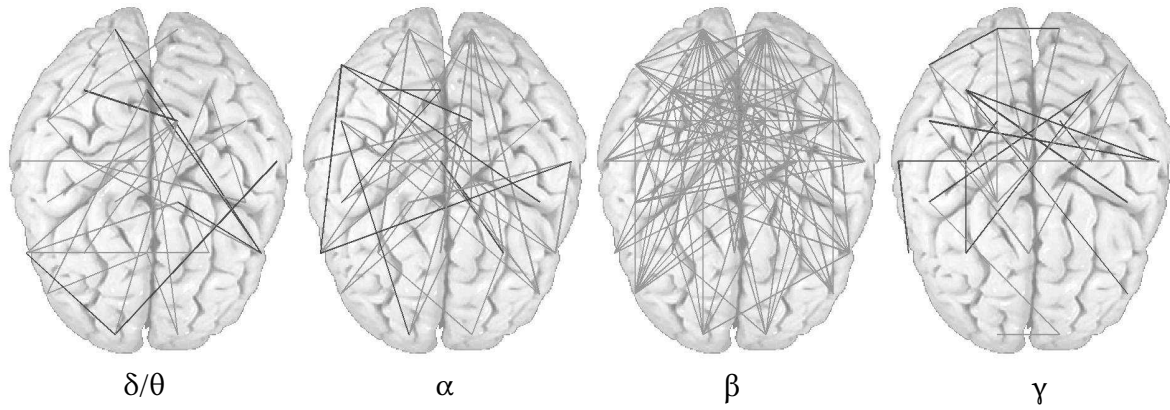


Figure 13.5: Significant propofol-induced changes of sTE in the (from left to right) θ : 0.5-8 Hz; α : 8-12 Hz; β : 12-24 Hz; γ : 25-47 Hz. Light grey lines indicate that with propofol absolute sTE is lower between two electrodes, i.e., there is less directed information flow. Only in the β -band a systematic change in cortical information transfer is visible.

13.4 Anesthetics affect EEG synchrony and information processing: Discussing the results

Multi-channel EEG recordings seem to be useful for several reasons.

13.4.1 Detection of adequate EEG recording positions

In contrast to single-channel EEG that is usually derived from the forehead, the quality of EEG recorded from other regions, i.e., temporal or occipital areas may be better. The forehead is the best spot to apply the commonly used self-adhesive electrodes. But EMG distortion may be higher than at other possible EEG electrode positions on the skull due to eye blinks and eye movements as well as frowning as well as due to the great number of contracting muscles (Goncharova, McFarland et al. 2003). The analysis of the multi-channel EEG recordings obtained from electrodes that were distributed over the scalp according to the international 10-20 system presented in section 13.2 showed that there are possibly better recording sites than the forehead, especially in the parietal area (Kreuzer, Paprotny et al. 2010). With EEG from these sites, a better performance of *ApEn* in separating consciousness from unconsciousness could be obtained in contrast to data recorded simultaneously from the forehead (section 13.2). Another reason to change EEG recording locations might be found in Alkire's article in which he proposes that frontal cortex may not be essential for anesthetic-induced unconsciousness (Alkire, Hudetz et al. 2008). Further, if single-channel EEG is analyzed, only temporal activity within a small patch of about six square centimeters

of the cortical network can be analyzed (Cooper, Winter et al. 1965). Spatial network activity properties can be additionally evaluated if multi-channel recordings are used.

13.4.2 Evaluating spatial EEG properties

In this context, multi-channel EEG data collected from volunteers undergoing propofol anesthesia was analyzed with *XApEn*, *BPeEn* and *sTE*. In the first step it could be determined that using *XApEn* and hence spatially evaluate EEG activity has more advantages than only using one EEG channel for differentiation between consciousness and unconsciousness (section 13.2) (Kreuzer, Paprotny et al. 2010). These calculations also revealed that analyzed electrode pairs including frontal electrodes show worse results than pairs from parietal and occipital regions, confirming the concerns as frontal EEG being the best solution. The use of two channel EEG recordings bears the benefit that long-range cortico-cortical signal processing can be dissected and not only intra-cortical activity or short-range cortico-cortical activity. Cortico-cortical communication seems to be based on a distinct frequency of neuronal oscillations. However, there is not yet a general consensus on which frequencies serve which function. Varela et al. propose that β -oscillations are responsible for establishing long-range connections while the γ -band seems to be more labile and more probably serve to build local patches of synchrony (Varela, Lachaux et al. 2001). John and Prichep claim β -frequencies to be responsible for intra-cortical and cortico-cortical activity and γ -activity is established in the cortico-thalamo-cortical (CTC-loop) (John and Prichep 2005). Other groups identified γ -frequencies as neuronal correlate of consciousness (Hameroff 2006; Alkire, Hudetz et al. 2008).

The results of the *XApEn* (section 13.3.1) and *BPeEn* (section 13.3.2) analysis of the γ -band seem to underline this dilemma, because no unitary result of changes in propofol induced-cortical synchrony changes could be obtained. In contrast to lower frequency bands there is no unitary directed effect of the anesthetic on spatial synchrony within these bands. Compared to the other frequency bands fewer connections (*BPeEn*) showed significant change and this change could be towards synchrony or asynchrony. Propofol-induced changes in the δ - to β -band were quite clear. Low frequent δ - and θ -synchrony (0.5-8 Hz) increased with propofol while α - and β -synchrony diminished. *BPeEn* showed significant desynchronization for all channel combinations in the α - and β -range. It is more robust to distortions due to its ordinal design. The fact that data points are coded without any tolerance seems to render *BPeEn* a parameter that evaluates also faster effects on neuronal dynamics. *BPeEn* preferentially seems to assess higher-frequent processes in the selected

frequency bands. *XApEn* determined frontal synchronization and desynchronization in parietal and occipital regions. Due to its design *XApEn* may mainly focus on the slower oscillations within the analyzed frequency range, since a tolerance parameter r suppresses low amplitude information which are mostly associated to rapid changes of the signal.

sTE presented in 13.3.3 evaluates directed information flow and the observed breakdown in β -communication, the frequency responsible for cortico-cortical tasks, indicates an altered cerebral state. The fact that *sTE* does not reflect changes in γ -frequencies may be based in the explained intra-cortical properties, i.e., the propofol effect on these frequencies is not observed by *sTE* on a large scale. Also the missing effect in the low frequencies seems plausible, since there may be no information content to broadcast.

Synchronization in the low frequency ranges may be caused by cortical neurons being driven by cortical relay neurons. In sleep, cortical neurons may be driven by thalamic relay neurons with δ -frequency (McCormick and Bal 1997). If the thalamus drives the cortex in δ -oscillations the global synchronization seems plausible. Another possibility might be due to the fact that some cortical cells oscillate with δ -frequencies when released from specific inputs (John and Prichep 2005). The α -frequency range seems to represent interactions of thalamic relay nuclei (TCR) with the cortex and α -oscillations further regulate and synchronize the excitability of cells in the thalamo-cortical pathway. This modulation is distributed cortico-cortically by interneuronal connections (John and Prichep 2005). If these mechanisms are disturbed by propofol the cortico-cortical synchronization may be negatively influenced. If thalamic TCR are hyperpolarized by the reticular nucleus transmission of sensory input by TCR neurons to the cortex is blocked and the decoupled cortical neurons start oscillations in the δ -range (John and Prichep 2005). Moreover, reticular nucleus neurons can inhibit thalamic pacemaker neurons slowing α -oscillations to the θ -range. These results add another possibility for the synchronizing effect of slow frequencies under anesthesia. Cortico-cortical transmissions are processed with β -frequencies (Varela, Lachaux et al. 2001; John and Prichep 2005). Desynchronization of β -oscillations may be caused by less γ -activity intra-cortically. γ -frequencies are used to compare cortical layer I and V in intra-cortical processes. This communication breaks down with anesthesia (Llinas, Leznik et al. 2002; John and Prichep 2005; Alkire, Hudetz et al. 2008). It could be hypothesized that if γ -communication breaks down, there is no information left to broadcast with β -oscillations. All these experiments point out, that there is sound knowledge of different tasks that are processed in cortical and subcortical areas but that the big scheme of anesthesia still lies in the dark.

13.5 Conclusion

Bivariate analyses seem capable of evaluating anesthetic-induced effects on spatiotemporal EEG properties and hence show better performance in distinguishing consciousness from unconsciousness than univariate measures. Further (de-) synchronization effects caused by propofol can be detected using the presented parameters. Low EEG frequencies in the δ - and θ -range become synchronized whereas higher frequencies become desynchronized. The analyses also identified the β -band as relevant EEG frequency to detect anesthetic induced effects.

14 Limitations

First of all, the data used for this manuscript were retrospectively analyzed, i.e., there was no chance of influencing the study design, i.e., choosing the anesthetics used and defining the anesthetic concentrations the cells, animals and humans are treated with. This leads to partly different drugs used in the single experiments as well as sometimes to concentrations of the drug that cause different hypnotic levels in the different experiments.

In order to achieve the distant goal to reliably assess the patient's state of consciousness the choice of the regimen should not influence the outcome of the signal analyses, i.e., the indicated state of consciousness. For evaluation of mechanistic issues, the choice of the regimen and their potentially different modes of action were considered.

In the *in vitro* experiments OTC were used. It can be argued that these cultured slices may not represent a fully functional cortical network. Still, this approach represents an established model for evaluating cortical effects as has been used in anesthesia research for many years (Antkowiak and Helfrich-Forster 1998; Antkowiak 1999; Dai, Perouansky et al. 2009). Further, it has to be mentioned that the effects detected on the *in vitro* down-state experiments are rather subtle and may hence be masked *in vivo* by drug actions on other cells such as thalamo-cortical neurons. In the *in vivo* experiments a potential limitation of the results may be the fact that the body temperature of the animals was not controlled, which in principle does not exclude moderate hypothermia. To minimize the influence of this phenomenon, the animals were placed into a plastic housing which provided some thermal insulation, and therefore at least it seems unlikely that they experienced severe hypothermia.

In the EEG studies especially with data derived from frontal recording sites on the patient's / volunteer's forehead EMG may superpose the useful signal. Especially in the higher EEG frequencies analyzed, EMG may influence the recording (Bonhomme and Hans 2007). In order to restrict the superposition of EMG and EEG we used only frequency ranges up to 30 Hz or focused on the EEG α - and β - frequency ranges. But still, influence of EMG cannot be completely excluded. In the transition studies the exact conscious state of the patient is of importance. Since the patient's state can only be evaluated by direct response from the patient to the investigator, this procedure could lead to possible inaccuracy in the evaluation of the state, which may pose an inherent problem in the experiments during the single-channel transition studies. But information processing changes in frontal cortical regions play a major role during propofol induced unconsciousness and *PeEn* –the

parameter used in these experiments– seems able to reflect these changes. Nevertheless, the underlying mechanisms triggering anesthetic-induced unconsciousness are not fully explored, i.e., a direct association of calculated *PeEn* with a specific state is not completely possible and has to be assumed to some degree. This limitation reflects the general problem when it comes to the evaluation of anesthetic-induced effects on brain electrical activity. The underlying sources that trigger these effects are still unknown. This is in contrast to examples from control systems engineering. If the control circuit and the disturbance are known the effect on the output is known as well. Here, the disturbance, the anesthetics induce cannot be precisely quantified as well as the control circuit, only the output, the LFP or EEG, can be observed. Hence, conclusions drawn may be assumptions. But with every result obtained during the analysis of anesthetic effects with different analyses techniques (signal analyses, imaging, ...), results can be combined, aligned and confirmed.

A last point to be mentioned is the knowledge transfer from experiments *ex vivo* to the animal model *in vivo* as well as from the animal model to humans. In the first case, effects observed *in vitro* may be superposed by effects on other cerebral regions *in vivo* and hence not be observed. In the second case, the translation from findings in animals to the more complex human brain may be questioned. But studies have shown that depth of anesthesia parameters as used in humans also work in the animal model (Silva, Campos et al. 2011) and the results presented in this thesis also reveal similarities between anesthetic induced effect in the animal and human.

15 Anesthetic-induced unconsciousness – a cortical point of view

15.1 Summary of the findings

Analyses of the data sets using the non-linear methods revealed significant anesthetic-induced effects for all experiments from the *in vitro* setup to multi-channel EEG recordings. Following observations that were determined are new, hence they should be pronounced.

15.1.1 LFP *in vitro*

LFP episodes not showing spontaneous activity – so called down-states – contain relevant information that changes with the presence of sevoflurane. So far, these down-states were considered cortical noise. Especially at sevoflurane concentrations corresponding to the loss of consciousness, a significant effect on *ORR* was observed (Drexler, Kreuzer et al. 2013). Further, activity during these down-states was not altered significantly by propofol, in contrast to the sevoflurane experiments (Kreuzer, Schneider et al. 2008).

15.1.2 LFP *in vivo*

Anesthetics concentration-dependently influence synchrony in the observed cortical network. These effects were revealed using bivariate entropy measures. The changes that are induced by volatile anesthetics are similar to changes found in analyses of EEG recordings. This leads to the conclusion that anesthetics unfold their effects on neuronal network activity of different size (Kreuzer, Hentschke et al. 2010).

Propofol has a significant effect on information processing between prefrontal cortex and hippocampus. Analysis of the relevant frequency range using bivariate entropy measures showed significantly decreased directed information flow between those areas, relevant for mnemonic processes. These effects may reflect a possible mechanism of anesthetic-induced amnesia (Kreuzer, Butovas et al. 2011).

15.1.3 Single and multi-channel EEG

The non-linear measure *PeEn* does not follow the phenomenon of paradoxical excitation during induction of anesthesia of EEG α - and β -frequencies as spectral measures do. It correctly reflects the fading of consciousness in contrast to the spectral analyses that stated a period of increased awareness. This finding may prove useful for the purpose of EEG based depth of anesthesia monitoring. During the anesthetic-induced state transition loss of consciousness different EEG oscillation have different reaction times to the state change.

Faster oscillations show an effect earlier than slower ones. Since faster EEG frequencies may be correlated with cortical processes and slower oscillations with processes in deeper, subcortical regions these results may deliver first clues pointing towards a cortical trigger of consciousness .

All these findings justify the evaluation of anesthetic induced effects using the applied analyses to determine effects on electrophysiological recordings from neuronal networks. The results pronounce the role of cortical areas for the process of anesthesia.

15.2 Discussing the role of the cortex

The presented work had two main objectives. The first one was to show that non-linear analyses are applicable to all sizes of neuronal networks and are able to reveal anesthetic-induced effects that may shed additional light to the process of anesthesia. These parameters were initially used to evaluate changes in EEG caused by anesthetic drugs (Bruhn, Ropcke et al. 2000; Jordan, Stockmanns et al. 2008; Olofsen, Sleight et al. 2008; Jordan 2010). Here, they were also utilized to evaluate effects on smaller patches of (cortical) activity, i.e., intra-cortically recorded LFP. And in another diminishing step, to analyze LFP derived from cultured isolated cortical networks lacking subcortical inputs. With the parameter set it was possible to detect significant effects of anesthetics in all sizes of neuronal networks using the same parameter setups. Nevertheless, different parameters revealed different effects. For example in the *in vitro* setup with cultured cortical cells, *ApEn* showed significant reaction on the lowest dose of sevoflurane whereas *ORR* reacted at a later concentration stage corresponding to the MAC_{awake} . In EEG recordings *PeEn* reliably distinguished consciousness from unconsciousness and *ApEn* reflected the different levels of anesthesia in a better way. With the introduction of bivariate measures to LFP analysis spatial information changes of electrophysiological recordings could be revealed. This work presents a first approach to evaluate an effect of anesthetics on electrical activity preferably in cortical networks at state transitions using non-linear analyses. So far, most analyses were performed at equilibrated concentrations of anesthetic regimens and dynamic processes happening during state transitions were neglected. Based on a dataset that allowed EEG analysis during LOC/ROC transitions initial attempts were made to investigate these transitions with the presented sets of parameters. This brings us to the second objective, the search for possible mechanisms of state transitions that can be observed in electrophysiological recordings. Different cerebral regions such as prefrontal cortex, thalamus and hippocampus were identified as major targets for general anesthetics,

mainly because of their high density of GABA_A receptors (Campagna, Miller et al. 2003). Numerous studies present significant effects of anesthetics in these areas but so far nothing can be said regarding the order of processes when unconsciousness is released. For example John and Prichep suggest a unitary mechanism for all anesthetics of inducing unconsciousness that starts with depression of the brainstem hence influencing the ascending reticular activating system. In further steps effects are released upon thalamic and mesolimbic connections with cortical areas. In the last step a depression of prefrontal cortex leads to reduced awareness (John and Prichep 2005). This theory of a unitary bottom-up approach was strongly questioned by other researches, arguing that different anesthetics act in different ways, i.e., ketamine and etomidate induce unconsciousness but do not affect thalamic structures. Experimental results lead to the suggestion that the cerebral cortex may be a trigger of consciousness and the process of losing consciousness may start there (Antkowiak 2005). Analysis of electrophysiological data recorded from different generating networks may help to gain new insights into this question. An initial hint may provide the results derived from isolated and cultured cortical networks. These preparations have no connection to subcortical areas, i.e., observed effects are purely cortical. It has been previously shown that action potential spiking activity is altered significantly with general anesthetics and that volatiles prolong LFP bursts (Antkowiak and Helfrich-Forster 1998; Antkowiak 1999). The presented results of this work reveal that volatiles represented by sevoflurane significantly affected activity in the down-state episodes even at subhypnotic concentrations of the regimen. Signal complexity of the LFP increased during down-states as reaction on sevoflurane, probably caused by a smaller signal to noise ratio. This could lead to the assumption that network dynamics which are necessary for consciousness are negatively influenced. A significant effect on LFP at concentrations corresponding to the MAC_{awake} represented by a switch-like change of *ORR* may deliver another clue towards a cortical mechanism of the process of losing consciousness. Furthermore, the fact that *ApEn* reacts on sedative and *ORR* on hypnotic sevoflurane concentrations suggests that sevoflurane alters down-state activity in qualitatively distinct ways which are concentration-dependent and that cerebral cortical areas are a major player in inducing sedation and unconsciousness. The fact that cortical down-states remain unaffected by propofol contradicts the theory of a unitary mechanism of anesthesia. If the cortical network is extended and subcortical inputs are added as in the *in vivo* recordings, volatiles cause a steady, concentration-dependent decrease in LFP complexity, but propofol does not. This inverse parameter behavior with volatiles can be explained by the absence of subcortical structures in the *in vitro* preparations. The fact that spectral power at low

frequencies is depressed with volatiles *in vitro* and activated *in vivo* supports these findings. For propofol no significant effect could be observed, neither for *in vitro*, nor for *in vivo* LFP. The cortex is disintegrated as observed *in vitro* and subcortical structures begin to drive the cortex at low frequencies resulting in more regular cortical activity as observed in the univariate analysis *in vivo*. This extended network seems also responsible that no switch-like behavior around the MAC_{awake} could be observed for volatile anesthetics *in vivo* as with *ORR in vitro*. Spatial, bivariate analyses revealed more regularity among the channels with volatiles leading to the assumption that the observed LFP activity is synchronized and that is why its information capacity is reduced. *XApEn* decreased monotonously with increasing concentrations of the volatile. Qualitative effects of *XApEn* on cortical *in vivo* activity and frontal interhemispheric EEG activity were notably similar. This leads to the suggestion that the synchronizing effects of general anesthetics are observable in small, intra-cortical networks as well as in activity that is spread cortico-cortically over long distances. A small number of interneurons control a large number of EEG generating cells (Brown, Lydic et al. 2010) and the results suggest that this synchronization may occur due to more synchronized interneuron activity. In addition to that, the results of multi-channel EEG analysis reveal that the strongest anesthetic effect is visible in the β -frequency range, i.e., the frequencies that seem responsible for long-range synchronization in the cortex. Information transfer is significantly decreased at these frequencies at concentration corresponding to LOC, giving another hint towards a cortical effect of losing consciousness. If long-range connections are disrupted or their state space is reduced the brain is not able to preserve consciousness. All these results were obtained during analyses of steady state conditions at equilibrated drug concentration levels. Since LOC seems to be similar to a first order state transition (Steyn-Ross, Steyn-Ross et al. 2004) and the mind switches from consciousness to unconsciousness, mechanistic issues cannot be processed by using steady state signal sequences. So the logical next step was to evaluate anesthetic-induced changes during LOC and ROC. Initially, LOC seems to be the more interesting transition since a phase of paradoxical excitation can be observed. Spectral power is activated during this phase in the α - and β -range causing spectral based measures to indicate a more aware state, i.e., falsely indicated consciousness (Kuizenga, Wierda et al. 2001). In contrast to spectral approaches, *PeEn* does not follow this excitation but reflects decreasing information content in the signal with increasing anesthetic concentrations. During this phase EEG activity becomes more synchronous leading to the activation but simultaneously the state space is reduced through more regular activity. The start of spectral activation in the β -

range lies before the state transition confirming the theory of a cortical trigger of consciousness. The transition analysis with *PeEn* also revealed a time hysteresis of the anesthetic effect. Faster frequencies seem to adapt quicker to the changed state than slower oscillations. Faster oscillations seem associated with cortical information processing, γ -frequencies represent intra-cortical communication or form patches of local synchrony whereas β -oscillations are responsible for cortical long range information transfer and synchronization between neighboring cortices (von Stein, Rappelsberger et al. 1999; von Stein and Sarnthein 2000; John and Prichep 2005). Frequencies in the α - and θ -range seem associated with mnemonic tasks (Bland 1986) and structuring working memory and mental imagery (von Stein and Sarnthein 2000; Sauseng, Griesmayr et al. 2010). θ -oscillations derived from frontal midline recording sites are assumed to share functional relationships with hippocampal oscillations in this frequency range (Mitchell, McNaughton et al. 2008). Furthermore, an inverse relation between scale of integration and frequency of interaction seems to exist, i.e., lower frequencies have a wider transmission range. And more generally low frequency interactions may be a characteristic feature for top-down interactions (von Stein and Sarnthein 2000). These results suggest that modification of EEG θ -oscillations by anesthetics has less to do with the hypnotic rather than with the amnestic component of anesthesia. In animal experiments an anesthetic-induced frequency shift towards lower frequencies could be observed, hence impairing memory consolidation (Butovas, Rudolph et al. 2010; Perouansky, Rau et al. 2010). In section 10.5 a direct influence of propofol on the cortico-hippocampal pathway is described. With the presented results the conclusion could be drawn that initial effects take place in the cortex and the mechanism of losing consciousness follows a top-down approach. This means that the cortical oscillations are suppressed (γ -waves) or hypersynchronized (β -waves) causing hypnosis. Effects in the EEG α - and θ -range lead to distortions in working memory tasks and memory consolidation causing amnesia. These conclusions are all based on the analysis of electrophysiological recordings and may function as a basis for further discussions concerning the yet unknown mechanisms of anesthesia-induced unconsciousness. The presented methods seem capable of gaining new information to these mechanisms and may serve as valuable extension to experiments identifying molecular and receptor specific effects or neuroimaging approaches. The next logical steps to conduct are analyses of specific pathways as presented for information processing between hippocampus and cortex in chapter 10. These information processes between neocortex and hippocampus seem responsible for mnemonic processes and an effect on this connection is estimated as reason for anesthetic-induced amnesia. First results of analyses in the pathway between amygdala and hippocampus

delivered promising results (Kreuzer, Kratzer et al. 2012). Similar experiments could be performed in the cortico-thalamo-cortical loop to shed light in the processes causing hypnosis. Derived results could help to undermine the presented cortical theories or identify the thalamus as trigger of consciousness. Taking all presented experiments and their results into consideration this work was able to show the potential of non-linear analysis of electrophysiological signals to detect anesthetic-induced effects. Bivariate approaches are capable of evaluating changes in synchrony and information transfer between two channels. Using these parameters, spatial information could also be included in the non-linear analyses. Results of the cortical *in vitro* and *in vivo* experiments and especially of the EEG recordings during state transitions point towards a cortical mechanism of losing consciousness. The presented methods and results may add another part of information to the general understanding of how anesthetics unfold their functional effects and to mechanistic differences between the single anesthetic drugs. Nevertheless, we cannot be sure that the potential of signal analysis methods is fully exploited. Potentially, one can still find undetected information in electrophysiological recordings of brain activity using different analyses. Further evaluation of how anesthetics trigger hypnotic and amnestic effects is essential in order to get the complete picture. Other methods like for instance functional magnetic resonance imaging of the brain in humans or voltage-sensitive dye imaging of cerebral structures *ex vivo* may help to gain further insights to the process of anesthesia. Every new piece of information may prove useful to work out new or optimize established signal analysis methods in order to develop an appropriate monitoring of anesthetic depth during surgical intervention. Analysis of the EEG during anesthesia is a promising, yet not fully developed approach to guide the patient through anesthesia. The analysis methods used in this thesis have proven useful for monitoring depth of anesthesia and seem to be superior to analyses, recently used by commercially available depth of anesthesia monitors, following a probabilistic approach (Jordan 2010). Hence optimization of the presented analyses combined with adaption new information regarding the process of anesthesia from other analytical approaches may help to ensure patient safety in the long run.

16 A cortical curiosity: Brain electrical activity obeys Benford's Law

The results presented in this section were also published as pre-release in *Anesthesia & Analgesia*. (Kreuzer, Jordan et al. 2014)

16.1 Background

In 1881 Simon Newcomb proposed that in many statistical and scientific tables the first non-zero digits are not distributed equally, but logarithmically. He found a formula, nowadays known as Benford's Law, describing a logarithmic distribution of the first digits (Newcomb 1881). In 1938, Frank Benford confirmed Newcomb's observation by creating an extensive database containing different kinds of data such as length of rivers, atomic weights, specific heat constants, the numbers occurring in a newspaper and many more (Benford 1938). In all of these collected data sets, the leading digits followed the logarithmic distribution reasonably well. Furthermore, Engel and Leuenberger showed that exponentially distributed numbers approximately obey Benford's Law (Engel and Leuenberger 2003). Today this distribution is used in macroeconomic statistics (Nye and Moul 2007) to detect fraud in accounting data (Durtschi, Hillison et al. 2004), income tax evasion (Nigrini 1996) or for the screening of large data sets (Brown 2005). Most recently Benford's Law was used to detect abnormalities in the 2009 Iranian election (Roukema 2009).

The idea of using Benford's Law on screening data is based on the observation that regular not faked data usually follow a logarithmic distribution while faked data show abnormalities in the distribution (Hill 1999). The law defined by Benford states that the first digits within many datasets that are not zero are distributed logarithmically and not equally as one may expect. This law can be written as

$$P(d) = \log_{10}\left(1 + \frac{1}{d}\right) \quad (16.1)$$

Where $P(d)$ is the probability of the first non-zero digit being d , with $d \in \{1,2,3,4,5,6,7,8,9\}$. The following example can explain the nature of this law: Imagine the stock price is rising from 10 to 20 points. The difference between both prices is 10 points and the price is doubled. If the price increases from 80 to 90 points, the difference is still 10 points, but the price only rises by $(9/8-1) = 12.5\%$. Even if the difference for both examples is ten points, it takes more effort to come from 10 to 20 than from 80 to 90. This implies that the 1 will show up more often than any other digit.

One property of Benford-distributed data is its scale-free behavior. Scale-free properties of neuronal networks have been observed in a number of publications. In organotypic cultures and acute slices of rat cortex the propagation of field potentials in neuronal avalanches as measure of network connectivity are scale-free (Beggs and Plenz 2003). In EEG analyses scale-free behavior was observed in α - and β - oscillations where amplitude fluctuations are scale free (Linkenkaer-Hansen, Nikouline et al. 2001), as well as in identifying networks involved in epileptic processes (Worrell, Cranstoun et al. 2002). In a graph theoretical approach scale-invariance was observed for connection durations in multi-electrode EEG recordings. This invariance persisted even when the test subject was anesthetized (Lee, Mashour et al. 2009). These experiments are only examples among a vast number of scale-invariant observations in neuronal networks. A data set was considered scale-invariant if its distribution followed a power-law, i.e., $y = ax^b$ with b being the exponent of the power law. In general, scale-free phenomena are considered to follow some kind of structured organization. Benford's law also indicates scale-invariance but with a logarithmic approach. In our experiments we did not focus on connectivity and correlation issues within the neuronal network, but on the distribution of voltage fluctuations in EEG and LFP time series under control conditions and during sevoflurane general anesthesia in order to reveal properties that can be used for evaluating the patients, respectively the neuronal networks state. For example, if the modulation of neuronal network activity through propofol alters the first digit distribution, it would then be an indicator for the patient's altered state of consciousness. It is unknown to what extent recorded LFP and EEG activity obey Benford's Law. We used anesthesia-induced changes of cortical processing of information as a general model of unconsciousness and amnesia.

16.2 Methods

For analysis, two independent data sets are considered. On the one hand sevoflurane data from the steady state study (section 5.4) was used for EEG analysis and on the other hand LFP activity *in vitro* from cultured cortical neurons (section 5.1) was analyzed. In this chapter the question is addressed whether biological signals derived from neuronal networks in the absence and also in the presence of an anesthetic drug follow Benford's Law. For both data sets, the distributions of first digits at control conditions were tested in accordance with Benford's law. Thereafter, it was analyzed whether the application of the volatile anesthetic sevoflurane modifies these distributions. EEG data were analyzed without additional filtering and after an additional 30 Hz low-pass filtering to minimize

EMG distortion at levels "awake", "light general anesthesia" (inter1) and "deep general anesthesia" (inter2) (section 5.4.1). A 10 s EEG sequence from each equilibrated level was extracted from each recording and the first digit distribution was checked for concordance with Benford's Law. In the LFP recordings also a 10 second sequence showing spiking activity and a resting signal (up- and down-states) was cut out at the end of each recording and the first digit distribution of these sequences was analyzed with respect to Benford's Law. In addition, the first digit distribution of the selected down-states also used for the analysis in section 8 was compared with the Benford distribution. Considered concentrations were 0 MAC ("awake"), 1 MAC ("light general anesthesia") and 1.5 MAC ("deep general anesthesia") (section 5.1.2).

The first digit distributions of the recordings without sevoflurane administration were compared to the distributions with sevoflurane. Comparison for accordance with the Benford distribution was performed as follows: data of one anesthetic level were pooled to one data set X for EEG or LFP data respectively. If the first digit distribution of the analyzed data set shows logarithmic behavior, the mantissas of the data's logarithm is uniformly distributed (Newcomb 1881). A set union can be defined as described in equation 16.2:

$$E_i := \bigcup_{k \in \mathbb{Z}} [i \cdot 10^k, (i+1) \cdot 10^k[\quad \text{for } i \in \{1, 2, \dots, 9\}, \text{ i.e., } \mathfrak{R}_+ = \bigcup_{i=1}^9 E_i \quad (16.2).$$

Hence, the probability of one data point having the first digit i is described in equation 16.3:

$$P(X \in E_i) = P(\langle \log(X) \rangle \in [\log i, \log(i+1)[) = \log(i+1) - \log i = \log\left(1 + \frac{1}{i}\right) \quad (16.3).$$

$\langle x \rangle$ is the mantissa of x , i.e., $x \bmod 1$.

$$P(X \in E_i) = \log\left(1 + \frac{1}{i}\right) \quad (16.4)$$

is the definition of Benford's Law. We compared the logarithmic, modulo 1 first digit distribution of the single data sets to a uniform distribution using the Kolmogorov-Smirnov test statistics. This test was performed using R 2.4.0 (R Foundation for Statistical Computing, Vienna, Austria) (R Development Core Team 2006). Additionally, similarity of the distributions was indicated by QQ-plots.

16.3 Results

Both, *in vitro* and EEG data lead to a test statistics ≤ 0.11 (Kolmogorov-Smirnov test) indicating a good similarity to the Benford distribution, related to a maximum deviation of 1. This is confirmed by corresponding QQ-plots which indicate only a small deviation from the bisecting line (Figure 16.1 and Figure 16.2). If the plotted EEG and *in vitro* data comply with the bisecting line a uniform distribution is indicated, i.e., the first digits of the data set show the Benford distribution. Small deviations of the data from the bisecting line still show accordance with the Benford distribution. Note that because of the large data set and of possible dependence of measurements, a p-value may be biased and therefore, is not included in the present analysis.

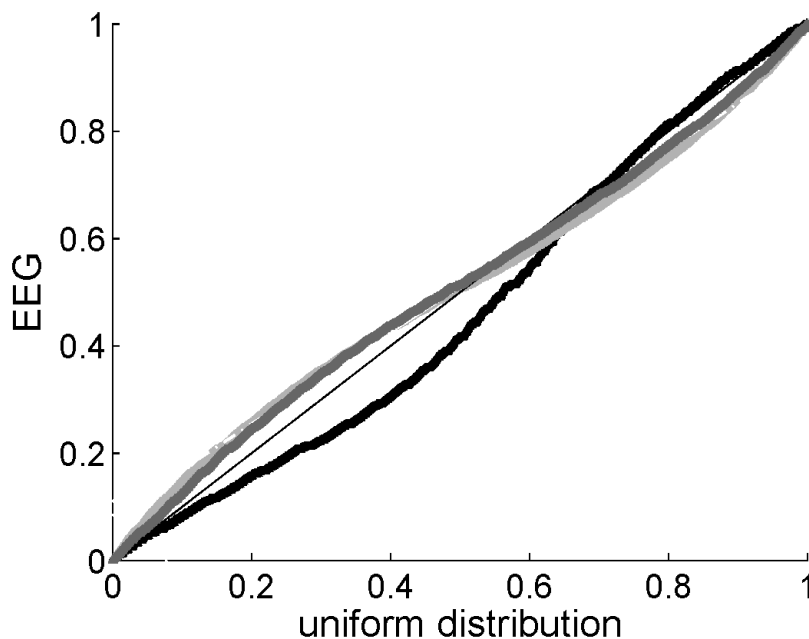


Figure 16.1: QQ-plots of the unfiltered EEG data, comparing the logarithmic, modulo 1 first digit distribution of the EEG sequences derived from the recordings at "awake" (black), "light general anesthesia" (grey) and "deep general anesthesia" (light grey) to a uniform distribution (black, thin line). All three EEG distributions are close to the bisecting line representing uniform distribution. The curvature of the EEG "awake" distribution is inverse to the EEG distributions recorded under sevoflurane. (Kreuzer, Jordan et al. 2014)

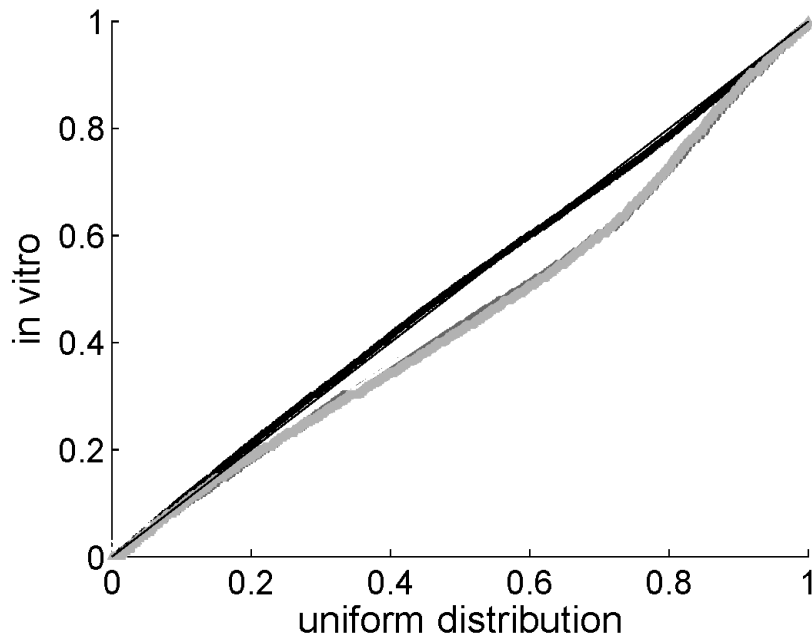


Figure 16.2: QQ-plots of the *in vitro* up and down-state sequences data, comparing the logarithmic, modulo 1 first digit distribution of the LFP sequences recorded at concentrations corresponding to "awake" (black), "light general anesthesia" (grey) and "deep general anesthesia" (light grey) to a uniform distribution (black, thin line). The distribution of the LFP "awake" sequences almost perfectly matches the Benford distribution, while the LFP "anesthesia" distributions still show good concordance to the bisecting line. (Kreuzer, Jordan et al. 2014)

The QQ-plots derived from EEG are close to the bisecting line for all anesthetic levels (Figure 16.1), i.e., the EEG recorded at different anesthetic levels is and remains Benford-like distributed. But the level "awake" can be distinguished from anesthetic levels by a different curvature in the QQ-plot. The "awake"-plot starts below the bisecting line while at anesthetic levels the plot is initially above the bisecting line. The curvature flips with delivery of sevoflurane. The state "awake" can be even better separated from "light general anesthesia" and "deep general anesthesia" by looking at the distribution of probabilities of the first digit being d . The curve of the first digit distribution from "awake" is more pronounced than the distributions from the recordings performed under anesthesia (Figure 16.3). The probability $P(d=1)$ and $P(d=2)$ is higher at the level "awake" than it is during anesthesia. The second plot of this figure shows the first digit distribution of the recorded data after 30 Hz low-pass filtering that was performed to exclude EMG activity from the analysis. This filtering does not have influence on the course of the anesthetic-induced change in the distribution.

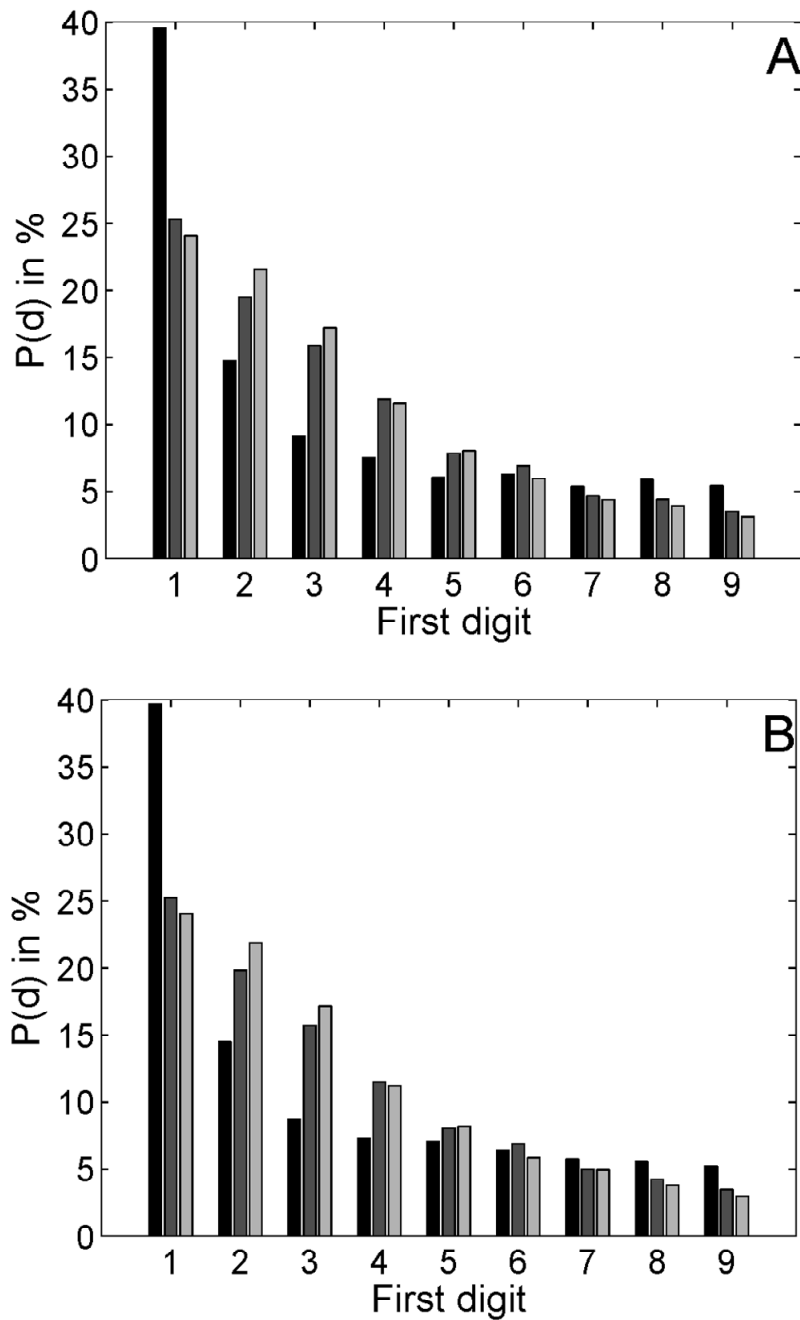


Figure 16.3: First digit distribution of unfiltered (A) and 30 Hz low-pass filtered (B) EEG data derived from sequences recorded at the levels “awake” (black), “light general anesthesia” (grey) and “deep general anesthesia” (light grey). The 30 Hz low-pass filtering does not influence the first digit distribution. After application of sevoflurane the first digit distribution becomes flatter. There are no significant differences in the distribution of the states “light general anesthesia” and “deep general anesthesia”. (Kreuzer, Jordan et al. 2014)

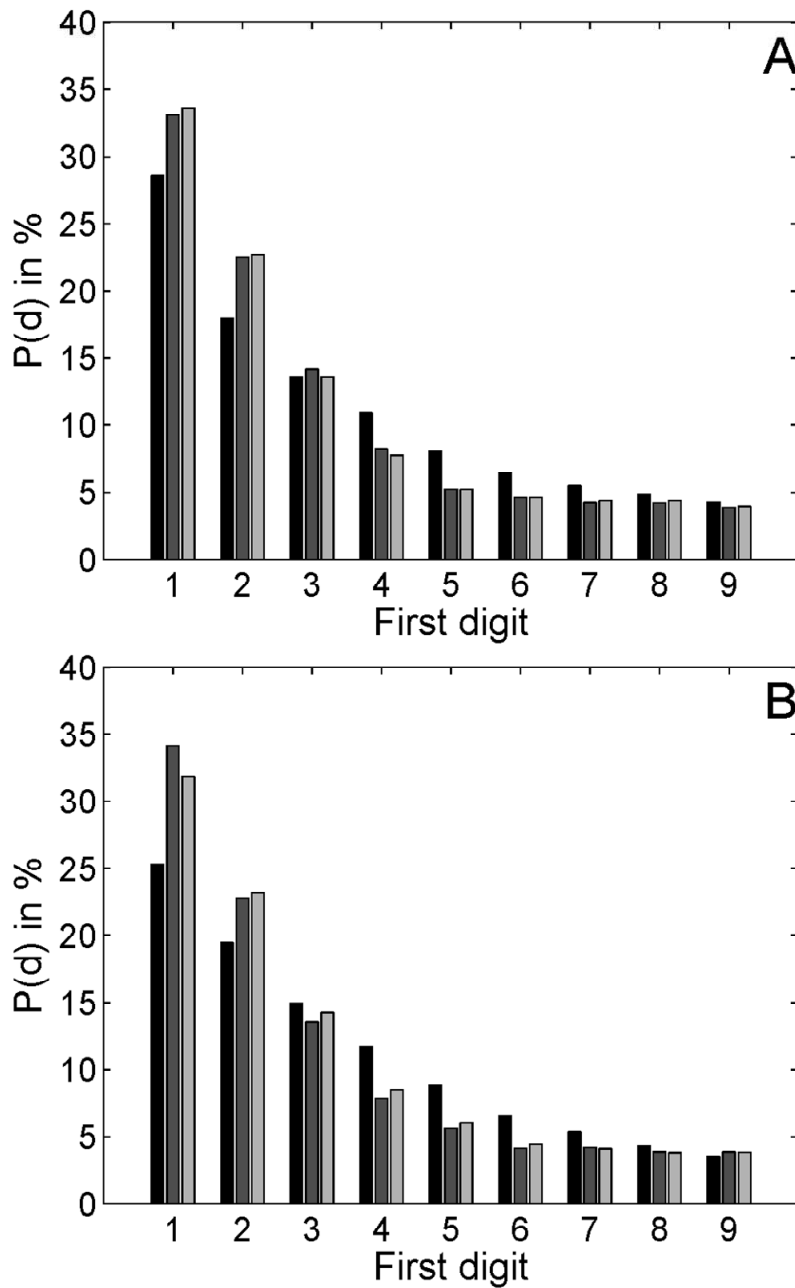


Figure 16.4: First digit distribution of the *in vitro* data (A: up- & down-state sequences; B: down-state sequences) recorded at the levels “awake” (black), “light general anesthesia” (grey) and “deep general anesthesia” (light grey). With application of sevoflurane, the first digit distribution of the recorded LFP sequences becomes steeper. There is no significant difference in the distributions of the analyzed sequences containing up- and down-states and the down-state only sequences. The sevoflurane concentration also seems to have only small impact on the distribution, because distributions recorded during light and deep general anesthesia only differ to a small degree. (Kreuzer, Jordan et al. 2014)

The *in vitro* QQ-Plot derived in absence of sevoflurane almost completely fits the bisecting line. The plots from the data with sevoflurane do not show this strong concordance, but are still very close to the bisecting line, i.e., agree with the Benford distribution (Figure 16.2). The flip in the curvature caused by sevoflurane is vaguely visible and it is inverse to the EEG data. The probability distribution of the leading digits was more pronounced after the cells were washed with sevoflurane, i.e., $P(d=1)$ and $P(d=2)$ was higher under sevoflurane delivery. This is contrary to the EEG observation. This distribution did not change significantly when the entire LFP recording containing up- and down-states or only down-states were analyzed. Spiking activity did not have influence on the resulting probability distribution (Figure 16.4).

16.4 Discussion

The presented results demonstrate that data sets representing information about the activity states of human brains and cultured neurons obey Benford's Law. Most important, this observation holds true for different states of neuronal activity corresponding to the states "awake", "light general anesthesia" and "deep general anesthesia" in human patients.

In other works, a global scale-free behavior according to power laws of neuronal network activity in terms of coupling of different cortical areas was observed in absence and presence of propofol (Lee, Mashour et al. 2009). Other results did also find power law distributions for neuronal network tasks such as LFP firing propagation (Beggs and Plenz 2003). All these findings suggest that neuronal processes and interactions are scale-free and follow a distinct organization. Our results indicate that scale-invariance also holds true for the analyzed EEG and LFP traces, independent of low-pass filtering. However, in order to gain knowledge for possible monitoring issues we did not evaluate the network connectivity but the first-digit distribution of voltage fluctuations in single channel EEG and LFP recordings. The *in vitro* experiments represent an isolated, cortical neuronal network (see section 5.1) whereas EEG is also influenced by subcortical structures. In the absence of drugs the first digit distribution of cortical activity complies with Benford's Law. This finding applies to LFP-recordings, carried out in cortical cultures and to EEG data sampled from human subjects equally well. The anesthetic sevoflurane was applied to modify the activity patterns of cortical neurons in a systematic and reproducible way. There is ample evidence in the literature that, at clinically relevant concentrations, this anesthetic enhances synaptic inhibition (Stucke, Zuperku et al. 2005; Ishizeki, Nishikawa et al. 2008). In cortical neurons, anesthetic-induced enhancement of synaptic inhibition shifts the balance between

excitatory and inhibitory synaptic inputs towards inhibition, thereby reducing neural excitability and activity (Hentschke, Schwarz et al. 2005). Benford's Law also applies to neuronal activity patterns induced by sevoflurane. Interestingly, there is a striking difference with regard to the actions of sevoflurane on cultured neurons and on the EEG of human subjects. In cultured neurons the anesthetic caused the distribution to "steepen", i.e., the probability of the first digit being 1 or 2 increased. This observation was made in the sequences containing phases of high- and low network activity (up- and down-states) and those containing exclusively down-states. However, an opposing action of sevoflurane was observed in the EEG-data as the distribution was flattened by sevoflurane, i.e., the probability of the first digit being 1 or 2 decreased.

Why does sevoflurane modify the distributions calculated from *in vitro* measurements and EEG-recordings in opposing ways?

The anesthetic sevoflurane decreases the activity of cortical neurons during up-states, which may result into prolonged up-states because the depletion of glutamate-containing synaptic vesicles is reduced. Sevoflurane-induced prolongation of down-states indicates that the anesthetic either delays recovery of neural excitability or increases the critical threshold that has to be crossed for triggering an up-state. Such a mechanism may explain the effects of sevoflurane on the activity patterns of cultured cortical neurons.

However, in an intact brain, cortical neurons display activity patterns which clearly deviate from those observed in isolated cortical networks. During wakefulness, asynchronous sensory input is transferred via thalamic relay neurons into the cortex. In this mode, relay neurons do not display synchronized firing (Steriade, McCormick et al. 1993). As a consequence, cortical neurons are receiving irregular synaptic inputs. In this mode cortical cells display irregular action potential firing and the EEG is desynchronized. During deep sleep and anesthesia, thalamic relay neurons oscillate in synchrony in the δ -frequency range (1-4 Hz). In this state, thalamic neurons produce strong and rhythmic synaptic excitation of cortical pyramidal neurons, forcing these cells to display a very similar activity pattern. Therefore, it is widely assumed that anesthetic-induced high-voltage low-frequency EEG activity is caused by a thalamic mechanism of action, pushing thalamic relay neurons into the mode of oscillatory δ -activity (Franks 2008).

16.5 Conclusion

Taken together, the different effects of sevoflurane on the distributions calculated from *in vitro* data and EEG-recordings most probably reflect actions on different neuronal substrates. In human subjects, sevoflurane affects both cortical and thalamic neurons. The thalamic effect strongly influences the EEG recording, thereby probably masking the direct actions of sevoflurane on cortical neurons. In cultured cortical neurons the influence of extra-cortical neurons is lacking, and as a consequence, the pure effect of sevoflurane on cortical neurons can be studied. Therefore, the different effects of sevoflurane on the Benford distribution as observed in the human EEG and in isolated cortical networks represent specific responses of different cell types and neural networks (cortex versus thalamus) to anesthetic-induced enhancement of synaptic inhibition. Most important, the distribution of data remained "Benford-like" under all experimental conditions tested in the present study. The latter finding opens new avenues for the screening of neurophysiologic data for irregularities.

17 Reference list

- Alkire, M. T., R. J. Haier, et al. (2000) "*Toward a Unified Theory of Narcosis: Brain Imaging Evidence for a Thalamocortical Switch as the Neurophysiologic Basis of Anesthetic-Induced Unconsciousness*" *Consciousness and Cognition* 9(3): 370-386.
- Alkire, M. T., J. R. McReynolds, et al. (2007) "*Thalamic microinjection of nicotine reverses sevoflurane-induced loss of righting reflex in the rat*" *Anesthesiology* 107(2): 264-272.
- Alkire, M. T., A. G. Hudetz, et al. (2008) "*Consciousness and Anesthesia*" *Science* 322(5903): 876-880.
- Antkowiak, B. and C. Helfrich-Forster (1998) "*Effects of small concentrations of volatile anesthetics on action potential firing of neocortical neurons in vitro*" *Anesthesiology* 88(6): 1592-1605.
- Antkowiak, B. (1999) "*Different actions of general anesthetics on the firing patterns of neocortical neurons mediated by the GABA(A) receptor*" *Anesthesiology* 91(2): 500-511.
- Antkowiak, B. (2002) "*In vitro networks: cortical mechanisms of anaesthetic action*" *British Journal of Anaesthesia* 89: 102-111.
- Antkowiak, B. (2005) "*The "Anesthetic Cascade": Fact or Fiction?*" *Anesthesiology* 103(4): 904-905.
- Antognini, J. F., X. W. Wang, et al. (1999) "*Quantitative and qualitative effects of isoflurane on movement occurring after noxious stimulation*" *Anesthesiology* 91(4): 1064-1071.
- Bandt, C. and B. Pompe (2002) "*Permutation Entropy: A Natural Complexity Measure for Time Series*" *Physical Review Letters* 88(17): 174102.
- Beck, T. W., T. J. Housh, et al. (2006) "*An examination of the Runs Test, Reverse Arrangements Test, and modified Reverse Arrangements Test for assessing surface EMG signal stationarity*" *Journal of Neuroscience Methods* 156(1-2): 242-248.
- Beggs, J. M. and D. Plenz (2003) "*Neuronal Avalanches in Neocortical Circuits*" *Journal of Neuroscience* 23(35): 11167-11177.
- Bendat, J. S. and A. G. Piersol (1986) "*Random data analysis and measurement procedures*" New York, John Wiley.
- Benford, F. (1938) "*The law of anomalous numbers*" *Proceedings of the American Mathematical Society* 78: 551-572.
- Benkowitz, C., M. Liao, et al. (2007) "*Determination of the EC50 Amnesic Concentration of Etomidate and Its Diffusion Profile in Brain Tissue: Implications for In Vitro Studies*" *Anesthesiology* 106(1): 114-123.
- Berens, P., G. A. Keliris, et al. (2008) "*Feature selectivity of the gamma-band of the local field potential in primate primary visual cortex*" *Frontiers in Neuroscience* 2(2): 199-207.
- Berger, H. (1929) "*Über das Elektroenzephalogram des Menschen*" *Archiv für Psychiatrie und Nervenkrankheiten* 87: 527-570.

- Berger, T., A. Borgdorff, et al. (2007) "*Combined Voltage and Calcium Epifluorescence Imaging In Vitro and In Vivo Reveals Subthreshold and Suprathreshold Dynamics of Mouse Barrel Cortex*" *Journal of Neurophysiology* 97(5): 3751-3762.
- Bland, B. H. (1986) "*The physiology and pharmacology of hippocampal formation theta rhythms*" *Progress in Neurobiology* 26(1): 1-54.
- Blatow, M., A. Rozov, et al. (2003) "*A Novel Network of Multipolar Bursting Interneurons Generates Theta Frequency Oscillations in Neocortex*" *Neuron* 38(5): 805-817.
- Bonhomme, V. and P. Hans (2007) "*Muscle relaxation and depth of anaesthesia: where is the missing link?*" *British Journal of Anaesthesia* 99(4): 456-460.
- Bower, J. and L. Parsons (2003) "*Rethinking the "Lesser Brain"*". *Scientific American*: 51-57.
- Braitenberg V and S. A (1998) "*Cortex: Statistics and Geometry of Neuronal Connectivity.*" Berlin, Heidelberg, Springer-Verlag.
- Brown, E. N., R. Lydic, et al. (2010) "*General Anesthesia, Sleep, and Coma*" *New England Journal of Medicine* 363(27): 2638-2650.
- Brown, R. J. C. (2005) "*Benford's Law and the screening of analytical data: the case of pollutant concentrations in ambient air*" *The Analyst* 9: 1280-1285.
- Bruhn, J., T. Bouillon, et al. (2000) "*Bispectral Index (BIS) and Burst Suppression: Revealing a Part of the BIS Algorithm*" *Journal of Clinical Monitoring and Computing* 16: 593-596.
- Bruhn, J., H. Ropcke, et al. (2000) "*Approximate Entropy as an Electroencephalographic Measure of Anesthetic Drug Effect during Desflurane Anesthesia.*" *Anesthesiology* 92(3): 715-726.
- Bryson, H. M., B. R. Fulton, et al. (1995) "*Propofol. An update of its use in anaesthesia and conscious sedation*" *Drugs* 50(3): 513-559.
- Butovas, S., U. Rudolph, et al. (2010) "*Activity Patterns in the Prefrontal Cortex and Hippocampus during and after Awakening from Etomidate Anesthesia*" *Anesthesiology* 113(1): 48-57.
- Buzsáki, G. and A. Kandel (1998) "*Somadendritic backpropagation of action potentials in cortical pyramidal cells of the awake rat*" *Journal of Neurophysiology* 79(3): 1587-1591.
- Buzsáki, G. (2007) "*The structure of consciousness*" *Nature* 446(7133): 267.
- Buzsáki, G. (2006) "*Rhythms of the brain*" Oxford ; New York, Oxford University Press.
- Buzsáki, G., C. A. Anastassiou, et al. (2012) "*The origin of extracellular fields and currents – EEG, ECoG, LFP and spikes*" *Nature Reviews Neuroscience* 13(6): 407-420.
- Campagna, J. A., K. W. Miller, et al. (2003) "*Mechanisms of Actions of Inhaled Anesthetics*" *The New England Journal of Medicine* 348(21): 2110-2124.
- Cash, S. S., E. Halgren, et al. (2009) "*The Human K-Complex Represents an Isolated Cortical Down-State*" *Science* 324(5930): 1084-1087.
- Cauller, L. J., B. Clancy, et al. (1998) "*Backward cortical projections to primary somatosensory cortex in rats extend long horizontal axons in layer I*" *Journal of Comparative Neurology* 390(2): 297-310.

- Chen, L. M., R. M. Friedman, et al. (2005) "*Optical imaging of SI topography in anesthetized and awake squirrel monkeys*" *Journal of Neuroscience* 25(33): 7648-7659.
- Ching, S., A. Cimenser, et al. (2010) "*Thalamocortical model for a propofol-induced α -rhythm associated with loss of consciousness*" *Proceedings of the National Academy of Sciences* 107(52): 22665-22670.
- Chmielowska, J., G. E. Carvell, et al. (1989) "*Spatial organization of thalamocortical and corticothalamic projection systems in the rat SmI barrel cortex*" *Journal of Comparative Neurology* 285(3): 325-338.
- Chris73 "*Action Potential*". ActionPotential.png, Wikipedia.
- Clausius, R. (1867) "*The mechanical theory of heat: with its applications to the steam-engine and to the physical properties of bodies*" London, John van Voorst.
- Cohen, B. A. and A. Sances, Jr. (1977) "*Stationarity of the human electroencephalogram*" *Medical & biological engineering & computing* 15(5): 513-518.
- Cooper, R., A. L. Winter, et al. (1965) "*Comparison Of Subcortical, Cortical And Scalp Activity Using Chronically Indwelling Electrodes In Man*" *Electroencephalography and Clinical Neurophysiology* 18: 217-228.
- Creutzfeldt, O. D., J. M. Fuster, et al. (1964) "*Experimenteller Nachweis von Beziehungen zwischen EEG-Wellen und Aktivitaet corticaler Nervenzellen*" *Naturwissenschaften* 51(7): 166-167.
- Dai, S., M. Perouansky, et al. (2009) "*Amnestic Concentrations of Etomidate Modulate GABAA,slow Synaptic Inhibition in Hippocampus*" *Anesthesiology* 111(4): 766-773.
- Detari, L., D. D. Rasmusson, et al. (1997) "*Phasic relationship between the activity of basal forebrain neurons and cortical EEG in urethane-anesthetized rat*" *Brain Research* 759(1): 112-121.
- Detsch, O., C. Vahle-Hinz, et al. (1999) "*Isoflurane induces dose-dependent changes of thalamic somatosensory information transfer*" *Brain Research* 829(1-2): 77-89.
- Drexler, B., C. Grasshoff, et al. (2006) "*Die GABAA-Rezeptor-Familie*" *Der Anaesthesist* 55(3): 287-295.
- Drexler, B., H. Hentschke, et al. (2010) "*Organotypic Cultures as Tools for Testing Neuroactive Drugs - Link Between In-Vitro and In-Vivo Experiments*" *Current Medicinal Chemistry* 17(36): 4538-4550.
- Drexler, B., M. Kreuzer, et al. (2013) "*Sevoflurane-induced loss of consciousness is paralleled by a prominent modification of neural activity during cortical down-states*" *Neuroscience Letters* 548: 149-154.
- Drummond, J. C. (1985) "*MAC for Halothane, Enflurane, and Isoflurane in the New Zealand White Rabbit: And a Test for the Validity of MAC Determinations*" *Anesthesiology* 62(3): 336-338.
- Durtschi, C., W. Hillison, et al. (2004) "*The Effective Use of Benford's Law to Assist in Detecting Fraud in Accounting Data*" *Journal of Forensic Accounting* 5: 17-34.
- Eger, E. I., L. J. Saidman, et al. (1965) "*Minimum alveolar anesthetic concentration: a standard of anesthetic potency*" *Anesthesiology* 26(6): 756-763.

- Elbert, T., W. J. Ray, et al. (1994) "*Chaos and physiology: deterministic chaos in excitable cell assemblies*" *Physiological reviews* 74(1): 1-47.
- Elul, R. and C. P. a. J. R. S. Carl (1972) "*The Genesis of the Eeg*", Academic Press. Volume 15: 227.
- Engel, H.-A. and C. Leuenberger (2003) "*Benford's law for exponential random variables*" *Statistics & Probability Letters* 63(4): 361-365.
- Erchova, I. A., M. A. Lebedev, et al. (2002) "*Somatosensory cortical neuronal population activity across states of anaesthesia*" *European Journal of Neuroscience* 15(4): 744-752.
- Fadlallah, B., B. Chen, et al. (2013) "*Weighted-permutation entropy: a complexity measure for time series incorporating amplitude information*" *Phys Rev E Stat Nonlin Soft Matter Phys* 87(2): 022911.
- Faure, P. and H. Korn (2001) "*Is there chaos in the brain? I. Concepts of nonlinear dynamics and methods of investigation*" *Comptes rendus de l'Académie des sciences. Série III* 324(9): 773-793.
- Fell, J., J. Röschke, et al. (1996) "*Discrimination of sleep stages: a comparison between spectral and nonlinear EEG measures*" *Electroencephalography and Clinical Neurophysiology* 98(5): 401-410.
- Ferezou, I., S. Bolea, et al. (2006) "*Visualizing the cortical representation of whisker touch: voltage-sensitive dye imaging in freely moving mice*" *Neuron* 50(4): 617-629.
- Ferrarelli, F., M. Massimini, et al. (2010) "*Breakdown in cortical effective connectivity during midazolam-induced loss of consciousness*" *Proceedings of the National Academy of Sciences* 107(6): 2681-2686.
- Fiset, P., T. Paus, et al. (1999) "*Brain Mechanisms of Propofol-Induced Loss of Consciousness in Humans: a Positron Emission Tomographic Study*" *Journal of Neuroscience* 19(13): 5506-5513.
- Franks, N. P. and W. R. Lieb (1982) "*Molecular mechanisms of general anaesthesia*" *Nature* 300(5892): 487-493.
- Franks, N. P. and W. R. Lieb (1986) "*Partitioning of long-chain alcohols into lipid bilayers: implications for mechanisms of general anesthesia*" *Proceedings of the National Academy of Sciences* 83(14): 5116-5120.
- Franks, N. P. (2006) "*Molecular targets underlying general anaesthesia*" *British Journal of Pharmacology* 147 Suppl 1: S72-81.
- Franks, N. P. (2008) "*General anaesthesia: from molecular targets to neuronal pathways of sleep and arousal*" *Nature Reviews Neuroscience* 9(5): 370-386.
- Friedman, E. B., Y. Sun, et al. (2010) "*A Conserved Behavioral State Barrier Impedes Transitions between Anesthetic-Induced Unconsciousness and Wakefulness: Evidence for Neural Inertia*" *PLoS ONE* 5(7): e11903.
- Gahwiler, B. H. (1981) "*Organotypic Monolayer-Cultures of Nervous-Tissue*" *Journal of Neuroscience Methods* 4(4): 329-342.

- Goard, M. and Y. Dan (2009) "*Basal forebrain activation enhances cortical coding of natural scenes*" *Nature Neuroscience* 12(11): 1444-1449.
- Gollo, L. L., C. R. Mirasso, et al. (2011) "*Theta Band Zero-Lag Long-Range Cortical Synchronization via Hippocampal Dynamical Relaying*" *PLoS ONE* 6(3): e17756.
- Goncharova, I. I., D. J. McFarland, et al. (2003) "*EMG contamination of EEG: spectral and topographical characteristics*" *Clinical Neurophysiology* 114(9): 1580-1593.
- Gottschalk, A. and S. A. Miotke (2009) "*Volatile anesthetic action in a computational model of the thalamic reticular nucleus*" *Anesthesiology* 110(5): 996-1010.
- Grasshoff, C. and B. Antkowiak (2004) "*Propofol and sevoflurane depress spinal neurons in vitro via different molecular targets*" *Anesthesiology* 101(5): 1167-1176.
- Gray, C. M., P. E. Maldonado, et al. (1995) "*Tetrodes markedly improve the reliability and yield of multiple single-unit isolation from multi-unit recordings in cat striate cortex*" *Journal of Neuroscience Methods* 63(1-2): 43-54.
- Gredell, J. A., P. A. Turnquist, et al. (2004) "*Determination of diffusion and partition coefficients of propofol in rat brain tissue: implications for studies of drug action in vitro*" *British Journal of Anaesthesia* 93(6): 810-817.
- Gregory, T. and D. Pettus (1986) "*An electroencephalographic processing algorithm specifically intended for analysis of cerebral electrical activity*" *Journal of Clinical Monitoring and Computing* 2(3): 190-197.
- Groth, A. (2006) "*Visualization of coupling in time series by order recurrence plots*" *Phys Rev E Stat Nonlin Soft Matter Phys* 72(4 Pt 2): 046220.
- Gugino, L. D., R. J. Chabot, et al. (2001) "*Quantitative EEG changes associated with loss and return of consciousness in healthy adult volunteers anaesthetized with propofol or sevoflurane*" *British Journal of Anaesthesia* 87(3): 421-428.
- Hameroff, S. R. (2006) "*The Entwined Mysteries of Anesthesia and Consciousness: Is There a Common Underlying Mechanism?*" *Anesthesiology* 105(2): 400-512.
- Harmony, T., T. Fernandez, et al. (1996) "*EEG delta activity: an indicator of attention to internal processing during performance of mental tasks*" *Int J Psychophysiol* 24(1-2): 161-171.
- Hasenstaub, A., Y. Shu, et al. (2005) "*Inhibitory postsynaptic potentials carry synchronized frequency information in active cortical networks*" *Neuron* 47(3): 423-435.
- Haslinger, R., I. Ulbert, et al. (2006) "*Analysis of LFP phase predicts sensory response of barrel cortex*" *Journal of Neurophysiology* 96(3): 1658-1663.
- Heinke, W. and S. Koelsch (2005) "*The effects of anesthetics on brain activity and cognitive function*" *Current Opinion in Anesthesiology* 18(6): 625-631.
- Hentschke, H., C. Schwarz, et al. (2005) "*Neocortex is the major target of sedative concentrations of volatile anaesthetics: strong depression of firing rates and increase of GABAA receptor-mediated inhibition*" *European Journal of Neuroscience* 21(1): 93-102.
- Hill, T. P. (1999) "*The Difficulty of Faking Data*" *Chance* 12(3): 27-31.

- Ho, K. K. L., G. B. Moody, et al. (1997) "*Predicting Survival in Heart Failure Case and Control Subjects by Use of Fully Automated Methods for Deriving Nonlinear and Conventional Indices of Heart Rate Dynamics*" *Circulation* 96(3): 842-848.
- Hobbhahn, J. and P. Conzen (2003) "*Sevofluran Kompendium*" Wiesbaden, Wissenschaftl. Verlagsabteilung, Abbott GmbH.
- Hoeflinger, B. F., C. A. Bennett-Clarke, et al. (1995) "*Patterning of local intracortical projections within the vibrissae representation of rat primary somatosensory cortex*" *Journal of Comparative Neurology* 354(4): 551-563.
- Horn, B., S. Pilge, et al. (2009) "*A combination of electroencephalogram and auditory evoked potentials separates different levels of anesthesia in volunteers*" *Anesthesia & Analgesia* 108(5): 1512-1521.
- Hornby, A. S. and J. Turnbull (2010) "*Oxford advanced learner's dictionary of current English*" Oxford [England], Oxford University Press.
- Hudetz, A. G. (2002) "*Effect of volatile anesthetics on interhemispheric EEG cross-approximate entropy in the rat*" *Brain Research* 954(1): 123-131.
- Hudetz, A. G., J. D. Wood, et al. (2003) "*Cholinergic Reversal of Isoflurane Anesthesia in Rats as Measured by Cross-approximate Entropy of the Electroencephalogram*" *Anesthesiology* 99(5): 1125-1131.
- Hudetz, A. G., J. A. Vizuet, et al. (2009) "*Desflurane selectively suppresses long-latency cortical neuronal response to flash in the rat*" *Anesthesiology* 111(2): 231-239.
- Imas, O. A., K. M. Ropella, et al. (2004) "*Halothane augments event-related gamma oscillations in rat visual cortex*" *Neuroscience* 123(1): 269-278.
- Imas, O. A., K. M. Ropella, et al. (2006) "*Isoflurane disrupts antero-posterior phase synchronization of flash-induced field potentials in the rat*" *Neuroscience Letters* 402(3): 216-221.
- Ishizeki, J., K. Nishikawa, et al. (2008) "*Amnestic concentrations of sevoflurane inhibit synaptic plasticity of hippocampal CA1 neurons through gamma-aminobutyric acid-mediated mechanisms*" *Anesthesiology* 108(3): 447-456.
- Izhikevich, E. M. (2007) "*Dynamical systems in neuroscience : the geometry of excitability and bursting*" Cambridge, Mass. ; London, MIT Press.
- Jääntti, V., E. Heikkinen, et al. (2008) "*Cortical Electroencephalogram from Subcortical Electrodes rather than Electrosuicorticoqram*" *Anesthesiology* 108(5): 963-964.
- Johansson, J. S. (2006) "*Central nervous system electrical synapses as likely targets for intravenous general anesthetics*" *Anesthesia & Analgesia* 102(6): 1689-1691.
- John, E. R., L. S. Prichep, et al. (2001) "*Invariant reversible QEEG effects of anesthetics*" *Conscious Cogn* 10(2): 165-183.
- John, E. R. and L. S. Prichep (2005) "*The Anesthetic Cascade: A Theory of How Anesthesia Suppresses Consciousness.*" *Anesthesiology* 102(2): 447-471.

- Jordan, C., C. Weller, et al. (1995) *"Monitoring evoked potentials during surgery to assess the level of anaesthesia"* Journal of Medical Engineering and Technology 19(2-3): 77-79.
- Jordan, D., A. Hock, et al. (2008) *"Are Non-Linear Measures of the EEG Justified in Monitoring Anesthesia? a Surrogate Based Test"* Anesthesiology 109: A-1287.
- Jordan, D., E. Kochs, et al. (2008) *"Influence of high frequency components on EEG-parameters in anaesthesia"* European Journal of Anaesthesiology 25: 5.
- Jordan, D., G. Stockmanns, et al. (2008) *"Electroencephalographic Order Pattern Analysis for the Separation of Consciousness and Unconsciousness: An Analysis of Approximate Entropy, Permutation Entropy, Recurrence Rate, and Phase Coupling of Order Recurrence Plots"* Anesthesiology 109(6): 1014-1022.
- Jordan, D., M. Kreuzer, et al. (2009) *"Mainly Linear Random Characteristics of the EEG may be detected by EEG Monitors of Anesthesia"* Proceedings of 5th Russian-Bavarian Conference: 235-236.
- Jordan, D., G. Stockmanns, et al. (2009) *"Is Detection of Different Anesthetic Levels Related to Nonlinearity of the Electroencephalogram?"* 4th European Conference of the International Federation for Medical and Biological Engineering. J. Sloten, P. Verdonck, M. Nyssen and J. Haueisen, Springer Berlin Heidelberg. 22: 335-339.
- Jordan, D. (2010) *"Signalanalysemethoden für das EEG-Narkosemonitoring"* Düsseldorf, VDI Verlag.
- Jordan, D., M. Steiner, et al. (2010) *"A Program for Computing the Prediction Probability and the Related Receiver Operating Characteristic Graph"* Anesthesia & Analgesia 111(6): 1416-1421.
- Jordan, D., G. Stockmanns, et al. (2010) *"Influence of signal length on EEG approximate and permutation entropy during anaesthesia"* Biomedizinische Technik 55(Suppl.1).
- Jordan, D., S. Paprotny, et al. (2011) *"Symbolic transfer entropy indicates changes of cortical flow of information between consciousness and propofol-induced unconsciousness: 7AP1-4"* European Journal of Anaesthesiology 28: 97.
- Jordan, D., R. Ilg, et al. (2013) *"Simultaneous Electroencephalographic and Functional Magnetic Resonance Imaging Indicate Impaired Cortical Top-Down Processing in Association with Anesthetic-induced Unconsciousness"* Anesthesiology 119(5): 1031-1042.
- Jurd, R., M. Arras, et al. (2005) *"[beta]3-containing GABAA receptors mediate the immobilizing and, in part, the hypnotic actions of etomidate and propofol"* International Congress Series Basic and Systemic Mechanisms of Anesthesia: Proceedings of the 7th International Conference on Basic and Systemic Mechanisms of Anesthesia held in Nara, Japan between 25 and 27 October 2005 1283: 143-148.
- Kamondi, A., L. Acsady, et al. (1998) *"Theta oscillations in somata and dendrites of hippocampal pyramidal cells in vivo: activity-dependent phase-precession of action potentials"* Hippocampus 8(3): 244-261.
- Kampa, B. M., J. J. Letzkus, et al. (2006) *"Cortical feed-forward networks for binding different streams of sensory information"* Nature Neuroscience 9(12): 1472-1473.

- Kandel, A. and G. Buzsaki (1997) "*Cellular-synaptic generation of sleep spindles, spike-and-wave discharges, and evoked thalamocortical responses in the neocortex of the rat*" *Journal of Neuroscience* 17(17): 6783-6797.
- Kaplan, B. J. (1985) "*The epileptic nature of rodent electrocortical polyspiking is still unproven*" *Experimental Neurology* 88(2): 425-436.
- Katzner, S., I. Nauhaus, et al. (2009) "*Local origin of field potentials in visual cortex*" *Neuron* 61(1): 35-41.
- Kawabata, N. (1976) "*Test of statistical stability of the electroencephalogram*" *Biological Cybernetics* 22(4): 235-238.
- Kelz, M. B., Y. Sun, et al. (2008) "*An essential role for orexins in emergence from general anesthesia*" *Proceedings of the National Academy of Sciences of the United States of America* 105(4): 1309-1314.
- Kerr, J. N., C. P. de Kock, et al. (2007) "*Spatial organization of neuronal population responses in layer 2/3 of rat barrel cortex*" *Journal of Neuroscience* 27(48): 13316-13328.
- Klimesch, W. (1999) "*EEG alpha and theta oscillations reflect cognitive and memory performance: a review and analysis*" *Brain Research Reviews* 29(2-3): 169-195.
- Korn, H. and P. Faure (2003) "*Is there chaos in the brain? II. Experimental evidence and related models*" *Comptes Rendus Biologies* 326(9): 787-840.
- Kortelainen, J., M. Koskinen, et al. (2008) "*Time-frequency properties of electroencephalogram during induction of anesthesia*" *Neuroscience Letters* 446(2-3): 70-74.
- Kreuzer, M., G. Schneider, et al. (2008) "*Sevoflurane and propofol have different effects on down states of local field potential activity in vitro*" *British Journal of Anaesthesia* 100: 868-880.
- Kreuzer, M., H. Hentschke, et al. (2010) "*Cross-approximate entropy of cortical local field potentials quantifies effects of anesthesia - a pilot study in rats*" *BMC Neuroscience* 11(1): 122.
- Kreuzer, M., D. Jordan, et al. (2010) "*Influence of anaesthesia on electroencephalographic stationarity*" *Biomedizinische Technik/Biomedical Engineering* 55(s1): P45.
- Kreuzer, M., S. Paprotny, et al. (2010) "*Influence of Electrode Position on Nonlinear EEG Analysis: An Example With Approximate And Cross Approximate Entropy*" *European Journal of Anaesthesiology* 27: S2-S32.
- Kreuzer, M., S. Butovas, et al. (2011) "*Propofol-induced Change in Information Processing between Neocortex and Hippocampus*" *ASA Abstracts*: 1163.
- Kreuzer, M., S. Kratzer, et al. (2012) "*Volatile Anesthetics Reduce Information Content of Amygdalo-Hippocampal Interactions, Thus Mediating Amnesia?: Results From Pilot Experiments*" *ASA Abstracts*: A216.
- Kreuzer, M., R. Zanner, et al. (2012) "*Time Delay of Monitors of the Hypnotic Component of Anesthesia: Analysis of State Entropy and Index of Consciousness*" *Anesthesia & Analgesia*.
- Kreuzer, M., D. Jordan, et al. (2014) "*Brain Electrical Activity Obeys Benford's Law*" *Anesthesia & Analgesia* 118(1): 183-191

- Ku, S.-W., U. Lee, et al. (2011) "*Preferential Inhibition of Frontal-to-Parietal Feedback Connectivity Is a Neurophysiologic Correlate of General Anesthesia in Surgical Patients*" PLoS ONE 6(10): e25155.
- Kuhn, B., W. Denk, et al. (2008) "*In vivo two-photon voltage-sensitive dye imaging reveals top-down control of cortical layers 1 and 2 during wakefulness*" Proceedings of the National Academy of Sciences of the United States of America 105(21): 7588-7593.
- Kuizenga, K., J. M. K. H. Wierda, et al. (2001) "*Biphasic EEG changes in relation to loss of consciousness during induction with thiopental, propofol, etomidate, midazolam or sevoflurane*" British Journal of Anaesthesia 86(3): 354-360.
- Laaris, N., G. C. Carlson, et al. (2000) "*Thalamic-evoked synaptic interactions in barrel cortex revealed by optical imaging*" Journal of Neuroscience 20(4): 1529-1537.
- Lamme, V. A., K. Zipser, et al. (1998) "*Figure-ground activity in primary visual cortex is suppressed by anesthesia*" Proceedings of the National Academy of Sciences of the United States of America 95(6): 3263-3268.
- Lampl I, Reichova I, et al. (1999) "*Synchronous membrane potential fluctuations in neurons of the cat visual cortex*" Neuron 22: 361-374.
- Lee, U., G. A. Mashour, et al. (2009) "*Propofol induction reduces the capacity for neural information integration: Implications for the mechanism of consciousness and general anesthesia*" Consciousness and Cognition 18(1): 56-64.
- Legatt, A. D., J. Arezzo, et al. (1980) "*Averaged multiple unit activity as an estimate of phasic changes in local neuronal activity: effects of volume-conducted potentials*" Journal of Neuroscience Methods 2(2): 203-217.
- Li, F. and J. Z. Tsien (2009) "*Memory and the NMDA Receptors*" New England Journal of Medicine 361(3): 302-303.
- Linkenkaer-Hansen, K., V. V. Nikouline, et al. (2001) "*Long-Range Temporal Correlations and Scaling Behavior in Human Brain Oscillations*" Journal of Neuroscience 21(4): 1370-1377.
- Llinas, R. R., E. Leznik, et al. (2002) "*Temporal binding via cortical coincidence detection of specific and nonspecific thalamocortical inputs: a voltage-dependent dye-imaging study in mouse brain slices*" Proceedings of the National Academy of Sciences of the United States of America 99(1): 449-454.
- MacIver, B. M., J. W. Mandema, et al. (1996) "*Thiopental Uncouples Hippocampal and Cortical Synchronized Electroencephalographic Activity*" Anesthesiology 84(6): 1411-1424.
- Manns, I. D., A. Alonso, et al. (2003) "*Rhythmically discharging basal forebrain units comprise cholinergic, GABAergic, and putative glutamatergic cells*" Journal of Neurophysiology 89(2): 1057-1066.
- Masimore, B., J. Kakalios, et al. (2004) "*Measuring fundamental frequencies in local field potentials*" Journal of Neuroscience Methods 138(1-2): 97.

- Mazze, R. I., S. A. Rice, et al. (1985) "*Halothane, isoflurane, and enflurane MAC in pregnant and nonpregnant female and male mice and rats*" *Anesthesiology* 62(3): 339-341.
- McCarthy, M. M., E. N. Brown, et al. (2008) "*Potential network mechanisms mediating electroencephalographic beta rhythm changes during propofol-induced paradoxical excitation*" *Journal of Neuroscience* 28(50): 13488-13504.
- McCormick, D. A. and T. Bal (1997) "*Sleep and arousal: thalamocortical mechanisms*" *Annual Review of Neuroscience* 20: 185-215.
- Meeren, H. K., J. P. Pijn, et al. (2002) "*Cortical focus drives widespread corticothalamic networks during spontaneous absence seizures in rats*" *Journal of Neuroscience* 22(4): 1480-1495.
- Mehboob, Z. and H. Yin (2008) "*Analysis of Non-stationary Neurobiological Signals Using Empirical Mode Decomposition*" *Hybrid Artificial Intelligence Systems*: 714.
- Meyer, H. (1899) "*Zur Theorie der Alkoholnarkose*" *Archiv für experimentelle Pathologie und Pharmakologie* 42(2-4): 109-118.
- Miller, R. D. (2005) "*Miller's Anesthesia*" Philadelphia, Elsevier.
- Mitchell, D. J., N. McNaughton, et al. (2008) "*Frontal-midline theta from the perspective of hippocampal "theta"*" *Progress in Neurobiology* 86(3): 156-185.
- Mitzdorf, U. (1987) "*Properties of the evoked potential generators: current source-density analysis of visually evoked potentials in the cat cortex*" *International Journal of Neuroscience* 33(1-2): 33-59.
- Murphy, M., M. Bruno, et al. (2011) "*Propofol anesthesia and sleep: a high-density EEG study*" *Sleep* 34(3): 9.
- Namba, T., T. M. Ishii, et al. (2000) "*Inhibition of the human intermediate conductance Ca²⁺-activated K⁺ channel, hIK1, by volatile anesthetics*" *European Journal of Pharmacology* 395(2): 95-101.
- Nauck, D., F. Klawonn, et al. (1996) "*Neuronale Netze und Fuzzy-Systeme Grundlagen des Konnektionismus, neuronaler Fuzzy-Systeme und der Kopplung mit wissensbasierten Methoden*" Braunschweig, Vieweg.
- Newcomb, S. (1881) "*Note on the frequency of use of the different digits in natural numbers*" *American Journal of Mathematics* 4: 39-40.
- Nickalls, R. W. and W. W. Mapleson (2003) "*Age-related iso-MAC charts for isoflurane, sevoflurane and desflurane in man*" *British Journal of Anaesthesia* 91(2): 170-174.
- Nicolelis, M. A. and E. E. Fanselow (2002) "*Thalamocortical [correction of Thalamocortical] optimization of tactile processing according to behavioral state*" *Nature Neuroscience* 5(6): 517-523.
- Nigrini, M. (1996) "*A taxpayer compliance application of Benford's law*" *Journal of the American Taxation Association* 18: 72-91.
- Norton, M. P. and D. G. Karczub (2003) "*Fundamentals of noise and vibration analysis for engineers*" Cambridge, Cambridge University Press.

- Nunes, C. S., D. A. Ferreira, et al. (2009) "*Individual effect-site concentrations of propofol at return of consciousness are related to the concentrations at loss of consciousness and age in neurosurgical patients*" *Journal of Clinical Anesthesia* 21(1): 3-8.
- Nunez, P. L. (1989) "*Generation of human EEG by a combination of long and short range neocortical interactions*" *Brain Topography* 1(3): 199-215.
- Nye, J. and C. Moul (2007) "*The Political Economy of Numbers: On the Application of Benford's Law to International Macroeconomic Statistics*" *The B.E. Journal of Macroeconomics* 7(1): -.
- Olofsen, E., J. W. Sleight, et al. (2008) "*Permutation entropy of the electroencephalogram: a measure of anaesthetic drug effect*" *British Journal of Anaesthesia* 101(6): 810-821.
- Overton, E. (1901) "*Studien über die Narkose zugleich ein Beitrag zur allgemeinen Pharmakologie*".
- Pan, W.-X. and N. McNaughton (1997) "*The medial supramammillary nucleus, spatial learning and the frequency of hippocampal theta activity*" *Brain Research* 764(1-2): 101-108.
- Paprotny, S., M. Kreuzer, et al. (2010) "*Analysis of EEG During Anaesthesia With Permutation Entropy: Is a Smaller Frequency Range Better?*" *European Journal of Anaesthesiology* 27: S2-S32.
- Patel, S. S. and K. L. Goa (1996) "*Sevoflurane. A review of its pharmacodynamic and pharmacokinetic properties and its clinical use in general anaesthesia*" *Drugs* 51(4): 658-700.
- Paz, R., E. P. Bauer, et al. (2008) "*Theta synchronizes the activity of medial prefrontal neurons during learning*" *Learning & Memory* 15(7): 524-531.
- Perouansky, M., V. Rau, et al. (2010) "*Slowing of the Hippocampal ? Rhythm Correlates with Anesthetic-induced Amnesia*" *Anesthesiology* 113(6): 1299-1309.
- Petersen, C. C., A. Grinvald, et al. (2003) "*Spatiotemporal dynamics of sensory responses in layer 2/3 of rat barrel cortex measured in vivo by voltage-sensitive dye imaging combined with whole-cell voltage recordings and neuron reconstructions*" *Journal of Neuroscience* 23(4): 1298-1309.
- Petersen, R. S. and M. E. Diamond (2000) "*Spatial-temporal distribution of whisker-evoked activity in rat somatosensory cortex and the coding of stimulus location*" *Journal of Neuroscience* 20(16): 6135-6143.
- Pikkujamsa, S. M., T. H. Makikallio, et al. (1999) "*Cardiac Interbeat Interval Dynamics From Childhood to Senescence : Comparison of Conventional and New Measures Based on Fractals and Chaos Theory*" *Circulation* 100(4): 393-399.
- Pilge, S., R. Zanner, et al. (2006) "*Time Delay of Index Calculation: Analysis of Cerebral State, Bispectral, and Narcotrend Indices*" *Anesthesiology* 104(3): 488-494.
- Pilge, S., J. Blum, et al. (2011) "*Does the Cerebral State Index Separate Consciousness from Unconsciousness?*" *Anesthesia & Analgesia* 113(6): 1403-1410.
- Pincus, S. (1991) "*Approximate entropy as a measure of system complexity*" *Proceedings of the National Academy of Sciences of the United States of America* 88: 2297-2301.
- Pincus, S. M. and A. L. Goldberger (1994) "*Physiological time-series analysis: what does regularity quantify?*" *American Journal of Physiology* 266(4 Pt 2): H1643-1656.

- Pincus, Steven M., T. Mulligan, et al. (1996) "*Older males secrete luteinizing hormone and testosterone more irregularly, and jointly more asynchronously, than younger males*" Proceedings of the National Academy of Sciences of the United States of America 93(24): 14100-14105.
- Polack, P. O. and S. Charpier (2006) "*Intracellular activity of cortical and thalamic neurones during high-voltage rhythmic spike discharge in Long-Evans rats in vivo*" The Journal of Physiology 571(Pt 2): 461-476.
- Poskanzer, K. E. and R. Yuste (2011) "*Astrocytic regulation of cortical UP states*" Proc Natl Acad Sci U S A 108(45): 18453-18458.
- Pryor, J. (2007). "*UA 1. Central Problems in Philosophy*" Retrieved 20.03, 2014, from <http://www.jimpryor.net/teaching/courses/intro/notes/causaltheory.html>.
- R Development Core Team (2006) "*R: A Language and Environment for Statistical Computing*" Vienna.
- Rampil, I. J. (1998) "*A Primer for EEG Signal Processing in Anesthesia*" Anesthesiology 89: 980-1002.
- Ray, W. J. and H. W. Cole (1985) "*EEG alpha activity reflects attentional demands, and beta activity reflects emotional and cognitive processes*" Science 228(4700): 750-752.
- Richman, J. S. and J. R. Moorman (2000) "*Physiological time-series analysis using approximate entropy and sample entropy*" Heart and Circulatory Physiology -American Journal of Physiology 278(6): H2039-2049.
- Riffenburgh, R. H. (1999) "*Statistics in medicine*" San Diego, Academic Press.
- Roukema, B. (2009) "*Benford's Law anomalies in the 2009 Iranian presidential election*" arXiv 0906.2789.
- Rudolph, U. and B. Antkowiak (2004) "*Molecular and neuronal substrates for general anesthetics*" Nature Reviews Neuroscience 5(9): 709-720.
- Sauseng, P., B. Griesmayr, et al. (2010) "*Control mechanisms in working memory: A possible function of EEG theta oscillations*" Neuroscience Biobehavioral Reviews 34(7): 1015-1022.
- Schmidt, G. (2001) "*Skriptum der Regelungs- und Steuerungstechnik 2*". München.
- Schmidt, G. N., J. Müller, et al. (2008) "*Messung der Narkosetiefe*" Der Anaesthesist 57(1): 9-36.
- Schneider, G., A. W. Gelb, et al. (2003) "*Detection of awareness in surgical patients with EEG-based indices-bispectral index and patient state index*" British Journal of Anaesthesia 91(3): 329-335.
- Schneider, G., E. Kochs, et al. (2004) "*Narcotrend(R) Does Not Adequately Detect the Transition between Awareness and Unconsciousness in Surgical Patients*" Anesthesiology 101(5): 1105-1111.
- Schneider, G., R. Hollweck, et al. (2005) "*Detection of consciousness by electroencephalogram and auditory evoked potentials*" Anesthesiology 103(5): 934-943.
- Schnider, T. W., C. F. Minto, et al. (1999) "*The Influence of Age on Propofol Pharmacodynamics*" Anesthesiology 90(6): 1502-1516.
- Schürmann, M., T. Demiralp, et al. (2000) "*Electroencephalogram alpha (8-15 Hz) responses to visual stimuli in cat cortex, thalamus, and hippocampus: a distributed alpha network?*" Neuroscience Letters 292(3): 175-178.

- Semba, K. and B. R. Komisaruk (1984) "*Neural substrates of two different rhythmical vibrissal movements in the rat*" *Neuroscience* 12(3): 761-774.
- Shannon, C. (1948) "*A Mathematical Theory of Communication*" *Bell System Technical Journal* 27: (379-423):623-356.
- Shaw, F. Z. (2004) "*Is spontaneous high-voltage rhythmic spike discharge in Long Evans rats an absence-like seizure activity?*" *Journal of Neurophysiology* 91(1): 63-77.
- Siapas, A. G., E. V. Lubenov, et al. (2005) "*Prefrontal Phase Locking to Hippocampal Theta Oscillations*" *Neuron* 46(1): 141-151.
- Silva, A., H. Cardoso-Cruz, et al. (2010) "*Comparison of Anesthetic Depth Indexes Based on Thalamocortical Local Field Potentials in Rats*" *Anesthesiology* 112(2): 355-363.
- Silva, A., S. Campos, et al. (2011) "*Performance of Anesthetic Depth Indexes in Rabbits under Propofol Anesthesia: Prediction Probabilities and Concentration-effect Relations*" *Anesthesiology* 115(2): 303-314.
- Simons, D. J., G. E. Carvell, et al. (1992) "*Responses of barrel cortex neurons in awake rats and effects of urethane anesthesia*" *Experimental Brain Research* 91(2): 259-272.
- Sleigh, J. W., J. A. Vizueté, et al. (2009) "*The electrocortical effects of enflurane: experiment and theory*" *Anesthesia & Analgesia* 109(4): 1253-1262.
- Smith, W. D., R. C. Dutton, et al. (1996) "*Measuring the performance of anesthetic depth indicators*" *Anesthesiology* 84(1): 38-51.
- Soanes, C. and A. Stevenson (2005) "*Oxford dictionary of English*" Oxford, Oxford University Press.
- Song, S., P. J. Sjöström, et al. (2005) "*Highly Nonrandom Features of Synaptic Connectivity in Local Cortical Circuits*" *PLoS Biology* 3(3): e68.
- Staley, K. J., M. Longacher, et al. (1998) "*Presynaptic modulation of CA3 network activity*" *Nature Neuroscience* 1(3): 201-209.
- Staniek, M. and K. Lehnertz (2008) "*Symbolic Transfer Entropy*" *Physical Review Letters* 100(15): 158101.
- Steriade, M., D. A. McCormick, et al. (1993) "*Thalamocortical oscillations in the sleeping and aroused brain*" *Science* 262(5134): 679-685.
- Steyn-Ross, A. (2002) "*Modelling the Anaestheto-dynamic Phase Transition of the Cerebral Cortex*", University of Waikato.
- Steyn-Ross, M. L., D. A. Steyn-Ross, et al. (2004) "*Modelling general anaesthesia as a first-order phase transition in the cortex*" *Progress in Biophysics and Molecular Biology* 85(2-3): 369-385.
- Stucke, A. G., E. J. Zuperku, et al. (2005) "*Sevoflurane enhances gamma-aminobutyric acid type A receptor function and overall inhibition of inspiratory premotor neurons in a decerebrate dog model*" *Anesthesiology* 103(1): 57-64.
- Thakor, N. V. and S. Tong (2004) "*Advances in quantitative electroencephalogram analysis methods*" *Annual Review of Biomedical Engineering* 6: 453-495.
- Tononi, G. and G. M. Edelman (1998) "*Consciousness and complexity*" *Science* 282(5395): 1846-1851.

- Uhlhaas, P. J., G. Pipa, et al. (2009) "*Neural synchrony in cortical networks: history, concept and current status*" *Frontiers in Integrative Neuroscience* 3: 17.
- Vardya, I., K. R. Drasbek, et al. (2008) "*Cell Type-Specific GABAA Receptor-Mediated Tonic Inhibition in Mouse Neocortex*" *Journal of Neurophysiology* 100(1): 526-532.
- Varela, F., J.-P. Lachaux, et al. (2001) "*The brainweb: phase synchronization and large-scale integration*" *Nature Reviews Neuroscience* 2(4): 229-239.
- Velly, L. J., M. F. Rey, et al. (2007) "*Differential Dynamic of Action on Cortical and Subcortical Structures of Anesthetic Agents during Induction of Anesthesia*" *Anesthesiology* 107(2): 202-212
- Verbny, Y. I., E. B. Merriam, et al. (2005) "*Modulation of gamma-aminobutyric acid type A receptor-mediated spontaneous inhibitory postsynaptic currents in auditory cortex by midazolam and isoflurane*" *Anesthesiology* 102(5): 962-969.
- Viertio-Oja, H., V. Maja, et al. (2004) "*Description of the Entropy algorithm as applied in the Datex-Ohmeda S/5 Entropy Module*" *Acta Anaesthesiologica Scandinavica* 48(2): 154-161.
- von Stein, A., P. Rappelsberger, et al. (1999) "*Synchronization Between Temporal and Parietal Cortex During Multimodal Object Processing in Man*" *Cerebral Cortex* 9(2): 137-150.
- von Stein, A. and J. Sarnthein (2000) "*Different frequencies for different scales of cortical integration: from local gamma to long range alpha/theta synchronization*" *International Journal of Psychophysiology* 38(3): 301-313.
- Welker, E., P. V. Hoogland, et al. (1988) "*Organization of feedback and feedforward projections of the barrel cortex: a PHA-L study in the mouse*" *Experimental Brain Research* 73(2): 411-435.
- Wiest, M. C. and M. A. Nicolelis (2003) "*Behavioral detection of tactile stimuli during 7-12 Hz cortical oscillations in awake rats*" *Nature Neuroscience* 6(9): 913-914.
- Wilhelm, W., J. Bruhn, et al. (2006) "*Überwachung der Narkosetiefe*" Köln, Deutscher Ärzte-Verlag.
- Woolsey, T. A. and H. Van der Loos (1970) "*The structural organization of layer IV in the somatosensory region (SI) of mouse cerebral cortex. The description of a cortical field composed of discrete cytoarchitectonic units*" *Brain Research* 17(2): 205-242.
- Worrell, G. A., S. D. Cranstoun, et al. (2002) "*Evidence for self-organized criticality in human epileptic hippocampus*" *Neuroreport* 13(16): 2017-2021.
- Zanner, R., S. Pilge, et al. (2009) "*Time delay of electroencephalogram index calculation: analysis of cerebral state, bispectral, and Narcotrend indices using perioperatively recorded electroencephalographic signals*" *British Journal of Anaesthesia* 103(3): 394-399.
- Zecharia, A. Y., L. E. Nelson, et al. (2009) "*The Involvement of Hypothalamic Sleep Pathways in General Anesthesia: Testing the Hypothesis Using the GABAA Receptor β 3N265M Knock-In Mouse*" *Journal of Neuroscience* 29(7): 2177-2187.

18 Supplement

List of figures

- Figure 2.1: The neuron consists of the soma where dendrites and one axon are spreading from. The dendrites are forming connections with other cells' axons and vice versa, hence building up a neuronal network where action potentials can be transmitted. (Pryor 2007) 7
- Figure 2.2: Two neurons can either communicate through direct coupling with gap junction channels (left) or via neurotransmitters through the synaptic cleft (right) (Johansson 2006). 8
- Figure 2.3: Schematic course of an action potential (Chris73)..... 9
- Figure 2.4: left side: recorded neuronal activity from an electrode that is placed extracellularly in an OTC (raw signal). This signal is processed by either low pass or high pass filtering to isolate LFP and action potentials. Right side: top: low frequent LFPs, bottom: action potentials; if action potential bursts are generated, simultaneously low frequent LFPs can be observed. These recordings were obtained from extracellular recordings in cortical OTC described in section 5.1. The action potentials can be extracted from the raw signal through high pass filtering, LFPs through low-pass filtering..... 11
- Figure 2.5: EEG generators: excitatory (left) and inhibitory (right) synapses generate an electrical signal on the scalp (Schmidt, Müller et al. 2008)..... 12
- Figure 3.1: Chemical structure of propofol..... 15
- Figure 3.2: Chemical structure the used volatile anesthetics..... 17
- Figure 3.3: The figure was taken from the work of Rudolph and Antkowiak (Rudolph and Antkowiak 2004). (a) When GABA is activated, chloride is released and can flow in the postsynaptic cell; (b) in the presence of general anesthetics IPSC's decay slower and hyperpolarization of the postsynaptic cell membrane is increased due to longer chloride flux; (c) pentameric design of the GABA_A receptor..... 18
- Figure 4.1: Anesthetic-induced changes in LFP observed from recordings used in this work; Left side (top down): Control, 0.2 μ M, 0.4 μ M propofol; Right side (top down): Control, 0.75 MAC, 1 MAC sevoflurane; The different spiking patterns for propofol and sevoflurane at control conditions (first row) may be due to the different age of the OTC. For the experiments with propofol older OTC were used (\rightarrow Section 5.1)..... 21
- Figure 4.2: Exemplary raw LFP sequences of 2 s length recorded from a multi-electrode array located in the rat barrel cortex as described in section 5.2 and presented in the paper of Kreuzer et al. (Kreuzer, Hentschke et al. 2010) . The recorded signal was filtered between 0.5 and 200 Hz. The displayed traces were recorded in the same animal at control, at a sedating concentration and an anesthetic concentration of isoflurane and after recovery (Kreuzer, Hentschke et al. 2010). Note the similarity of the signals within each row (lines 1-7 and 9-14) and particularly between adjacent pairs

of electrodes. Row two is placed approximately 300 μm deeper in the cortex than row one, possibly targeting another layer. 22

Figure 4.3: Excerpt from the recorded multi-channel LFP in mouse neocortex at control conditions and after a hypnotic dose of propofol. More regular oscillations in the α -range can be observed in the presence of propofol. 23

Figure 4.4: Excerpt from the recorded multi-channel LFP in mouse hippocampus at control conditions and after a hypnotic dose of propofol. Single rows display LFP traces obtained from the single recording electrodes. In the presence of propofol, dominating frequencies become slower and amplitudes increase. The signals seem to follow a more regular pattern. 23

Figure 4.5: Anesthetic-induced changes in EEG patterns that were recorded from EEG-electrodes placed on the forehead. In a conscious subject EEG is characterized by high frequencies and low amplitudes (1st row). With increasing concentrations of the drug (2nd and 3rd row) the EEG becomes slower but of higher amplitude. At very high concentrations burst suppression represented by activity patterns interrupted by isoelectric sequences occurs (4th row). 25

Figure 5.1: Extraction of a down-state episode from the *in vitro* recording. The recorded raw signal (1st row) was low-pass filtered to obtain the LFP trace (2nd row) or high-pass filtered to isolate action potentials (3rd row). Down-state sequences were extracted from the LFP trace. (Drexler, Kreuzer et al. 2013) 28

Figure 5.2: Positions of the multi-electrode arrays in the somatosensory (“barrel”) cortex of the rats. (Hentschke, Schwarz et al. 2005; Kreuzer, Hentschke et al. 2010) 31

Figure 5.3: Course of the anesthetic concentration vs. time in the EEG recording protocol. Arrows indicate the starting point of the steady concentration level. Horizontal bars mark the time of EEG recording. (Jordan 2010)..... 35

Figure 5.4: Study design with simulated intraoperative awareness. The figure was taken from (Pilge, Blum et al. 2011) and modified..... 38

Figure 6.1: A system can be considered linear if the sum of inputs sequences that is transformed leads to the same output signal as the sum of transformed input signals. It does not matter, if signals $ax_1(t)$ and $bx_2(t)$ are added before or after the transformation operation. The resulting output $y(t)$ will be equal..... 42

Figure 6.2: A: The continuous time series $x(t)$ can be presented as series of equally spaced and weighted, Dirac impulses leading to a discrete time series $x[n]$, according to formulas 6.10 and 6.11. The time between the Dirac impulses is defined by the sampling rate f_s , i.e. $T_s = 1/f_s$. That means that only the amplitude values of $x(t)$ at the time points defined by f_s are considered for further processing. B: Example for aliasing: In case of a too low f_s , here f_{sa} , to little sample points are recorded and the original cannot be assumed. Instead something like the red signal will be estimated. Once aliasing has occurred the lost information cannot be regained. 46

Figure 6.3: exemplary time series $x[t]$ of length $N = 11$ used for description of the SR calculation. 50

Figure 6.4: exemplary time series $x[n]$ of length $N = 11$ used for description of the Shannon-Entropy calculation. 53

Figure 6.5: exemplary time series $x[n]$ of length $N = 11$ used for description of the $ApEn$ calculation..... 57

Figure 6.6: The six possible order patterns for a dimension of $m = 3$ adapted from Groth’s article (Groth 2006). 58

Figure 6.7: exemplary time series $x[n]$ of length $N = 11$ used for description of the $PeEn$ calculation..... 60

Figure 6.8: exemplary time series $x[t]$ of length $N = 11$ used for description of the ORR calculation..... 62

Figure 6.9: $ApEn$, $PeEn$, and ORR of the undistorted exemplary time series (top) and with increasing influence of random noise (center and bottom). $ApEn$ is less influenced than $PeEn$ and ORR 64

Figure 6.10: $ApEn$, $PeEn$, and ORR of the undistorted exemplary time series (top) and with a linear drift (bottom). ORR and $PeEn$ are not influenced by the drift, whereas $ApEn$ increases.... 65

Figure 6.11: exemplary time series $x[n]$ (black, long dashes) and $y[n]$ (grey, short dashes) of length $N = 10$ used for description of the $XApEn$ calculation. 67

Figure 6.12: exemplary time series $x[n]$ (black, long dashes) and $y[t]$ (grey, short dashes) of length $N = 10$ used for description of the $BPeEn$ calculation. 68

Figure 6.13: exemplary time series $x[n]$ (black, long dashes) and $y[n]$ (grey, short dashes) of length $N = 10$ used for description of sTE calculation. 71

Figure 7.1: Left side & center: Example for different distributions of an EEG parameter values at states “awake” and “unconscious”. On the left side, the example represents a P_K of 0.56 and the arrows indicate concordant (parameter at “awake” > parameter at “unconscious”, solid black line), discordant (parameter at “awake” < parameter at “unconscious”, solid gray line), and tied (parameter at “awake” = parameter at “unconscious”, dashed black line), relationships. The right side represents a distribution with $P_K = 1$, i.e., there is perfect separation of the parameter values derived from the different levels. Only concordant relationships exist. Right side: In case of using P_K to evaluate a parameter's performance of separating different anesthetic levels, the evaluation of relationships has to be performed over all combinations of states. Here for "awake" vs. "light anesthesia", "awake" vs. "deep anesthesia" and "light anesthesia" vs. "deep anesthesia"..... 73

- Figure 8.1: *PSD* average of all propofol recordings; top: low frequencies 0-15 Hz, bottom: high frequencies 15-50 Hz; Low frequencies up to approximately 4 Hz are dominant. With increasing propofol concentration, *PSD* decreases..... 78
- Figure 8.2: *PSD* average of all sevoflurane recordings; top: low frequencies 0-15 Hz, bottom: high frequencies 15-50 Hz; *PSD* shows activation at low concentrations at 0.25 MAC followed by suppression at higher concentrations. 79
- Figure 8.3: Averaged *PSD* of down-state sequences. The power spectrum shows activation especially in low frequencies for low doses (0.25 and partially 0.5 MAC) and strong inhibition at higher doses. At 0 MAC and recovery a small side peak at approx. 4 Hz is visible. 80
- Figure 8.4: *PSD* at control conditions, of blocked cellular activity and recordings of background and setup noise only (empty cell). *PSD* was highest during control conditions at low frequencies when cells were put in the measuring container, and was still above the *PSD* of background noise even if their activity was blocked. 81
- Figure 8.5: top: *ApEn* of down-states rises significantly with sevoflurane . *Pooled sedating concentrations (light grey) and hypnotic concentrations (grey) significantly differ from control conditions ($p < 0.05$, Bonferroni corrected). bottom: Different propofol concentrations cannot be distinguished with *ApEn*. *ApEn* at control conditions and recovery do not differ significantly, neither for sevoflurane nor for propofol. Higher *ApEn* at propofol control conditions compared to sevoflurane may be explained by the different age of the OTC used for the experiments..... 84
- Figure 8.6: *PeEn* rises significantly (*, $p < 0.05$, Bonferroni corrected) with sevoflurane for grouped sedating (light grey) and hypnotic (grey) concentrations..... 85
- Figure 8.7: *ORR* ($m = 4$) significantly separates control conditions from hypnotic concentrations (*, light grey, 0.75 -1.5 MAC) as well as sedating concentrations from hypnotic concentrations (#, 0.25 & 0.5 MAC vs. 0.75 to 1.5 MAC, grey) of sevoflurane. ($p < 0.05$, Bonferroni corrected) It shows a switch-like behavior at concentrations around the MAC_{awake} . *ORR* at control conditions and recovery is not significantly different. 86
- Figure 8.8: *PSD* of the recordings from cultures with the GABA antagonist bicuculline (black) and bicuculline and 0.75 MAC sevoflurane. *PSD* generally decreases as soon as sevoflurane is delivered pointing to a non GABAergic effect of sevoflurane on network activity..... 88
- Figure 8.9: Top: Even in the presence of the GABA antagonist bicuculline *ApEn* ($m = 2, r = 0.2SD$) shows a significant ($p < 0.05$) increase after delivery of 0.75 MAC sevoflurane, a hypnotic concentration. *Significantly different from BICU. Bottom: In contrast to the experiments without bicuculline, there is no significant effect to *ORR* ($m = 4$) when 0.75 MAC sevoflurane was applied. 89

- Figure 9.1: averaged PSD of the selected sequences for isoflurane (A), enflurane (B) and halothane (C). PSD differs depending on the used anesthetic agent, but generally it shows activation at low δ - to α - frequencies and suppression at high frequencies in the γ -band. Note the logarithmic representation..... 93
- Figure 9.2: Normalized $ApEn$ ($m = 2, r = 0.2SD$) for the single recording channels in the single animals (from top to bottom: rat1, rat2, rat3). For each channel at each level the mean parameter value of the analysis of the three segments was used. $ApEn$ decreases with increasing MAC for all three regimens, whereas halothane seems to show the lightest decline. Significant difference $ApEn$ values compared to control conditions are marked with * (isoflurane), # (enflurane) and § (halothane), ($p < 0.05$, Bonferroni corrected). In rat3 we desisted from significance testing because of only three recording channels. 95
- Figure 9.3: Exponential regression of $ApEn$. Isoflurane shows strongest concentration-dependent decrease..... 96
- Figure 9.4: Normalized $PeEn$ ($m = 5$) for the single recording channels in the single animals (from top to bottom: rat1, rat2, rat3). For each channel at each level the mean parameter value of the analysis of the three segments was used. $PeEn$ tends to decrease with increasing MAC for all three regimens, whereas halothane seems to show the lightest decline. Significant difference $PeEn$ values compared to control conditions are marked with * (isoflurane), # (enflurane) and § (halothane), ($p < 0.05$, Bonferroni corrected). In rat3 we desisted from significance testing because of only three recording channels. 97
- Figure 9.5: Normalized ORR ($m = 4$) for the single recording channels in the single animals (from top to bottom: rat1, rat2, rat3). For each channel at each level the mean parameter value of the analysis of the three segments was used. ORR tends to increase with increasing MAC for all three regimens, whereas halothane seems to show the lightest increase. Significant difference ORR values compared to control conditions are marked with * (isoflurane), # (enflurane) and § (halothane), ($p < 0.05$, Bonferroni corrected). In rat3 we desisted from significance testing because of only three recording channels. 98
- Figure 9.6: Anesthetic-induced changes of $XApEn$. Each color-coded matrix contains values obtained from non-redundant paired combinations of recording sites. The animal was exposed, in separate experimental sessions, to increasing concentrations of isoflurane (left subcolumn) and halothane (right subcolumn). Increasing blue colors indicate more similarity among the compared channels. (Kreuzer, Hentschke et al. 2010). x- and y- axis represent the single channels of the electrode array 100
- Figure 9.7: Dose-response curves of $XApEn$. Dependence of $XApEn$ on anesthetic concentration is expressed in MAC. The data points represent values from all non-redundant paired combinations of recording sites, normalized to control and averaged (\pm standard deviation). Single detached data points at negative abscissa values represent values after recovery (open symbols; no recovery data

were recorded for rat 3). The lines are fits of the data to the monoexponential function $y = \exp(-x/b)$ with b as the only free parameter. Adjusted R^2 values ranged from 0.85 to 0.91, indicating that the fits were adequate. (Kreuzer, Hentschke et al. 2010)..... 101

Figure 9.8: *XApEn* compared to cross correlation: A: raw data excerpts of 30 s length from channels 1, 2 and 7 of the same recording as shown in Figure 4.2. (control condition). Note the sequence of 'high voltage rhythmic spikes' (HVRS) starting at ~12 s. B: *XApEn* values calculated from non-overlapping 1 s sequences of all combinations of the three channels shown. C: peak cross correlation values of the same channel combinations and time intervals as shown in B. The peak of each non-overlapping 1 second segment was determined from the respective cross correlation function in an interval of ± 50 ms relative to zero lag. (Kreuzer, Hentschke et al. 2010)..... 102

Figure 10.1: Propofol-induced modification of *PSD* in the 2-16 Hz range in the neocortex (top) and the hippocampus (bottom) at control conditions (black) and after delivery of propofol (grey). Besides the increase in the spectral power at very low frequencies ~2 Hz there are no changes in the neocortical power spectrum, whereas in the hippocampus a clear shift of peak frequency from approximately 8 to about 5 Hz is visible..... 107

Figure 10.2: Boxplots of *XApEn* analysis after 100 Hz low-pass filtering at control conditions and at hypnotic concentrations of propofol. No significant effect in the cerebral regions could be detected..... 108

Figure 10.3: Propofol-induced, significant changes of *BPeEn* in the θ - (top), α - (middle) and β - (bottom) range in the hippocampus. Data presented in the left column were obtained during control conditions and in the right column after delivery of propofol. Channels become more regular in the θ -range and more irregular in the α -range for all channel combinations, whereas in the β -range *BPeEn* significantly decreases but the pattern is not as specific as observed for the other two slower frequencies. 110

Figure 10.4: Propofol-induced, significant change of *BPeEn* in the α -range in the neocortical region. Left column was obtained during control conditions, the right one after delivery of propofol. Channels become more irregular in the α -range for all channel combinations. 111

Figure 10.5: Propofol-induced, significant change of *BPeEn* in the θ - (top) and α -range (middle) between all hippocampus-neocortex channel combinations. Results in the left column were obtained during control conditions, in the right one after delivery of propofol. Channels become more regular in the θ -range and more irregular in the α -range for all channel combinations..... 111

Figure 10.6: *sTE* in the θ - and α -range for all channel combinations within neocortical (A) and hippocampal regions (B) and between both areas (C). Within the single recording areas *sTE* does not alter significantly with delivery of propofol. Information flow, detected with *sTE*, significantly decreases between hippocampus and neocortex with propofol in the α -range. At θ -frequencies, *sTE* also decreases, but not significantly. Still, a trend can be revealed with a significantly

decreasing result derived from the sign test whereas there is no unitary change in $sTE(\theta)$ within the areas..... 113

Figure 11.1: PSD (0-15 Hz/15-50 Hz) at different anesthetic levels for sevoflurane (A) and propofol (B) anesthesia. Low frequencies are activated with the used anesthetics, while high frequencies are suppressed. At levels LOC and inter1 α - and β -frequencies become activated. 118

Figure 11.2: $ApEn$ ($m = 2; r = 0.2SD$) of 0.5-400 Hz unfiltered (top) and 30 Hz low-pass filtered (bottom) EEG recorded at different anesthetic levels with sevoflurane and propofol. Significant differences from control conditions are indicated with * (sevoflurane) and # (propofol), ($p < 0.05$ Bonferroni corrected)..... 119

Figure 11.3: Course of $ApEn$ related to MAC for the frequency bands 0.5 to 400 Hz (white) and 0.5 to 30 Hz (black). A biphasic course at subhypnotic sevoflurane concentrations can be observed followed by a steady decrease of $ApEn$. During high frequency analysis a strong drop of $ApEn$ is visible at the onset of the drug..... 120

Figure 11.4: $PeEn$ ($m = 5$) (top) and ORR ($m = 4$) (bottom) at different anesthetic levels. Both parameters are affected by the anesthetic regimen and seem to be appropriate to be used for separation between the conscious state and anesthetic levels. Exception is the special state of BS. The detailed performance of separating different states is presented in Table 11.1 122

Figure 12.1: Boxplots for normalized $PeEn$ (top) and SR (bottom) of α - and β -frequencies during the transition from awake to LOC. $PeEn$ of α -frequencies shows no significant change during LOC but $PeEn(\beta)$ is significantly lower after LOC than before. $SR(\alpha)$ is significantly higher than 92 s after LOC compared to values derived from 60s before the event, indicating slow activation of these frequencies. $SR(\beta)$ shows a biphasic activation with significant higher SR 8 s after LOC compared to SR 60 s before the transition. The dashed line at 1 was inserted for better orientation. *Significant compared to parameter value obtained at - 60 s..... 126

Figure 12.2: $PeEn$ of LOC (black) and ROC (dark grey) transitions in the different frequency bands. From top to bottom: δ -, θ -, α -, β -, γ -band. Data are presented as mean and standard deviation of the normalized parameter series. Mean $PeEn(\delta)$ shows no anesthetic-dependent effect in the state transitions. Mean $PeEn(\theta)$ increases during LOC and shows no change during ROC. Mean $PeEn(\alpha)$ does not react on changing propofol concentrations at LOC but increases after ROC. Mean $PeEn(\beta)$ and $PeEn(\gamma)$ decrease during LOC and increase with the emergence of anesthesia. 128

Figure 12.3: Slew Rate of LOC (black) and ROC (dark grey) transitions in the different frequency bands. From top to bottom: δ -, θ -, α -, β -, γ -band. Data is presented as mean and standard deviation from the normalized parameter series. Mean $SR(\delta)$ and $SR(\theta)$ show no obvious effects during LOC and ROC, only standard deviation is smaller after LOC. Mean $SR(\alpha)$ displays an activation in the transition from awake to LOC and steadily decreases during the recovery from anesthesia. Mean

$SR(\beta)$ is also activated during induction and also increases during the recovery phase. Mean $SR(\gamma)$ decreases during LOC and increases at ROC. 130

Figure 13.1: Averaged PSD obtained from the multi-channel study. With propofol activation at low frequencies and in the α - and β -band can be observed while PSD is higher during wakefulness at frequencies above approximately 37 Hz. 136

Figure 13.2: P_K for single-channel ($ApEn$, left) and all channel combinations ($XApEn$, right). Black dots/lines indicate $0.5 \leq P_K < 0.6$; dark grey represents $0.6 \leq P_K < 0.8$ and grey indicates $P_K \geq 0.8$. Orientation: top: frontal 137

Figure 13.3: Significant propofol-induced changes of $XApEn$ in inter-channel synchrony in frequency bands: from left to right: 0.5-8 Hz; 8-12 Hz; 12-24 Hz; 25-47 Hz. Grey indicates increasing synchrony with propofol whereas black indicates a gain in asynchrony. Top: frontal; 138

Figure 13.4: Significant propofol-induced changes of $BPeEn$ in inter-channel synchrony in frequency bands: from left to right: δ , θ : 0.5-8 Hz; α : 8-12 Hz; β : 12-24 Hz; γ : 25-47 Hz. Grey indicates increasing synchrony with propofol whereas black indicates a gain in asynchrony. Top: frontal; . 139

Figure 13.5: Significant propofol-induced changes of sTE in the (from left to right) θ : 0.5-8 Hz; α : 8-12 Hz; β : 12-24 Hz; γ : 25-47 Hz. Light grey lines indicate that with propofol absolute sTE is lower between two electrodes, i.e., there is less directed information flow. Only in the β -band a systematic change in cortical information transfer is visible. 140

Figure 16.1: QQ-plots of the unfiltered EEG data, comparing the logarithmic, modulo 1 first digit distribution of the EEG sequences derived from the recordings at "awake" (black), "light general anesthesia" (grey) and "deep general anesthesia" (light grey) to a uniform distribution (black, thin line). All three EEG distributions are close to the bisecting line representing uniform distribution. The curvature of the EEG "awake" distribution is inverse to the EEG distributions recorded under sevoflurane. (Kreuzer, Jordan et al. 2014)..... 155

Figure 16.2: QQ-plots of the *in vitro* up and down-state sequences data, comparing the logarithmic, modulo 1 first digit distribution of the LFP sequences recorded at concentrations corresponding to "awake" (black), "light general anesthesia" (grey) and "deep general anesthesia" (light grey) to a uniform distribution (black, thin line). The distribution of the LFP "awake" sequences almost perfectly matches the Benford distribution, while the LFP "anesthesia" distributions still show good concordance to the bisecting line. (Kreuzer, Jordan et al. 2014)..... 156

Figure 16.3: First digit distribution of unfiltered (A) and 30 Hz low-pass filtered (B) EEG data derived from sequences recorded at the levels "awake" (black), "light general anesthesia" (grey) and "deep general anesthesia" (light grey). The 30 Hz low-pass filtering does not influence the first digit distribution. After application of sevoflurane the first digit distribution becomes flatter. There are no significant differences in the distribution of the states "light general anesthesia" and "deep general anesthesia". (Kreuzer, Jordan et al. 2014)..... 157

Figure 16.4: First digit distribution of the *in vitro* data (A: up- & down-state sequences; B: down-state sequences) recorded at the levels “awake” (black), “light general anesthesia” (grey) and “deep general anesthesia” (light grey). With application of sevoflurane, the first digit distribution of the recorded LFP sequences becomes steeper. There is no significant difference in the distributions of the analyzed sequences containing up- and down-states and the down-state only sequences. The sevoflurane concentration also seems to have only small impact on the distribution, because distributions recorded during light and deep general anesthesia only differ to a small degree. (Kreuzer, Jordan et al. 2014)..... 158

List of tables

Table 2.1: Classic EEG frequencies and some of their assumed cerebral processing tasks	13
Table 6.1: Sampling rates and quantization resolution of the data that was recorded in the single experiments	47
Table 8.1: <i>ApEn</i> in the absence and presence of sevoflurane calculated from 2 s LFP down-state epochs obtained from cortical OTC. *Indicates significance ($p < 0.05$, Bonferroni corrected) of an anesthetic concentration level vs. control conditions.	83
Table 8.2: P_K values and their confidence intervals of the different non-linear parameters for distinguishing (i) the different levels from each other, (ii) 0 MAC vs. all other concentrations and (iii) concentrations below MAC “awake” vs. concentrations above the MAC “awake”	86
Table 8.3: P_K values and their confidence intervals of the different non-linear parameters for distinguishing (i) the different levels from each other, (ii) 0 MAC vs. all other concentrations and (iii) concentrations below MAC “awake” vs. concentrations above the MAC “awake” for the parameter average of the three selected down-state episodes.....	87
Table 10.1: <i>BPeEn</i> and <i>STE</i> values (mean (standard deviation)) for the different analyses within and between the different regions. Displayed values represent the average over all channel combinations. Significant changes caused by propofol are printed in bold numbers. Non-significant changes that still reveal some propofol-induced trend are kept in bold and italic numbers.	112
Table 11.1: P_K values and their confidence intervals of the different non-linear parameters for distinguishing (i) the different levels from each other and (ii) consciousness from unconsciousness. Recordings from BS were excluded from P_K analysis due to its special status. <i>PeEn</i> seems potent to reliably distinguish between consciousness and unconsciousness whereas <i>ApEn</i> seems suitable for separating different sedating and anesthetic levels. The presented results are from the 0.5-30 Hz analyses.	121
Table 11.2: <i>ApEn</i> values (mean and standard deviation) for the EEG sequences at different anesthetic levels filtered to the classical frequency ranges. Bold entries indicate significance against the awake state ($p < 0.05$, Bonferroni corrected).....	123
Table 11.3: <i>PeEn</i> values (mean and standard deviation) for the EEG sequences at different anesthetic levels filtered to the classical frequency ranges. Bold entries indicate significance against the awake state ($p < 0.05$, Bonferroni corrected).....	123
Table 12.1: Median values (25%-, 75%-quantile) of <i>PeEn</i> and <i>SR</i> of the α - and β -band at selected time points 60 s before and 8, 60 and 92 s after LOC. * indicates a significant change of the parameter values compared to the time point “60 s before LOC”	125

Acknowledgements

Ich bedanke mich herzlich bei den zahlreichen Menschen, die zum Gelingen dieser Arbeit beigetragen haben. Insbesondere geht mein Dank an:

Herrn Prof. Dr. E. Kochs, der mir die Möglichkeit gab und gibt, an der Klinik für Anaesthesiologie zu forschen und meine Promotion durchzuführen, sowie für die Durchsicht, Korrektur und Begutachtung der Arbeit.

Herrn Prof. Dr. G. Schneider, für die hervorragenden Ratschläge und fruchtbaren Diskussionen und den guten Start in mein „Forscherleben“.

Herrn Dr. D. Jordan, der mir immer ein Ansprechpartner und Mentor war und diese Arbeit durch seine Ideen mitgeprägt hat.

Prof. Dr. B. Antkowiak, Dr. B. Drexler, Dr. H. Hentschke, PD C. Grasshoff, sowie Dr. S. Butovas aus Tübingen, ohne deren Hilfe die Ergebnisse zu den *in vitro* und *in vivo* Experimenten nie zu Stande gekommen wären. Von Euch habe ich unglaublich viel gelernt.

Herrn Prof. Dr. M. Schemann für die Bereitschaft als Zweitbetreuer zu fungieren.

Meinen (ehemaligen) Mitarbeitern der Arbeitsgruppe: Dipl.-Ing. Adem Omerovic, Dipl.-Ing. Sebastian Berger, Dr. Stefanie Pilge, Dr. Robert Zanner, Dr. Martin Bretschneider, Dr. Sabine Grimberg und noch viele mehr. Durch Euch hatte ich stets Spaß an der Arbeit und der rege wissenschaftliche Austausch hat uns alle nach vorne gebracht.

Der größte Dank gilt jedoch meinen Eltern, die mich stets unterstützt haben und daher einen nicht unerheblichen Anteil am Gelingen dieser Arbeit haben. Meinen Großeltern danke ich für die stetigen Aufmunterungen und ihre motivierende, positive Lebenseinstellung. Weiterer Dank gilt natürlich auch meiner Schwester Vroni und ihrer Familie.

Last but not least möchte ich meiner Freundin Sandra danken. Sie hat mich all die Jahre unterstützt und motiviert. Danke für die sprachliche Unterstützung und die Korrektur dieser Arbeit. Danke für Deine Geduld und deine Zielstrebigkeit, wenn sie mir gefehlt hat.

Publications

Schneider G, Kochs E, Horn B, **Kreuzer M**, Ningler M: *Narcotrend[®] Does Not Adequately Detect the Transition between Awareness and Unconsciousness in Surgical Patients.* *Anesthesiology* 2004; 101: 1105-1111

Jenkins DM, Chami B, **Kreuzer M**, Presting G, Alvarez AM, Liaw BY: *Hybridization probe for femtomolar quantification of selected nucleic acid sequences on a disposable electrode.* *Anal Chem* 2006; 78: 2314-8

Pilge S, Zanner R, Schneider G, Blum J, **Kreuzer M**, Kochs E: *Time Delay of Index Calculation: Analysis of Cerebral State, Bispectral, and Narcotrend Indices.* *Anesthesiology* 2006; 104: 488-494

Kreuzer M, Kochs EF, Pilge S, Stockmanns G, Schneider G: *Construction of the Electroencephalogram Player: A Device to Present Electroencephalogram Data to Electroencephalogram-Based Anesthesia Monitors.* *Anesth Analg* 2007; 104: 135-139

Zanner R, Pilge S, Kochs EF, **Kreuzer M**, Schneider G: *Time delay of electroencephalogram index calculation: analysis of cerebral state, bispectral, and Narcotrend indices using perioperatively recorded electroencephalographic signals.* *Br. J. Anaesth.* 2009; 103: 394-399

Kreuzer M, Hentschke H, Antkowiak B, Schwarz C, Kochs E, Schneider G: *Cross-approximate entropy of cortical local field potentials quantifies effects of anesthesia - a pilot study in rats.* *BMC Neuroscience* 2010; 11: 122

Pilge S, Blum J, Kochs EF, Schöniger S-A, **Kreuzer M**, Schneider G: *Does the Cerebral State Index Separate Consciousness from Unconsciousness?* *Anesthesia & Analgesia* 2011; 113: 1403-10

Schulz C, Mayer V, **Kreuzer M**, Kochs E, Schneider G: *A tool for immediate and automated assessment of resuscitation skills for a full-scale simulator.* *BMC Research Notes* 2011; 4: 550

Pilge S, **Kreuzer M**[§], Kochs EF, Zanner R, Paprotny S, Schneider G: *Monitors of the hypnotic component of anesthesia - correlation between bispectral index and cerebral state index.* Minerva Anesthesiol 2012; 78: 636-45

Kellermann K, **Kreuzer M**[§], Omerovich A, Hoetzing F, Kochs E, Jungwirth B: *A mobile phone based alarm system for supervising vital parameters in free moving rats.* BMC Research Notes 2012; 5: 119

Kreuzer M, Zanner R, Pilge S, Paprotny S, Kochs EF, Schneider G: *Time Delay of Monitors of the Hypnotic Component of Anesthesia: Analysis of State Entropy and Index of Consciousness.* Anesth Analg 2012; 115(2):315-9

Drexler B, **Kreuzer M**[§], Jordan D, Antkowiak B, Schneider G: *Sevoflurane-induced loss of consciousness is paralleled by a prominent modification of neural activity during cortical down-states.* Neuroscience Letters 2013; 548: 149-154

Kreuzer M, Jordan D, Antkowiak B, Drexler B, Kochs EF, Schneider G: *Brain electrical activity obeys Benford's Law,* Anesth Analg, status: accepted after minor corrections

[§]: both authors contributed equally

Selected Abstracts / contributions to a congress

Kreuzer M, Schneider G, Drexler B, Antkowiak B, Jordan D, Kochs EF. *Sevoflurane-induced changes of field potential activity are detected by Benford's Law*, EJA 2006; 23 (Suppl.37): A-385

Horn B, **Kreuzer M**, Kochs EF, Schneider G. *Different states of anesthesia can be detected by Benford's Law*, J Neurosurg Anesthesiol 2006; 18(4): 328-329

Bretschneider M, **Kreuzer M**, Drexler B, Hentschke H, Antkowiak B, Schwarz C, Kochs EF, Schneider G. *Coherence of in vitro and in vivo field potential activity and EEG, detected by ordinal analysis*, J Neurosurg Anesthesiol 2006; 18(4): 309

Kreuzer M, Drexler B, Hentschke H, Schwarz C, Antkowiak B, Stockmanns G, Kochs EF, Schneider G, *Die Approximate Entropie als universeller Parameter zur Analyse anästhetika-abhängiger Signaländerungen auf zellulärer Ebene bis hin zur EEG-Oberflächenableitung*, Biomedizinische Technik 2007; 52 (Suppl.): 48991

Kreuzer M, Schwarz C, Schneider G, Hentschke H, Kochs EF, *Cross-Approximate-Entropy as a Measure of Isoflurane-Induced Changes in Recordings of Neuronal Population Signals in Vivo*, EJA 2007, 24 (Suppl. 39): 7AP5-5

Kreuzer M, Drexler B, Antkowiak B, Kochs EF, Schneider G, *Order Recurrence Can Detect the MAC“Awake” in Local Field Potential Activity in Vitro and in EEG*, Anesthesiology 2008; 109 A733

Kreuzer M, Schneider G, Drexler B, Hentschke H, Antkowiak B, Kochs EF, *Sevoflurane and propofol have different effects on down-states of local field potential activity in vitro*, BJA 2008; 100: 868 – 880

Kreuzer M, Jordan D, Kochs EF, Pilge S, Schneider G, *Cross Approximate Entropy Proves To Be Partially Superior to Approximate Entropy in EEG Analysis*, Anesthesiology 2009; A221

Kreuzer M, Paprotny S, Jordan D, Kochs EF, Schneider G, *Influence of Electrode Position on Non-linear EEG Analysis: An Example With Approximate And Cross Approximate Entropy* , EJA 2010; 27 (Suppl. 47): 3AP3-4

Paprotny S, **Kreuzer M**, Jordan D, Kochs EF, Schneider G, Permutation entropy for EEG-analysis during anaesthesia depends on frequency ranges, EJA 2010; 27 (Suppl. 47): 3AP6-5

Kreuzer M, Jordan D, Paprotny S, Kochs EF, Schneider G, *Bivariate Permutation Entropy Evaluates Propofol Induced Changes in EEG Synchrony*, Anesthesiology 2010; A049

Kreuzer M, Kochs EF, Schneider G, Jordan D, *Hysteresis of EEG during propofol induced loss of consciousness*, EJA 2011, Vol 28 (Suppl. 48): 7AP1-1

Kreuzer M, Butovas S, Kochs EF, Antkowiak B, Schneider G, Jordan D, *Propofol-induced Change in Information Processing between Neocortex and Hippocampus*, Anesthesiology 2011; A1163

Kreuzer M, Jordan D, Steyn-Ross A, Schneider G, Kochs EF, *Permutation Entropy does not follow EEG α - and β - activation during propofol induction*, EJA 2012, Vol 29 (Suppl. 50): 7AP3-1

Curriculum Vitae

Matthias Kreuzer

Personal Data

Date of Birth: August 4, 1978
Place of Birth: Munich, Germany
Nationality: German

Education

1988-1997 Certificate of General University Maturity, Fürstfeldbruck, Germany
1997-1998 Civilian Service at Fürstfeldbruck General Hospital
1998-2003 Diploma studies of electrical engineering, Technische Universität München, Germany
2003-2005 Masters programme biomedical engineering, Technische Universität München, Germany and University of Hawai'i at Manoa, Honolulu, USA
Since 2005 Research fellow at the department of anaesthesiology of the Klinikum rechts der Isar, Technische Universität München